Synthesis and characterisation of low band gap polymers for organic photovoltaics and transistors

David Ian James

Submitted in partial fulfilment of the requirements for the degree of
Doctor of Philosophy in Organic Chemistry

Imperial College London
Physics Department

April 2014

菲菲，她的耐心，爱心和理解。

Declaration

The work performed in this thesis was carried out in the Chemistry Department, Imperial College London, between October 2010 and September 2013 under the joint supervision of Iain McCulloch and James Durrant and is the work of the author unless otherwise stated.

David Ian James April 2014

'The copyright of this thesis rests with the author and is made available under a Creative Commons Attribution Non-Commercial No Derivatives licence. Researchers are free to copy, distribute or transmit the thesis on the condition that they attribute it, that they do not use it for commercial purposes and that they do not alter, transform or build upon it. For any reuse or redistribution, researchers must make clear to others the licence terms of this work'

Contributions

The work presented in this thesis was carried out in collaboration with a wide variety of people due to the interdisciplinary nature of the research and would not have been possible without their input.

The organic solar cells were fabricated at Imperial College London in Prof. James Durrant's group by Dr. Raja Shahid Ashraf and at Eindhoven University in Prof René Janssen's group by Dr Youngju Kim.

The organic transistors were fabricated in Thomas Anthopoulos' group at Imperial College London by Dr Youngju Kim, Dr Kigook Song, Dr Nir Yaacobi-Gross, David Beasley and Stephan Rossbauer, at Eindhoven University in Prof René Janssen's group by Dr Youngju Kim (once she had moved group) and at Cambridge University in Prof Henning Sirringhaus' group by Dr Auke Jisk Kronemeijer.

AFM measurements were carried out by David Beasley and Dr Youngju Kim at Imperial College London and Eindhoven University respectively.

PESA measurements were carried out in CSIRO (Melbourne, Australia) by Dr Scott Watkins.

Single crystal structure measurement and analysis was carried out by Dr Andrew White at Imperial College London.

X-ray diffraction measurements were carried out at Imperial College London in Prof. Natalie Stingelin-Stutzmann's group by Dr Paul Westacott.

The work presented in Chapter 2 was carried out in collaboration with Dr Hugo Bronstein, who helped to bring the project to completion. The work presented in Chapter 3 section 3.3 was carried out in close collaboration with Dr. Raja Shahid Ashraf who developed the synthesis of the thiophene isoindigo monomer (**3.25**) and copolymer **IGT-BT**. Other collaborations were with Dr Bob Schroeder who provided

monomers (**3.11**) and (**3.12**), and Iain Meager who helped with the development of furan isoindigo.

Acknowledgements

First and foremost I would like to thank my supervisor Prof. Iain McCulloch for giving me the opportunity to work in his research group. I am very grateful for his patience, encouragement and helpful advice over the last few years, that has enabled me to bring this Ph.D. to completion and develop in a professional and personal capacity. I would also like to thank my second supervisor Prof James Durrant for some useful discussions and helpful advice over the course of the project.

A big thank you also goes to Dr Weimin Zhang, Dr Hugo Bronstein, Dr. Raja Shahid Ashraf, Dr Laure Biniek, Dr Christian Nielsen, Dr Martin Heeney, Dr Zhuping Fei, Dr Mohammed Al- Hashimi, Dr Hongliang Zhong, Dr Munazza Shahid, Dr Junping Du and Dr Yonek Hleba for always having time to answer my questions and teaching me how to do chemistry.

I would like to express my immense gratitude to the people that I worked with on a daily basis in the lab who made being there such a pleasure. In particular I would like to thank George Barnes, the best Man at my wedding, for his constant optimism and charisma and Bob Schroeder for all his help, useful insights and guidance. Also on the list are Chin Pang Yau, Johnny Marshall, Iain Meager, Craig Combe, Jenny Donaghey, Dickson Koroma, Thomas McCarthy-Ward, Joe Rumer, Pierre Boufflet, Jessica Shaw, Sarah Holliday, Josh Green, Christopher Russel, Michael Hurhangee, Rolf Andernach, Mindaugas Kirkus, Dan Beatrup, Miquel A Planells Dillunde, Samuel Cryer, Johnathan Jeck, Dorith Meischler, Barnaby Walker, Raj, Matt, Andrea, Stef and Yang, for all of the great times in the lab and in the pub!

I would also like to thank all the people that made devices and tested my polymers, in particular Dr Youngju Kim, David Beasley, Auke Jisk Kronemeijer, Dr Nir Yaacobi-Gross, Dr Kigook Song for ever so diligently making transistors and Dr Paul Westacott who spent many hours performing X-ray diffraction measurements. A large thank you also goes to Dr Scott Watkins for performing all of my PESA measurements.

I would also like to thank Pete Haycock and Dick Shephard for all the hours that they put in running the NMR service as well as Lisa Haigh and John Barton for never giving up on my somewhat tricky mass spec samples. Also I would like to thank Stefanos Karapanagiotidis for constantly fixing and maintaining my pump, as well as Peter Sulsh for maintaining the chemistry building.

I am very grateful to all the friends that I made within the doctoral training centre for all the great times and collaborations, as well as all of the friends that I made within the wider centre for plastic electronics community.

A large thank you goes to my parents Malcolm and Trudy as well as my two sisters Christine and Michelle for all their affection and encouragement to pursue my studies.

Lastly, a special thank you goes to my wife, Feifei for putting up with me spending so much time in the lab and for all her love and encouragement over the years.

Abstract

The replacement of silicon as a semiconductor within photovoltaics and transistors is key to producing cheaper and easier to produce devices, which can go some way towards tackling global issues such as global warming. Organic electronics have many advantages over silicon due to the fact that they can be solution processed, are cheap and can be deposited on flexible substrates. However, current efficiencies of organics photovoltaics (OPVs) and transistors (OFETs) are lagging behind those based on inorganic materials and thus the development of new materials will be the focus of this thesis.

The first part of this thesis is devoted to the synthesis of a novel fused hexacyclic thiophene donor molecule, **4T** with the primary aim of producing a novel copolymer for OPVs and OFETs. A variety of synthetic routes are explored to produce the desired **4T** monomer with the final outcome being the production and characterisation of the novel copolymer **P4T-BT**.

The next section incorporates the development of more environmentally friendly novel phenyl isoindigo copolymers which show high efficiencies in OPVs and OFETS. Further modification of the isoindigo core produced a novel thiophene isoindigo monomer, which improved the planarity of the copolymers subsequently synthesised. These copolymers had substantially lower band gaps than the analogous Phenyl isoindigo copolymers that were synthesised for comparison. Random terpolymers of the thiophene and phenyl isoindigo monomers were subsequently synthesised to incorporate the properties of the two monomers into one polymer, in order to broaden the spectral absorption of the polymers. Further attempts to produce thiazole isoindigo and furan isoindigo are also outlined in this section.

The third part of this work explores the development of polymers based on Pechmann dyes for application in OFET devices.

Contents

Declaration III
Contributions IV
Acknowledgements VI
Abstract VIII
Contents IX
Publications XV
Abbreviations XVI
Chapter 1 - Introduction 1
1.1 The Challenges of Our Times 2
1.2 Background to Polymers 4
1.3 Background to Conducting Polymers 5
1.3.1 The nature of bonding 5
1.3.2 Origins of conductivity in semiconducting polymers 6
1.3.3 Optoelectronic properties of semiconducting polymers 8
1.3.4 Exciton diffusion and charge transport 10
1.4 Organic Photovoltaics 14
1.4.1 Background 14
1.4.2 OPV device architecture and characterisation 18
1.5 Organic Field Effect Transistors (OFETs) 21
1.5.1 Background 21
1.6 Polymer Design Principles 27
1.7 Band Gap Engineering and Charge Transport Mobility Considerations 29
1.8 Polymer Solubility 34
1.9 Synthetic Aspects 35
1.10 Aim of Thesis 37
Chapter 2 - 4T polymer for OPVs and OFETs 39
2.1 Introduction 40
2.2 Synthesis of the 4T Monomer 42
2.3 Synthesis of 4T Based Polymer 55
2.4 Polymer Properties 57
2.4.1 Polymer molecular weight 57
2.4.2 Polymer UV-Vis 57
2.4.3 Polymer performance in OFETs 58

2.4.4 Polymer performance in OPV 60
2.5 Conclusion and Subsequent Impact 61
Chapter 3 Isoindigo 63
3.1 Introduction to Isoindigo 64
3.2 Furan Flanked Isoindigo Based Polymers 67
3.2.1 Synthesis of furan flanked isoindigo monomer 68
3.2.2 Synthesis of furan flanked isoindigo based copolymers 69
3.2.3 Physical properties of furan flanked isoindigo based polymers 70
3.2.4 Optical properties of furan flanked isoindigo based polymers 71
3.2.5 Energy levels of furan flanked isoindigo based polymers 74
3.2.6 DSC of furan flanked isoindigo based polymers 78
3.2.7 XRD of furan flanked isoindigo based polymers 79
3.2.8 OFET device performance of furan flanked isoindigo based polymers 80
3.2.9 OPV device performance of furan flanked isoindigo based polymers 81
3.2.10 Atomic force microscopy (AFM) characterisation of blend films 85
3.2.11 Conclusion 86
3.3 Thiophene Isoindigo 87
3.3.1 Synthesis of thiophene isoindigo monomer 87
3.3.2 Synthesis of IGT-BT copolymer 90
3.3.3 Properties of the IGT-BT copolymer 90
3.3.4 Optical properties of IGT-BT copolymer 91
3.3.5 Energy levels of IGT-BT copolymer 91
3.3.6 OFET device performance of IGT-BT copolymer 93
3.3.7 AFM of IGT-BT copolymer 95
3.3.8 XRD of IGT-BT copolymer 95
3.3.9 Density functional theory calculations for IGT-BT 96
3.3.10 Conclusion 97
3.4 Thiophene Isoindigo Part 2 – A Comparison with Phenyl Isoindigo 98
3.4.1 Synthesis of thiophene isoindigo and phenyl isoindigo copolymers 98
3.4.2 Physical properties of thiophene and phenyl isoindigo copolymers. 101
3.4.3 Optical properties of thiophene and phenyl isoindigo copolymers. 103
3.4.4 PESA determination of energy levels of thiophene and phenyl isoindigo copolymers. 106
3.4.5 DFT of thiophene and phenyl isoindigo copolymers. 108
3.4.6 DSC of thiophene and phenyl isoindigo copolymers. 115
3.4.7 OFET device performance of thiophene and phenyl isoindigo copolymers 116

3.4.8 OPV device performance of thiophene and phenyl isoindigo copolymers 120
3.4.9 Conclusion 122
3.5 Thiophene and Phenyl Isoindigo Based Terpolymers 123
3.5.1 Synthesis of random thiophene isoindigo and phenyl isoindigo terpolymers 124
3.5.2 Properties of random thiophene isoindigo and phenyl isoindigo terpolymers 125
3.5.3 Optical properties of random thiophene isoindigo and phenyl isoindigo terpolymers 126
3.5.4 DSC of random thiophene and phenyl isoindigo terpolymers. 128
3.5.5 PESA determination of energy levels of random thiophene and phenyl isoindigo terpolymers. 128
3.5.6 OPV device performance of random thiophene isoindigo and phenyl isoindigo terpolymers. 130
3.5.7 OFET device performance of random thiophene isoindigo and phenyl isoindigo terpolymers. 131
3.5.8 Conclusion 135
3.6 Thiazole Isoindigo 135
3.6.1 Towards the synthesis of thiazole isoindigo. 136
3.6.2 Conclusion 141
3.7 Furan Isoindigo 141
3.7.1 Towards the synthesis of furan isoindigo. 142
3.7.2 Conclusion 145
Chapter 4 Pechmann Dyes 146
4.1 Introduction to Pechmann Dyes 147
4.2 Synthesis of Pechmann Dye Based Monomers 149
4.3 Synthesis of Pechmann Dye Based Polymers 155
4.4 Physical Properties of the Pechmann Dye Homo Polymer hPMA 157
4.5 Optical Properties of Pechmann Dye Homo polymer hPMA 158
4.6 DSC of Pechmann Dye Homo Polymer hPMA 159
4.7 Optical Properties of Pechmann Dye Homo Polymer hPMA Revisited. 160
4.8 Energy Levels of Pechmann Dye Homo Polymer hPMA 161
4.9 OFET Device Performance of Pechmann Dye Homo Polymer hPMA. 161
4.10 Density Functional Theory Calculations for hPMA 163
4.11 Conclusion and Broader Application 165
Chapter 5 Experimental Procedures 166
5.1 General Procedures 167
5.2 Field Effect Transistor Fabrication and Characterisation. 168
5.3 Solar Cell Fabrication and Characterisation 170

5.4 Synthesis of 2,5-dibromothieno[3,2-b]thiophene (2.11) 171
5.5 Synthesis of 3,6-Dibromo-thieno[3,2-b]thiophene (2.12) 171
5.6 Synthesis of thieno[3,2-b]thiophene-3,6-dicarboxylic acid (2.13) 172
5.7 Synthesis of 2,5-dibromothieno[3,2-b]thiophene-3,6-dicarboxylic acid (2.14) 172
5.8 Synthesis of diethyl 2,5-dibromothieno[3,2-b]thiophene-3,6-dicarboxylate (2.16) 173
5.9 Synthesis of diethyl 2,5-di(thiophen-2-yl)thieno[3,2-b]thiophene-3,6-dicarboxylate (2.18) 173
5.10 Synthesis of 2,5-di(thiophen-2-yl)thieno[3,2-b]thiophene-3,6-dicarboxylic acid (2.19) 174
5.11 Synthesis of thieno[3',2':4,5]cyclopenta[1,2-b]thieno[2",3":3',4']cyclopenta[1',2':4,5] thieno[2,3-d]thiophene-4,9-dione (2.21) 175
5.12 Synthesis of thieno[3',2':4,5]cyclopenta[1,2-b]thieno[2",3":3',4']cyclopenta[1',2':4,5] thieno[2,3-d]thiophene-4,9-diol (2.25) 175
5.13 Synthesis of triisopropyl(thiophen-2-yl)silane (2.27) 176
5.14 Synthesis of triisopropyl(5-(trimethylstannyl)thiophen-2-yl)silane (2.28) 176
5.15 Synthesis of diethyl 2,5-bis(5-(triisopropylsilyl)thiophen-2-yl)thieno[3,2-b]thiophene-3,6-dicarboxylate (2.29) 177
5.16 Synthesis of 2,5-bis(5-(triisopropylsilyl)thiophen-2-yl)thieno[3,2-b]thiophene-3,6-dicarboxylic acid (2.30) 178
5.17 Synthesis of 2 bromo thiophene 3 ethyl ester (2.41) 179
5.18 Synthesis of 2,5-bis(trimethylstannyl)thieno[3,2-b]thiophene (2.42) 179
5.19 Synthesis of diethyl 2,2'-thieno[3,2-b]thiene-2,5-diyldithiophene-3-carboxylate (2.43) 180
5.20 Synthesis of 7,7'-(2,2'-(thieno[3,2-b]thiophene-2,5-diyl)bis(thiophene-3,2-diyl))bis(5,9-diethyltridecan-7-ol) (2.44) 181
5.21 Synthesis of 7,7'-(2,5-di(thiophen-2-yl)thieno[3,2-b]thiophene-3,6-diyl)bis(5,9-diethyltridecan-7-ol) (2.51) 181
5.22 Synthesis of 4T (2.53) 182
5.23 Synthesis of 4T-Br2 (2.54) 183
5.24 Synthesis of P4TBT 184
5.25 Synthesis of (E)-6,6'-dibromo-[3,3'-biindolinylidene]-2,2'-dione (3.3). 185
5.26 Synthesis of 9-(iodomethyl)nonadecane (3.5). 185
5.27 Synthesis of 6,6'-dibromo-N,N'-(2-octyldodecanyl)-isoindigo (3.6). 186
5.28 Synthesis of furan-2-yltrimethylstannane (3.8). 186
5.29 Synthesis of (E)-6,6'-di(furan-2-yl)-1,1'-bis(2-octyldodecyl)-[3,3'-biindolinylidene]-2,2'-dione (3.9). 187
5.30 Synthesis of (E)-6,6'-bis(5-bromofuran-2-yl)-1,1'-bis(2-octyldodecyl)-[3,3'-biindolinylidene]-2,2'-dione (3.10) 188

5.31 Synthesis of Poly((E)-6-(furan-2-yl)-1,1'-bis(2-octyldodecyl)-6'-(5-(thiophen-2-yl)furan-2-yl)-[3,3'-biindolinylidene]-2,2'-dione) (PFTFI). 188
5.32 Synthesis of Poly((E)-6-(furan-2-yl)-1,1'-bis(2-octyldodecyl)-6'-(5-(thieno[3,2-b]thiophen-2-yl)furan-2-yl)-[3,3'-biindolinylidene]-2,2'-dione) (PFTTFI). 189
5.33 Synthesis of 9-(azidomethyl)nonadecane (3.18) 190
5.34 Synthesis of 2-octyldodecan-1-amine (3.19) 191
5.35 Synthesis of n-(2-octyldodecyl)thiophen-3-amine (3.21 branched) 192
5.36 Synthesis of N-hexadecylthiophen-3-amine (3.21 linear) 192
5.37 Synthesis of 4-(2-octyldodecyl)-4H-thieno[3,2-b]pyrrole-5,6-dione (3.22 branched) 193
5.38 Synthesis of 4-(hexadecyl)-4H-thieno[3,2-b]pyrrole-5,6-dione (3.22 linear) 194
5.39 Synthesis of (E)-4,4'-bis(2-octyldodecyl)-[6,6'-bithieno[3,2-b]pyrrolylidene]-5,5'(4H,4'H)-dione (3.24 branched) 194
5.40 Synthesis of (E)-4,4'-dihexadecyl-[6,6'-bithieno[3,2-b]pyrrolylidene]-5,5'(4H,4'H)-dione (3.24 linear) 195
5.41 Synthesis of (E)-2,2'-dibromo-4,4'-bis(2-octyldodecyl)-[6,6'-bithieno[3,2-b]pyrrolylidene]-5,5'(4H,4'H)-dione (3.25 branched) 196
5.42 Synthesis of (E)-2,2'-dibromo-4,4'-dihexadecyl-[6,6'-bithieno[3,2-b]pyrrolylidene]-5,5'(4H,4'H)-dione (3.25 linear) 197
5.43 Synthesis of IGT-BT 197
5.44 Synthesis of IGT-T 198
5.45 Synthesis of IGT-TT 199
5.46 Synthesis of IGPh-T 200
5.47 Synthesis of IGPh-TT 201
5.48 Synthesis of polymer IGT-Ph 202
5.49 Synthesis of IGT-Na 203
5.50 Synthesis of IGPh-Ph 203
5.51 Synthesis of IGPh-Na 204
5.52 Synthesis of rIGPhPhIGT0.25 205
5.53 Synthesis of rIGPhPhIGT0.50 206
5.54 Synthesis of rIGPhPhIGT0.75 206
5.55 Synthesis of tert-butyl thiazol-4-ylcarbamate (3.35) 207
5.56 Synthesis of tert-butyl (2-octyldodecyl)(thiazol-4-yl)carbamate (3.36) 208
5.57 Synthesis of tert-butyl palmitoyl(thiazol-4-yl)carbamate (3.37) 208
5.58 Synthesis of N-(thiazol-4-yl)palmitamide (3.38) 209
5.59 Synthesis of 2-bromothiazol-4-amine (3.40) 210
5.60 Synthesis of N-(2-bromothiazol-4-yl)palmitamide (3.41) 210

5.61 Synthesis of N-hexadecylthiazol-4-amine (3.42) 211
5.62 Synthesis of N-(2-bromothiazol-4-yl)-2,2,2-trichloroacetamide (3.45) 211
5.63 Synthesis of (E)-N-(2-bromothiazol-4-yl)-2-(hydroxyimino)acetamide (3.44) 212
5.64 Synthesis of tert-butyl furan-3-ylcarbamate (3.52) 212
5.65 Synthesis of tert-butyl furan-3-yl(2-octyldodecyl)carbamate (3.53) 213
5.66 Synthesis of 2-octyldodecanoic acid (3.56) 213
5.67 Synthesis of 2-octyldodecanoyl chloride (3.57) 214
5.68 Synthesis of tert-butyl furan-3-yl(palmitoyl)carbamate (3.54) 214
5.69 Synthesis of tert-butyl furan-3-yl(2-octyldodecanoyl)carbamate (3.58) 215
5.70 Synthesis of N-(furan-3-yl)palmitamide (3.59) 216
5.71 Synthesis of N-(furan-3-yl)-2-octyldodecanamide (3.60) 216
5.72 Synthesis of 4-hexadecyl-4H-furo[3,2-b]pyrrole-5,6-dione (3.62) 217
5.73 Synthesis of 2-hydroxy-4-oxo-4-(thiophen-2-yl)butanoic acid (4.3) 218
5.74 Synthesis of (E)-5,5'-di(thiophen-2-yl)-2H,2'H-[3,3'-bifuranylidene]-2,2'-dione (4.4) 218
5.75 Synthesis of (E)-1,1'-bis(2-octyldodecyl)-5,5'-di(thiophen-2-yl)-[3,3'-bipyrrolylidene]-2,2'(1H,1'H)-dione (4.8) 219
5.76 Synthesis of 4-(5-bromothiophen-2-yl)-2-hydroxy-4-oxobutanoic acid (4.11) 220
5.77 Synthesis of (E)-5,5'-bis(5-bromothiophen-2-yl)-2H,2'H-[3,3'-bifuranylidene]-2,2'-dione (4.12) 220
5.78 Synthesis of (E)-5,5'-bis(5-bromothiophen-2-yl)-1,1'-dihexadecyl-[3,3'-bipyrrolylidene]-2,2'(1H,1'H)-dione (4.14) 221
5.79 Synthesis of (E)-4-(3-dodecylthiophen-2-yl)-4-oxobut-2-enoic acid (4.17) 221
5.80 Synthesis of (E)-5,5'-(3-dodecylthiophen-2-yl)bifuranylidenedione (4.18) 222
5.81 Synthesis of 1-(3-dodecylthiophen-2-yl)ethanone (4.22) 222
5.82 Synthesis of (E)-1,1'-didodecyl-5,5'-bis(3-dodecylthiophen-2-yl)-[3,3'-bipyrrolylidene]-2,2'(1H,1'H)-dione (4.24) 223
5.83 Synthesis of (E)-5,5'-bis(5-bromo-3-dodecylthiophen-2-yl)-1,1'-didodecyl-[3,3'-bipyrrolylidene]-2,2'(1H,1'H)-dione (4.25) 224
5.84 Synthesis of hPMA 224
Chapter 6 References 226
Chapter 7 Appendix 238
7.1 The X-ray crystal structure of 4T-Br2 (2.54) 239

Publications

The following publications have been produced as a result of this work and will be discussed in the following chapters:

Chapter 2

• Synthesis of a novel fused thiophene-thieno[3,2-*b*]thiophene-thiophene donor monomer and co-polymer for use in OPV and OFETs., *Macromol Rapid Commun*, 2011, Vol:32. Pages:1664-1668 DOI: 10.1002/marc.201100417

Chapter 3

• A new thiophene substituted isoindigo based copolymer for high performance ambipolar transistors, *Chemical Communications*, 2012, Vol: 48. Pages:3939-3941 DOI**:** 10.1039/C2CC30169E

• Bis-lactam-based donor polymers for organic solar cells: Evolution by design, *Thin Solid Films* 2013

• High performance isoindigo based polymers for efficient solar cells, J. Mat. Chem, 2014, Manuscript in preparation.

The work for the following publications was undertaken over the course of my time at Imperial but will not be included in this thesis:

•Compartmentalization of Electrophoretically Separated Analytes in a Multiphase Microfluidic Platform, *Analytical Chemistry*, 2012, Vol:84. DOI**:** 10.1021/ac301141x

•Design of Semiconducting Indacenodithiophene Polymers for High Performance Transistors and Solar Cells, *Accounts of Chemical Research*, 2012, Vol:45. DOI**:** 10.1021/ar200208g

•James DI, Smith J, Heeney M, Anthopoulos TD, Salleo A, McCulloch I, Organic Semiconductor materials for transistors, Organic Electronics II: More materials and applications, Editor: Klauk, Wiley-VCH, 2012, Pages: 3-26, ISBN:9783527640225

•Synthesis and photo-induced charge separation of confined conjugation length phenylene vinylene-based polymers., *Polym. Chem.*, 2013, Advance Article DOI: 10.1039/C3PY00061C

Abbreviations

(A) – Acceptor
AcOH - Acetic acid
AM – Air mass
AFM - Atomic force microscopy
BT - Benzothiadiazole
BHJ – Bulk heterojunction
Calc. – Calculated molecular ion peak
CB - Chlorobenzene
CF - Chloroform
CMOS – Complementary metal oxide semiconductor
CPDT – Cyclopenta[2,1-b:3,4-b']dithophene
DFT - Density functional theory
DP – Degree of polymerisation
DNA – Deoxyribonucleic acid
dba - dibenzylideneacetone
PQX- 5,8-dibromo-phenanthrenequinoxaline
DCM - Dichloromethane
DCC - N,N'-dicyclohexylcarbodiimide
Et_2O – Diethyl ether
DIAD - Diisopropyl azodicarboxylate
DSC - Differential scanning calorimetry
DPP - Diketopyrrolopyrrole
DMAP - 4-dimethylaminopyridine
DMF - Dimethylformamide
DMSO – Dimethyl sulphoxide
PDTG–TPD - dithienogermole–thienopyrrolodione
(D) – Donor
V_D – Drain voltage
EI – Electron ionisation
ETL – Electron transport layer
eV – Electron volt
ES – Electrospray
EtOAc – Ethyl acetate
EQE - External quantum efficiency
FF - Fill factor
fs – femtoseconds
V_G – Gate voltage
GPC – Gel permeation chromatography
HMDS - Hexamethyldisilazane
HOMO – Highest occupied molecular orbital
HRMS – High resolution mass spectroscopy
HTL – Hole transport layer
h - hours
IDT – Indacenodithiophene
ITO - Indium tin oxide
ICT - Internal charge transfer
kDa – Kilo Daltons
$LiAlH_4$ - Lithium aluminium hydride
LDA - Lithium diisopropyl amide
LUMO – Lowest unoccupied molecular orbital
MS – Mass spectroscopy
MALDI - Matrix-assisted laser desorption ionization
P_{max} - Maximum power
meV – Milli-electron volts
min - Minutes
M - Molar
m/z – Molecular ion peak
nm – Nanometers
NBS - N-bromosuccinimide
nBuLi - n butyl lithium
NDI - N,N-dialkylnaphthalene-1,8:4,5-tetracarboxydiimides
TPD – n-octylthienopyrrolodione
NMR – Nuclear magnetic resonance spectroscopy
M_n – Number average molecular mass
V_{oc} - Open circuit voltage
OFET – Organic field effect transistor
OPV – Organic photovoltaic
ODCB - Ortho dichlorobenzene
p –TSA - Para-toluene sulphonic acid
PPM – Parts per million
PFBT - Pentafluorobenzenethiol
PTCBI - 3,4,9,10-perylenetetracarboxylic bis-benzimidazole
$PC_{61}BM$ - [6,6]-phenyl-C_{61}-butyric acid methyl ester
$PC_{71}BM$ - [6,6]-phenyl-C_{71}-butyric acid methyl ester
PCE - Photocurrent conversion efficiency
PESA - Photo electron spectroscopy in air
PDI - Polydispersity index

PEDOT - Poly(3,4-ethylenedioxythiophene)
P3HT – Poly-3-hexyl thiophene
PITN – Polyisothianaphthalene
PMMA - Poly(methylmethacrylate)
MEH-PPV – poly(2-methoxy-5-(2′-ethyl-hexyloxy)-1,4-phenylene vinylene)
PCDTBT – poly[N-9'-heptadecanyl-2,7-carbazole-alt-5,5-(4',7'-di-2-thienyl-2',1',3'-benzothiadiazole)]
PPV – Poly(phenylenevinylene)
PSS - Poly(styrenesulfonate)
recSEC - Recycling size exclusion chromatography
rpm – Revolutions per minute
rt – Room temperature
SAM – Self assembled monolayer
$\mathbf{J_{sc}}$ - Short circuit current density
$\mathbf{I_{SD}}$ – Source-drain current
TW – Terawatts
Boc - Tertiary-Butoxycarbonyl
TBAF - Tertiary butyl amine fluoride
TCE – Tetrachloroethane
THF - Tetrahydrofuran
TMEDA - Tetramethylethylenediamine
TT – thieno[3,2-*b*]thiophene
TLC – Thin layer chromatography
V_T - Threshold voltage
TOF – Time of flight
TCB - trichlorobenzene
$\mathbf{Et_3N}$ - triethyl amine
TFA - Trifluoroacetic acid
TIPS – Triisopropyl silyl
TIPS-Cl - Triisopropylsilyl chloride
$\mathbf{P(}o\mathbf{\text{-}tol)_3}$ - Tri(*o*-tolyl)phosphine
$\mathbf{PPh_3}$ - Triphenyl phosphine
$\mathbf{M_w}$ – Weight average molecular mass
XRD - X-ray diffraction

Chapter 1 - Introduction

I believe there is no philosophical high-road in science, with epistemological signposts. No, we are in a jungle and find our way by trial and error, building our road behind us as we proceed.

Max Born (1882-1970) German Physicist. Nobel Prize, 1954

1.1 The Challenges of Our Times

Since the development of the first stream engine which could produce continuous rotary motion by James Watt in 1781,[1] man has been using ever increasing amounts of fossil fuels in the drive to improve living standards through industrialisation. This has had the adverse effect of releasing large quantities of greenhouse gases which have been accumulating in the atmosphere. As a result of the rise in carbon dioxide levels there has been shown to be a correlated increase in global surface temperatures, **Figure 1.1**.

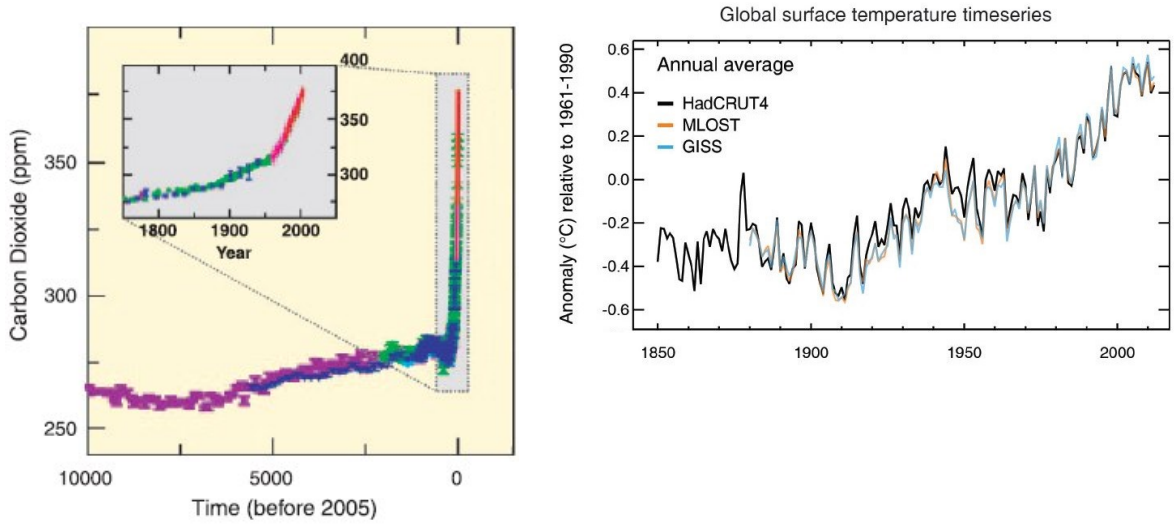


Figure 1.1: Historical atmospheric concentrations of CO_2 from the last 10,000 years up to 2005. Measurements are shown from ice cores (symbols with different colours for different studies) and atmospheric samples (red lines) (left).[2] Global surface annual average temperature change since 1850 (right).[3]

If emissions of greenhouse gases continue at their present rate of growth it is anticipated that by 2056 emissions of CO_2 will have doubled, which will take the atmospheric concentration of CO_2 beyond 560 ppm. It is at this concentration that it is anticipated that anthropogenic global warming will trigger severe changes in climate.[4] These changes include a higher risk of flooding as sea levels rise, melting of glaciers and polar ice caps, changes to crop yields, a decrease in biodiversity and changes to the availability of water.[5] However as the world energy demand is around 16 TW (2009 figure)[6] with fossil fuels accounting for just over 80% of energy production,[7] reducing CO_2 levels will not be an easy task. Additionally the demand for energy is anticipated to increase to ~27 TW by 2050 as a result of increases in world population

and projected economic growth in developing countries.[8] With reserves of fossil fuels slowly declining[9] the use of renewable energy sources will need to be substantially increased to not only compensate for the increased demand for energy but also to lower CO_2 levels. As 120,000 TW of solar energy illuminates the earth, there is more than enough energy in sunlight to supply the world's energy demands. In fact, more solar energy strikes the earth in one hour (4.3×10^{20}J) than the world uses in an entire year (4.1×10^{20}J in 2001).[8] However currently only 1% of the energy produced by renewable energy sources is made up of solar energy.[7] This is due to the intermittency of solar radiation, as well as the high costs associated with the production of crystalline silicon solar cells as despite the fact that silicon is the second most abundant element within the earth's crust, its extraction and purification to the >99.9999% grade required for electronic applications is very energy intensive. Not only does this cause a lot of CO_2 to be produced in the production of a technology designed to be environmentally benign but a lot of hazardous waste is also generated in the process.[10] Thus alternative semiconducting materials are required that can be produced cheaply with minimal environmental impact to replace the functions currently carried out by silicon.

Semiconducting polymers and small molecules are a viable substitute for silicon and can be used in organic photovoltaics (OPVs) and organic field effect transistors (OFETs). Even though the device performances of OPVs and OFETS are currently considerably lower than their inorganic counterparts, the fact that they can be easily solution processed via roll to roll fabrication techniques due to their flexible nature means that low cost large area devices can be made.[11] For OPVs organic materials have several technological advantages over silicon such as their higher extinction coefficients (usually $\geq 10^5$ cm^{-1}), and low band gaps on the order of 1-3 eV, which can be chemically tailored,[12] meaning that layers of just 100 nm thick are required to absorb most of the incident light.[13] This means that the costs of the materials for OPV devices are considerably lower than silicon and with inexpensive low temperature solution processing, the energy payback time and amount of CO_2 emissions released during production are expected to be much lower than silicon based devices.[14-17] Thus there is the potential for OPVs to solve the world energy crisis as even with just 10% efficient solar cells only 0.16% of the worlds land mass would need to be covered to provide the world with enough energy. To put this in perspective this is roughly the

equivalent of the amount of land area covered by America's federal highways.[18] As for OFETs, there are a variety of applications that don't require high performance switching speeds such as radio frequency identification tags, pixel drivers and smart cards that they can be used for.[19, 20]

1.2 Background to Polymers

A polymer is defined as a substance that has a molecular structure built up chiefly or completely from a large number of similar units bonded together.[21] Typically polymers are synthesised via either a chain growth process in which the monomers are added one unit at a time to a growing chain, or a step growth process in which chains of monomers add directly to each other. As polymerisation is generally a random process (except for the synthesis of DNA) the molecular weights of the individual chains within the polymer will vary. This means that unlike small molecules that have a fixed molecular weight, the molecular weight distribution of polymers need to be modelled statistically. Thus the molecular weight distribution of a polymer is typically defined by the following three parameters:

$$M_n = \frac{\sum_i N_i M_i}{\sum_i N_i} \quad (\mathbf{1}) \qquad M_w = \frac{\sum_i N_i M_i^2}{\sum_i N_i M_i} \quad (\mathbf{2}) \qquad PDI = \frac{M_w}{M_n} \quad (\mathbf{3})$$

M_n is the number average molecular mass where N_i is the number of polymer chains composed of i monomers, M_i is the mass of a polymer chain composed of i monomers. M_w is an alternative measure that defines the mass average molecular mass of the polymer chains. The polydispersity index (PDI) defines the mass distribution of the polymer chains and is always greater than or equal to 1.[22]

These values are typically measured by a technique known as gel permeation chromatography (GPC) which is a type of size exclusion chromatography in which the polymer is passed through a column of porous beads. If the polymer chain is small it can become retained within the pores of the beads while larger chains pass straight through. By comparing the retention times of the polymer against polystyrene standards of known molecular weight the molecular weight of the polymer can be deduced.

The length of a polymer chain has a pronounced effect on its properties. Factors such as viscosity, tensile strength, crystallinity, chain entanglements, melting temperature, energy levels, charge carrier mobility and solubility can all be affected.[23] For example low molecular weight polymers show a high amount of crystallinity but show poor charge carrier mobilities as their crystalline domains are separated by grain boundaries.[24] By increasing the molecular weight to an M_n value above 20 KDa the polymers can form more chain entanglements which improve the links between crystalline domains thus increasing the charge carrier mobility.[25, 26] However if the M_n exceeds 150 KDa the polymer has a higher viscosity, which can hinder crystallisation during annealing, leading to reduced mobilities.[27] Thus it is very important for synthetic chemists to control the molecular weights of the polymers. This can be achieved to some extent by controlling the reaction temperature, monomer ratios and reaction time. Additionally, as will be seen later on in this thesis the desired molecular weight of a polymer can be extracted out of a batch of polymer by recycling size exclusion chromatography (rSEC).

1.3 Background to Conducting Polymers

1.3.1 The nature of bonding

Traditionally polymers have been seen as being non conductive insulator materials. Examples of this class of material include polymers such as polyethylene, polyvinyl alcohol and polyvinyl chloride. The reason that these polymers are insulating is due to their molecular structure. When looking at the bonds that make up these polymers' backbones it is evident that the carbon atoms are bonded solely through σ-bonds. σ-bonds are formed when a carbon atom promotes an electron from a 2s orbital to an empty 2p orbital in a process called hybridisation to give four sp^3 hybridised orbitals, in a tetrahedral arrangement, each of which can become filled by sharing an electron with an sp^3 hybridised orbital of a neighbouring carbon atom. It is this sharing of electrons that forms the σ-bond. As the electrons within these bonds are localised solely between the two bonding carbon atoms there are no electrons available for the conduction of electricity or heat.[28]

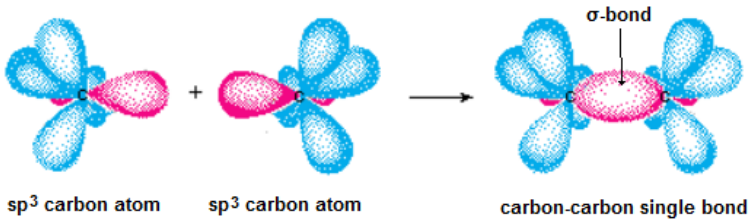


Figure 1.2: Formation of σ-bond.

Semiconducting polymers, on the other hand have backbones that incorporate π-bonds between the carbon atoms in an alternating σ- bond π-bond arrangement that allows for the conduction of charge. π-bonds are formed when a carbon atom promotes an electron from a 2s orbital to an empty 2p orbital to give three sp^2 hybridised orbitals that lie in a plane at 120º to each other, leaving the remaining p_z orbital unhybridised at 90º out of the plane of the other three orbitals. The three sp^2 orbitals can form σ-bonds with neighbouring orbitals while the remaining electrons in the p_z orbital can bond with the electrons in a neighbouring p_z orbital thus forming a π-bond. Whilst the electrons in the σ-bonds are vital for the structural integrity of the polymer backbone the electrons in the π-bonds are not and are thus free to be delocalised by conjugation with adjacent π-bonds, which allows the polymer to be conducting.[28]

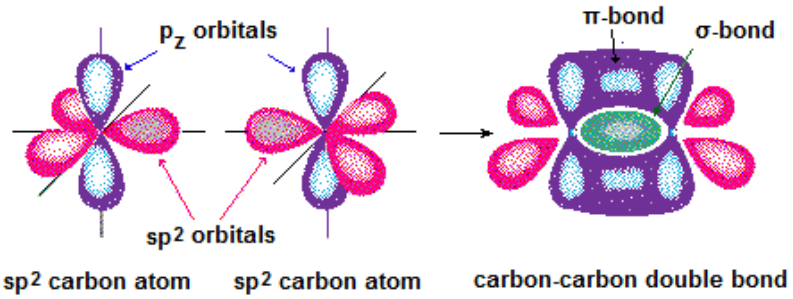


Figure 1.3: Formation of π-bond.

1.3.2 Origins of conductivity in semiconducting polymers.

The field of plastic electronics started in 1977 when it was discovered that polyacetylene is conductive when doped.[29] Polyacetylene like all conductive polymers is composed of alternating single and double bonds in which the electrons in the π orbitals can be delocalised along the polymer chain, providing that the neighbouring π orbitals are not occupied. It is the requirement for the electrons to go into non filled

orbitals, due to the Pauli Exclusion Principle,[30] that the polymer needs to be doped under non illuminated conditions for the conductivity to be observed.[31]

Semiconducting polymers can show both n-type and p-type behaviour in which electrons transport charge in n-type materials and holes transport charge in p-type materials.[32] However, the majority of polymers that are available exhibit p-type behaviour. The reason for this can be deduced from looking at an illustration of what happens in a crystalline film in which two ethylene units are stacked on top of each other, **Figure 1.4.**

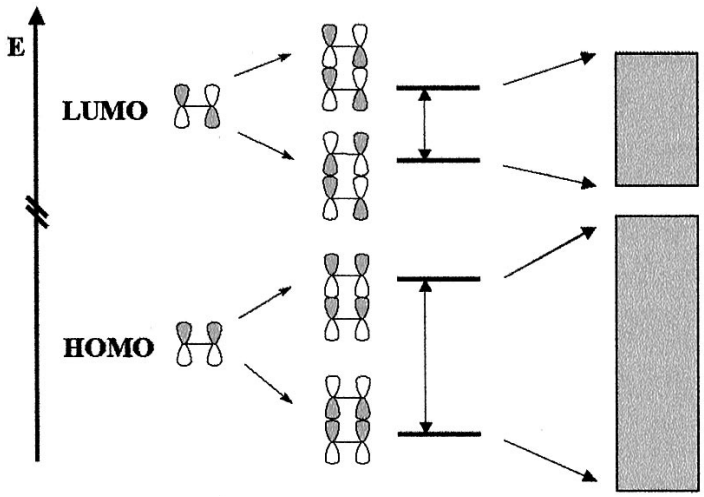


Figure 1.4: Illustration of the bonding and antibonding interactions between the HOMO/LUMO levels of two ethylene molecules in a cofacial configuration. The conduction bands formed when a large number of stacked molecules interact are also illustrated.[32]

From the illustration (**Figure 1.4**) it can be seen that in the isolated ethylene molecule the highest occupied molecular orbital (HOMO) is formed of two p_z orbitals that have lobes where the signs of the wavefunctions are the same meaning that they can form a bond. Thus there is no node in the electronic wavefunction for the HOMO. The lowest unoccupied molecular orbital (LUMO) level corresponds to the two p_z orbitals in which lobes of opposite sign are interacting thus forming an antibonding interaction. Thus there is a node in the electronic wavefunction of the LUMO. In the two ethylene units that are stacked in a cofacial arrangement the interaction between the two molecules leads to a splitting of the HOMO level and the LUMO level. The HOMO splitting is large as the interaction between the HOMOs of the two molecules results in either a fully bonding situation in which the HOMO-1 of the dimer is fully

stabilised or a fully antibonding situation in which the HOMO level of the dimer is completely destabilised. As for the LUMO the splitting is considerably smaller. This is due to the direct bonding interactions being compensated for by diagonal antibonding interactions in the LUMO of the dimer and in the LUMO+1 of the dimer the direct antibonding interactions are compensated for by the diagonal bonding interactions. This means that as a qualitative rule that for perfectly cofacial configurations the lower the number of nodes in the wavefunction the larger the splitting will be for the particular level in question. So as the HOMO has one less node than the LUMO the splitting of the HOMO will be greater. This effect is further amplified when going to larger stacks and so can explain why the hole mobility is generally expected to be larger than the electron mobility for organic semiconductors in crystals or crystalline films.[32]

1.3.3 Optoelectronic properties of semiconducting polymers

Upon covalently linking a series of acetylene monomers together an orbital interaction between the π- bonds occurs, which gives rise to an energy level splitting between HOMO and the LUMO. In this case the HOMO is a π and the LUMO is a π* orbital. It can be seen in **Figure 1.5** that the HOMO and LUMO are dependant on the distance that the electrons can delocalise over, otherwise known as the persistence length. As the number of monomer units increases the amount of orbital interaction increases leading to a decrease in the band gap between the HOMO and LUMO energy levels, until the persistence length is so large that the band gap reaches a saturation point and can't be decreased any further. As this point, typically between 10-15 monomer units,[33] the energy levels rather than being discrete show a 'band' like structure similar to that seen in inorganic semiconductors.[34]

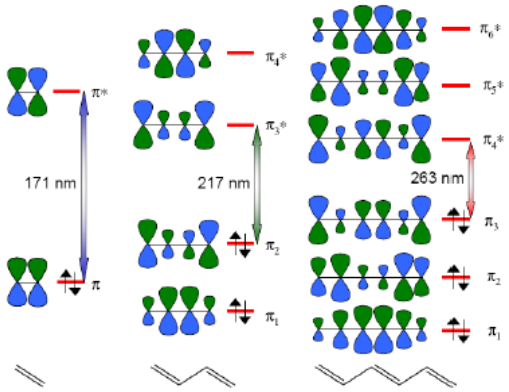


Figure 1.5: Red shifting of optical absorption with increasing conjugation length.[35]

As previously mentioned doping can either add or remove an electron from the polymer thus making it conducting. The same effect can be achieved by electrical charge injection or photoexcitation. When an electron is either added or removed there is a redistribution of charge within the polymeric structure in order to minimise the total energy of the polymer. Thus the nuclear positions of the atoms, bond angles and bond lengths change within the polymer, resulting in the formation of a polaron around the charge, as shown in **Figure 1.6**.[36]

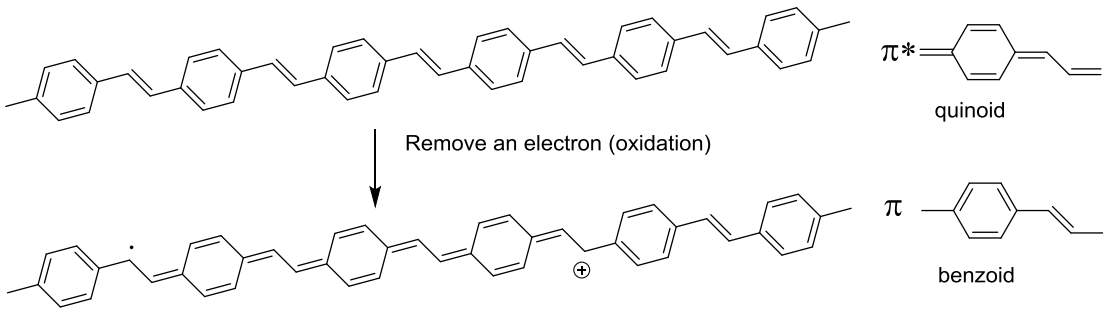


Figure 1.6: Changes in bond alternation from benzoid to quinoid upon formation of a hole polaron.

The formation of the polaron also introduces additional energy levels between the HOMO and the LUMO energy gap which can either be empty (hole polaron) or filled (electron polaron). If a hole polaron and an electron polaron come into contact an exciton is formed in which further structural relaxation occurs due to the coulombic attraction between the electron and the hole. This process releases a small amount of energy which is termed the exciton binding energy.[37] Excitons can be either singlet excitons (generated upon photoexcitation or charge injection) or triplet excitons (generated by charge injection) depending on the relevant spins of the electrons involved, as shown in **Figure 1.7**.

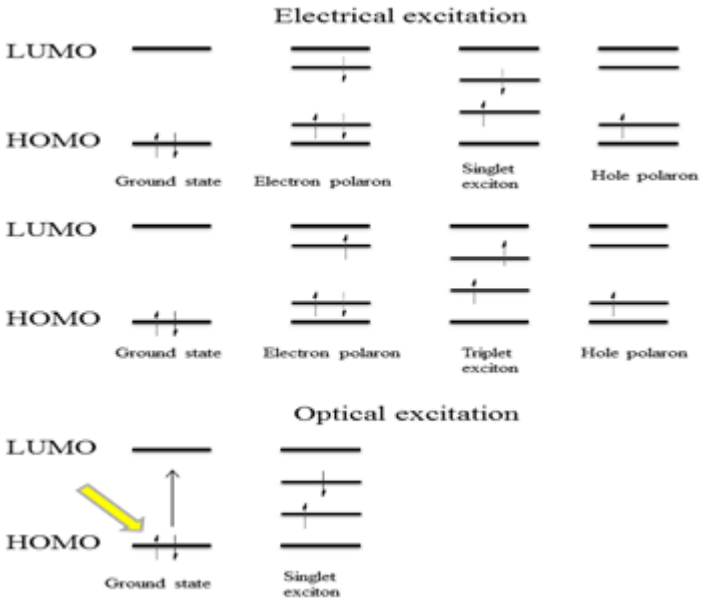


Figure 1.7: Formation of polarons and singlet and triplet excitons.

The structural relaxation caused as a result of exciton formation leads to the polymer having a more rigid and planar conformation in the excited state. This effect can clearly be seen in polymers such as polyvinylchloride in which the structure is converted from benzoid to quinoid via a change in bond order which persists over six monomer units.[38]

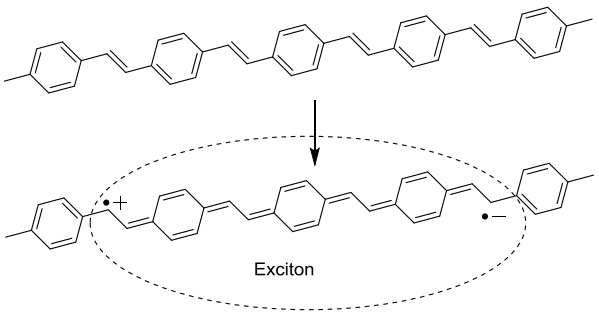


Figure 1.8: Change in bond alternation upon exciton formation.

1.3.4 Exciton diffusion and charge transport

Excitons are affected by the length of the polymer chain that they are on. For chains that are longer that the exciton wavefunction the energy of the exciton can be roughly described by the relationship $E \sim 1/L^2$ where E is the energy and L is the length of the polymer chain. However for shorter chains the energy dependence changes to $E \sim 1/L$ as the electron-hole pair becomes 'squeezed' due to the effect of the ends of the

polymer chain. This exciton wavelength confinement effect forces the electron and hole to be closer together than their equilibrium separation and thus an additional energy 'cost' is paid for this as the kinetic energy of the electron and hole increases which in turn increases the energy gap.[28]

When looking at an ideal polymer that is perfectly straight it is possible to envisage that the exciton wavefunction could be delocalised over the entire chain. However in reality the polymer chain is disordered with kinks and twists disrupting the exciton wavefunction, giving rise to different length segments that each have a different energy gap. Thus to minimise their energy, excitons diffuse to the longest possible segment of polymer chain.[28] The excitons have a lifetime of 100 ps-1 ns[37] and so can diffuse roughly 5-10 nm before undergoing non radiative decay.[39] The effect of this can be seen by looking at the fluorescence of polymers, as short wavelength light can be absorbed but it is long wavelength light that gets emitted as the exciton undergoes radiative recombination.[28]

Excitons can move through organic semiconductors. They achieve this by a number of different mechanisms that include Förster energy transfer, Dexter energy transfer and trivial energy transfer.

Förster energy transfer is limited to being only able to transport singlet excitons. The energy transfer involves a one step process in which the movement of an electron on an excited state donor [D*] sets up an oscillating dipole which creates an electric field. This electric field induces an oscillating dipole on a neighbouring acceptor molecule [A] thus causing the [D*] and [A] to be coupled thus allowing the energy transfer to occur. Once the transfer is complete the electron in the excited state donor relaxes back to the ground state thus diminishing the probability of back transfer. This process is not only distance dependant but also dependant on the precise orientation of the two dipoles involved. An additional requirement is that for efficient energy transfer to occur the emission of [D*] must overlap with the absorbance of [A]. The process could be summarised as $[D^*] + [A] \rightarrow [D] + [A^*]$.[40]

Dexter energy transfer is able to operate for both singlet and triplet excitons. The mechanism is based on an electron transfer process in which the electron in an excited

state donor [D*] is exchanged for a ground state electron from the acceptor [A]. This process can take place in either a concerted manner or in two steps as shown in **Figure 1.9**. Dexter energy transfer is however limited by the requirement that the wavefunctions of [D*] and [A] must overlap and the rate of energy transfer is also limited by the distance that separates the [D*] and [A].[41]

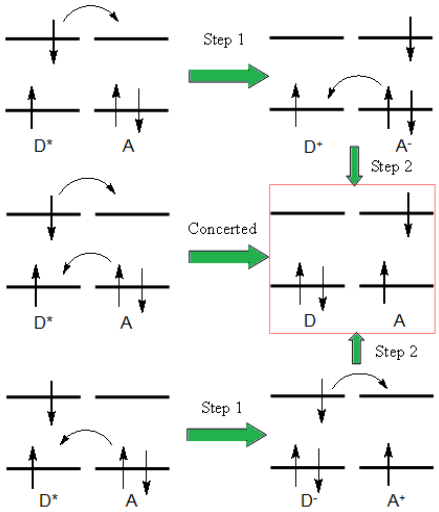


Figure 1.9: Dexter energy transfer pathways.[41]

Trivial transfer is a two step mechanism in which the excited state donor [D*] decays radiatively with the acceptor [A] absorbing the light that was emitted.[41] It can be represented as follows:

$$[D^*] \rightarrow [D] + h\nu$$
$$[A] + h\nu \rightarrow [A^*]$$

In the bulk, charge transport in organic semiconductors is regarded as a hopping process that takes place between localised molecular orbitals. This is unlike the transport found in inorganic semiconductors such as silicon, as in silicon the Mott-Wannier excitons formed have much lower binding energies (<50 meV) as a result of the high dielectric constant of silicon ($\varepsilon_r \sim 11.9$), which can effectively screen the charges. This allows the distance between the electrons and holes to be greater than the silicon lattice spacing, meaning that the excitons in silicon dissociate freely enabling the charges to be transported by band conduction. In organic semiconductors as the dielectric constants of the polymers are low (roughly $\varepsilon_r \sim$ 2-4) this provides an inadequate screening of charges meaning that tightly bound Frenkel excitons are formed with binding energies of up to 1 eV.[28, 34]

One can define two types of charge transport in organic semiconductors, the first is intramolecular and the second is intermolecular. Intramolecular charge transport (or intrachain transport) occurs along the chain of the polymer. Due to defects along the chain (such as twists due to entropic disorder and chemical defects that disrupt conjugation) the intramolecular charge transport along the chain is insufficient to transport the charge over the macroscopic distances required.[28] Intermolecular charge transport (or interchain transport) allows the charges to pass from one molecule to the next. A requirement for this to happen is that the π orbitals on each molecule must be coupled and thus intermolecular charge transport is more favourable in polymers that exhibit high degrees of crystallinity and close π-π stacking arrangements.[42] Polymers that are amorphous or semicrystalline typically show low mobilities due to being restricted solely to intrachain charge transport.[43] However it has been shown that amorphous polymers with high enough molecular weights can still exhibit high hole mobilities a notable example being a diketopyrrolopyrrole-based polymer reported by Bronstein et al[44] that achieved a mobility of 1.95 $cm^2V^{-1}s^{-1}$.

The transport of charges is characterised by measuring the macroscopic mobility of the charges. The equation that relates the mobility to an applied electric field is given by **Equation (4)**.

$$\mu = \frac{v_d}{E} \qquad (4)$$

Where μ is the mobility, v_d is the drift velocity of the electrons and E is the applied field.

Mobilities for organic semiconductors are considerably lower than those obtained for crystalline silicon (1000 $cm^2V^{-1}s^{-1}$) being typically on the order of (~1-15 $cm^2V^{-1}s^{-1}$) for the very best devices.[45] However not all applications of organic semiconductors require high mobilities as will be seen in the next section.

1.4 Organic Photovoltaics

1.4.1 Background

Organic solar cells based on polymers and small molecules are otherwise known as excitonic solar cells.[46] Unlike inorganic solar cells that upon absorbing a photon of light directly produce a free electron and hole due to their high dielectric constant, organic solar cells produce a coulombically bound exciton due to their low dielectric constant which is insufficient to screen the electron and hole from each other. Thus in order to produce a current the exciton in organic solar cells needs to be split. Early devices attempted to split the exciton using a single photoactive layer sandwiched between two electrodes, in a Schottky diode architecture. However these devices only yielded poor efficiencies (0.07%)[47] as the Schottky contact effect is insufficient to separate the electrons and holes. The development of a bilayered device by Tang[48] incorporating copper phthalocyanine (CuPc) as an electron donor and 3,4,9,10-perylenetetracarboxylic bis-benzimidazole (PTCBI) as an electron acceptor increased efficiencies to 1%. This increase in efficiency was as a result of the energy offset between the LUMO energy levels of the two materials at the bilayer interface, which was enough to drive exciton dissociation.

If we look at the processes that occurred within Tang's solar cell in detail, a simplified model can be envisaged in which there are six key steps, **Figure 1.10**.

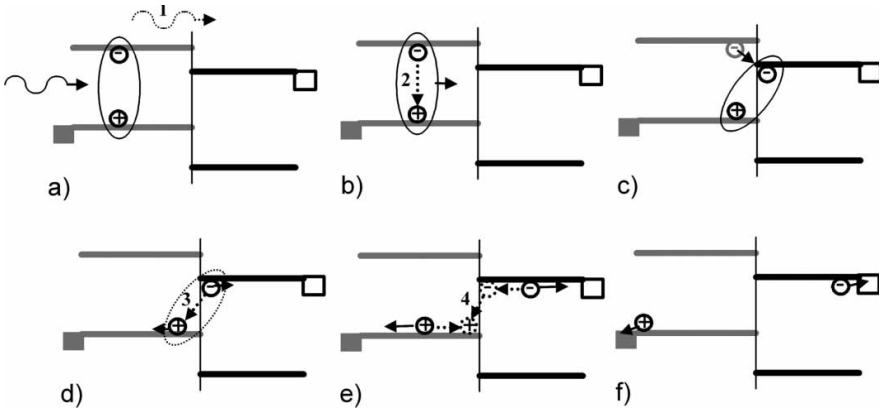


Figure 1.10: Charge generation in a donor - acceptor OPV. a) absorption of a photon to give an exciton, b) diffusion of the exciton towards the donor acceptor interface, c) electron transfer from donor to acceptor, d) dissociation of the exciplex into free carriers, e) transport of free carriers towards the electrodes, f) collection at the electrodes. Loss mechanisms are shown: 1) non absorbed photons, 2) exciton decay, 3) geminate recombination of the bound pair, 4) bimolecular recombination.[49]

The six steps are as follows:[49]

1) Absorption of a photon to give a singlet exciton – this requires photoactive materials with high extinction coefficients and band gaps that are equal to or less than the wavelengths of the incident photons. Additionally the photoactive layer needs to be thick enough to absorb all of the incident light to avoid energy losses through non absorbed photons.[49]
2) Diffusion of the exciton towards the donor acceptor interface – this requires the interface to be within 10 nm of the position that the exciton is generated otherwise the exciton will decay.[49]
3) Electron transfer from the donor to the acceptor to form an exciplex (excited state complex) – this requires the LUMO to LUMO offset to be greater than the exciton binding energy for thermodynamically favourable charge separation to occur. At this point it is possible for geminant recombination of the bound pair to occur in which the excited state electron on the acceptor recombines with the hole on the donor to waste the energy as heat.[49]
4) Dissociation of the bound pair into free carriers – the free carriers can recombine in the bulk material in a process called bimolecular recombination to lose the energy as heat.[49]
5) Transport of the charges to the electrodes – occurs under the influence of the internal electric field caused by the Fermi level pinning effect that is due to the work functions of the two electrodes being different. This stage requires the materials to have good mobilities as well as percolation pathways to the electrodes as otherwise bimolecular recombination can also occur at this stage.[49]
6) Collection of the charges at the electrodes – the work functions of the electrodes must be compatible with the HOMO or LUMO levels of the materials to avoid blocking contacts being formed.[49]

However the reason that the efficiency of Tang's solar cell was only 1% was due to the fact that the photocurrent was low. In order to increase the photocurrent it is essential to absorb as many photons as possible. This can be achieved through increasing the thickness of the active layer as most materials have an optical absorption depth of 100 nm.[50] However if the active layer is thicker than the 10 nm exciton diffusion length then the excitons will decay before reaching the donor-

acceptor interface, thus meaning that the photocurrent will be limited to just the excitons generated 10 nm from the interface. A solution to this problem was found by Yu et al[51] through the introduction of the bulk heterojunction (BHJ) concept in which the donor and the acceptor are randomly blended to form a device morphology that has interpenetrating networks of donor and acceptor with bi-continuous charge percolation pathways to the electrodes. This enables the use of a thicker film for optimal light absorption whilst enabling the excitons to be created within 10 nm from the interface. Using this concept, device efficiencies were increased to 2.9% using poly(2-methoxy-5-(2′-ethyl-hexyloxy)-1,4-phenylene vinylene) (**MEH-PPV**) as an electron donor and a Buckminster fullerene C_{60} as the electron acceptor. Since then, vast improvements in efficiencies have been made with the development of better polymers such as poly 3-hexyl thiophene (**P3HT**) (5%),[52] poly[N-9'-heptadecanyl-2,7-carbazole-alt-5,5-(4',7'-di-2-thienyl-2',1',3'-benzothiadiazole)] (**PCDTBT**) (6.1%)[53], dithienogermole–thienopyrrolodione (**PDTG–TPD**) (7.4%)[54] and (**PTB7**) (7.4%),[55] which has been shown to give performances of 9.2% in inverted devices.[56] The structures are given in **Figure 1.11**.

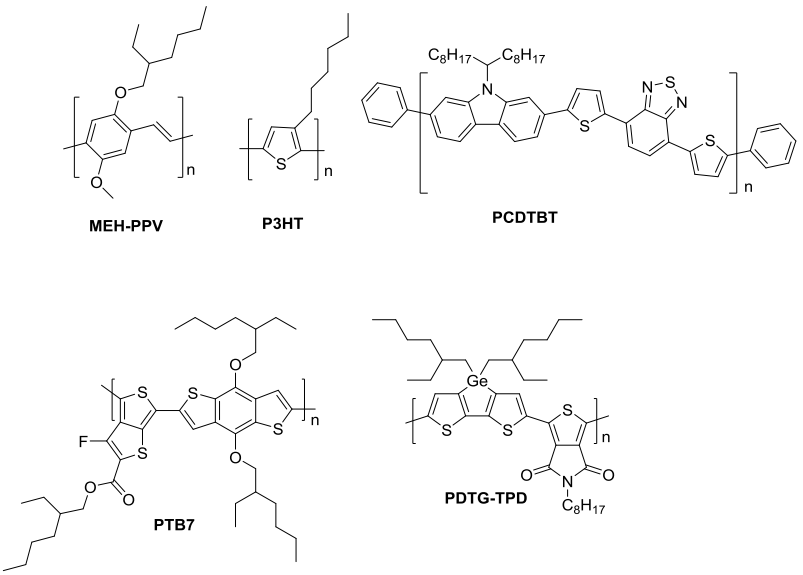


Figure 1.11: Structures of **MEH-PPV**, **P3HT**, **PCDTBT**, **PTB7** and **PDTG-TPD**.

In addition to the improvements in the structure of the donor polymers the acceptors used have improved as well. Initially the acceptor used in conjunction with the BHJ approach was a C_{60} Buckminster fullerene. C_{60} proved to be a useful n-type acceptor material due to its low lying triply degenerate LUMO which means that it is thermodynamically favourable for it to accept up to six electrons.[57] As electron

transfer from the excited state of a donor molecule to the C_{60} can occur on a timescale of 45 femtoseconds (fs) which is faster than the rate of back electron transfer or the rate of exciton decay, the quantum efficiency of charge separation can reach up to 100%.[58, 59] The ultrafast electron transfer has another beneficial effect in improving the photostability of the donor material against photooxidation as the express quenching of the reactive polymer excited state decreases the chance of it reacting with oxygen. C_{60} also shows high mobilities as measured in thin film transistors. However C_{60} is not particularly soluble meaning that it has the tendency to crystallise which thus makes it unsuitable for solution processing. Thus the next step in improving fullerene acceptors is to add solubilising side chains. With this in mind [6,6]-phenyl-C_{61}-butyric acid methyl ester (**$PC_{61}BM$**) was developed which due to its enhanced solubility has become one of the most commonly used acceptors within organic photovoltaic devices.[60] As the **$PC_{61}BM$** has a spherical fullerene it means that it is very poor at absorbing light, as its symmetry forbids low energy transitions from taking place. However the solution to this issue has been to use the **$PC_{71}BM$** analogue in which the asymmetry of the C_{71} fullerene allows low energy transitions to occur which in turn enables the **$PC_{71}BM$** to contribute to the photocurrent in OPV devices.[61]

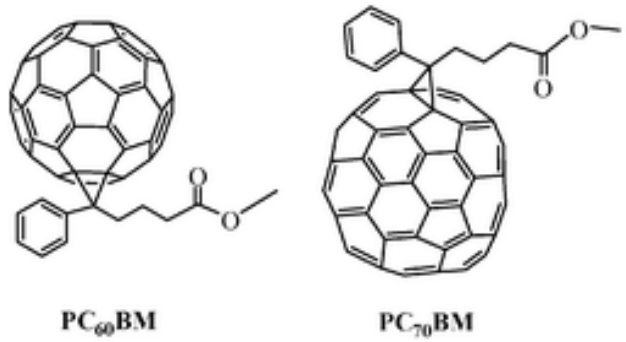


Figure 1.12: Structures **$PC_{61}BM$** and **$PC_{71}BM$**.

1.4.2 OPV device architecture and characterisation

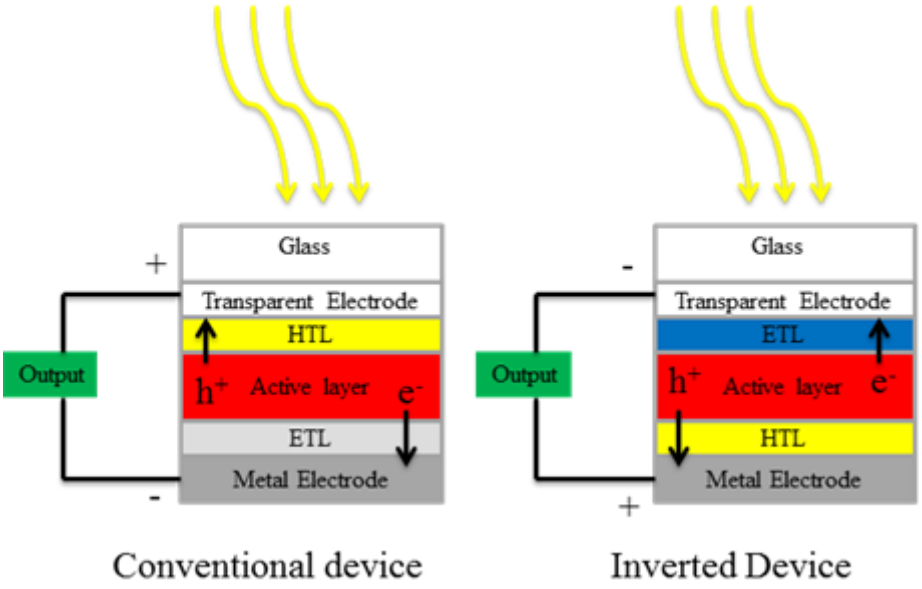


Figure 1.13: Architecture of conventional and inverted devices.

Traditionally the conventional device architecture for OPV devices, **Figure 1.13**, has been based on using a glass substrate upon which indium tin oxide or a thin layer of metal is deposited.[62] This layer acts as a high work function anode for collecting holes. The next layer is typically composed of a blend of Poly(3,4-ethylenedioxythiophene): Polystyrene sulfonate (PEDOT:PSS) as a transparent hole transport layer. This layer helps to not only adjust the energy levels between the active layer and electrode, select for holes thus blocking electrons from reaching the electrodes where they can non radiatively recombine,[63] but also helps to smooth out the electrode surface thus improving the electrical contact and preventing shorts that may occur due to defects on the electrode surface.[64] The active layer is composed of the donor polymer and fullerene acceptor in a variety of ratios which are designed to improve the morphology of the blend through ensuring adequate nanoscale phase separation of the donor and the acceptor in order to get optimal device performance.[65] The conjugated polymers used for the donor are not particularly soluble as a result of their rigid rod backbone structures, which enhance intermolecular π-π stacking interactions between polymer chains and thus cause the polymers to aggregate in solution.[66] This means that when the donor polymers are mixed with the acceptor, the polymers tend to phase separate, thus reducing the extent of the mixing, which in turn disrupts the nanoscale morphology of the blend. Thus upon depositing the polymer and fullerene into the

active layer, the solvent must be removed quickly to prevent the fullerene from being fully extruded from the polymer as the polymer starts to aggregate. This can be achieved by removing the solvent quickly via spin coating, which prevents full phase separation. The choice of deposition solvent or mix of solvents will also affect the morphology as certain solvents can preferentially solvate the polymer or the fullerene. Thus this has an effect on the stacking and domain sizes of the polymer as well as the extent to which fullerene aggregates are formed, which are somewhat necessary for charge percolation pathways.[50] Additional factors that affect the morphology and stability of the blend are the use of thermal annealing, solvent annealing, additives, use of crosslinkers, UV light, low level light soaking and the design and molecular weight of the donor polymer.[31, 67-71] The electron transport layer is typically composed of lithium fluoride, which helps to adjust the energy levels between the active layer and the electrode and select for electrons thus blocking holes from reaching the electrodes and non radiatively recombining.[63] The final layer is the low work function cathode for collecting the electrons which is typically comprised of aluminium, calcium or magnesium.[72]

However the issue with these conventional devices is that the indium in the indium tin oxide layer is a rare and expensive metal which increases the price of the device.[73] Thus various replacements for ITO such as carbon nanotubes,[74] graphene oxide[75] and semitransparent metal layers[76] to name but a few are being tried as potential substitutes. The PEDOT:PSS layer is also troublesome as the acidic nature of the sulfonate can degrade the electrodes.[77] Thus alternative materials such as TiO_2, MoO_3 and ZnO are being investigated as possible substitutes.[63] The main problem though is that the metal electrode that is deposited last is typically a reactive metal which needs to be deposited under vacuum. This is not ideal for large area roll to roll processing and also means that the device is prone to have a short lifetime due to the oxidative instability of the reactive metal.[54]

Due to the lack of oxidative stability of the cathode, an inverted device architecture incorporating high work function metals such as gold and silver can be used to form the top electrode. This improves the oxidative stability of the device enabling it to have a longer lifetime and additionally as gold and silver are not reactive the device can be fabricated in a large scale roll to roll fashion. The hole transporting layer in

these devices is typically composed of transparent MoO_3, ZnO_3 or TiO_2 which not only prevents the electrons from reaching the top electrode but can also improve the amount of light absorbed within the device by acting as an optical spacer.[62]

A variety of other device architectures are also present in the literature, which aim to enhance the amount of light that can be absorbed. These include folded solar cells,[78] the incorporation of plasmonic layers[79] and the use of multiple active layers in tandem devices.[6] It is the use of both high and low band gap materials in tandem devices that has yielded the greatest device efficiencies so far with a record 10.6% having been achieved for an inverted tandem device.[80, 81]

All of these organic solar cells are characterised by measuring both the current-voltage (*J-V*) characteristics and the external quantum efficiency as shown in **Figure 1.14**.

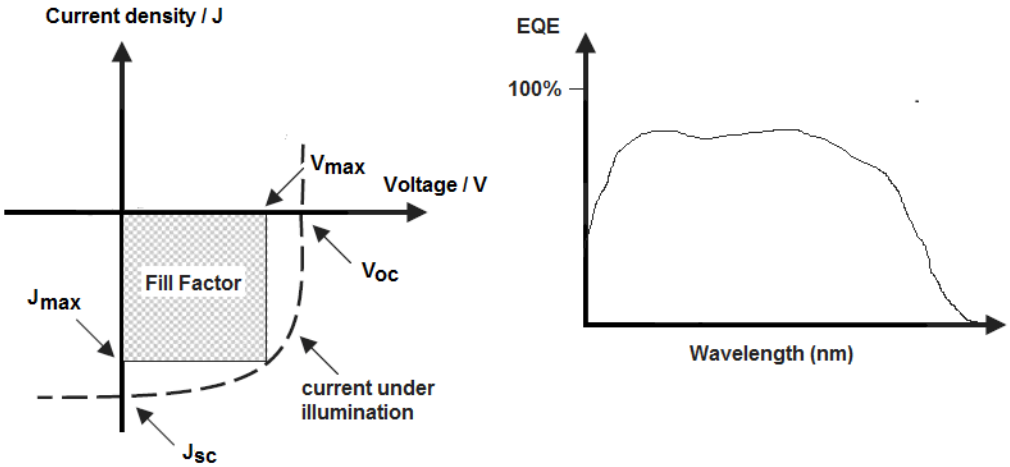


Figure 1.14: *J-V* curve of an OPV cell under illuminated conditions (Left). The parameters shown are: V_{OC} (open circuit voltage), V_{max} = maximum voltage, J_{SC} (short circuit current density), J_{max} = maximum current density. An illustration of the external quantum efficiency plotted against wavelength (right).[82]

The performance characteristics are defined as follows:[82]

- J_{sc} - The short circuit current density is the maximum current density attainable when the voltage across the device is zero whilst the solar cell is illuminated. The reason that the short circuit current density is used rather than the short circuit current is due to the fact that the short circuit current depends on the device area. The factors that affect the J_{SC} are the level of illumination, efficiency of charge separation, efficiency of charge collection and photon absorption.[82]

- V_{OC} - The open-circuit voltage is the maximum voltage that can be obtained when the current across the device is zero. The V_{OC} is proportional to the energy difference between the HOMO of the donor and the LUMO of the acceptor[11] and is typically about 0.5-1.5 V.[50]
- P_{max} -The maximum power is given by:

$$P_{max} = J_{max}V_{max} \quad (5)$$

- *FF* - The fill factor is a measure of the squareness of the *J-V* curve and is the ratio between the obtained power output and the theoretical power output.

$$FF = \frac{J_{max}V_{max}}{J_{sc}V_{oc}} = \frac{P_{max}}{J_{sc}V_{oc}} \quad (6)$$

- PCE - Photocurrent conversion efficiency is the most common figure of merit used to compare solar cells and is given by the following formula:

$$PCE = \frac{FFJ_{sc}V_{oc}}{P_{in}} = \frac{P_{max}}{P_{in}} \quad (7)$$

where P_{in} is power input which is determined by the photon flux incident on the device.[59]

The external quantum efficiency (EQE) is shown in **Figure 1.14**, which is defined as the number of charges collected at the electrodes divided by the number of incident photons at a particular wavelength λ_i. The formula is:

$$EQE = 1240\frac{J_{sc}}{\lambda_i P_{in}} \quad (8)$$

where the factor of 1240 is the wavelength of a 1 eV photon under vacuum.[41]

Ideally the EQE should equal 100% across the entire wavelength range which would indicate that all photons absorbed were converted to charges, however in practice the effect of charge recombination limits the EQE.

1.5 Organic Field Effect Transistors (OFETs)

1.5.1 Background

Traditionally transistors are based on amorphous silicon and are used as the amplifying and switching components in modern electronics.[83] These require a variety of energy intensive batch manufacturing techniques such as material deposition and patterning steps which require a number of high vacuum and high temperature

processing steps. Additionally amorphous silicon transistor fabrication is wasteful in terms of the materials used as several subtractive lithographic patterning and mask steps are required which also limit the manufacturing throughput. Although the cost of an individual transistor is very low due to the fact that a very high density of transistors that can be attained on a single piece of silicon, the actual cost per unit area is very high. This presents an opportunity for organic semiconductors to be used instead as they can be formulated into inks and deposited via low cost and non energy intensive solution based printing techniques.[84-86] This enables the manufacture of large area, low temperature, high throughput OFETs which not only lowers the cost but also enables the development of flexible circuitry, as the lower temperatures used in the fabrication process enable the use of plastic substrates. A number of potential applications for these cheap, flexible transistors can be envisaged ranging from radio frequency identification tags that could be used instead of barcodes in the supermarket to flexible backplanes in active matrix displays.[27]

OFETs can be p-type or n-type devices that are made up of a source and drain electrode that are connected via an organic semiconductor, with a gate electrode that is insulated from the semiconductor via a dielectric material. The source and drain electrodes are used for injecting and extracting charges, in the case of a p-type device the source electrode would inject holes into the HOMO of the organic semiconductor upon the application of a negative gate voltage. The holes migrate to the interface between the semiconductor and the dielectric where they form an accumulation layer and are subsequently transported to the drain electrode upon the application of an electric field between the source and drain electrodes. By modulating the gate voltage the transistor can be turned ON and OFF, with the values of the ON current and voltage required to turn a transistor ON being the considered to be the figures of merit when looking at the electrical performance of the device. Additionally the charge carrier mobility of the semiconductor is another factor that affects the transistor performance as it determines the charging speed of the device. Ideally high mobilities in excess of 0.5 $cm^2V^{-1}s^{-1}$ are required for applications such as liquid crystal displays which have a requirement for fast pixel charging speeds in order to have fast refresh rates for video rate displays.[27] These mobilities are now obtainable with plastic electronics leading to greater industrial interest in these materials.

There are four different device architectures that are commonly employed and are dependant on whether the gate electrode is deposited before or after the semiconductor layer and whether the source and drain electrodes reside in the same plane as the dielectric in a coplanar arrangement or whether they are in a staggered arrangement, **Figure 1.15**. These configurations can affect both the ease of manufacture and the performance of the device. The bottom-gate, bottom contact configuration is typically used when screening new materials as these transistors are quick and easy to fabricate. However, the coplanar geometry of the electrodes is not the optimal device architecture for high performance as improved gate-field enhanced charge injection can be obtained by using a staggered electrode configuration.[27]

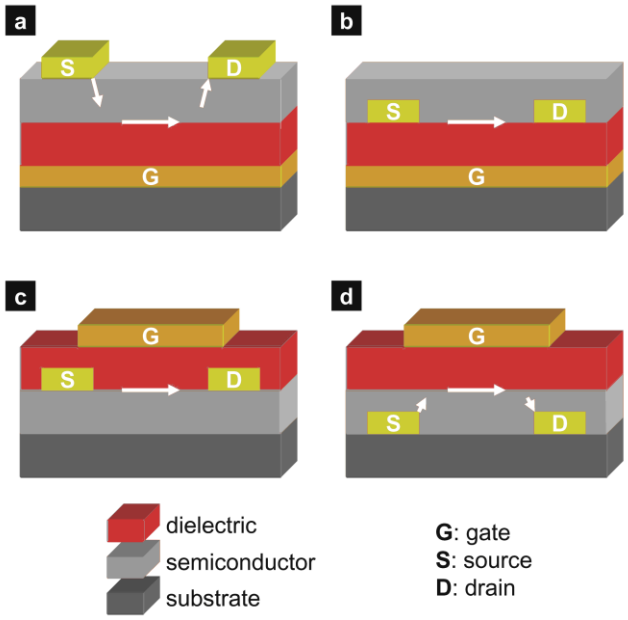


Figure 1.15: OFET device architectures a) top contact, bottom gate. b) bottom-contact, bottom-gate. c) top-contact, top-gate. d) bottom-contact, top-gate. The arrows represent charge carrier pathways in the device and illustrate the difference between the coplanar and staggered electrode arrangements.[27]

Transistors are characterised by measuring the transfer and output characteristics, **Figure 1.16**, in order to determine the key parameters which are the linear and saturation mobility of the semiconductor, the ON/OFF ratio and the threshold voltage (V_T).

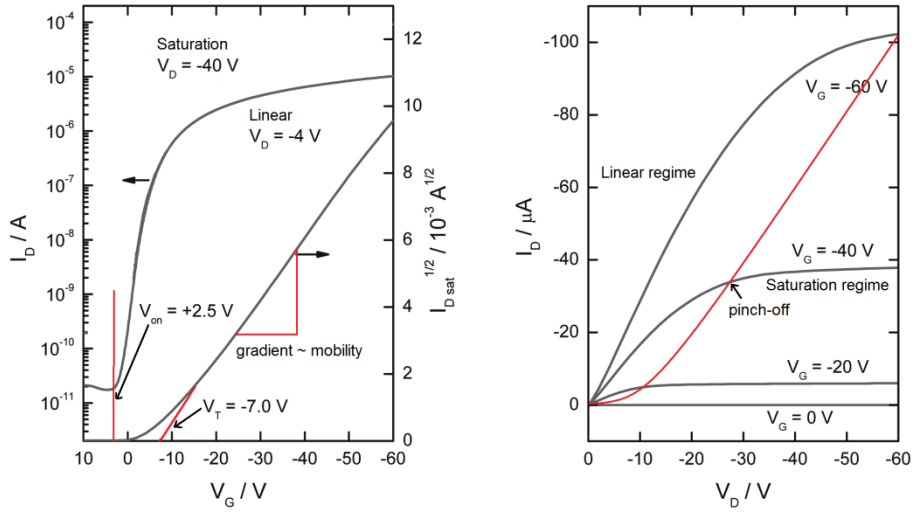


Figure 1.16: Transfer (left) and output (right) characteristics of a high mobility p-type material.[27]

The basic relationships describing the drain current are:

$$(I_{SD})_{\mu_{lin}} = \frac{W}{L}\mu_{lin}C_i(V_G - V_T)V_D \quad \textbf{(9)}$$

$$(I_{SD})_{sat} = \frac{W}{2L}\mu_{sat}C_i(V_G - V_T)^2 \quad \textbf{(10)}$$

Where $(I_{SD})_{\mu_{lin}}$ is the drain current in the linear regime, $(I_{SD})_{sat}$ is the drain current in the saturation regime, W is the channel width, L is the channel length, μ_{lin} is the mobility in the linear regime, μ_{sat} is the mobility in the saturation regime, C_i is the capacitance per unit area of the insulator layer, V_G is the gate voltage, V_T is the threshold voltage and V_D is the drain voltage.[27, 87]

On initially increasing the magnitudes of V_D and V_G an initially linear current regime is observed at low drain voltages ($V_D < V_G$) as given by equation (**9**). When the drain voltage exceeds the gate voltage, the transistor enters the saturation regime and the channel pinches off as the channel current (I_{SD}) saturates and becomes independent of the drain voltage as shown by equation (**10**). From experimental data, equations (**9**) and (**10**) can be used to determine the linear mobility and the saturation mobility of the organic semiconductor, with the saturation mobility being the figure typically quoted in literature due to it being the larger measure. The ON/OFF ratio can be calculated from equation (**11**);[87]

$$\frac{I_{on}}{I_{off}} = \frac{\mu C_i V_G}{2\mu_T q N_A t} \quad (\mathbf{11})$$

where μ_T is the semiconductor mobility in the off state, N_A is the carrier concentration in the off state, t is the semiconductor film thickness and q is the charge of an electron.[87]

The choice of materials for each layer of the OFET is important in obtaining optimal device performance. The source and drain contacts need to be able to inject and extract charges from the organic semiconductor and so the interface between the metallic contacts and the semiconductor needs to be carefully designed. When a metal and semiconductor come into contact the Fermi levels equalise in a similar way to when two metals come into contact. Thus the electrons or holes must overcome any energetic barriers created for injection or extraction from the metal into the LUMO for the electrons or HOMO for the holes. However unlike the situation with the two metals, the size of the energetic barrier is dependant not only on the work function of the metal but also the size of the interface dipole created by the organic material, which can shift the work function of the metal.[88] Thus the source and drain contacts are chosen to have work functions that match either the LUMO of the semiconductor for n-type devices or the HOMO of the semiconductor for p-type devices. As the majority of conducting polymers exhibit p-type performance, high work function gold or silver contacts are typically used to ensure that charge injection is not limited by a charge injection barrier. Self assembled monolayers (SAMs) composed of small organic molecules such as thiols can also be used to modify the interface between the metal contacts and the organic semiconductor and change the work function of the metal thus improving charge injection.[89]

As can be seen from equations (**9**), (**10**) and (**11**) the transistor performance is governed by the capacitance of the dielectric which can be expressed by equation (**12**);

$$C_i = \varepsilon_0 \frac{k}{d} \quad (\mathbf{12})$$

where ε_0 is the permittivity of a vacuum, k is the dielectric constant and d is the thickness of the dielectric.[87]

The choice of dielectric material used has to be optimised for each organic semiconductor and device architecture due to various effects such as whether or not the semiconductor is able to properly wet the surface of the dielectric and form a thin film. While the thickness of the dielectric can be controlled during the deposition process the dielectric constant k is an intrinsic property of the material. Traditionally SiO_2 is used for bottom-gate, bottom-contact devices. However, while thin layers of SiO_2 can be achieved to increase capacitance, there is a limit to how thin the layers can be to produce pin-hole free films. As the dielectric constant for SiO_2 is low (k = 3.9) a lot of research into alternative materials with higher k dielectrics has been carried out in order to reduce the OFET operating voltages. This is due to the fact that while high mobilities for semiconducting materials can be demonstrated their operating voltages are typically between 30-50 V meaning that the devices consume large amounts of power. Whilst a wide variety of dielectrics have been investigated, a couple of examples being barium zirconate titanate (k = 17.3) and Ta_2O_5 (k = 23), SiO_2 is still the most commonly used due to the fact that it enables the various semiconducting materials that are being screened to have the same basis for comparison. For top gate device architectures, solution processable polymer dielectrics are required. Some common dielectrics in use are CYTOP^{TM} (k = 2.1) which is a fluorinated polymer and poly(methyl methacrylate) (PMMA) (k = 2.6).[87]

The organic layer is the region in which charge transport takes place within just a few monolayers of material, in a two dimensional fashion, at the semiconductor-dielectric interface.[90] Thus factors such as the way the polymers are ordered within the monolayers are important. Through designing polymers with stiff backbones, interdigitating alkyl chains and π-π stacking interactions the polymers can be made to be more crystalline thus improving charge transport.[91] There are also many synthetic design parameters that affect the performance of the semiconductor. Molecular weight,[24, 92-97] polydispersity,[98] levels of impurities,[99] chemical defects and end groups in the polymer backbone[100-102] are all important as they influence both the electrical and morphological properties of the organic semiconductor within devices. In addition the band gap of the materials should be controlled as although wide bandgap materials can be used for either n-type or p-type devices, low band gap polymers can exhibit ambipolar behaviour which is a favourable characteristic for use in complementary metal-oxide semiconductor (CMOS) digital integrated circuits.[103]

1.6 Polymer Design Principles

For OPV devices the band gap of the polymer is a key design consideration as only photons that are equal to or greater than the band gap of the polymer can be absorbed. When looking at the solar emission spectrum, **Figure 1.17**, it is clear that the solar spectrum has its maximum photon flux at 1.8 eV or approximately 700 nm.[46]

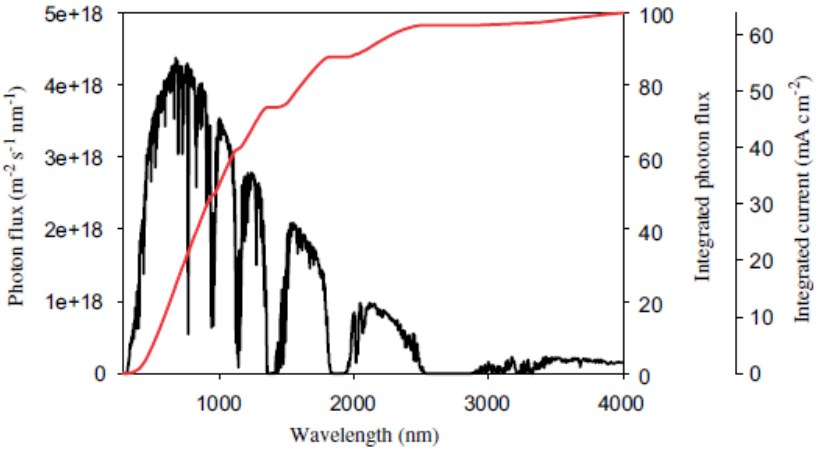


Figure 1.17: Solar photon flux at air mass (AM) 1.5 as a function of wavelength. The integral of the photon flux is shown on the right y axis as a percentage of the total number of photons and as the obtainable current density.[67]

In order to collect the majority of the photons that are at low energies a low band gap is required. In an ideal case a band gap of 1.1 eV is needed to absorb 70% of the incident photons at AM 1.5 assuming 100% absorption of the solar emission intensity.[82] However when looking at the energy levels of the donor and the acceptor needed for charge separation, it is clear that the LUMO to LUMO offset between the donor and the acceptor must be greater than the exciton binding energy for the charge separation to be thermodynamically favourable, and is typically specified as being around 0.2 - 0.3 eV. If the LUMO to LUMO offset is greater than the minimum offset required then energy is lost from the system as heat upon electron transfer, which in turn decreases the V_{oc}.[104] If the LUMO of the donor is lowered to decrease the band gap of the polymer and thus increase the photon absorption there is a possibility that the LUMO can become lower than the LUMO of the acceptor which will prevent electron transfer from occurring. Thus a compromise between efficient electron transfer and a low band gap is required. So if the acceptor used is $PC_{61}BM$ with a LUMO value of -4.2 eV below vacuum level,[46] the ideal LUMO value for the donor

polymer would be around -3.9 eV. As for the HOMO levels, increasing the HOMO level of the donor polymer in order to decrease the band gap and thus increase the photocurrent is not a good design strategy. This is due to the fact that this would have two distinctly detrimental effects on device performance and stability. The first effect would be to reduce the V_{oc} of OPV device, as the V_{oc} is proportional to the energy offset between the HOMO of the donor and the LUMO of the acceptor. The second effect would be to make the donor polymer more susceptible to oxidation, as in order for a polymer to be air stable the HOMO energy level should be below the air oxidation threshold which has been estimated by cyclic voltammetry to be about -5.27 eV.[104, 105] However if the HOMO energy is lowered too much then the band gap of the polymer will be too large to sufficiently complement the solar absorption spectrum and would thus lead to a decrease in photocurrent. Thus a compromise between a large V_{oc} and J_{sc} is required and so a HOMO energy level of between -5.3eV and -5.8 eV would be optimal thus giving a band gap of between 1.2 and 1.9 eV.[104]

For OFET devices the precise band gap of the semiconducting polymer is of less importance as the electrode materials can be tailored to the energy levels of the polymer. The main consideration for designing an OFET polymer is to use coplanar aromatic molecules that can form highly crystalline thin film microstructures so that optimal charge transport in the monolayers at the dielectric interface can occur. Thus features that enhance the ability of the polymers to form highly ordered, closely packed π stacks with correctly orientated and interconnected domains are required. Additionally polymers that pack in an edge on orientation to the plane of the substrate are favourable for OFETs, as this enables the charges to hop from one π stack to the next in the required direction for charge transport between the electrodes. This is unlike the polymers required for OPV devices in which a face on orientation is required for optimal charge transport, due to the electrodes being in a different spatial configuration.[106]

1.7 Band Gap Engineering and Charge Transport Mobility Considerations

As previously mentioned the band gap of a polymer can be decreased through extending the conjugation length of the polymer chain. However this is only feasible up until a persistence length of around 10 - 15 monomer units at which point the decrease in band gap reaches a saturation point and can't be decreased any further.[59]

Alternative means of decreasing the band gap can also be employed. One particular technique involves using the quinoidal effect in which the bond length alternation along a polymer backbone is reversed. A particular example is polythiophene which can have two forms. The first form is the aromatic form in which the π electrons are localised solely on the thiophene rings meaning that the thiophene retains its aromaticity. The other form is the quinoid form in which π electrons are delocalised along the polymer backbone causing the bond length alternation of the single and double bonds to be reversed. As the quinoid form is energetically less stabilised in comparison to the aromatic form, the HOMO energy level of the quinoid form is raised relative to the aromatic form thus resulting in the quinoid form having a lower band gap. The strength of the quinoidal effect can be seen when comparing poly(phenylene), poly(phenylenevinylene) (**PPV**), polythiophene and polyisothianaphthene (**PITN)**. The polymer with the largest band gap is poly(phenylene) with a band gap of 3.2 eV due to the fact that it is composed solely of highly aromatic phenyl rings. **PPV** introduces a vinyl link between the aromatic phenyl rings which helps to dilute the effect of the aromaticity which thus decreases the band gap to 2.5 eV. Polythiophene is made up of thiophene rings which are inherently less aromatic than phenyl rings meaning that the polythiophene exhibits a greater quinoidal effect and thus has a lower band gap of 2 eV. **PITN** exploits these observations of the quinoidal effect by having a phenyl ring fused in the β position of the thiophene. As the thiophene ring has a lower aromatic resonance energy than the phenyl ring (1.26 eV verses 1.56 eV) the π electrons reside on the phenyl thus forcing the thiophene rings to remain in the quinoid form. This significantly lowers the band gap to 1 eV. The polymeric structures are given in **Figure 1.18**.[59]

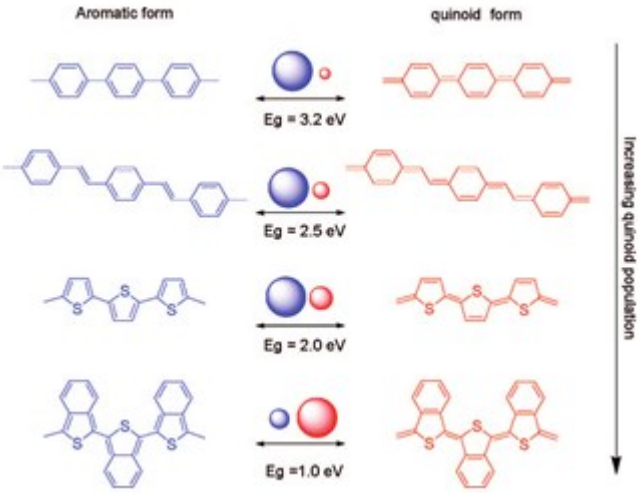


Figure 1.18: Structures of resonance forms of polyphenylene, poly(phenylenevinylene) (**PPV**), polythiophene and polyisothianaphthene (**PITN**). The coloured circles represent the relative contribution of the aromatic and quinoid forms to the polymer backbone.[59]

As can also be seen from comparing polyphenylene and **PPV**, the aromatic resonance energy, which prevents electron delocalisation, can be minimised by decreasing the torsion angle between the neighbouring phenyl units. The increase in planarity allows greater conjugation between the aromatic rings which stabilises the backbone and decreases the polymer band gap. As can be seen from comparing polyphenylene and polythiophene the difference in aromatic resonance energy is not the only factor in lowering the band gap. When looking at the torsion angle between two neighbouring phenyl units and two neighbouring thiophene units, **Figure 1.19**, it is clear that the hydrogens on the carbons β to the carbons bonding the two units together sterically hinder the two phenyls from being planar. This steric hindrance is not present in the thiophene-thiophene dimer, resulting in greater planarity and thus a lowered band gap.[107]

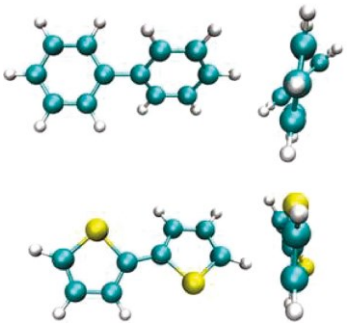
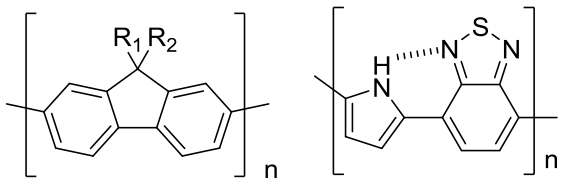


Figure 1.19: Overhead (left) and cross-section (right) view of both a phenyl-phenyl (top) and thiophene-thiophene (bottom) coupled dimer molecule.[107]

The torsion angle can also be dictated by side group substituents on the monomer units that can sterically hinder the polymer from being planar. If the side groups are sufficiently small then the torsion angle will be small. However as the side groups that are used are typically alkyl chains for solubility, reducing the size of the side groups will decrease the solubility of the polymer, which may limit the ability to solution process the polymer. This means that a compromise between the torsion angle and solubility may be needed. However, an alternative way of overcoming this problem is to use a bridging group to enforce planarity between the rings. This can be done via either covalent bonds as used in fluorene polymers (**P1**) or hydrogen bonding as used in pyrrol benzothiadiazole (**P2**), **Figure 1.20**.



P1 **P2**

Figure 1.20: Structures for fluorene polymer (**P1**) and pyrrol benzothiadiazole (**P2**).

The energy levels of the polymer can be manipulated by changing the aromatic units that make up the polymer. By using heteroaromatics, the heteroatoms such as nitrogen, oxygen and sulphur can use their unpaired electrons to directly conjugate into the π system via mesomeric donation. While these atoms are more electronegative than carbon and so would be expected to withdraw electron density, the mesomeric donation effect overcomes the effect of the electronegativity to increase the electron density of the aromatic ring and thus raises the HOMO energy level. For silicon based heteroaromatics, due to the fact that silicon is less electronegative than carbon the silicon atom donates its electrons inductively to raise the HOMO energy level. However when the lone pair of the heteroatom is unable to conjugate into the π system, such as the nitrogen atom in thiazole or pyridine, the effect of the electronegativity of the heteroatom dominates thus withdrawing electron density from the π system, which in turn lowers the HOMO.[107]

The HOMO and LUMO energy levels can also be independently modulated via directly incorporating electron donating or electron withdrawing groups onto the aromatic ring. The use of substituents such as cyano, nitro or trifluoromethyl groups

can withdraw electron density through either inductive or mesomeric effects thereby lowering the HOMO and LUMO energy levels. Substituents such as alkoxy, alkyl and amine groups can act as electron donating groups which can raise the HOMO energy level.[49, 59]

The most commonly used strategy to lower the polymer band gap is to copolymerise conjugated electron rich donor monomers (D) with conjugated electron poor acceptor monomers (A). This facilitates a push-pull single –double bond resonance effect ($D - A \leftrightarrow D^{+} = A^{-}$) which increases the quinoidal character of the polymer backbone and in turn lowers the polymer band gap. The use of copolymerisation also hybridises the two HOMOs and the two LUMOs which results in a further decrease in the polymer band gap as shown in **Figure 1.21**.[67]

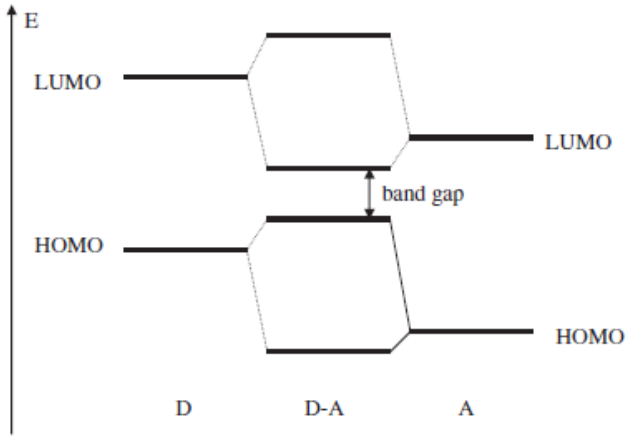


Figure 1.21: Orbital mixing of alternating donor and acceptor units to lower the polymer band gap.[67]

Copolymerisation of a donor monomer with an acceptor monomer also has another beneficial effect. Upon photoexcitation of the copolymer the photo excited electron in the LUMO of the donor part of the copolymer undergoes intramolecular charge transfer to the lower lying LUMO of the acceptor part of the copolymer thus forming an intrachain exciplex (excited state complex). This is also partly responsible for the lower optical band gap obtained for copolymers in relation to their respective homopolymers, as the copolymers appear red shifted. This has another beneficial effect in that the emission lifetime of the copolymer is longer lived due to the increased spatial charge separation.[108]

The way that the polymer chains interact with neighbouring polymer chains also has an influence on the polymer band gap. By forming π-π stacking arrangements in the solid state, the polymers can facilitate interchain charge delocalisation which lowers the polymer band gap. For polymers to display these properties they need to be composed of planar aromatic units which are regioregular and have an extended coplanar conformation, as these properties enable closely packed crystalline domains to form.[59]

The charge carrier mobility of the polymers is another factor that is important for obtaining large photocurrents in OPVs and fast charging rates in OFETs. As the mechanism for charge transfer is via a hopping mechanism between π-π stacks, the properties that enable the polymers to be crystalline, such as using poly fused aromatics to give coplanar 'rigid rod like' polymers, and using interdigitating side chains to form 3 dimensional oriented domains need to be employed.[109] However it should be noted that obtaining a high charge carrier mobility in an OFET device does not mean that a high photocurrent in an OPV device will be observed as the mobility of the polymers in OFETs is affected by the ability of the polymer to form edge on π-π stacks to the plane of the substrate whereas the mobility of the polymer in an OPV device is affected by the ability of the polymer to form face on π-π stacks to the plane of the substrate.[110]

The crystallinity of rigid rod type polymers can go through two phases upon heating. These phases are a crystalline phase at low temperatures and an isotropic (melt) phase at higher temperatures.[27] As seen from **Figure 1.22**, the temperature at which the transition between the two phases occurs at is determined by the Gibbs free energy of each phase with respect to the temperature, with the lowest free energy phase being exhibited. Typically polymers that are flexible will go from the isotropic phase directly to the crystalline phase. However, for polymers with a rigid rod like backbone the polymers can exhibit a liquid crystalline phase which occurs between the isotropic melt phase and the crystalline phase. If the rigid polymer is deposited during the liquid crystalline phase then the films formed are highly crystalline which is beneficial to obtaining high charge mobilities. Thus it is evident that the liquid crystalline phase is a desirable property for polymers to have and so to produce high charge carrier mobility polymers for OFET devices the backbones of the polymers

should be stiff. This can be achieved through using aromatic molecules that are locked in coplanar arrangements along the polymer backbone.[27]

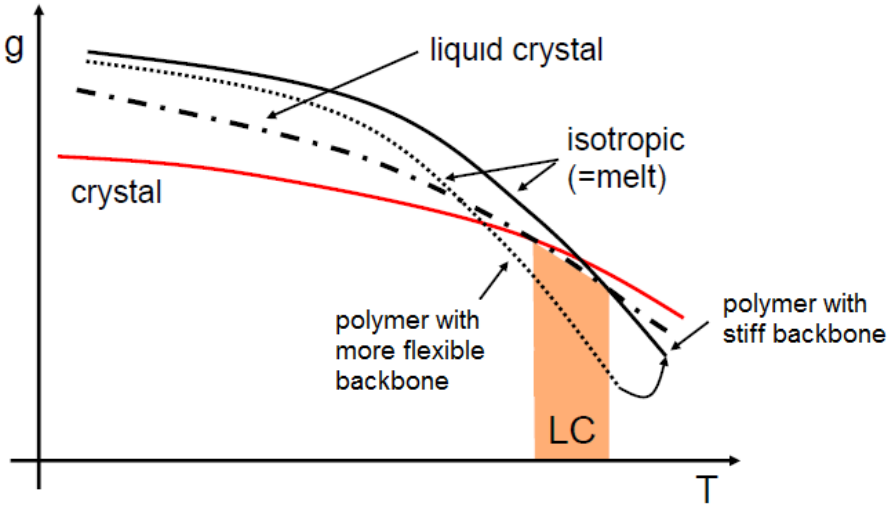


Figure 1.22: Effect of stiffening polymer backbone on the polymer phase free energy.[27]

1.8 Polymer Solubility

Conjugated polymers tend not to be very soluble due to their ability to form π-π stacks which cause them to aggregate out of solution. Thus in order for conjugated polymers to be able to be formulated into inks for solution processing into OPV and OFET devices, solubilising alkyl chains need to be incorporated along the polymer backbone. The use of branched alkyl side chains makes the polymers more soluble compared to linear side chains as they disrupt the crystalline packing and ordering of the polymers. However this increases the π-π stacking distance and thus lowers the charge carrier mobility of the polymer.[111] Using longer alkyl chains has been shown to increase the solubility of the polymers as well, although the use of longer aliphatic side chains can increase the distance required for hopping transport which thus has a detrimental effect on the charge carrier mobility.[112, 113] The aliphatic side chains can be considered to act as an insulator and so it has been found that upon increasing the fraction of the side chains relative to the hole conducting portion of the polymer backbone the charge carrier mobility decreases.[59]

The position of the side chains along the polymer backbone is another factor that needs to be considered. It is thought that incorporating the alkyl chains on just the donor portion of the donor acceptor copolymer is beneficial for charge separation. This is due to the fact that the donor portion of the copolymer will be sterically hindered from the fullerene whereas the acceptor part of the copolymer is naked allowing the fullerene to dock in the vicinity of the acceptor portion. Thus if intrachain transport occurs, which initially separates the electron and hole, it becomes easier for the fullerene to accept the electron as the coulombic binding energy between the electron and hole has already been decreased due to the greater spatial separation between them.[110]

When branched side chains have been used in polymers, it has been found that it is beneficial to move the branching point of the side chain further from the polymer backbone. This reduces the amount of steric hindrance between neighbouring polymer chains and thus promotes the formation of more crystalline domains, which has been shown to improve the performance of both OPV and OFET devices.[114]

Other factors that also influence polymer solubility are the regioregularity, rigidity of the polymer backbone, the molecular weight, the polarity of any attached substituents and any intermolecular interactions between neighbouring polymer chains. All these factors affect not just the polymer solubility but also the microscopic morphology phase behaviour, the crystallinity and the contact effects between the various components of the device, all of which have an influence on the performance of the device.[59]

1.9 Synthetic Aspects

A variety of factors in relation to the design of the synthesis affect the performance of the semiconductor. Molecular weight,[24, 92-97] polydispersity[98], levels of impurities[99], chemical defects in the polymer backbone and end groups[100-102] are all important as they determine both the morphological and electrical properties of the polymeric semiconductor within devices. All of these factors are affected by the polymerisation conditions that are used, with the subsequent work up and purification techniques

such as Soxhlet extraction, washing with diethyldithiocarbamate trihydrate to remove residual palladium, and recycling size exclusion chromatography being able to control the molecular weight, polydispersity and levels of impurities to some extent.[24, 93, 94, 96-99]

However the molecular weight is also affected by the choice of alkyl chains used in the monomers, as to obtain high molecular weights ultra pure monomers are required to obtain the correct stoichiometry for the polymerisation reaction. This is easier to achieve with soluble monomers as they can be easily purified by column chromatography. Additionally the alkyl chains affect the solubility of the growing polymer chain during the polymerisation reaction as if the polymer is not soluble enough then the growing polymer chain will drop out of solution before the desired molecular weight is achieved.

The choice of synthetic route is also important as if the chosen route were to give defects that are structurally similar to the semiconductor then these would be very tricky to separate out. The inclusion of these impurities within the film can result in the disruption of the local crystalline order within the polymer film. This would create defect sites that serve as traps within the polymer film, which would immobilise charge carriers and thus lead to a decrease in the charge carrier mobility of the polymer.[115]

Conjugated semiconducting polymers are made up of aromatic units that are linked via carbon – carbon single bonds. There are many methods that are employed to form carbon – carbon single bonds, including Gilch polymerisation,[116] electrochemical polymerisations[117], chemical oxidative polymerisations[118], Grignard metathesis,[119] and transition metal catalysed cross coupling reactions.[120] The methods most commonly employed to link aromatic units together are Suzuki, Stille, Negishi and Yamamoto couplings. Of these Stille and Suzuki are the two coupling reactions that are most widely used, both of which have pros and cons. The Stille coupling is an effective reaction that is able to tolerate a wide variety of functional groups. However, this specific reaction produces vast quantities of organotin residues which are hydrophobic and so can become entrained within the hydrophobic polymer making them difficult to separate out. The Suzuki reaction, on the other hand, is far less toxic

but needs to be carried out under aqueous conditions meaning that it is less able to endure such a wide range of functional groups. However, the pros of the Suzuki reaction are that it is high yielding and also far easier to work up than the Stille reaction as the residual boron containing species are easier to extract from the product mixture. Unfortunately, Stille, Suzuki, Negishi and Yamamoto coupling reactions all use metal catalysts, Sn, Pd, Zn, and Ni respectively, which can become entrained into the polymer. If the purification techniques cannot adequately remove these metal impurities from the polymer then they can not only act as charge traps within the polymer but also cause the polymer to degrade faster. Thus the purification techniques that are used in the final stages of polymer synthesis are crucial to device performance.[115]

1.10 Aim of Thesis

The objective of this doctoral work is to synthesise both novel monomers for use in donor acceptor copolymers and use existing monomers to synthesise a variety of novel copolymers for use in both OPV and OFET devices.

The first part of this thesis involves the development of a novel fused hexacyclic thiophene donor molecule, **4T** with the primary aim of developing a donor material which extends the range of spectral absorption of cyclopenta[2,1-b:3,4-b']dithiophene (**CPDT**), a monomer that has been shown to give PCEs of up to 5.8%.[121]

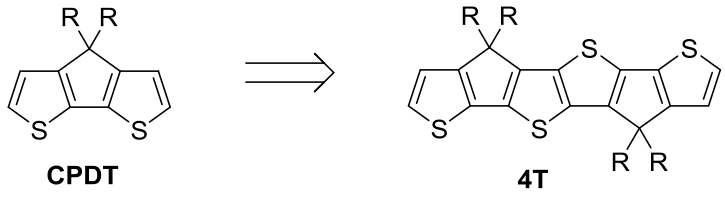


Figure 1.23: Structural extension of **CPDT** to give **4T**.

The next section involves the development of novel isoindigo based[115] copolymers using phenyl isoindigo initially and then in order to improve polymer planarity developing a novel thiophene isoindigo monomer. A comparison between the phenyl isoindigo and the thiophene isoindigo monomers will then be explored in detail

followed by the synthesis of a variety of novel random terpolymers consisting of the phenyl and thiophene isoindigo units designed to extend the spectral range of the individual components of the polymer. Finally the aim of this section was to extend the isoindigo family to thiazole isoindigo and furan isoindigo to see the effects of electron poor and electron rich isoindigo based monomers, however this aim was not fully realised and so the synthetic efforts towards these monomers are shown.

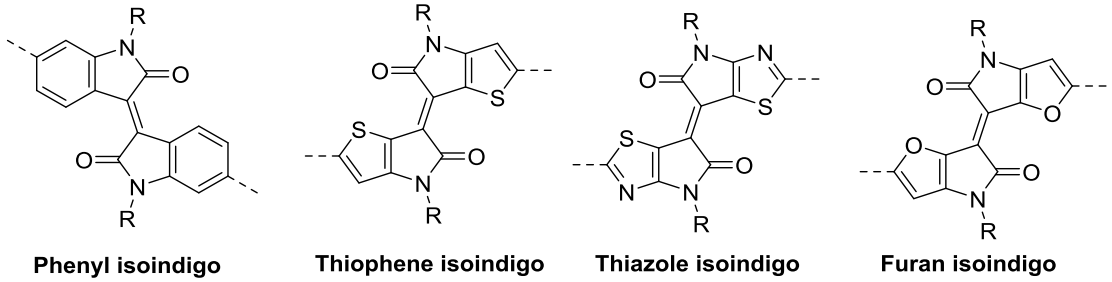


Figure 1.24: Structures of isoindigo derivatives.

The final section involves the development of new monomers and polymers based on Pechmann dyes, which due to being somewhat structurally similar to thiophene isoindigo are anticipated to show properties which are similar.

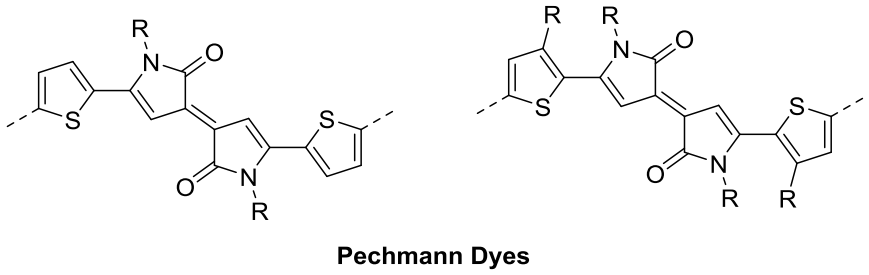


Figure 1.25: Structures of Pechmann dye derivatives.

Chapter 2 - 4T polymer for OPVs and OFETs

Every honest researcher I know admits he's just a professional amateur. He's doing whatever he's doing for the first time. That makes him an amateur. He has sense enough to know that he's going to have a lot of trouble, so that makes him a professional.

Charles Franklin Kettering (1876-1958) U. S. Engineer and Inventor.

2.1 Introduction

The synthesis of a **4T** based polymer is motivated by the success of a previously reported bithiophene monomer that has been bridged with a carbon atom to give cyclopenta[2,1-b:3,4-b']dithiophene (**CPDT**). This unit has the advantage of being perfectly planar as the central bridging carbon enforces planarity between the neighbouring thiophene rings, which in turn allows the electron density on the thiophenes to become delocalised over the whole monomer unit. This not only lowers the band gap of the monomer but when incorporated into a donor – acceptor copolymer also enables the band gap of the overall copolymer to be lowered through enhanced electron delocalisation over the persistence length of the polymer chain. **CPDT** has been copolymerised with a variety of acceptor units the most notable examples being n-octylthienopyrrolodione (**TPD**) and 2,1,3-benzothiadiazole (**BT**) to give **PDTC**[122] and **PCPDTBT**[121, 123] respectively as shown in **Figure 2.1.**

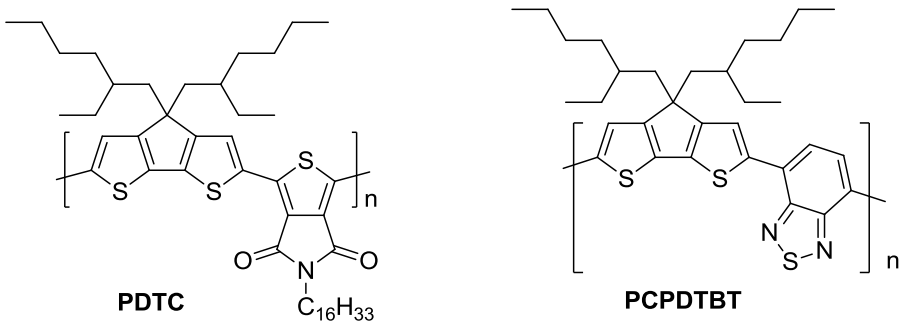


Figure 2.1: Structure of bithiophene copolymers **PDTC** and **PCPDTBT**.

For these copolymers the **PDTC** copolymer gives a moderate PCE of 3.74% with $PC_{71}BM$ primarily due to its poor fill factor of 0.47.[122] **PCPDTBT** initially gave a PCE of 2.67% with $PC_{61}BM$ but was able to be improved to 3.16% when blended with the more optically active $PC_{71}BM$.[123] The PCE of **PCPDTBT** was able to be further improved with the use of a small amount of 1,8-octanedithiol additive which improved the morphology of the blend to give a maximum PCE of 5.8% with an average PCE of 5.5% over 1000 devices.[3] The distinct decrease in optical band gap on going from **PDTC** to **PCPDTBT** from 1.67 eV to 1.46 eV has a pronounced effect on the J_{sc} with it increasing from 10.04 $mAcm^{-2}$ to 16.2 $mAcm^{-2}$ due to an increase in the number of photons from the long wavelength end of the solar spectrum that can be absorbed.

Another class of monomer that has inspired the synthesis of the **4T** monomer is the **IDT** unit. This unit was first reported by Shu-Hua Chan et al in 2008,[124] and was specifically designed as a way of overcoming the limitations of the widely used poly-3-hexylthiophene (**P3HT**) polymer. **P3HT**, despite achieving transistor hole mobilities of 0.2 $cm^2V^{-1}s^{-1}$ [125] and power conversion efficiencies of up to 6.5% in organic photovoltaic devices,[126] suffers from having a wide band gap that does not fully match the solar spectrum. Additionally, at high molecular weights, **P3HT** is susceptible to chain folding, due to its flexibility, which may limit charge carrier mobility and thus be detrimental to device performance.[127-130] The **IDT** unit, comprised of two thiophene units bridged to a central phenyl ring by two planarising sp^3 carbon atoms, overcomes these difficulties as the ladder type unit with its rigid structure not only increases the persistence length of the polymer[131, 132] but also reduces the amount of rotational disorder around the interannular single bonds.[133-136] These parameters enable the band gap of the polymer to be lowered which allows greater low energy photon absorption thus giving rise to a higher short circuit current, as well as enabling the polymer to have a lower reorganisation energy, which can enhance the intrinsic charge carrier mobility.[133-136] Synthetically, the bridging carbon has been functionalised with a variety of alkyl chains which both influence the crystallinity of the backbones through steric effects as well as have an effect on polymer miscibility with other materials within blends.[110] Examples of the effect of the choice of alkyl chain can be see through comparing linear hexadecyl alkyl chains against bulkier 4-phenyl hexyl alkyl chains. In the case of the linear alkyl chain the organic field effect transistors produced obtain high hole mobilities (3.6 cm^2/Vs) for non annealed devices,[137-139] while for the bulkier side chains the morphology of the fullerene and polymer blends was substantially improved leading to a high J_{sc} of (11.2 $mAcm^{-2}$) and PCEs of 6.4%.[140, 141]

Another unit that is of interest with regards to **4T** polymer synthesis is thieno[3,2-*b*]thiophene (**TT**) – a planar, symmetrical, aromatic unit consisting of two thiophene units in an antiperiplanar conformation fused at the central position. **TT** has been incorporated into a variety of polymers such as **pBTTT** where it has been shown to improve hole mobility as a result of the strong interchain interactions which enable the polymer chains to pack in an ordered fashion.[42] For polymers designed for OPV applications **TT** has been shown to increase the V_{oc} as a result of the polymers having

deeper HOMO energy levels.[142-144] This can be ascribed to the fact that **TT** has greater aromaticity than the more commonly used thiophene unit, which thus reduces the amount of quinoidal effect that the polymer exhibits leading to the lowered HOMO. However, polymers incorporating **TT** are typically less soluble and so a common method of overcoming this limitation is to add alkyl chains onto the β position.[142-144] Despite the fact that this enables the polymers to be solubilised it also introduces a twist between neighbouring units due to steric hindrance which in turn leads to reduced conjugation.[145, 146]

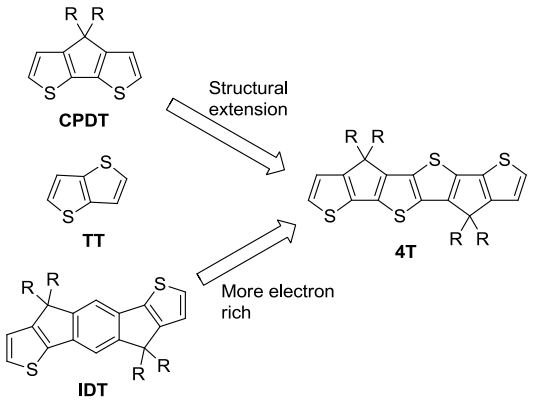


Figure 2.2: The chemical structures of **CPDT**, **TT**, **IDT** and **4T**. R = alkyl chain.

From looking at **CPDT**, **IDT**, and **TT** it can envisaged that by replacing the central phenyl group in **IDT** with **TT**, a rigid, ladder type electron rich donor molecule resembling two **CPDT** molecules fused together can be designed. This new unit, **4T**, with extended conjugation should reduce conformational disorder further compared to **IDT** and further lower the band gap relative to **CPDT** allowing for a greater number of low energy photons in the solar spectrum to be harvested. In addition, the two bridging sp^3 carbon atoms allow for four solubilising alkyl side chains to be attached which will allow for the polymer to be solution processed.

2.2 Synthesis of the 4T Monomer

The synthesis of the **4T** monomer proved to be rather synthetically challenging resulting in a number of different routes being developed to attain the desired monomer.

One of the routes tried was based on the route developed by Zhang et al for achieving the synthesis of **IDT**.[139] Zhang's route involves the Negishi coupling of diethyl 2,5-dibromoterephthalate (**2.1**) with 2-thienylzinc bromide (**2.2**) to give 2,5-dithien-2-ylterephthalic acid diethyl ester (**2.3**). Saponification of ester (**2.3**) yielded 2,5-dithien-2-ylterephthalic acid (**2.4**), which was converted to the acid chloride (**2.5**) and ring closed via a Friedel Crafts reaction with $AlCl_3$ to give 4,9-dihydro-s-indaceno[1,2-b:5,6-b']-dithiophene-4,9-dione (**2.6**). Wolff Kishner reduction of (**2.6**) at 180 ºC with hydrazine monohydrate and potassium hydroxide afforded 4,9-dihydro-s-indaceno[1,2-b:5,6-b']-dithiophene (**2.7**) which was subsequently alkylated to give (**2.8**) and brominated to give the **IDT** monomer (**2.9**), as seen in **Figure 2.3**.

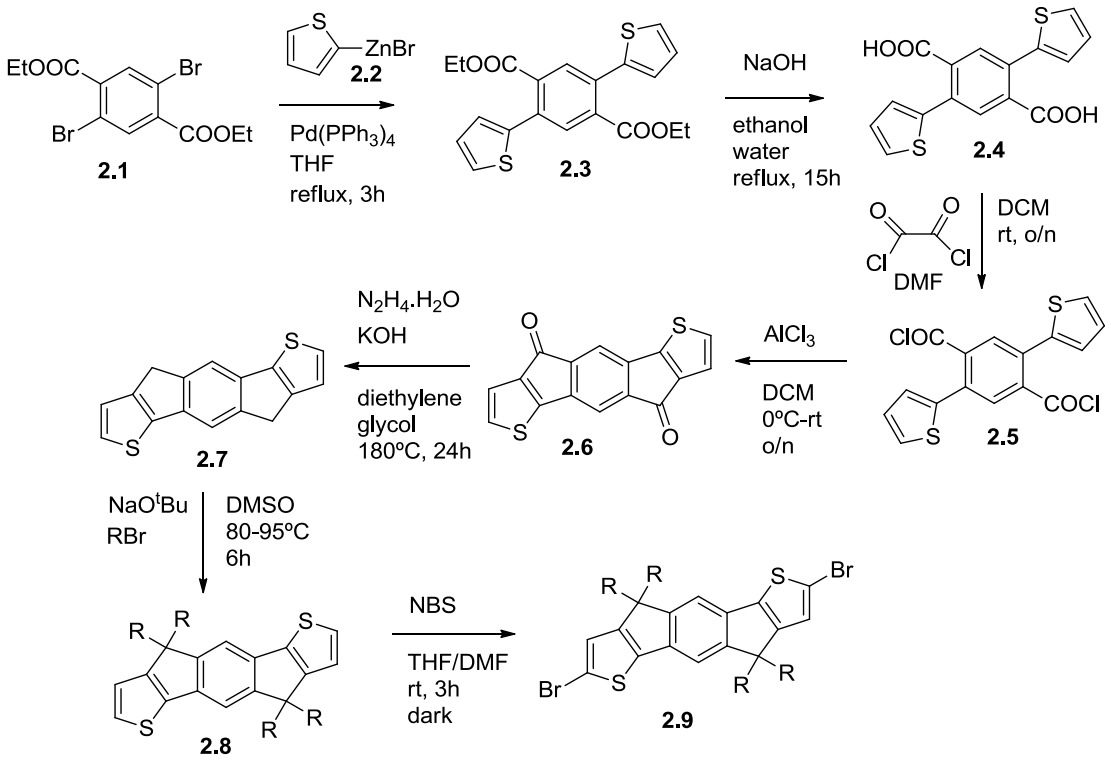


Figure 2.3: Synthesis of IDT monomer (**2.9**). R = hexadecyl alkyl chain[139]

Based on the synthesis of **IDT** the first step was to synthesise a thieno[3,2-*b*]thiophene equivalent of diethyl 2,5-dibromoterephthalate (**2.1**). This was achieved through initially using *N*-bromosuccinimide (NBS) to chemoselectively brominate thieno[3,2-*b*]thiophene (**2.10**) in the 2 and 5 positions in accordance to a method described by Liu et al.[147] The next step involved using a halogen dance reaction as described by Miguel et al[148] to rearrange the bromines from the 2 and 5 positions to the 3 and 6 positions using lithium diisopropyl amide (LDA) to give a 96% yield of 3,6 dibromothieno[3,2-*b*]thiophene (**2.12**). This was in agreement with the 96%

obtained in literature. Compound (**2.12**) was subsequently chemoselectively dilithiated in the 3 and 6 positions with *n*-butyllithium (nBuLi) and reacted directly with dry ice (CO_2) to give thieno[3,2-*b*]thiophene-3,6-dicarboxylic acid (**2.13**). The dry ice used would have been slightly wet due to condensation of moisture on the dry ice pellets. This moisture would have quenched the lithiated thieno[3,2-*b*]thiophene species and thus lowered the yield. However using anhydrous CO_2 would have lead to the formation of ketonic by products through further reaction of the lithiated species with the intermediate carboxylate salt that is formed during the reaction.[149] Thus a yield of 97% was obtained after a simple work up which involved quenching the excess nBuLi with sodium hydrogen carbonate and then acidifying the reaction mixture so that the carboxylate salt was protonated and the product precipitated out. The next 2 steps were more problematic as initial attempts to esterify the dicarboxylic acid (**2.13**) and then brominate failed as unfortunately the esterification using para-toluene sulphonic acid (p–TSA) in neat refluxing ethanol degraded the thieno[3,2-*b*]thiophene. Thus it was decided to block the α positions through brominating the dicarboxylic acid (**2.13**) with NBS using the same conditions as Liu et al.[147] However using these conditions failed to make the reaction go to completion as the electron withdrawing carboxylic acids deactivated the α positions towards electrophilic attack by the bromine. Thus an excess, 4 equivalents, of NBS was used and the reaction was run for 2 days instead of just overnight to give yields of around 60%. The next step initially involved trying to esterify the dibromo dicarboxylic acid (**2.14**) using p–TSA in neat refluxing ethanol. However this debrominated the α positions of the thieno[3,2-*b*]thiophene and so an alternative method was sought. The next method involved using N,N'-dicyclohexylcarbodiimide (DCC) and 4-dimethylaminopyridine (DMAP) in dichloromethane (DCM) with ethanol but unfortunately this method also failed to yield the desired product and just returned starting material. Thus it was decided to convert the carboxylic acid functionalities into acid chloride functionalities using oxalyl chloride with a catalytic amount of dimethylformamide (DMF) and then quench the acid chloride (**2.15**) with ethanol to form diethyl 2,5-dibromothieno[3,2-*b*]thiophene-3,6-dicarboxylate (**2.16**). This method worked to give a satisfactory yield of 62%.

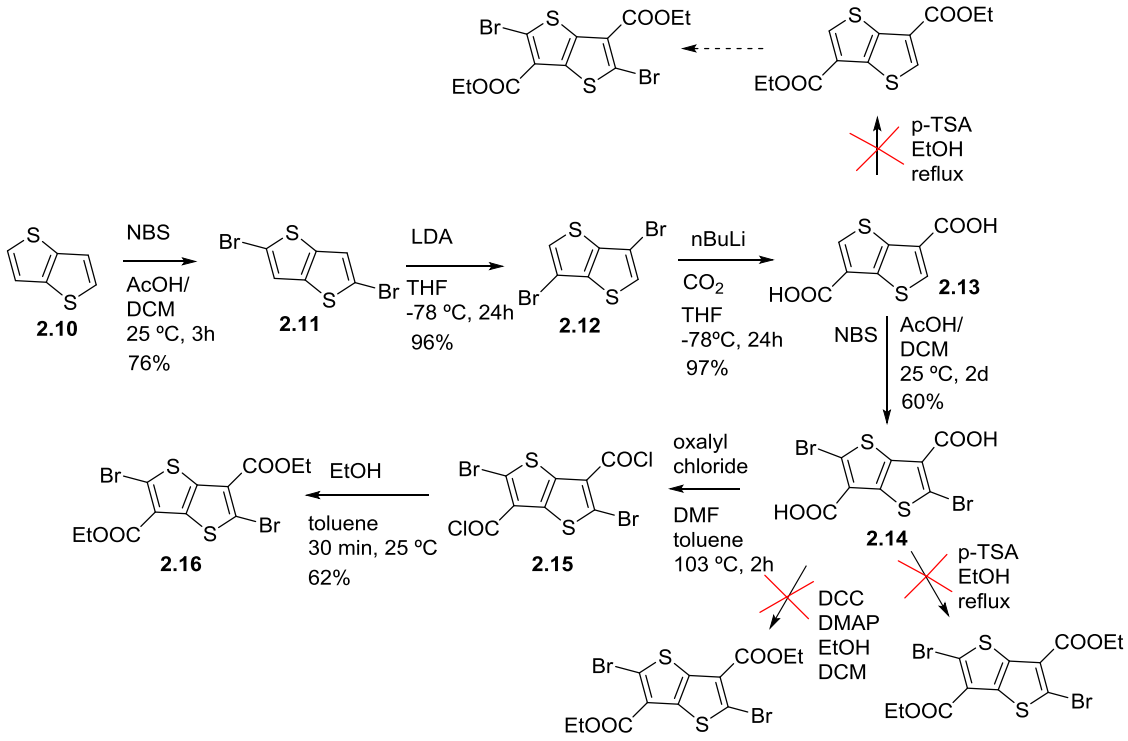


Figure 2.4: Synthesis of diethyl 2,5-dibromothieno[3,2-*b*]thiophene-3,6-dicarboxylate (**2.16**) indicating the various routes attempted.

The ester (**2.16**) was Stille coupled with tributyl(thiophen-2-yl)stannane (**2.17**) using catalytic $Pd_2(dba)_3$ with tri(*o*-tolyl)phosphine (P(*o*-tol)$_3$) ligands in a microwave heated to 200 ºC for 10 min to give diethyl 2,5-di(thiophen-2-yl)thieno[3,2-*b*]thiophene-3,6-dicarboxylate (**2.18**) as a yellow solid in 76% yield. Subsequent base catalysed saponification with sodium hydroxide converted the ester functional groups to carboxylic acid groups to give 2,5-di(thiophen-2-yl)thieno[3,2-*b*]thiophene-3,6-dicarboxylic acid (**2.19**) as a yellow solid in 78% yield. The next 2 steps involving the conversion of the carboxylic acid functionalities to acid chlorides to give (**2.20**) and then Friedel Crafts ring closure with $AlCl_3$ to give the diketone (**2.21**) proved to be trickier. Initially the carboxylic acid (**2.19**) was dissolved in tetrahydrofuran (THF) and oxalyl chloride and a catalytic amount of DMF were added. The reaction was run overnight to yield the acid chloride (**2.20**). Due to the unstable nature of acid chlorides this compound was not isolated for analysis and so was used directly for the next step. $AlCl_3$ was added directly to the reaction mixture to attempt the ring closure. However, as the acid chloride (**2.20**) was not soluble in THF and had precipitated out after forming, the ring closure reaction failed. Thus an alternative solvent, anhydrous DCM was tried. However, this time the initial carboxylic acid (**2.20**) was insoluble in the

DCM and so the acid chloride failed to form. The solution to this problem was to run the acid chloride formation reaction in THF and then evaporate off the THF and excess oxalyl chloride once the acid chloride had fully precipitated out of solution. Next anhydrous DCM was added to fully dissolve the acid chloride, which enabled the Friedel Crafts ring closure reaction to go to completion. This yielded the diketone (**2.21**) as a black insoluble product. Wolff Kishner reduction of the diketone (**2.21**) was attempted and initial efforts seemed promising as a distinct colour change from black to reddish brown was observed. Due to the insoluble nature of this product (**2.22**), alkylation was attempted directly using potassium tertiary butoxide and ethyl hexyl bromine in the hope of recovering the tetra alkylated product (**2.23**). Unfortunately no alkylated product was obtained.

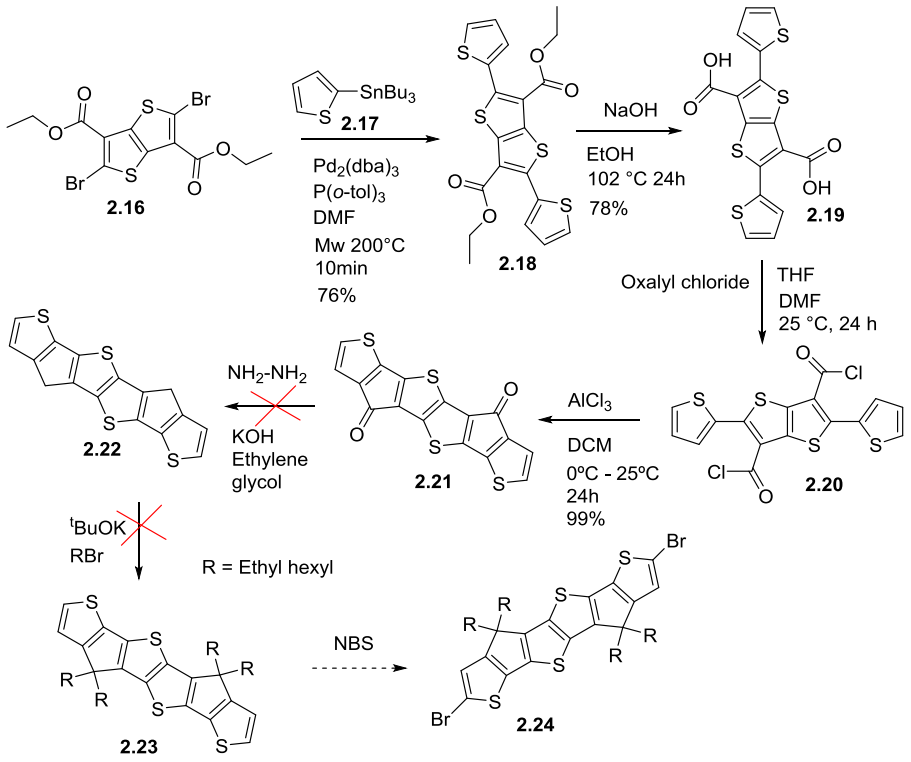


Figure 2.5: Synthetic route attempted to obtain monomer (**2.24**).

Thus a closer inspection of the previous Wolff Kishner reduction was required. As it turned out the black diketone (**2.21**) was not thermally stable as heating in pure diethylene glycol without the addition of hydrazine at 120 ºC was enough to turn it reddish brown. Thus as the high temperature Wolff Kishner reduction was not a viable option, a couple of alternative low temperature reduction routes were tried.

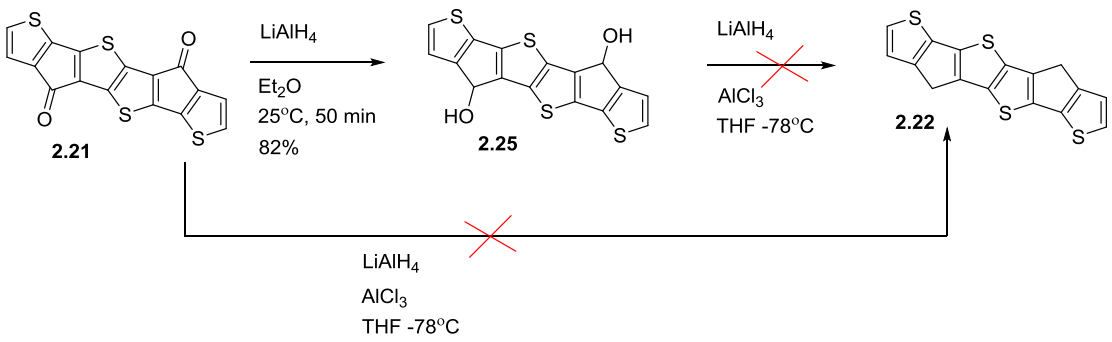


Figure 2.6: Two attempted synthetic routes to reduce diketone (**2.21**).

The use of lithium aluminium hydride ($LiAlH_4$) to reduce diketone (**2.21**) to dialcohol (**2.25**) at 25 °C yielded an insoluble black powder which was shown to be a mixture of the desired product and the starting material by mass spectroscopy. This crude mixture was taken directly to the next step, which involved the reduction of the alcohol with $LiAlH_4$ and $AlCl_3$ to give a black insoluble product assumed to be product (**2.22**). In tandem a direct route to product (**2.22**) was tried by directly subjecting diketone (**2.21**) to $LiAlH_4$ and $AlCl_3$ to yield a black insoluble product. Both batches of the assumed reduced (**2.22**) products were used directly in the next alkylation step to attempt to get the tetra alkylated product (**2.23**). However upon purification of the resulting products it was found that in both cases the ring opened products had been formed. Due to the insoluble nature of the starting materials it is hard to say at which point the product had become ring opened. Thus it was decided to try an alternative route which would not involve harsh reduction conditions.

Based on the notion that a Wittig reaction could functionalise the ketone functional groups of diketone (**2.21**) with alkyl chains, an attempt was made to improve the solubility of the diketone. Thus the first step was to lithiate thiophene (**2.26**) with one equivalent of nBuLi at -78 ºC, and quench the mono lithiated thiophene with triisopropylsilyl chloride (TIPS-Cl) to give triisopropyl(thiophen-2-yl)silane (**2.27**).

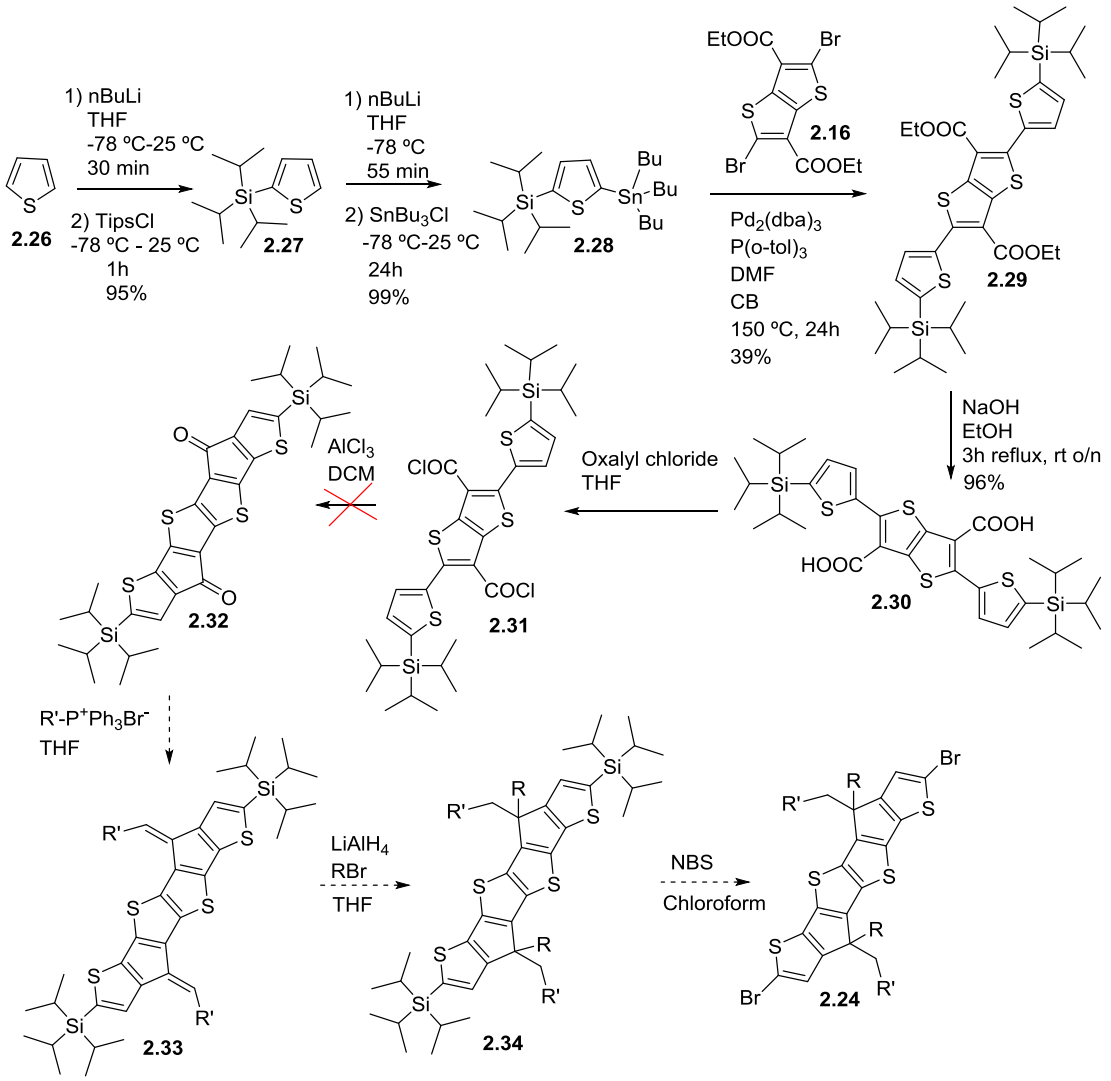


Figure 2.7: Attempted synthetic route towards final monomer (**2.24**).

Subsequent lithiation of TIPS protected thiophene (**2.27**) with nBuLi and quenching with tributyl stannyl chloride gave triisopropyl(5-(trimethylstannyl)thiophen-2-yl)silane (**2.28**) as a pale orange oil in 99% yield. Stille coupling of ester (**2.16**) with tin compound (**2.28**) using catalytic $Pd_2(dba)_3$ in an oil bath heated to 150 ºC for 24 h gave diethyl 2,5-bis(5-(triisopropylsilyl)thiophen-2-yl)thieno[3,2-*b*]thiophene-3,6-dicarboxylate (**2.29**) as a yellow solid in 39% yield. Subsequent base catalysed saponification with sodium hydroxide converted the ester functional groups to carboxylic acid groups to give 2,5-bis(5-(triisopropylsilyl)thiophen-2-yl)thieno[3,2-*b*]thiophene-3,6-dicarboxylic acid (**2.30**) as a yellow solid in 96% yield. The next step involved the conversion of the two carboxylic acid functionalities into acid chlorides using oxalyl chloride in anhydrous THF. After rotary evaporating off the THF and any excess oxalyl chloride the crude acid chloride (**2.31**) obtained was used directly in

the next step. Changing the solvent to anhydrous DCM and using $AlCl_3$ to Friedel Crafts ring close the acid chloride proved effective, and the resulting product (**2.32**) would have been taken on to be alkylated through a Wittig reaction, the resulting alkene (**2.33**) would have been simultaneously reduced and alkylated in a one pot reaction with $LiAlH_4$ and a bromo alkane, in accordance to a method developed by Aso Yoshio et al,[150] to give (**2.34**) with the final step being the direct replacement of the TIPS protecting groups with bromine using NBS (**Figure 2.7**). However, the black product obtained from the Friedel Crafts ring closure had become TIPS deprotected as a result of either the acidic conditions sustained in the conversion to the acid chloride functionality or the acidic conditions of the Friedel Crafts ring closure. This meant that the resulting product was no longer soluble and thus the subsequent planned steps could not be attempted.

The next route tried was based on Van Mierloo's[151] three step synthetic approach to obtaining symmetrically and asymmetrically functionalised 4H-cyclopenta[2,1-b:3,4-b′]dithiophenes. Van Mierloo's route involves Kumada coupling 3-bromo-2,2′-bithiophene (**2.35**) with 2-thienylmagnesium bromide (**2.36**), followed by lithiation of (**2.37**) and subsequent reaction with dialkyl ketones to give symmetric and asymmetric dialkylated tertiary alcohol derivatives (**2.38**) depending on which alkyl groups were used in the ketones. The next step is the key step with a Friedel Crafts ring closure using sulphuric acid in octane to give 4,4-dialkyl-4H-cyclopenta[2,1-b:3,4-b′]dithiophenes (**2.39**) as shown in **Figure 2.8**.

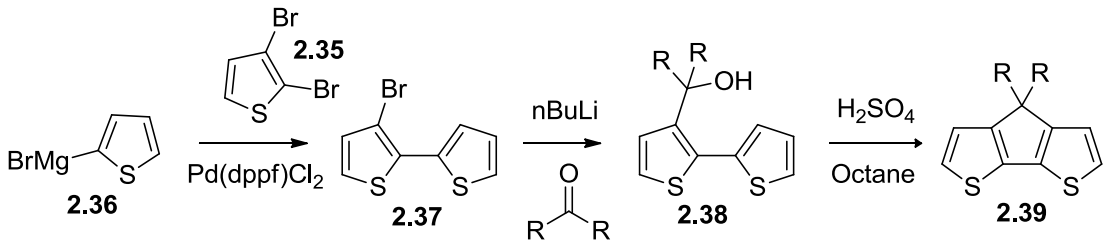


Figure 2.8: Synthesis of 4,4-dialkyl-4H-cyclopenta[2,1-b:3,4-b′]dithiophenes.[151]

Based on the afore mentioned synthesis of 4,4-dialkyl-4H-cyclopenta[2,1-b:3,4-b′]dithiophenes (**2.39**) the first step was to synthesise a tetra alkylated tertiary alcohol equivalent to compound (**2.38**). This was achieved after a number of synthetic steps, **Figure 2.9**.

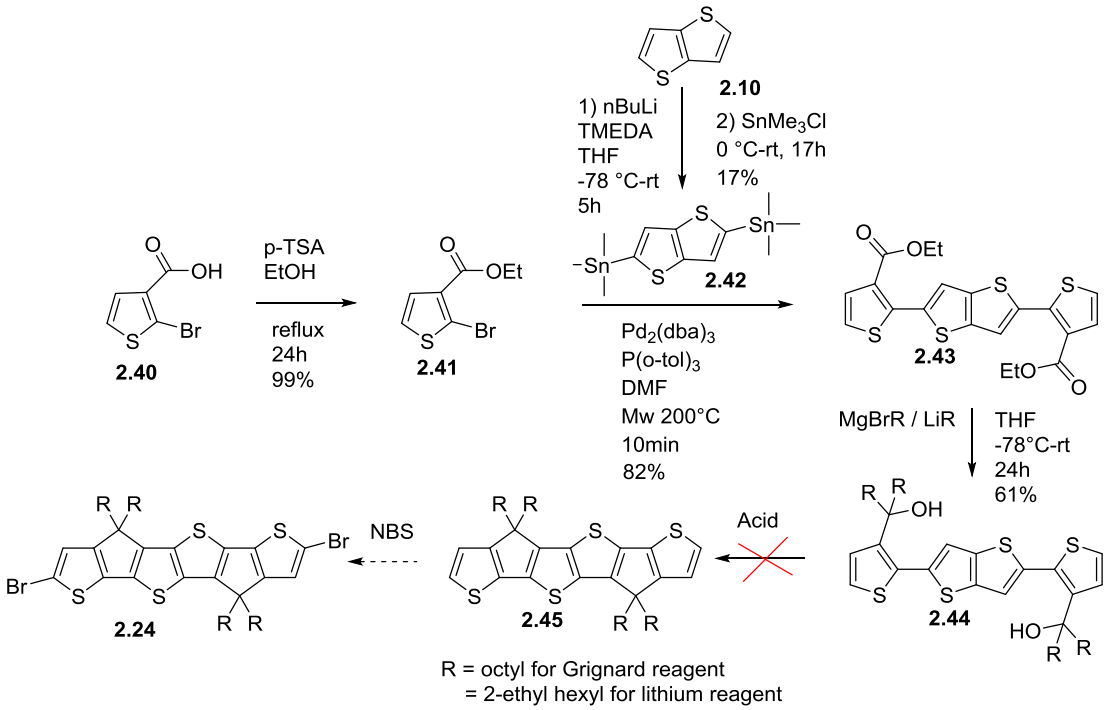


Figure 2.9: Attempted synthetic route towards final monomer (**2.24**).

The first step was to esterify commercially available 2-bromo -3 thiophenecarboxylic acid (**2.40**) by refluxing it in neat ethanol using p-TSA as a catalyst overnight. Upon work up excellent yields of between 86-99% were obtained of 2-bromo thiophene-3-ethyl ester (**2.41**). In tandem, 2,5-bis(trimethylstannyl)thieno[3,2-*b*]thiophene (**2.42**) was synthesised from commercially available thieno[3,2-*b*]thiophene (**2.10**) through lithiation, using nBuLi and tetramethylethylenediamine (TMEDA) to improve the reactivity of the nBuLi,[152] and quenching the lithiated species with trimethyltin chloride. Subsequent Stille coupling of the tin monomer (**2.42**) with the ester (**2.41**) gave the coupled ester (**2.43**) with an initial yield of 67% which was increased to 94%. The improvements in yield was a result of optimising the purification conditions from a recrystallisation from hot ethyl acetate to just a hot filtration from ethyl acetate to get rid of the palladium. The next step involved using 2-ethyl hexyl magnesium bromide as a Grignard reagent to alkylate coupled ester (**2.43**) and obtain tetra alkylated dialcohol (**2.44**). The crude tetra alkylated dialcohol (**2.44**) was subsequently ring closed with sulphuric acid in octane stirring at room temperature overnight. However the yield for this step was very low ~7% and the 133mg of product (**2.45**) obtained after extensive flash chromatography in hexane was still impure so it was difficult to ascertain if the product had actually ring closed. The low

yield was as a result of the product being destroyed by the acid, through forming a black plastic, presumed to be a result of an acid catalysed cross coupling reaction. Additionally the yield of the previous alkylation step may also have been low as having isolated the purified dialcohol with octyl side chains (**2.44**) only an 8% yield was obtained. So it was decided to optimise the alkylation step in the hope of achieving greater yields for the ring closure step as well as use less harsh acidic ring closure conditions. Thus 2-ethylhexyllithium reagent was used instead of a Grignard reagent, as with Grignard reagents side reactions such as single electron transfer reactions which cause E2 eliminations thus forming alkenes can generate unwanted products and thus lower the yield.[149] The use of the lithium reagent gave a 60% yield of pure dialcohol with ethyl hexyl side chains (**2.44**) after column chromatograph with hexane. Ring closure of the purified dialcohol with ethyl hexyl side chains (**2.44**) in sulphuric acid was subsequently attempted using a shorter reaction time of 1 hour (h), however only the alkene product (**2.46**) was formed (**Figure 2.10**) Allowing the reaction to go on for another 4 h resulted in the product being almost completely destroyed. Thus alternative acids such as amberlyst 15, $AlCl_3$ and BF_3 using various reaction times and temperatures were tried but unfortunately all of these acids only formed the alkene product (**2.46**).

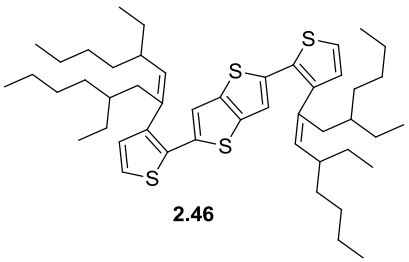


Figure 2.10: Isolated alkene product (**2.46**).

Based on Van Mierloo's[151] three step synthetic approach it can be seen that it is possible to ring close bithiophenes with tertiary alcohols such as 3-([2,2'-Bithiophen]-3-yl)pentan-3-ol (**2.38**) using H_2SO_4. Mechanistically this reaction also proceeds via an alkene intermediate (**2.47**) due to E2 elimination of the tertiary alcohol. This however is followed by the protonation of the double bond (**2.48**) and an electrophilic attack on the formed tertiary carbocation by the electron rich β position of the thiophene to form the ring closed carbocation (**2.49**) which subsequently eliminates the β hydrogen to form the ring closed product (**2.39**) as shown in **Figure 2.11**.

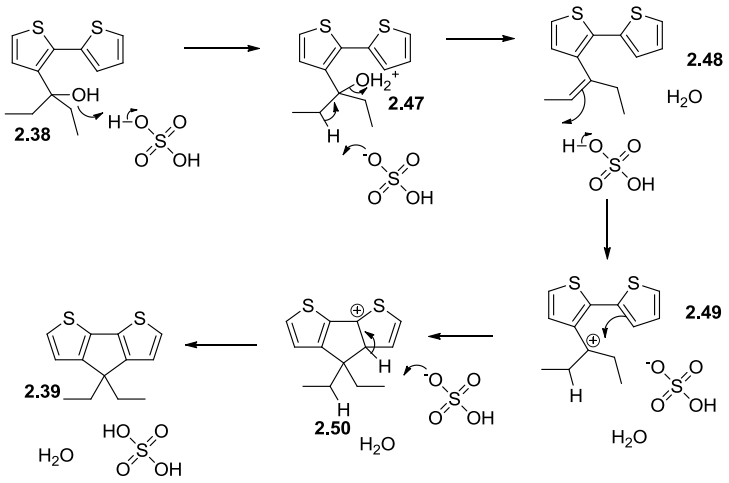


Figure 2.11: Mechanism of ring closure of 3-([2,2'-Bithiophen]-3-yl)pentan-3-ol (**2.38**).

However a possible reason that just the alkene (**2.46**) is formed in this reaction is that the β position of the thieno[3,2-*b*]thiophene is less electron rich than that of the β position of thiophene, as the electron density is more delocalised in the bigger aromatic π system of the thieno[3,2-*b*]thiophene, and so electrophilic attack of the carbocation intermediate is less likely. Thus at longer reaction times the acid catalysed cross coupling shown in **Figure 2.12** is more likely to occur.

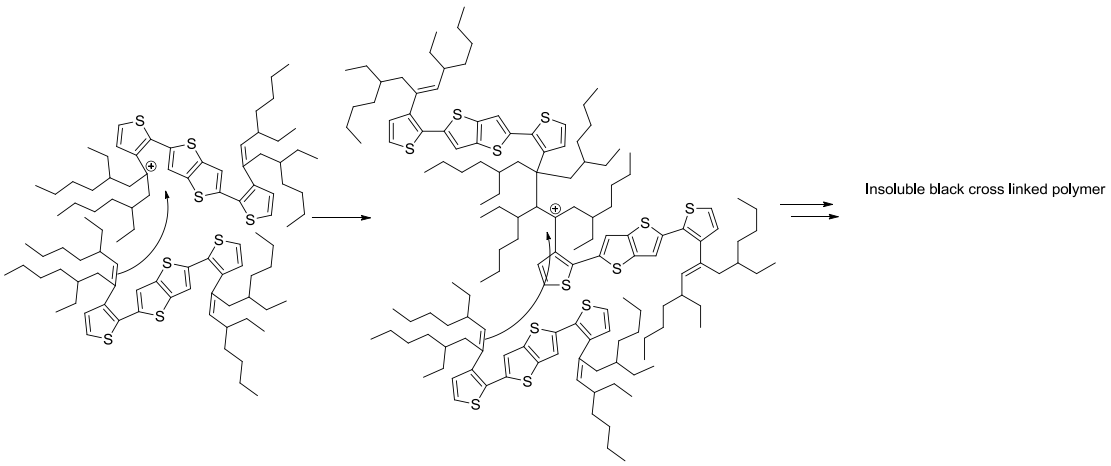


Figure 2.12: Postulated acid catalysed cross coupling mechanism.

As a result of these synthetic difficulties, an alternative strategy of ring closing using the thiophene as the nucleophile, rather than the thieno[3,2-*b*]thiophene was envisaged, **Figure 2.13**. The idea behind using this strategy was that the thiophene having its electron density less delocalised than the thieno[3,2-*b*]thiophene should be

more nucleophilic and thus the rate of ring closure verses the rate of acid catalysed cross coupling should be greater.

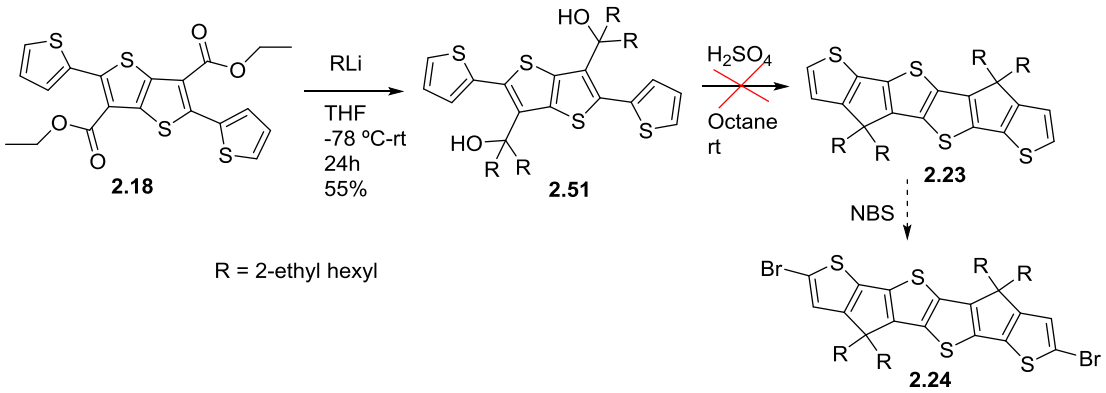


Figure 2.13: Attempted synthetic route towards final monomer (**2.24**).

Having remade ester (**2.18**), it was reacted with 2-ethylhexyl lithium to give the dialcohol (**2.51**) as a yellow oil in 55% yield. The addition of concentrated sulphuric acid to dialcohol (**2.51**) initially resulted in an alkene being formed on the ethyl hexyl side chains. This was expected as this is an intermediate in the reaction pathway towards ring closure. However upon leaving the reaction for a longer period of time it was found that no further reaction occurred. So an additional amount of sulphuric acid was added to the alkene and it was found that the compound decomposed after about 5 minutes. This may have been due to the same crosslinking effect of the alkene with neighbouring alkenes as previously shown in **Figure 2.12**.

Based on these findings an alternative alkyl side chain which employed phenyl groups to both sterically hinder the attack on the intermediate carbocation and also provide stabilisation for the intermediate carbocation was employed. This work was carried out in collaboration with Dr. Hugo Bronstein.[153] Using the method developed to synthesise ester (**2.43**), the ester (**2.43**) was alkylated via a Grignard reaction with freshly prepared 4-n-hexylphenyl magnesium bromide. The crude dialcohol (**2.52**) obtained as a viscous oil was used without further purification and directly ring closed via acid catalysis by dissolving the dialcohol (**2.52**) in hot glacial acetic acid and adding sulphuric acid dropwise in accordance to the method used for the synthesis of IDT.[154] This procedure produced the novel fused hexacyclic ring system (**2.53**) as a light yellow solid in 9% yield. The low yield for this step is as a result of some of the starting material forming oligomers, although in this case as no intermediate alkene is

formed, the nucleophilic attack on the intermediate carbocation must come from the thiophenes flanking the central thieno[3,2-*b*]thiophene core. The formation of these oligomers was evident as a significant amount of insoluble black plastic like material is obtained upon addition of the sulphuric acid. However, the product (**2.53**) could be obtained through filtering off the black plastic material upon work up and then extracting the entrained product (**2.53**) from the oligomers by dissolving the black plastic material in chloroform using sonication. After filtering off the oligomers the product (**2.53**) was isolated from the filtrate via column chromatography. Using NBS for the final bromination step and a subsequent recrystallisation from acetone provided the final 4T monomer (**2.54**) as a pale yellow solid in 76% yield, **Figure 2.14**.

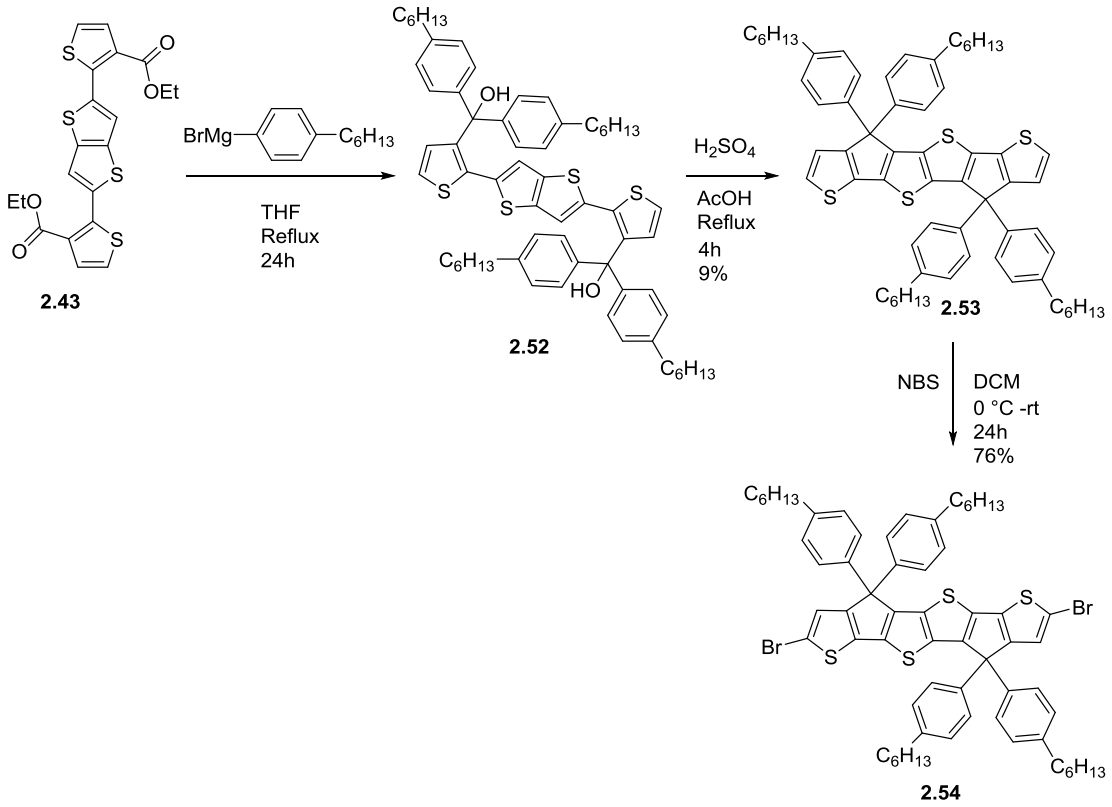


Figure 2.14: Synthetic route of towards novel 4T monomer (**2.54**).

The structure and planar nature of monomer (**2.54**) was confirmed by analysing a single crystal of monomer (**2.54**), grown from hexane, using single crystal X-ray diffraction (XRD), **Figure 2.15**.

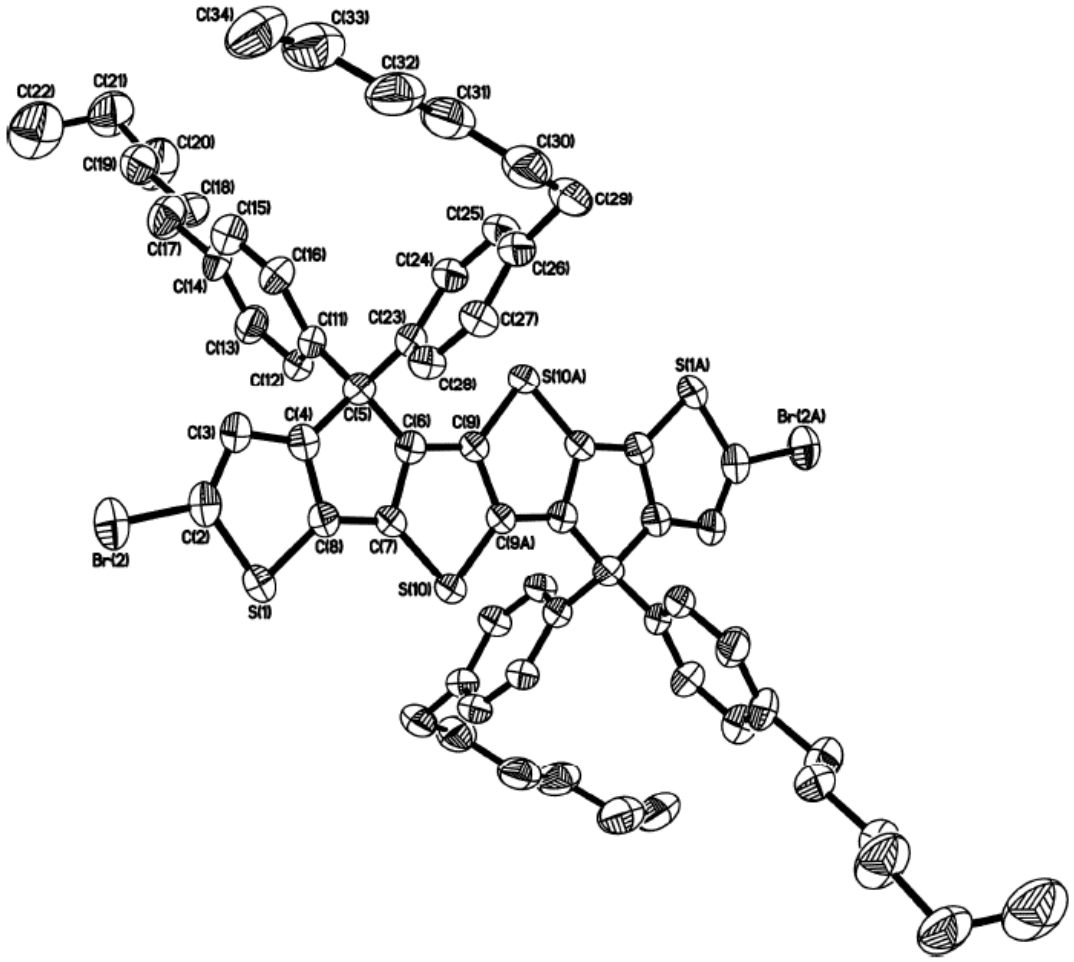


Figure 2.15: Molecular structure of 4T monomer (**2.54**). 30% probability ellipsoids are indicated.

The single crystal of the monomer obtained was a long thin needle and thus the XRD measurement required an 83 hour collection time as only a small volume of the crystal could be bathed in the X-ray beam, giving rise to only weak scattering. Despite the fact that only weak data could be obtained for this sample, the molecule was found to have a centre of symmetry in the middle of the C(9) – C(9A) bond, a coplanar core structure, with the C(11) to C(22) 4-n-hexylphenyl groups being found to be disordered.

2.3 Synthesis of 4T Based Polymer

As it has been demonstrated that using **BT** as an acceptor with **CPDT** gives greater OPV device efficiencies than with **TPD** (5.5% for **BT**[121] as opposed to 3.74% for

TPD[122]) it was decided to copolymerise the donor 4T monomer (**2.54**) with **BT**. Additionally this allows one to make a direct comparison with the copolymer **IDT-BT** which showed an impressive PCE of 6.41%.[155]

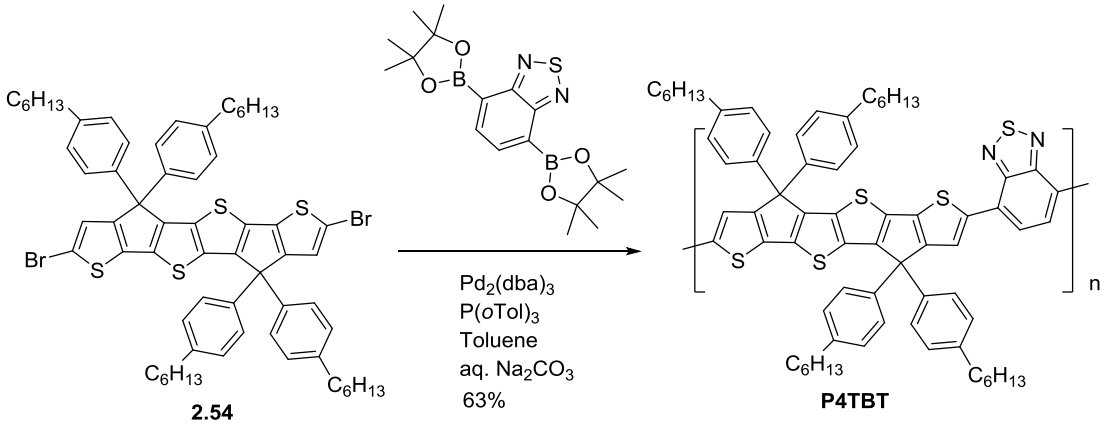


Figure 2.16: Synthesis of novel polymer **P4TBT**.

Suzuki coupling of the 4T monomer (**2.54**) with 2,1,3-benzothiadiazole-4,7-bis(boronic acid pinacol ester) in an exact 1:1 ratio, using $Pd_2(dba)_3$ as catalyst, P(*o*-tol)$_3$ ligands, toluene as solvent, aqueous sodium carbonate as the base and Aliquat 336 as the phase transfer agent, was carried out using conventional heating over the course of 72 h at 110 ºC in accordance to the method reported by Zhang et al.[139] The resulting polymer **P4TBT** was precipitated into methanol, before being filtered off as a dark solid. The polymer was purified via Soxhlet extraction in acetone, hexane and chloroform in order to reduce the polydispersity index (PDI) of the crude polymer. By removing both the low molecular weight oligomers and catalytic impurities the performance of the polymer within devices can be enhanced. This is due to the fact that minor impurities such as oligomers and structural defects can decrease the charge carrier mobility and act as charge traps which increase the amount of charge recombination.[156] This not only reduces the photocurrent within OPV devices but the low molecular weight impurities also decrease the device lifetime even in the absence of atmospheric moisture and oxygen.[157] The next stage of the polymer purification was to dissolve the polymer in hot chloroform and with vigorous stirring remove any residual catalytic palladium impurities via chelation with aqueous sodium diethyldithiocarbamate.[158] This was followed by an aqueous extraction to remove any residual inorganic impurities. The removal of these inorganic impurities is also

important as these could not only act as charge traps but it has been shown that even at levels of 6.1×10^{-6}% the optical properties of conjugated materials can be detrimentally affected.[159]

2.4 Polymer Properties

2.4.1 Polymer molecular weight

The molecular weight of **P4TBT** was estimated using gel permeation chromatography (GPC) calibrated against polystyrene standards. The eluent used was chlorobenzene in which the polymer is readily soluble and the measurement was carried out at 80 ºC to give M_n = 19 kDa, M_w = 50 kDa, PDI = 2.6. This gives a degree of polymerisation (DP) of 16 meaning that the average polymer chain contains 16 repeat units. This means that the length of the polymer chain is greater than the persistence length which is typically 10 repeat units and thus means that the lowest possible band gap for the polymer can be attained.

2.4.2 Polymer UV-Vis

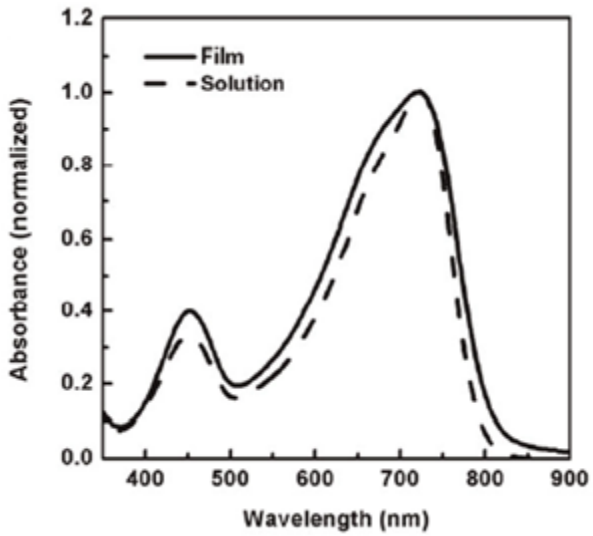


Figure 2.17: UV-Vis absorption spectrum of **4T-BT** in chloroform solution and in thin film spun from chlorobenzene solution.

The optical properties of the polymer were characterised using UV-Vis absorption spectroscopy. In chloroform at room temperature the solution UV-Vis sprectum shows two strong absorption bands with maxima at 449 nm and 729 nm. The maximum at 449 nm corresponds to the π- π* transition, while the second much stronger absorption at 729 nm corresponds to an internal charge transfer (ICT) absorption band. The appearance of these two distinct bands reveals the donor-acceptor (D-A) nature of the polymer, while the fact that the polymer exhibits a broad absorption over a large range of wavelengths shows that the polymer is suitable for use in an OPV device. For the thin film UV-Vis spectrum of the polymer, with the exception of a slight broadening of the absorption, the polymer shows an almost identical absorption to the solution UV-Vis spectrum. The thin film absorption also shows a maximum absorption at 729 nm, indicating that upon going from solution to thin film the polymer has not become more ordered, as otherwise a red shift would be observed. The lack of crystallinity observed in the thin film can be attributed to the fact that the sterically bulky 4-n-phenylhexyl side chains may prevent π-π stacking of the polymer backbones thus rendering the polymer amorphous. The onset of the absorption in the film of the polymer can be seen at ~820 nm, indicating that the polymer has a very narrow optical band gap of 1.5 eV. Based on photo electron spectroscopy in air (PESA) the HOMO energy level was measured to be at -5.2 eV, relative to the vacuum energy level. Combining the data from PESA with that of the UV-Vis spectrum the LUMO was estimated to be at -3.7 eV.

Compared to **IDT-BT** the HOMO level of **4T-BT** is approximately 0.2 eV higher. This means that **4T-BT** is considerably more electron donating than **IDT-BT**. This is as expected as the substitution of the electron poor phenyl in the **IDT** analogue for electron rich thieno[3,2-*b*] thiophene would raise the HOMO. This also explains why the optical bandgap for **4T-BT** is somewhat lower than the optical bandgap of **IDT-BT** (1.5 eV verses 1.75eV[155] respectively).

2.4.3 Polymer performance in OFETs

To evaluate the hole mobility of **4T-BT**, top gate, bottom contact field effect transistors were fabricated. The fabrication process involved evaporating gold source and drain electrodes onto cleaned glass substrates and then functionalising the

electrodes with a self assembled mono layer (SAM) composed of pentafluorobenzenethiol (**PFBT**). The purpose of the **PFBT** is to lower the work function of the gold electrodes, by being electron withdrawing, thus facilitating hole injection into the HOMO of the polymer. The polymer, dissolved in hot chlorobenzene (5 mg / mL) was spin cast on top of the **PFBT** monolayer at 2000 rpm for 1 min and annealed at either 150 ºC or 200 ºC for 10 min to produce thin films. A CYTOP^{TM} (a fluoropolymer with a high dielectric constant) dielectric was spin cast at 2000 rpm for 1 min on top of the polymer layer and annealed at 95 ºC for 20 min. Finally an aluminium gate electrode was thermally evaporated on top. The obtained transfer and output characteristics for a typical device annealed at 200 ºC are shown in **Figure 2.18** below.

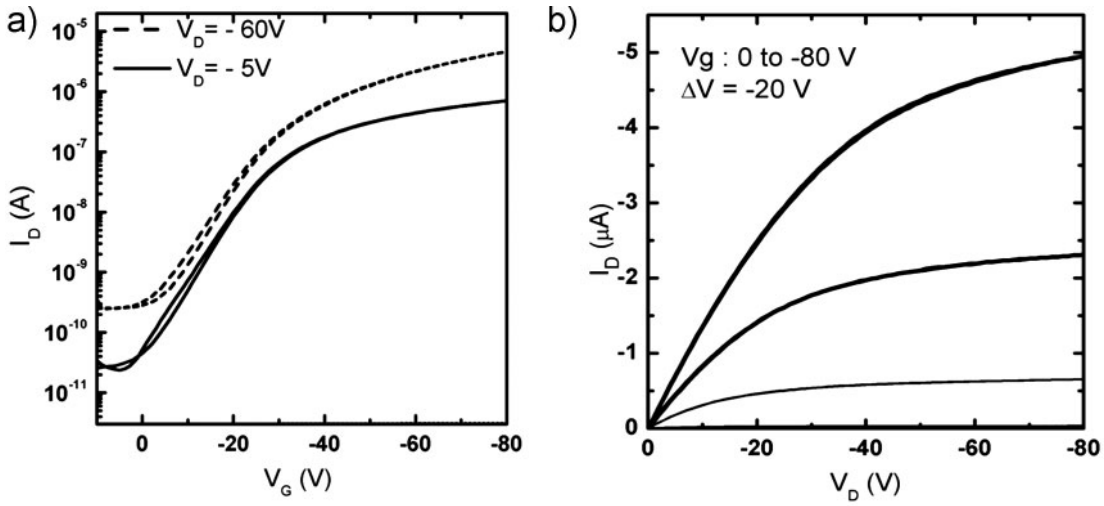


Figure 2.18: a) Transfer characteristics of a **4T-BT** device annealed at 200 ºC. b) Output characteristics of a **4T-BT** device annealed at 200 ºC.

Using the Mott-Gurney law the saturated field effect mobilities for the novel copolymer were found to be in the range of 0.05-0.07 $cm^2V^{-1}s^{-1}$ with on/off ratios of ~10^4. It was found that for the output characteristics of the samples annealed at 150 ºC a small amount of hysteresis was observed. Upon annealing at 200 ºC the hysteresis completely disappeared, most probably as a result of an improvement in thin film morphology. The field effect mobilities obtained could have been improved further through the use of alternative device configurations utilising higher surface energy substrates as the polymer solution showed poor wettability on the substrate. However, despite the poor film formation these values are substantially greater than the 0.020 $cm^2V^{-1}s^{-1}$ value for saturation field effect hole mobility obtained for the analogous 4-

hexylphenyl **IDT-BT** copolymer, although it should be mentioned that an alternative bottom gate, top contact device configuration was used for this polymer.[160] The improvement in mobility from going from **IDT-BT** to **4T-BT** can be attributed to the replacement of the central phenyl unit with thieno[3,2-*b*]thiophene as the thieno[3,2-*b*]thiophene extends the planarity of the polymer. It has been found that for **IDT-BT** that when the 4-hexylphenyl side chains are replaced with long linear alkyl chains mobilities in excess of 1 $cm^2V^{-1}s^{-1}$ can be obtained as a result of less steric hindrance between neighbouring polymer backbones which leads to greater crystallinity.[139] It was hoped that a similar result could be obtained for **4T-BT** but unfortunately due to synthetic limitations attempts to include linear alkyl side chains failed.

2.4.4 Polymer performance in OPV

To evaluate the solar cell performance of **4T-BT** solar cell devices were made with the device architecture indium tin oxide (ITO): poly(3,4-ethylenedioxythiophene) (PEDOT) / poly(styrenesulfonate) (PSS): Active layer: LiF: Al. The fabrication process involved spin coating an aqueous solution of PEDOT/PSS onto pre patterned ITO substrates. A solution of **4T-BT** and $PC_{70}BM$ in ortho dichlorobenzene (ODCB) in a ratio of 1:4 was spin coated on top of the ITO to form an 80 nm thick active layer, followed by the vacuum deposition of LiF and Al to form the counter electrode. The solar cell current density voltage characteristics (*J-V*) and external quantum efficiency (EQE) are shown in **Figure 2.19** below.

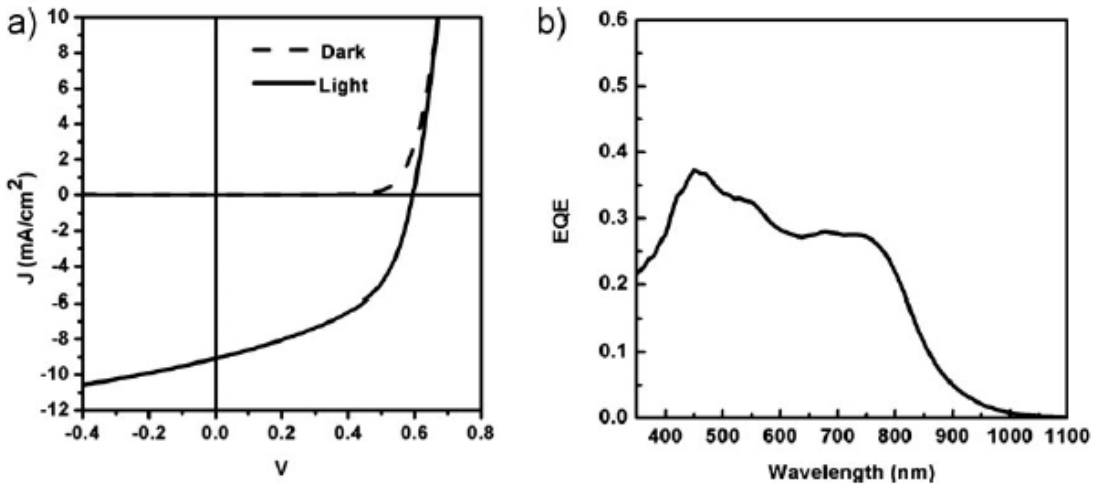


Figure 2.19: a) *J-V* curve of OPV device. b) EQE spectra of OPV device.

Under AM 1.5 conditions the *J-V* curve, **Figure 2.19 a)**, gives the open circuit voltage (V_{oc}) as 0.59 V, the short circuit current (J_{sc}) as -9.1 $mAcm^{-2}$, a fill factor (FF) as 0.49 and a photocurrent conversion efficiency (PCE) of 2.5%. The fairly modest device efficiency can be attributed to the low FF, which is possibly due to a poor blend morphology which in this case has given rise to shunt resistance. The EQE, **Figure 2.19 b)**, shows a broad coverage over a large proportion of the solar spectrum which gives rise to the favourable J_{sc}. The maxima at ~450 nm is attributed to the contribution of the $PC_{70}BM$, with the rest of the EQE spectrum exhibiting matching characteristics to the polymer UV-Vis absorption spectra. However, even though the EQE exhibits a broad range, the EQE for any given wavelength does not exceed 40%. The reason for this is not considered to be due to an insufficient energetic offset between the LUMO of the polymer and the LUMO of the fullerene as **IDT-BT**, which performs well, shows similar LUMO energy levels to **4T-BT**.[34] Thus the low EQE can be accredited to the poor FF, which was a result of the detrimental nanoscale morphology. It is expected though that further improvements can be made to optimise the morphology and thus improve the FF through the use of additives, as has been shown for other materials with similar solubilising groups.[140]

2.5 Conclusion and Subsequent Impact

The development of the 4T monomer (**2.54**) has been synthetically challenging with a variety of synthetic intermediates and synthetic routes being tried and tested along the way. The novel 4T monomer (**2.54**) was finally synthesised via a Friedel crafts ring closure reaction in which the use of 4-hexyl phenyl side chains proved crucial. The 4T monomer (**2.54**) was fully characterised using single crystal X-ray diffraction and copolymerised with benzothiadiazole to give the novel low bandgap, high molecular weight **4T-BT** copolymer. The copolymer showed promising mobilities in both the linear and saturated regimes, in top gate, bottom contact in OFET devices, with mobilities approaching 0.1 $cm^2V^{-1}s^{-1}$. In the initial OPV devices that were fabricated with $PC_{70}BM$ the polymer gave a modest PCE of 2.5% which can be mainly attributed to a high J_{sc} due to the polymer's broad absorption and low bandgap.

Another research group has subsequently developed copolymers based on the 4T core using the route outlined in **Figure 2.14**, but with 4-(octyloxy)phenyl side chains

instead of 4 hexyl phenyl side chains.[161] Using 5,8-dibromo-phenanthrenequinoxaline (PQX), TPD and BT as comonomers, 3 new copolymers were synthesised. These copolymers gave OPV device efficiencies in the range of 1.91 – 2.59 % and OFET performances in the range of 2.5×10^{-4} – 0.053 $cm^2V^{-1}s^{-1}$ showing the promising performance values that the **4T** core can give.

Additionally another group has independently developed a small molecule based on the 4T core using a similar route to that outlined in **Figure 2.7**, although rather than using TIPS protecting groups to ensure the solubility of the diketone (**2.32)** alkyl chains are used instead. Also rather than employing a Wittig reaction to functionalise the diketone a Knoevenagel condensation was used to incorporate dicyanovinylene moieties onto the molecule. This small molecule gave OFET devices with impressive electron mobilities of 0.16 $cm^2V^{-1}s^{-1}$.[162]

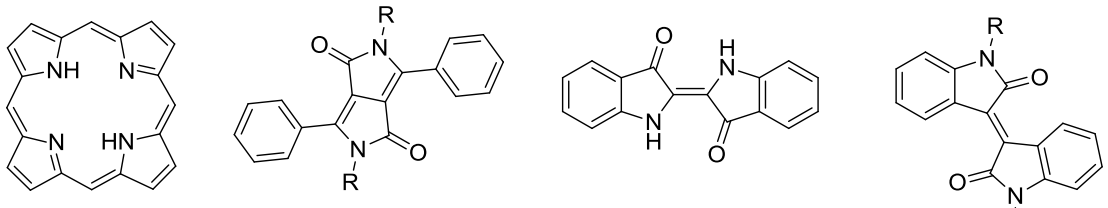
The results from both the work reported in this thesis and the work of other research groups show that the novel fused hexacyclic thiophene donor molecule with the right adjustments to the side chains and choice of comonomer shows great potential for use in the field of organic electronics.

Chapter 3 Isoindigo

Make everything as simple as possible, but not simpler.
Albert Einstein (1879-1955), theoretical physicist

3.1 Introduction to Isoindigo

Much of the development of new materials for plastic electronics has been either based on naturally occurring compounds such as porphyrins from plants or industrially available dyes and pigments such as diketopyrrolopyrrole (DPP), which is commercially used in high performance paints. Indigo is another dye which was first isolated from a species of predatory sea snails in the family Muricidae as far back as 2000 BC by the ancient Indus Valley civilisation.[163] Used for dying royal clothing throughout antiquity, the dye called Tyrian purple at the time, was prized because its colour did not fade easily and became brighter as it was exposed to sunlight and weathering. More recently Tyrian purple, found to consist mainly of 6,6' dibromoisoindigo, was used to fabricate ambipolar transistors with reasonable hole and electron mobilities of 0.22 cm^2/Vs and 0.03 cm^2/Vs respectively.[164] These mobilities were obtained as the planar indigo molecule is able to form hydrogen bonds between neighbouring molecules enabling highly ordered crystalline domains to form. This results in the intermolecular π stacking that is necessary for charge transport. However, these mobilities were obtained despite the fact that indigo is not through conjugated. Thus the development of a through conjugated version of indigo was required for improved performance. Fortunately, isoindigo, a structural analogue of indigo, is also available with its synthesis being reported as far back as 1910.[165] More recently isoindigo has been discovered as a minor isomer of the indigoid dyes found in the leaves of the plant Isatis tinctoria (Woad).[166]



Porphyrin DPP Indigo Isoindigo

Figure 3.1: Structures of porphyrin, DPP, indigo and isoindigo

Isoindigo is a symmetrical molecule, composed of two indolin-2-one units which give rise to its electron withdrawing ability thus making it suitable as an electron acceptor within donor acceptor copolymers. The precise conformation of isoindigo is however a matter for debate as it would seem that there is evidence to suggest that it is in some cases planar and in other cases twisted about the central double bond.

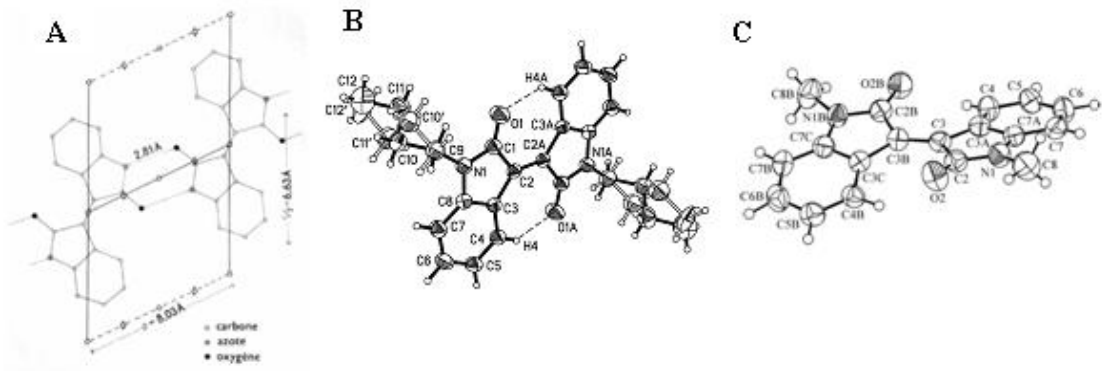


Figure 3.2: X-ray crystal structures a) non alkylated isoindigo[167] b) 1,1' dibutyl isoindigo[168] c) 1,1' dimethyl isoindigo[169]

Based on X-ray crystallography data of non alkylated isoindigo crystals formed via sublimation[167] and 1,1' dibutyl isoindigo (1,1'-Dibutyl-3,3'-biindolinylidene-2,2'-dione 1,1'-Dibutyl-3,3'-biindolinylidene-2,2'-dione) crystals formed via crystallisation from THF,[168] the molecule is designated as being completely planar with a weak intermolecular interaction between the oxygen atom and the neighbouring hydrogen atom on the adjacent phenyl ring enforcing planarity. However a crystal structure of 1,1' dimethyl isoindigo formed via crystallisation from chloroform shows a distinct rotation of the two oxindole rings relative to the double bond with an angle of 22.3(2)° between the planes.[169] This rotation could have an effect on the conjugation of the molecule as the rotation causes a decrease in the amount of orbital overlap required for efficient electron delocalisation. Fortunately the crystal structure for this conformation also shows that the overall molecule is conjugated, the proof being that the central double bond has a bond length of 1.363(4) Å – an intermediate value between a single bond 1.397 Å and a double bond 1.321 Å. Despite the fact that the authors of this paper cannot provide an unambiguous explanation for this conformation, isoindigo has been extensively used as a conjugated acceptor for organic electronics.

The first use of isoindigo in solar cells was reported by Mei et al[170] in which two novel small molecules (**Figure 3.3**), one consisting of an isoindigo core flanked by two bithiophene units in a donor-acceptor-donor (D-A-D) configuration and the other consisting of a bithiophene core flanked by two isoindigo units in an acceptor-donor-acceptor (A-D-A) configuration, were used. As it turned out the D-A-D isoindigo small molecule gave the better photocurrent conversion efficiency (PCE) with a PCE

of 1.76% as opposed to the 0.55% obtained by the A-D-A small molecule. The difference in the performance between these two molecules was attributed to the fact that the D-A-D small molecule exhibited a higher degree of molecular ordering as well as a lower band gap.

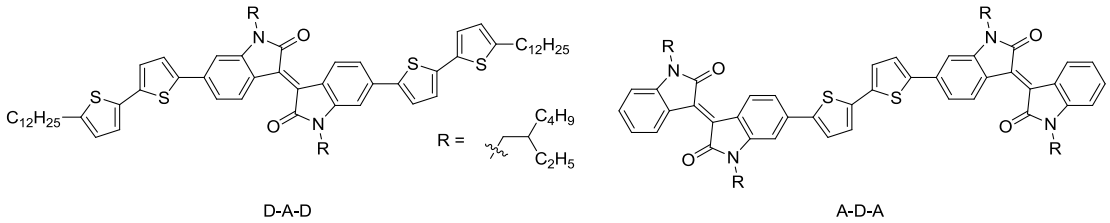


Figure 3.3: Isoindigo D-A-D and A-D-A small molecules.[170]

Despite the fact that Stalder et al[171] reported the first donor acceptor copolymers based on isoindigo, it was Wang et al[172] who first used an isoindigo based copolymer **PTI-1** in solar cells (**Figure 3.4**). Through increasing the alkyl side chain length on the isoindigo unit from 2-ethylhexane to 2-hexyldecyl Wang et al ensured that the polymer would remain in solution during the polymerisation which thus gave rise to a higher molecular weight polymer (Mn 86 kDa compared to Mn 2.4 kDa for the thiophene copolymer first reported by Stalder et al[171]). This isoindigo – thiophene copolymer gave an improved PCE of 3% along with a high open circuit voltage (V_{OC}) of 0.89V.

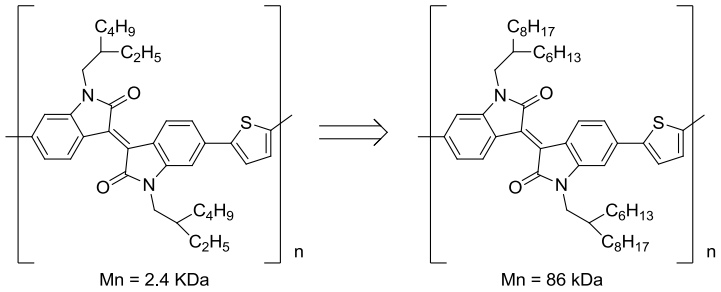


Figure 3.4: Side chain improvement in **PTI-1**

However as **PTI-1** only contained one thiophene as the donor unit, it only exhibited a low absorption in the high energy band of its UV absorption spectrum. Thus to increase the absorption intensity in the high energy band Wang et al increased the conjugation length of the donor unit by incorporating a terthiophene unit, which was also favourable for π-π stacking of polymer backbones, as terthiophene is quite planar.[173] Synthetically this was achieved by flanking the isoindigo monomer with

thiophene, alkylated in the β position for solubility, and copolymerised with thiophene to give the polymer **P3TI** (**Figure 3.5**).

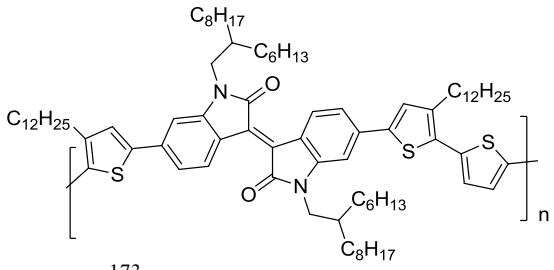


Figure 3.5: Structure of **P3TI**[173]

Whilst the alkyl side chains situated on the flanking thiophene enhanced the solubility of the polymer allowing high molecular weighs of up to Mn 73 kDa to be obtained, they also lower the band gap as a result of the electron donating alkyl chain raising the HOMO energy level. This improved the photocurrent giving a large J_{sc} of 13.1 $mAcm^{-2}$ and a record PCE of 6.3% at the time. However, the V_{oc} dropped to 0.70 V due to the decrease in the offset between the HOMO of the donor polymer and the LUMO of the $PC_{71}BM$ acceptor. Thus to improve the performance of isoindigo polymers it is important to obtain a larger V_{oc} whilst maintaining the J_{sc} and solubility parameters.

3.2 Furan Flanked Isoindigo Based Polymers

The majority of the currently used polymers for organic electronics are based on building blocks that originate from non renewable feedstocks such as oil and coal. To make the production of OPVs and OFETs truly sustainable, one should aim to use bio renewable materials derived from plants. Isoindigo being derived from natural sources is a good start towards this goal, but as thiophene based electron donor units are derived from coal, reducing the use of thiophene within polymers would make them more eco-friendly.

Furan, being similar in structure to thiophene and being derived from corn is an ideal substitute. Along with being able to enhance solid state order through having high backbone coplanarity and short inter-ring bond lengths,[174, 175] furan has been shown to improve the solubility of polymers when compared to thiophene equivalents, with a recent example being the development of furan based DPP polymers.[176] This enables

less bulky solubilising groups to be used which in turn can promote closer polymer packing in blend films and thus lead to improved OPV device performance.[177] Furan is more electron rich than thiophene and so would be expected as a result to raise the HOMO energy level of a polymer in which thiophene is substituted for furan. However if as a result of the solubility enhancement that furan provides, the alkyl chains that are required in thiophene based polymers can be omitted, the lack of an electron donating alkyl chain on the furan will mean that the furan based polymer will have a lower HOMO energy compared to an alkyl thiophene based polymer. In turn this will enable the polymer to have a greater Voc.

3.2.1 Synthesis of furan flanked isoindigo monomer

The isoindigo core was synthesised in accordance to the method published by Wang et al.[172] Commercially available 6-bromooxindole (**3.1**) and 6-bromoisatin (**3.2**) were converted via acid catalysed aldol condensation and dehydration in refluxing acetic acid to give 6,6'-dibromoisoindigo (**3.3**) in 90% yield. No purification of the insoluble 6,6'-dibromoisoindigo (**3.3**) was required as it can be simply filtered out of the reaction mixture and washed. As it has been shown that longer alkyl chains attached to the isoindigo core increase solubility and thus improve polymer molecular weight[172] it was decided to use a slightly longer 2-octyl-1-dodecane alkyl chain. To synthesise the required halogenated alkyl chain, the method reported by Classon et al[178] was employed. This involved reacting 2-octyl-1-dodecanol (**3.4**) with triphenylphosphine, iodine and imidazole in DCM. The imidazole in this reaction is used to neutralise liberated halogen acids as well as enhance reactivity, to give 9-(iodomethyl)nonadecane (**3.5**) in 90% yield. N alkylation of 6,6'-dibromoisoindigo (**3.3**) with branched iodoalkane (**3.5**) using potassium carbonate to deprotonate the nitrogen of the 6,6'-dibromoisoindigo (**3.3**) gave the 6,6'-dibromoisoindigo derivative (**3.6**) in 55% yield after column chromatography. In parallel, furan (**3.7**) was mono lithiated using sec BuLi and N,N,N′,N′-Tetramethylethylenediamine (TMEDA) for increased reactivity and subsequently mono stannylated with trimethyl tin chloride to give furan-2-yltrimethylstannane (**3.8**) as an orange oil in 71% yield. Stille coupling of 6,6'-dibromoisoindigo derivative (**3.6**) and furan-2-yltrimethylstannane (**3.8**) using tetrakis(triphenylphosphine)palladium (0) gave 6,6'-difuranisoindigo (**3.9**) as a red solid in 65% yield. The dibrominated monomer (**3.10**) was obtained using NBS and

isolated using column chromatography in 36% yield. This yield was somewhat less than expected due to the reaction not having gone to full completion as a fair amount of mono brominated compound was recovered. However, unlike Ma et al[179] who encountered difficulties upon brominating isoindigo flanked with thiophene, no such difficulties arose. In the case of Ma et al[179] the bromination was not selective, as it was found that monobromo, dibromo and tribromo compounds were formed simultaneously. This meant that an extensive and long column had to be employed to separate the mixture resulting in a low yield of monomer. The explanation given for this is that the strong electron withdrawing effect of the isoindigo group reduced the electron cloud density on the α positions of the thiophene flanking units. This reduced electron density on the α positions means that this position is less favourable for electrophilic attack and thus makes the β position more susceptible to being brominated. However in the case of furan, furan is more electron rich than thiophene and so may counteract the electron withdrawing effect of the isoindigo. Thus no tribromo compounds were detected, meaning that the purification of the dibrominated monomer (**3.10**) was a lot easier.

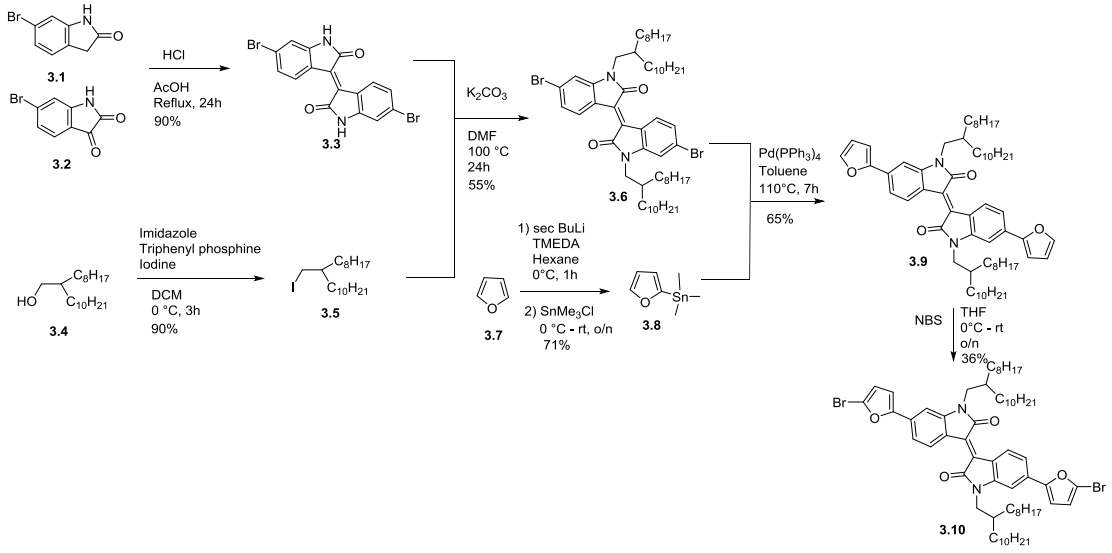


Figure 3.6: Synthesis of monomer **3.10**

3.2.2 Synthesis of furan flanked isoindigo based copolymers

The monomer was polymerised via Pd-catalysed Stille coupling with both 2,5-bis(trimethylstannyl)thiophene (**3.11**) and 2,5-bis(trimethylstannyl)thieno[3,2-

b]thiophene (**3.12**) to give copolymers **PFTFI** and **PFTTFI** respectively. These copolymers were both end capped with 2-trimethylstannyl thiophene (**3.13**) and 2-bromothiophene (**3.14**) to remove both tin and bromine moieties from the ends of the polymer chains to remove charge traps from the polymers[176, 180]. After precipitation into methanol, the polymers were purified via Soxhlet extraction in acetone, hexane and chloroform (CF). Glass Soxhlet thimbles were used for this to avoid the incorporation of cellulose into the polymers. **PFTTFI** being a higher molecular weight polymer required additional extraction with chlorobenzene (CB) and trichlorobenzene (TCB). The chloroform fraction for **PFTFI** and the chloroform, chlorobenzene and trichlorobenzene fractions for **PFTTFI** were each heated with sodium diethyldithiocarbamate trihydrate to remove residual palladium, which has been shown to be detrimental to device performance.[181] The polymers were finally re-precipitated into methanol and filtered to afford the novel dark green copolymers **PFTFI** and **PFTTFI**.

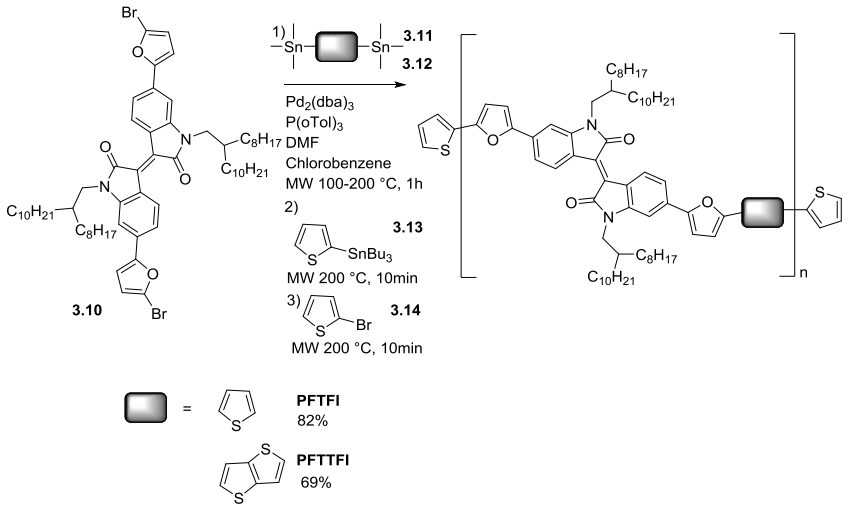


Figure 3.7: Synthesis of copolymers **PFTFI** and **PFTTFI**.

3.2.3 Physical properties of furan flanked isoindigo based polymers

The molecular weights of the polymers were measured by GPC calibrated against polystyrene standards. For the chloroform fraction of **PFTFI** the molecular weight was reasonable with the values obtained being M_n = 15.7 kDa, M_w = 40.6 kDa and a PDI of 2.58. For **PFTTFI** the values for the chloroform fraction were rather low with M_n = 6.8 kDa, M_w = 13.8 kDa and a PDI of 2.03. However the values for the

chlorobenzene fraction of **PFTTFI**, M_n = 29.1 kDa, M_w = 76.3 kDa, PDI= 2.61, and the trichlorobenzene fraction, M_n = 48.8 kDa, M_w = 71.4 kDa, PDI = 1.46 were considerably higher. The fact that the molecular weight of **PFTTFI** increases upon going from chloroform to chlorobenzene, a stronger solvent, shows that the polymer becomes less soluble as its molecular weight increases. This is evident from the fact that the even higher molecular weight trichlorobenzene fraction was practically insoluble as only a small amount was able to be dissolved in chlorobenzene for GPC analysis. The difference in solubility between **PFTFI** and **PFTTFI** can be attributed to the fact that thieno[3,2-*b*]thiophene is a larger unit than thiophene meaning that for a given polymer chain length there is less solubilising alkyl chain density along the polymer backbone.[182] In order to obtain a fair comparison between **PFTFI** and **PFTTFI** only the chlorobenzene fraction of **PFTTFI** was used in subsequent characterisation as this fraction of **PFTTFI** is closest to the **PFTFI** polymer in terms of molecular weight and PDI.

3.2.4 Optical properties of furan flanked isoindigo based polymers

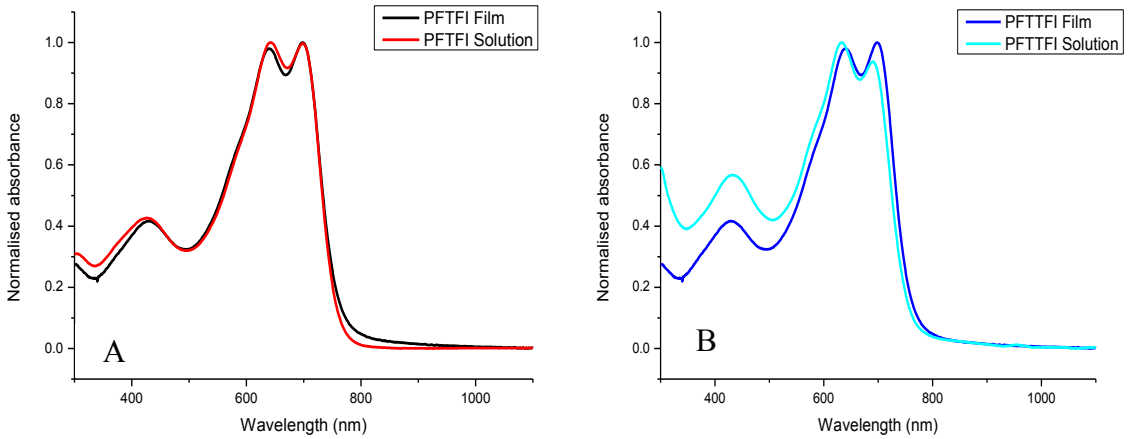


Figure 3.8: Solution (chlorobenzene at 25 ºC) and thin film UV-Vis absorption spectra of a) **PFTFI** and b) **PFTTFI**.

Figure 3.8 shows the UV-Vis absorption spectra of **PFTFI** and **PFTTFI** in dilute chlorobenzene solution at 25 ºC and in thin film spun from chlorobenzene solution (5 mg/mL, 1000 rpm, 1 min). Both copolymers show two absorption bands and an aggregation peak for both the solution and thin film spectra. The low energy band at

642nm and 640 nm for **PFTFI** solution and thin film respectively and 632nm and 640 nm for **PFTTFI** solution and thin film respectively correspond to the intermolecular charge transfer band of the electron donating units to the electron accepting isoindigo core. The high energy band at 426 nm and 429 nm for **PFTFI** solution and film respectively and 433 nm and 429 nm for **PFTTFI** solution and film respectively corresponds to the π–π* transition. In general it is expected that the polymer in a thin film should be more ordered due to π-π stacking interactions between neighbouring conjugated polymer chains leading to a bathochromic shift (red shift) going from solution to thin film, as seen for **PFTTFI**. However the 2 nm hypsochromic shift (blue shift) on going from solution to thin film for **PFTFI** shows that this is not always the case. This effect has been seen before in a study on the variation of side chain length on isoindigo units, in which longer side chains retarded intermolecular π-π interactions in solid state leading to a hypsochromic shift in absorption.[183] As the side chains are both the same length for **PFTFI** and **PFTTFI** the difference in behaviour can only be explained in terms of side chain density, with the greater side chain density for a given polymer chain length for **PFTFI** having a greater effect on the spatial arrangement of the copolymers, which retards intermolecular π-π interactions and thus leads to the hypsochromic shift. From looking at the absorption onsets of the thin film spectra, 765 nm and 760 nm for **PFTFI** and **PFTTFI** respectively, it can be calculated that the bandgaps are 1.62 eV and 1.63 eV for **PFTFI** and **PFTTFI** respectively. The hypsochromic shift of **PFTTFI** with respect to **PFTFI** can be attributed to the fact that thieno[3,2-*b*]thiophene is more aromatic than thiophene and thus shows less quinoidal character which in turn leads to the greater bandgap.

In both the solution and thin films for both of the copolymers an absorption at 699 nm (690 nm for **PFTTFI** solution) can be seen which can be attributed to aggregation. To show this temperature dependant UV-Vis measurements of **PFTFI** and **PFTTFI** in chlorobenzene were taken. **Figure 3.9** shows that as the polymer cools from 80 °C to 20 °C the molar absorption coefficient increases as the absorption maxima gradually red shift towards 642 nm and 632 nm for **PFTFI** and **PFTTFI** respectively. The red shift can be explained in terms of solution aggregation causing polymer backbones to become less twisted and thus more conjugated. The appearance of a completely new peak at 699 nm and 690 nm, for **PFTFI** and **PFTTFI** respectively, indicates the

occurrence of solution aggregation. It should be noted that due to a lack of **PFTTFI** an old solution of **PFTTFI** was used for the temperature dependant UV-Vis measurement. This explains why the absorption profile of the solution spectra of **PFTTFI** in **Figure 3.9 b)** appears to be somewhat either degraded or shows the formation of nanowires[184] compared to the absorption profile seen in **Figure 3.8 b)**. However, despite the solution degradation/ nanowire formation the same trend in aggregation can be observed for **PFTTFI** as **PFTFI**.

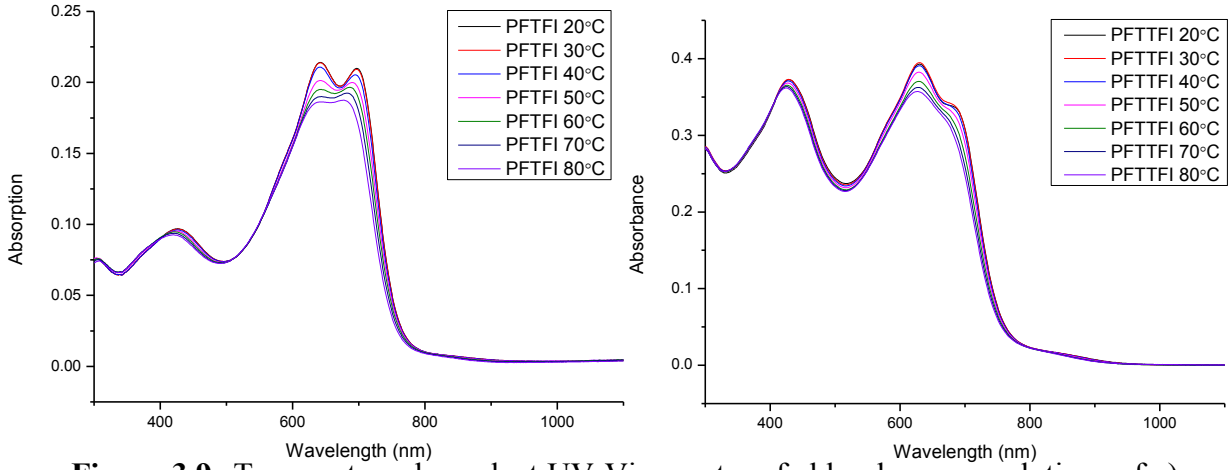


Figure 3.9: Temperature dependant UV-Vis spectra of chlorobenzene solutions of a) **PFTFI** and b) **PFTTFI**.

The molar extinction coefficients for the two polymers were also measured. To do this, solutions of known concentration were made by accurately weighing out a sample of polymer and dissolving it in a known volume of chlorobenzene. The concentration of the solution was calculated using equation 13:

$$c = \frac{(m/M)}{V} \qquad \textbf{(13)}$$

where c is the concentration, m is the mass of the polymer sample, M is the molecular weight of the donor and acceptor repeat unit and V is the volume of the solution. Next the absorbance of the polymers was measured by UV-Vis and plots of absorbance verses concentration shown in **Figure 3.10** were plotted.

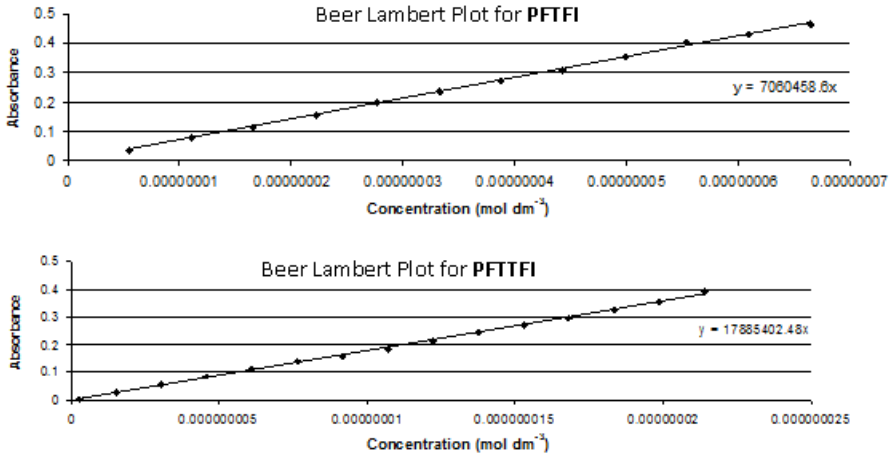


Figure 3.10: Beer Lambert plots of absorbance verses concentration for **PFTFI** (top) and **PFTTFI** (bottom)

Using the Beer Lambert Law, equation 14;

$$A = \varepsilon l c \qquad (14)$$

where A is the absorbance, ε is the molar extinction coefficient, l is the path length and c is the concentration, the molar extinction coefficients for **PFTFI** and **PFTTFI** can be calculated as 7×10^5 $M^{-1}cm^{-1}$ and 1×10^6 $M^{-1}cm^{-1}$ respectively. It is interesting to note that the molar extinction coefficient of **PFTTFI** is 1.5 times greater than **PFTFI**. This could be due to the fact that the thieno[3,2-*b*]thiophene in **PFTTFI** has more π electrons than thiophene and thus more light can be absorbed.

3.2.5 Energy levels of furan flanked isoindigo based polymers

The HOMO energy levels of **PFTFI** and **PFTTFI** were measured by PESA (photoelectron spectroscopy in air) and found to be -5.42 eV and -5.41 eV respectively in relation to the vacuum energy level. The fact that the HOMO energy level for **PFTTFI** is 0.01 eV higher than **PFTFI** is due to the more electron rich nature of thieno[3,2-*b*]thiophene. Using the optical bandgaps, estimated from the absorption onset of the thin film UV-Vis spectrums the LUMO energy levels were calculated to be -3.80 eV and -3.78 eV for **PFTFI** and **PFTTFI** respectively with respect to the vacuum energy level. The fact that the LUMO of **PFTFI** is 0.02 eV lower than **PFTTFI** is due to the fact that thiophene is less aromatic than thieno[3,2-*b*]thiophene and thus shows greater quinoidal character which in turn leads to the lower band gap.

Quantum chemical calculations of the energy levels and band gaps of **PFTFI** and **PFTTFI** were performed using density functional theory (DFT) with Gaussian 09, in accordance to literature precedent.[185] The B3LYP/6-31G* functional and basis set was used to calculate optimised ground state geometries, from which the frontier orbital energies were deduced. Methylated trimers were used an approximation to the polymers as full alkyl chains or using more repeat units in the calculation would have been computationally expensive and would have only marginally increased the accuracy of the calculation. To calculate the optical band gaps, non adiabatic linear response calculations using time dependant density functional theory in Gaussian 09 were carried out. This involved using the same B3LYP/6-31G* functional and basis set as before. However as these calculations are carried out on the ground state geometries and not the excited state geometries these can only be regarded as an approximation to the absorption of the materials. From these calculations the HOMO energy levels were found to be -4.759 eV and -4.755 eV for **PFTFI** and **PFTTFI** respectively. The optical band gaps were found to be 1.592 eV and 1.599 eV for **PFTFI** and **PFTTFI** respectively, thus giving LUMO values of -3.167 eV and -3.156 eV for **PFTFI** and **PFTTFI** respectively. From the values obtained it can be seen that the calculated HOMO energy level of **PFTFI** is lower than **PFTTFI**, a trend that correlates well with the experimental HOMO energy levels derived from PESA, and is due to the fact that thiophene is less electron rich than thieno[3,2-*b*]thiophene. The calculated optical band gap of **PFTFI** is smaller than **PFTTFI**, which also corresponds well with the trend seen in the experimentally determined optical band gaps. This is due to the fact that for **PFTFI** as thiophene is less aromatic than thieno[3,2-*b*]thiophene the polymer can exhibit a greater quinoidal effect and thus have a lower band gap. On closer inspection of the actual values obtained in these calculations it can be seen that the values for the optical band gaps in the region of 1.59 eV are very close to the experimental band gaps of 1.62 -1.63 eV. However the values for the HOMO energy levels are off by 0.661 eV and 0.655 eV for **PFTFI** and **PFTTFI** respectively as seen in **Figure 3.11**.

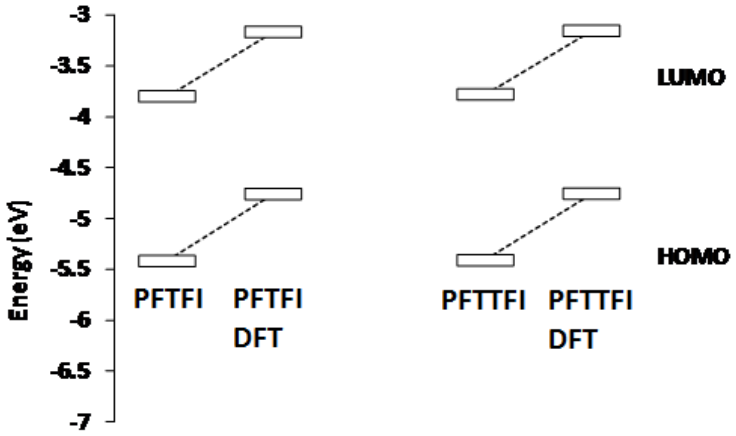


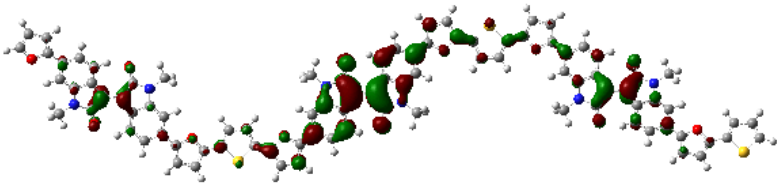
Figure 3.11: Experimental and calculated HOMO and LUMO energy levels of **PFTFI** and **PFTTFI**.

The large systematic shift in energy levels from going from experimental values to DFT calculations can be explained by the fact that the DFT calculations are carried out in vacuum and completely ignore dielectric solvation in the solid state. For this reason it is also important to calculate the LUMO energy levels using the same DFT methods to keep the errors consistent so that accurate trends can be observed.[185]

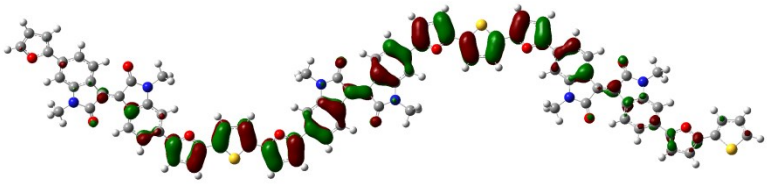
The molecular orbitals of the HOMO and LUMO of the two polymers can be visualised as seen in **Figure 3.12**.

PFTFI

LUMO

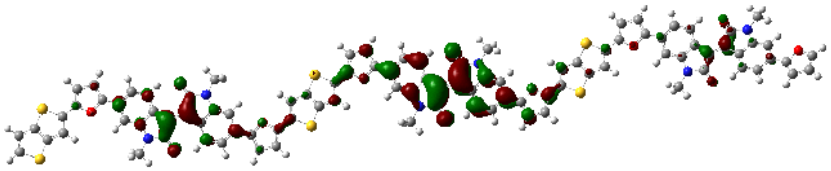


HOMO



PFTTFI

LUMO



HOMO

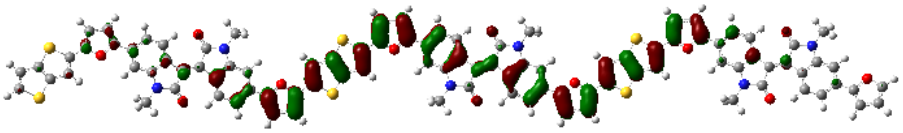


Figure 3.12: HOMO and LUMO distributions for the minimum energy conformations of methyl substituted **PFTFI** and **PFTTFI** trimers optimised with Gaussian at the B3LYP/6-31G* level.

It can be seen that the HOMO wave function is delocalised along the whole of the polymer backbone for both polymers, which should be good for hole transport. The LUMO however is mostly localised on the isoindigo units for both polymers, which means that this should facilitate efficient charge separation, a trait required for good device efficiencies. From looking at the backbone curvature of the two polymers it can be seen that they both form a sine wave structure, although for **PFTTFI** the frequency of the sine wave is double that of **PFTFI**. This doesn't seem to have any effect on the delocalisation but may have an impact on the molecular packing between neighbouring backbones.

3.2.6 DSC of furan flanked isoindigo based polymers

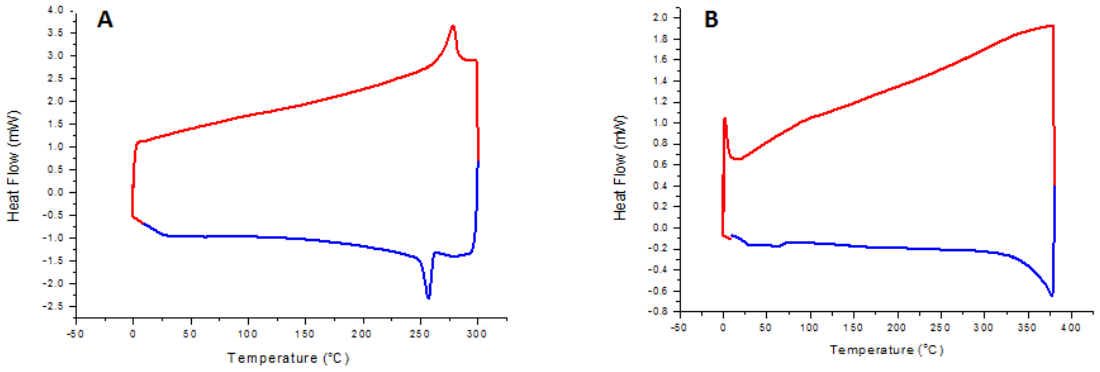


Figure 3.13: DSC curves of **PFTFI** (A) and **PFTTFI** (B). The red lines indicate heating while the blue lines indicate cooling. Positive peaks are endothermic events and negative peaks are exothermic events.

The molecular packing of the polymers was probed using differential scanning calorimetry (DSC). As expected, **PFTFI** showed a melt peak at 271 °C and its corresponding crystallization on cooling at 261 °C (**Figure 3.13 a**). The enthalpy of melt and crystallization were both 7.7 J/g indicating the reversibility of the phase transition. The fact that this polymer exhibits such a defined melt and crystallisation indicates that this polymer is very crystalline, indicating good π-π stacking which should be favourable for charge transport. By comparison **PFTTFI** (**Figure 3.13 b**) showed no transitions at all, suggesting a lack of molecular order in the polymer. However, it is impossible to definitively draw a conclusion based solely on DSC data as the shape of the DSC curve can be affected by factors such as sample preparation and scan rate. For this particular sample, being a fibrous polymer it is possible that the polymer sample didn't completely cover the bottom of the DSC pan and thus heat transfer to the polymer was ineffective meaning that no phase transitions were observed. Thus it is pertinent to perform a second scan cycle so that once the polymer has melted over the course of the first cycle it will cover the base of the DSC pan allowing the phase transitions to be detected on the second cycle. It is important to note that the first cycle as well as yielding information about impurities such as residual solvent can also tell us about the kinetics of the polymer. For instance a polymer that has been heated beyond its melting point and then cooled quickly can become crystallised not at its thermodynamic minimum but at a kinetic minimum thus giving rise to different enthalpies of melting and crystallisation. However these effects were not observed for the first or second cycles of **PFTTFI** and so an alternative

technique such as X-ray diffraction (XRD) must be employed to ascertain something about the polymer's structure.

3.2.7 XRD of furan flanked isoindigo based polymers

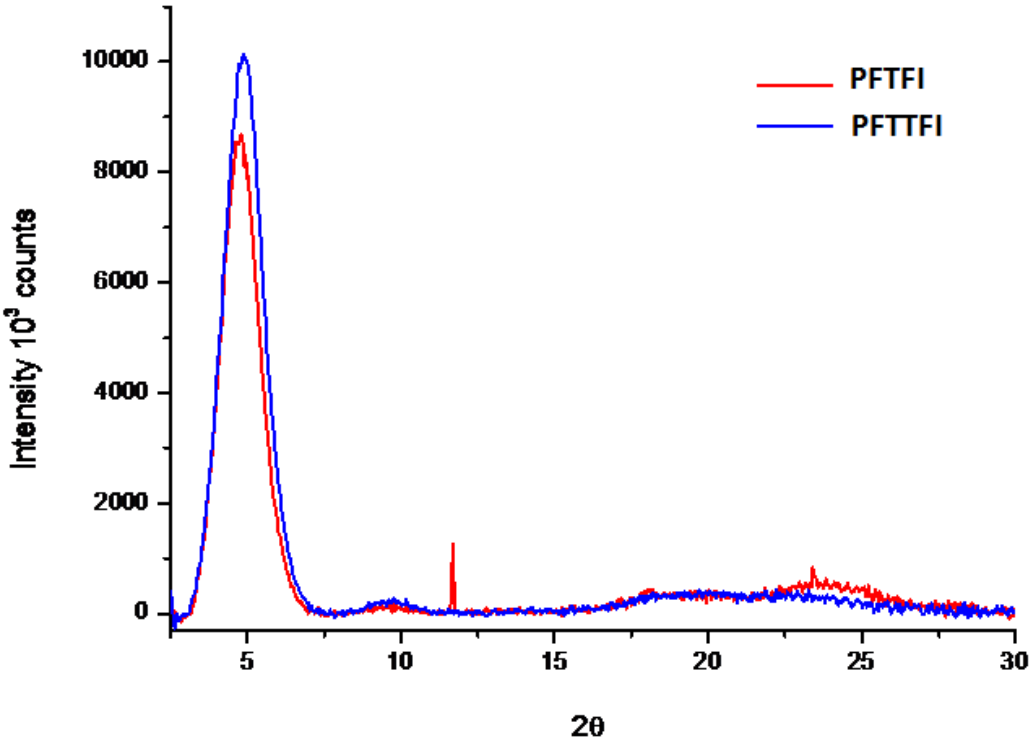


Figure 3.14: X-ray diffraction patterns of drop cast thin films of **PFTFI** (red) and **PFTTFI** (blue).

XRD samples were prepared by dissolving 10 mg/mL of **PFTFI** and **PFTTFI** in chlorobenzene and drop casting the solutions onto silicon wafers to form thin films, which were subsequently annealed at 100 ºC for 10 min. **Figure 3.14** shows the XRD spectra obtained and indicates that both copolymers are crystalline, with the 100 peak, assigned in accordance to literature precedent,[186] clearly seen. This indicates that in a neat film **PFTFI** and **PFTTFI** adopt a lamellar type packing motif, with lamella d – spacings calculated to be 18.4 Å and 18.1 Å respectively. The greater lamella spacing for **PFTFI** is further proof of the effect of greater side chain density affecting the spatial arrangement between polymer chains, as seen previously in the UV-Vis spectra.

3.2.8 OFET device performance of furan flanked isoindigo based polymers

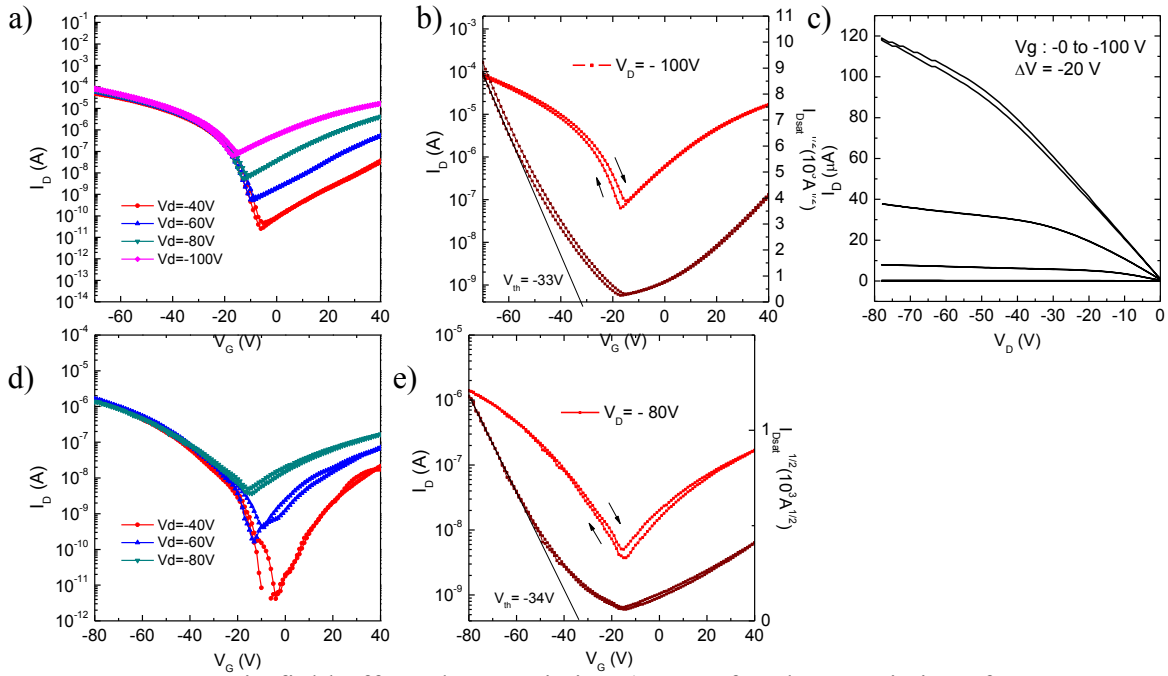


Figure 3.15: Organic field effect characteristics a) Transfer characteristics of **PFTFI** at various drain voltages. b) Transfer characteristics of **PFTFI** at -100V. c) Output characteristics of **PFTFI**. d) Transfer characteristics of **PFTTFI** at various drain voltages. e) Transfer characteristics of **PFTTFI** at -80V.

Top-gate, bottom-contact organic field effect transistors (OFETs) were fabricated on glass with Au-PFBT electrodes, a CYTOP^{TM} dielectric and an Al gate. The channel length was 20 µm and the channel width was 1000 µm. Polymer films were spin cast at 2000 rpm from dichlorobenzene solution and annealed at 200 °C for 10 min. **Figure 3.15** shows the OFET characteristics of **PFTFI** and **PFTTFI**. From looking at the transfer characteristics of **PFTFI** it can be seen that the polymer exhibits ambipolar behaviour with saturation hole mobilities of 0.423 cm^2/Vs and electron mobilities of 0.079 cm^2/Vs. The threshold voltage for **PFTFI** was found to be -33V while the on/off ratio at -40 V was 10^5. **PFTTFI** also showed ambipolar behaviour with saturation hole mobilities of 0.027 cm^2/Vs and electron mobilities of 0.002 cm^2/Vs. Despite the fact that the threshold voltage for **PFTTFI** (-34 V) was comparable to **PFTFI** as well as the on/off ratio being the same order of magnitude (10^5), it is clear from the mobilities that **PFTTFI** shows considerably lower device performance. This poor performance is due to the fact that the more insoluble **PFTTFI** was harder to process into uniform films. Unfortunately, no output

measurements for **PFTTFI** were performed so it is not possible to make a full comparison of OFET performance between the two polymers.

3.2.9 OPV device performance of furan flanked isoindigo based polymers

Bulk heterojunction solar cells with an indium tin oxide (ITO) / poly(3,4-ethylenedioxythiophene):poly(styrene sulfonic acid) (PEDOT:PSS) / **PFTFI** or **PFTTFI** : $PC_{70}BM$ / LiF / Al structure were fabricated, with the polymer ; fullerene layer being spin cast from chlorobenzene (CB) and mixed chloroform (CF) / ortho dichlorobenzene (ODCB) solvents. **Figure 3.16** shows the current-voltage (*J-V*) characteristics and external quantum efficiency (EQE) of the solar cell devices that were initially fabricated from **PFTFI**.

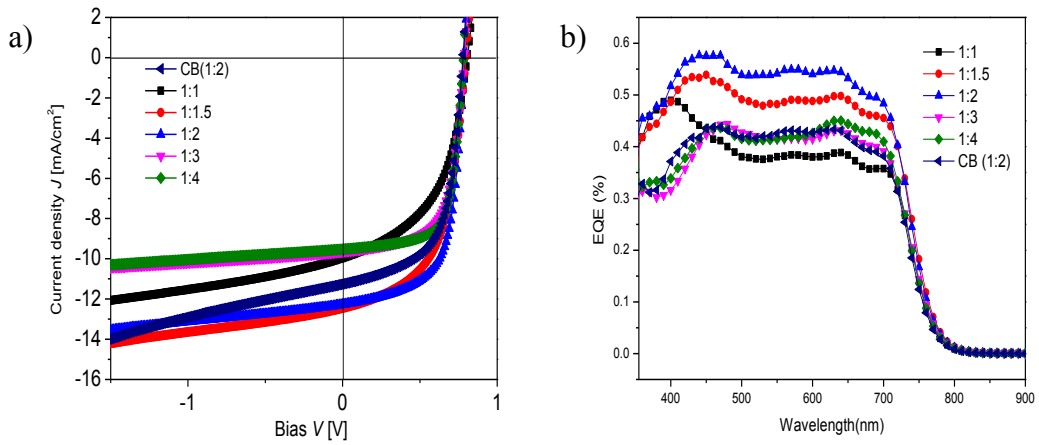


Figure 3.16: Initial OPV device data from **PFTFI** a) J-V b) EQE

The Jsc and PCE values obtained from the *J-V* characteristics for **PFTFI** (**Figure 3.16 a**) were corrected using the EQE (**Figure 3.16 b**) to give the values shown in **Table 3.1**.

PFTFI: $PC_{70}BM$ ratio	Solvent	Area (cm^2)	Active layer thickness (nm)	V_{oc} (V)	J_{sc} (mA/cm^2)	FF	PCE (%)
1:2	CB	0.36	90	0.78	9.45	0.61	4.5
1:1	CF:ODCB 9:1	0.36	90	0.81	9.05	0.50	3.67
1:1.15	CF:ODCB 9:1	0.36	90	0.80	10.8	0.57	5.16
1:2	CF:ODCB 9:1	0.09	90	0.79	12.24	0.65	6.29
1:3	CF:ODCB 9:1	0.09	90	0.79	9.43	0.65	4.84
1:4	CF:ODCB 9:1	0.09	107	0.76	9.6	0.70	5.23

Table 3.1: Initial device performance of **PFTFI**.

The first device produced using a 1:2 blend of **PFTFI** : $PC_{70}BM$ spin cast from chlorobenzene showed a favourable PCE of 4.5%. This was then methodically optimised using a CF:ODCB solvent mixture of 9:1, which has been shown to enhance polymer aggregation thereby causing a red shift in absorption and thus lead to an improved J_{sc}.[187] The device utilising a 1:1 blend of **PFTFI** : $PC_{70}BM$ shows the lowest J_{sc}, FF and PCE. This is as a result of ineffective charge extraction due to low fullerene loading. Upon slightly increasing the ratio of **PFTFI** : $PC_{70}BM$ to 1:1.15 and then to 1:2 both the J_{sc} and FF increased thus giving rise to an increased PCE of 6.29%. This is reflected in the stepwise increase in the EQE absorption across the wavelength range from 350 - 730 nm, which is an indication of greater exciton dissociation and charge collection. However upon increasing the fullerene loading to blend ratios of 1:3 and 1:4 there is a significant drop in the EQE leading to PCEs of 4.84% and 5.23% respectively. This is attributed to increased fullerene aggregation, as seen from atomic force microscopy (AFM) data (see section **3.2.10**) which causes charge traps thus hindering charge percolation to the electrodes.

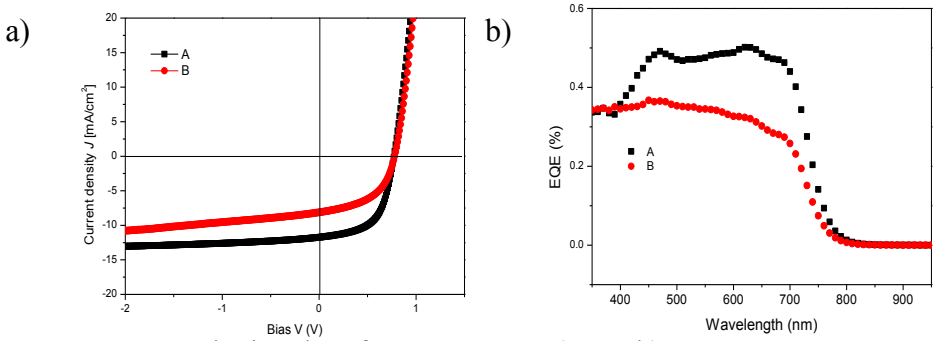


Figure 3.17: OPV device data from **PFTTFI** a) J-V b) EQE

Figure 3.17 shows the J-V characteristics and EQE of the solar cell devices fabricated from **PFTTFI** : $PC_{70}BM$ 1:2 blends. The J_{sc} and PCE values obtained from the *J-V*

characteristics for **PFTTFI** (**Figure 3.17 a**) were corrected using the EQE (**Figure 3.17 b**) to give the values shown in **Table 3.2**.

Device	Solvent	Area (cm^2)	Active layer thickness (nm)	V_{oc} (V)	J_{sc} (mA/cm^2)	FF	PCE (%)
A	CF:ODCB 9:1	0.16	100	0.77	10.64	0.58	4.75
B	CF:ODCB 1:9	0.09	100	0.78	7.8	0.50	3.0

Table 3.2: Device performance of **PFTTFI**.

Device A based on the initially optimised conditions for **PFTFI** gave a PCE of 4.75%. Due to the lower solubility of **PFTTFI** an alternative solvent system with greater ODCB content (device B) was tested. However despite the marginal improvement in V_{oc} this failed to improve the PCE as a result of the reduction in J_{sc}.

As favourable initial results were obtained for the **PFTFI** OPV devices, further optimisation was carried out to see if reproducible results could be obtained. The optimised device *J-V* and EQE spectra are shown in **Figure 3.18**.

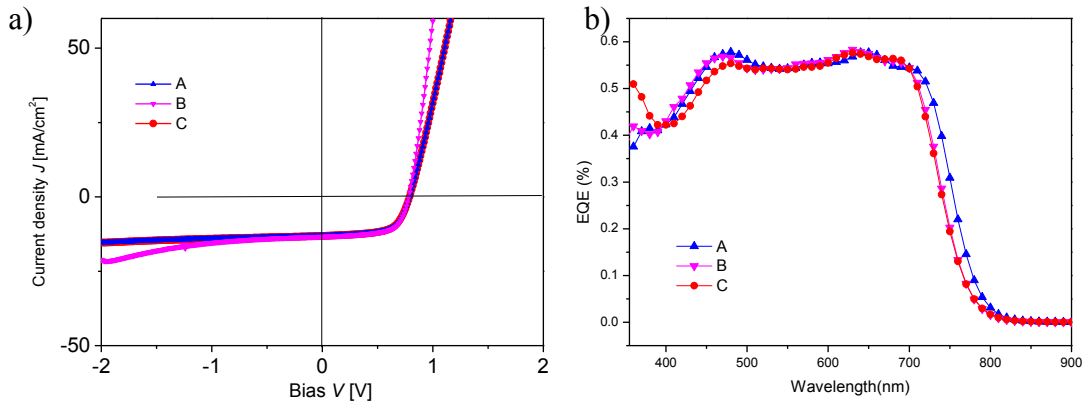


Figure 3.18: Optimised OPV device data from **PFTFI** a) J-V b) EQE

The J_{sc} and PCE values obtained from the *J-V* characteristics for **PFTFI** (**Figure 3.18 a**) were corrected using the EQE (**Figure 3.18 b**) to give the values shown in **Table 3.3**.

Device	Concentration (mg/mL)	Spin speed (rpm)	Thickness (nm)	Area (cm^2)	V_{oc}	J_{sc}	FF	PCE (%)
A	18	2500	90	0.16	0.79	12.69	0.64	6.42
B	25	3000	90	0.09	0.78	12.66	0.65	6.42
C	25	2000	130	0.09	0.77	12.45	0.67	6.42

Table 3.3: Device performance of fully optimised devices of **PFTFI**.

The corrected PCE values of 6.42% show that despite slight changes in the concentration of **PFTFI** used, as well as changes in spin speed, device thickness and device area the same overall PCE could be obtained. This shows that the processing parameters do not have to be entirely the same to achieve high performance, which is encouraging in terms of device to device uniformity and reproducibility required for large scale manufacturing.

3.2.10 Atomic force microscopy (AFM) characterisation of blend films

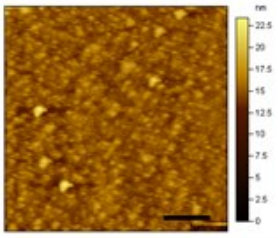
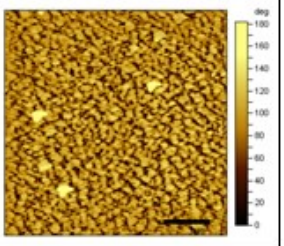
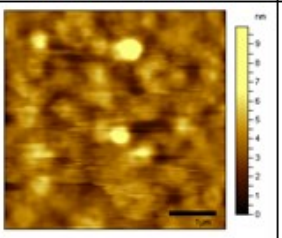
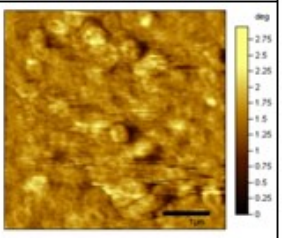
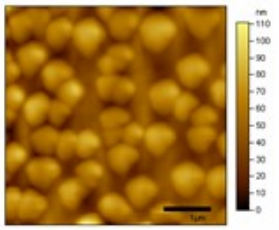
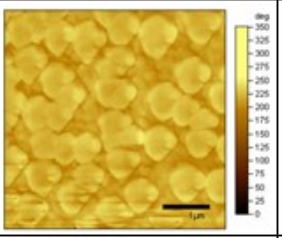
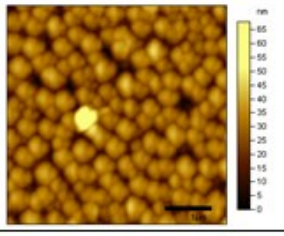
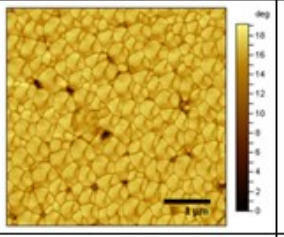
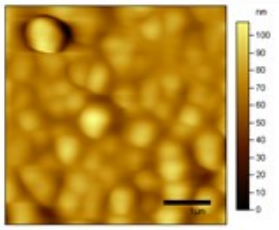
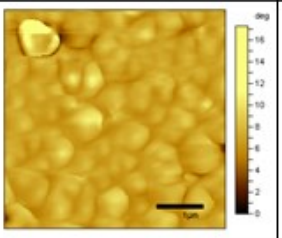
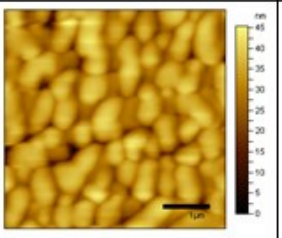
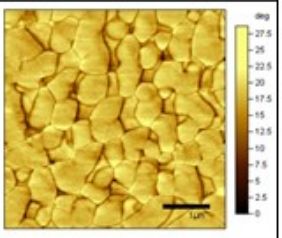
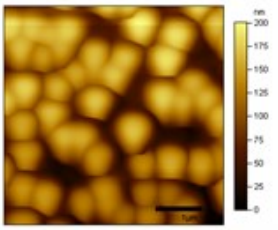
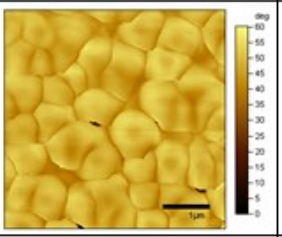
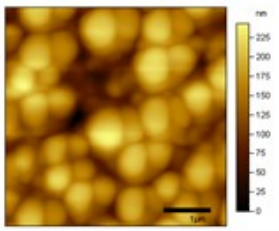
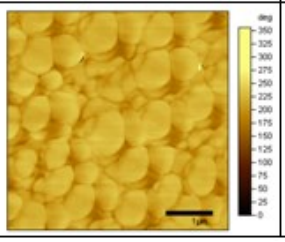
Polymer: $PC_{70}BM$	**PFTFI** Tapping Mode	**PFTFI** Phase Mode	**PFTTFI** Tapping Mode	**PFTTFI** Phase Mode
Pristine				
1:1				
1:1.5				
1:2				
1:3				
1:4				

Table 3.4: Polymer: $PC_{70}BM$ blends for AFMs prepared from chlorobenzene solution and spin coated onto cleaned glass substrates. The dimensions are 5 ×5 μm and the scale bars are 1 μm.

Due to not having the actual OPV devices to perform the AFMs on, a model system on glass was devised. Although this is not an optimal reproduction of the OPV devices produced in this research, it can be seen from this model system that for **PFTFI** the 1:1 ratio of **PFTFI**:$PC_{70}BM$ shows large separated polymer and fullerene domains leading to poor change separation and percolation pathways as illustrated by the poor device performance. Increasing the fullerene loading to 1:1.15 improves the mixing leading to the PCE increasing to 5.16%. Upon a further increase in fullerene loading to 1:2 it can be seen that there is almost homogeneous mixing of polymer and fullerene domains leading to the high efficiencies of over 6%. Increasing the fullerene loading to give the 1:3 and 1:4 blends is detrimental to device performance as seen by the greater segregation of domains, more clearly illustrated in the **PFTFI** phase AFMs. This is due to greater fullerene aggregation, which leads to more charge traps and thus a lower photocurrent. As for **PFTTFI** it can be seen that optimal blending of polymer and fullerene has not been achieved using a 1:2 blend ratio which explains the lower PCE obtained.

3.2.11 Conclusion

In conclusion, two new polymers have been synthesised which are almost isostructural to **P3T1** by incorporating furan flanking groups rather than alkyl thiophene flanking groups around an isoindigo core. These 2 novel materials display contrasting UV-Vis absorption spectra which can be explained in terms of their alkyl chain density per unit length. DSC (for **PFTFI**) and XRD indicate the crystalline nature of these polymers. Solar cell devices fabricated using **PFTFI** gave significantly increased open circuit voltages in comparison to **P3T1** at the cost of a slightly decreased short circuit current as a result of the wider band gap. However due to the increased open circuit voltage the overall PCE for **PFTFI** was marginally higher than for **P3T1** indicating that furan is a viable environmentally friendly replacement for alkyl thiophene in this system.

3.3 Thiophene Isoindigo

The success of isoindigo as a viable alternative to DPP lies in the fact that like DPP it contains two electron withdrawing units which assist in molecular hybridisation and thus lower the band gap of the polymer. Additionally as the pyrrole functionality within these units is strongly polar, intermolecular interactions are facilitated allowing for enhanced charge transport. Synthetically both DPP and isoindigo are able to be functionalised with solubilising alkyl chains on the nitrogen atoms during the final stages of synthesis allowing the polymers to be soluble. However, unlike DPP which typically contains peripheral thiophene units which can assist in planarising the polymer backbone, isoindigo with its peripheral phenyl units may exhibit a more twisted backbone. The twisted backbone for isoindigo can occur when there is steric overlap between the substituents on the carbon atom adjacent to the bonded carbon atom. So for example when isoindigo is copolymerised with phenyl the two alpha hydrogens to the carbon coupling the two ring systems will sterically hinder the rings from being coplanar. This steric effect will not only increase the band gap but also repress intermolecular π-π interactions between polymer chains meaning that the polymer will show more amorphous character. By changing the phenyl in isoindigo to a thiophene unit it is hoped that the steric effect between neighbouring units will be minimised thus reducing the out of plain twist between them. Additionally as thiophene is aromatically less stable than phenyl, the bond character between neighbouring units will be more sp^2 like, due to the quinoidal effect, which thus promotes coplanarity. This should allow for more crystalline polymers, as a result of better intermolecular π-π interactions, to be synthesised, which will exhibit lower band gaps.

3.3.1 Synthesis of thiophene isoindigo monomer

The thiophene isoindigo monomer was synthesised in collaboration with Dr Raja Shahid Ashraf.[188] For making the monomer with a branched alkyl chain the first step was to convert 2-octyldodecan-1-ol (**3.15**) to an azide (**3.19**) using a Mitsunobu reaction involving the use of diphenyl phosphorazidate (**3.16**), diisopropyl azodicarboxylate (DIAD) (**3.17**) and triphenyl phosphine (PPh_3). Using lithium

aluminium hydride ($LiAlH_4$) the resultant azide was reduced to an amide in 66% yield, as shown in **Figure 3.19**.

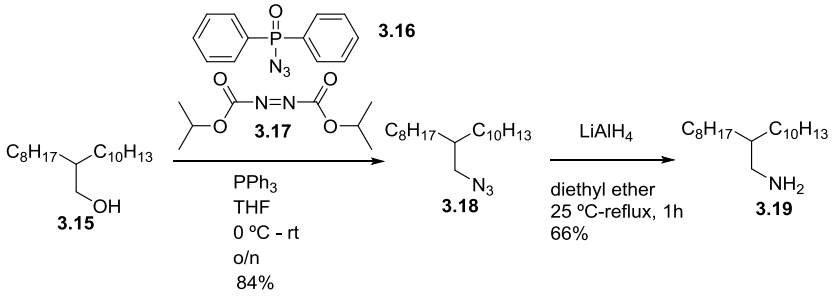


Figure 3.19: Synthesis of branched amine (**3.19**)

Using either the branched amine (**3.19**) or commercially available hexadecylamine, 3-bromothiophene (**3.20**) was nucleophilically attacked in a copper catalysed Ullmann coupling reaction with one of the amines to afford thiophene amine (**3.21**). These thiophene amines (**3.21**) were fairly unstable if left for long periods of time in air, and so as soon as they had been isolated via flash chromatography were immediately taken on the next step. Cyclising the thiophene amine (**3.21**) with oxalyl chloride and triethyl amine (Et_3N) via a Friedel Crafts reaction gave the cyclised thiophene (**3.22**) as either an orange oil for the branched alkyl chain or an orange solid for the linear alkyl chain, **Figure 3.20**. At first these proved very tricky to purify as flash chromatography using hexane and ethyl acetate, a procedure devised by Dr Ashraf, resulted in a large amount of black impurities eluting at roughly the same rf as the product, which resulted in a reduced yield. By changing the eluting solvent to neat DCM the yield was substantially increased by 27%.

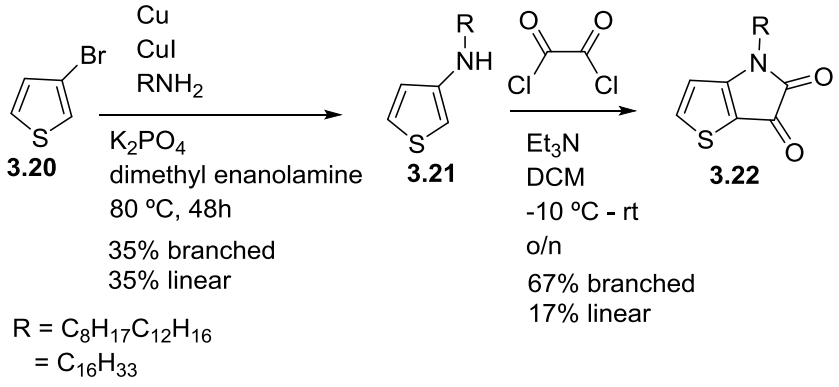


Figure 3.20: Synthesis of cyclised thiophene (**3.21**)

At this stage Dr Ashraf attempted a number of routes to dimerise the cyclised thiophene (**3.22**). The initial route (Route 1) involved reducing one of the keto groups

using a Wolff Kishner reduction to give the product (**3.23**) and subsequently using an acid catalysed condensation reaction to dimerise the reactant (**3.22**) and the product (**3.23**) of the previous reaction together. However as this route proved to be low yielding and the target compound was hard to purify, two other routes, Route 2 and Route 3 involving the direct dimerisation of the cyclised thiophene (**3.22**) in one step were also evaluated. As both routes 2 and 3 gave almost quantitative yields it was decided to carry on with route 3 due to the fact that as well as giving good yields it also takes place under mild conditions. The 3 routes are shown in **Figure 3.21**.

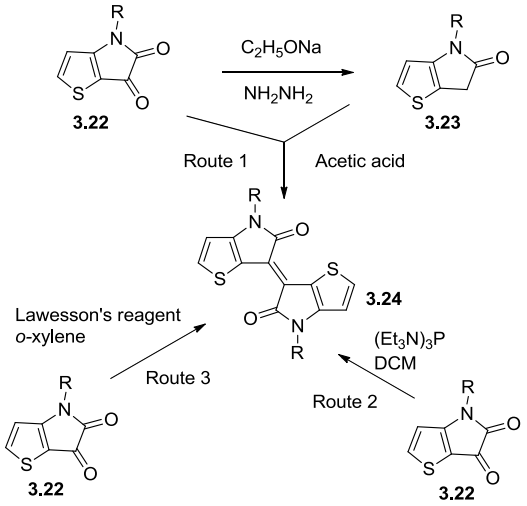


Figure 3.21: Various routes evaluated for the synthesis of thiophene isoindigo (**3.24**)

Thus dimerisation of cyclised thiophene (**3.22**) with Lawesson's reagent gave thiophene isoindigo (**3.24**) after a 2 h reaction in xylene at 60 ºC. Bromination of thiophene isoindigo (**3.24**) with NBS afforded the final monomer (**3.25**) in 75% yield for the branched chain monomer and a poor 20% yield for the linear chain monomer as it was considerably harder to purify, **Figure 3.22.**

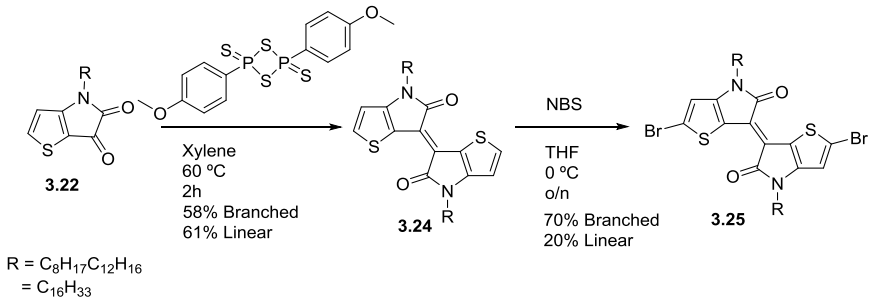


Figure 3.22: Synthesis of thiophene isoindigo monomer (**3.25**)

3.3.2 Synthesis of IGT-BT copolymer

To produce a very low band gap polymer for transistor applications it was decided to copolymerise the branched chain thiophene isoindigo monomer (**3.25**) with an electron withdrawing benzothiadiazole (BT) unit. Using Suzuki cross coupling the two monomers, thiophene isoindigo monomer (**3.25**) and 4,7-bis(4,4,5,5-tetramethyl-1,3,2-dioxaborolan-2-yl)benzo[c][1,2,5]thiadiazole (**3.26**) were polymerised to give the **IGT-BT** copolymer, which was precipitated into methanol, filtered and purified via Soxhlet extraction in methanol, acetone, hexane and chloroform to remove catalytic impurities and short chain oligomers. The chloroform fraction was concentrated down and the polymer was precipitated into methanol before being filtered and dried.

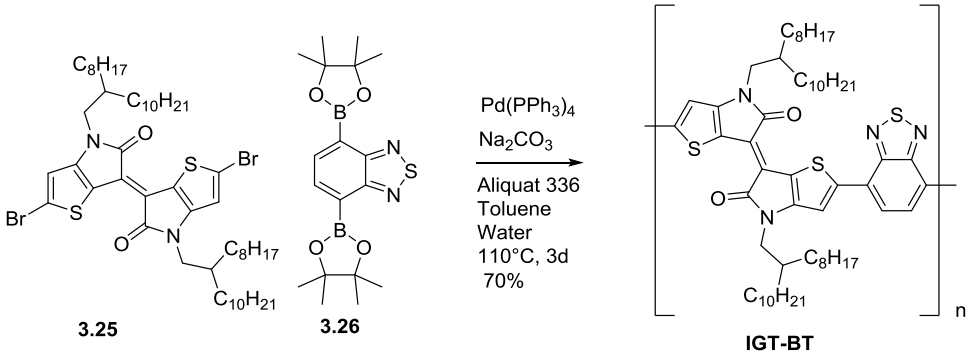


Figure 3.23: Synthesis of **IGT-BT** copolymer.

3.3.3 Properties of the IGT-BT copolymer

The **IGT-BT** copolymer was soluble in a variety of solvents namely chloroform, tetrahydrofuran (THF), toluene and chlorobenzene. Using gel permeation chromatography (GPC), calibrated against polystyrene standards, running on chlorobenzene at 80 ºC, the molecular weight of the copolymer was found to be M_n = 40000 g/mol, Mw = 90000 g/mol giving a PDI of 2.25 and a degree of polymerisation of 41 units, which is well above the persistence length of the polymer chain meaning that the lowest band gap for this polymer system can be attained.

3.3.4 Optical properties of IGT-BT copolymer

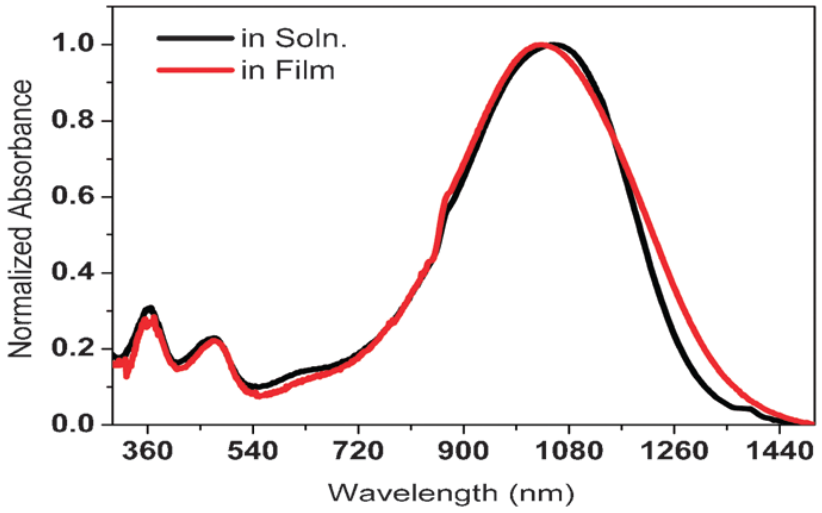


Figure 3.24: UV-Vis absorption spectra of IGT-BT copolymer in chlorobenzene solution and in thin film (spin coated from chlorobenzene).

The optical absorption spectra of both the polymer solution and thin film show remarkably long wavelength maxima. It is interesting to note that the lambda max of the thin film at 1035 nm is slightly blue shifted when compared to the corresponding lambda max of the solution at 1054 nm. From the absorption onset of the thin film at 1370 nm the optical band gap of the polymer can be determined to be 0.92 eV, which is 0.82 eV lower compared to the analogous phenyl isoindigo-BT copolymer (E_g = 1.74 eV).[189] This considerable decrease in bandgap can be attributed to the fact that the use of thiophene in the thiophene isoindigo monomer planarises the polymer backbone as a result of reduced steric effects and the increased sp^2 nature of the interannular single bonds that link the monomer units together.

3.3.5 Energy levels of IGT-BT copolymer

The HOMO energy level of **IGT-BT** was measured using PESA and found to be -4.8 eV in relation to the vacuum energy level. The fact that the HOMO energy level for **IGT-BT** is 0.88 eV higher than that of the analogous phenyl isoindigo-BT (-5.68 eV)[189] is due the electron rich nature of the thiophene unit which raises the HOMO energy level. Using the optical band gap, estimated from the absorption onset of the thin film UV-Vis spectrum the LUMO energy level of **IGT-BT** was calculated to be -3.88 eV. This is considerably lower than the LUMO level of phenyl isoindigo-BT (-

3.54 eV)[189] owing to the large difference in optical band gap. The HOMO and LUMO energy levels for **IGT-BT** were also measured by cyclic voltammetry, **Figure 3.25**.

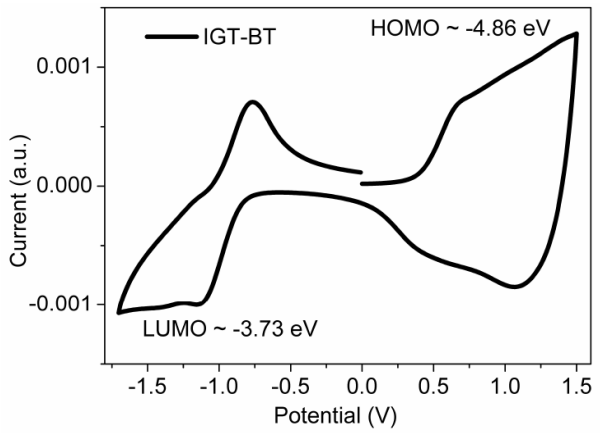


Figure 3.25: Cyclic voltammogram of **IGT-BT** in CH_3CN/0.1M $[nBu4N]^+[PF_6]$ at $0.1Vs^{-1}$.

The HOMO energy level was calculated using the equation:

$$E_{HOMO}\,(eV) = -\left(E_{ox}^{onset} - E_{Fc/Fc^+}^{onset}\right) - 4.80\,(eV) \qquad (\mathbf{15})$$

where E_{ox}^{onset} and E_{Fc/Fc^+}^{onset} are the onset oxidation potentials for the polymer sample and the ferrocene against the Ag/AgCl reference electrode, while the value – 4.8 eV is the HOMO energy level of ferrocene against vacuum.[190]

The LUMO energy level was calculated using the equation:

$$E_{LUMO}\,(eV) = -\left(E_{red}^{onset} - E_{Fc/Fc^+}^{onset}\right) - 4.80\,(eV) \qquad (\mathbf{16})$$

where E_{red}^{onset} and E_{Fc/Fc^+}^{onset} are the onset reduction potentials for the polymer sample and the ferrocene against the Ag/AgCl reference electrode, while the value – 4.8 eV is the HOMO energy level of ferrocene against vacuum.[190]

Using these equations the HOMO energy level was determined as -4.86 eV based on the onset of the oxidation potential and the LUMO energy level was determined as -3.73 eV based on the onset of the reduction potential. These obtained values are in rough agreement with the obtained PESA results despite being obtained in solution rather than in air.

3.3.6 OFET device performance of IGT-BT copolymer

OFET devices were fabricated using a top gate bottom contact configuration on a glass substrate. Gold was used for the source and drain electrodes and was patterned by photolithography utilising a double layer resist. The **IGT-BT** polymer was subsequently dissolved in dichloromethane and spin coated on top of the electrodes under nitrogen, before the films were annealed at a variety of temperatures namely 80 ºC, 250 ºC and 300 ºC for 2 h and allowed to cool to room temperature. Poly(methylmethacrylate) (PMMA) with n-butylacetate was used as the dielectric and deposited on top of the polymer film via spin coating to give a layer that was 500 nm thick. The dielectric was subsequently dried at 80 ºC for 30 minutes before the gold top gate electrode was evaporated on top of the dielectric.

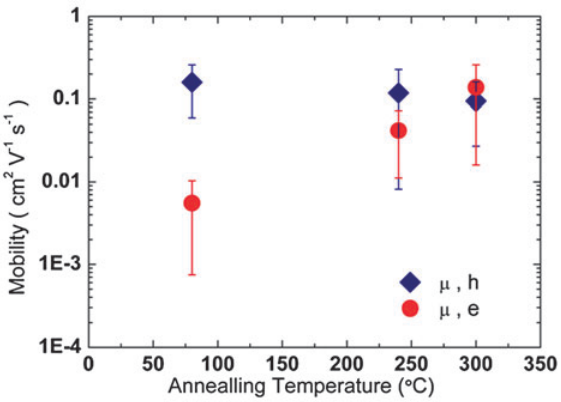


Figure 3.26: Saturation hole and electron mobilities of OFET devices at various annealing temperatures. Transistor dimensions: L = 20 µm and W = 1000 µm.

Figure 3.26 shows the hole and electron mobilities determined from the saturation regime of the transfer curves of a variety of devices annealed at various temperatures. The as-spun saturation hole and electron mobility was found to be ~0.16 $cm^2V^{-1}s^{-1}$ and ~6×10^{-3} $cm^2V^{-1}s^{-1}$ respectively. Whilst the saturated hole mobility was found to be almost unaffected by changes in annealing temperature going from 80 ºC to 300 ºC, the electron mobility increased linearly with increasing annealing temperature from 6×10^{-3} $cm^2V^{-1}s^{-1}$ to 0.14 $cm^2V^{-1}s^{-1}$. At an annealing temperature of 300 ºC the hole and electron mobilities become almost balanced, the champion device characteristics at the 300 ºC annealing temperature are shown in **Figure 3.27**.

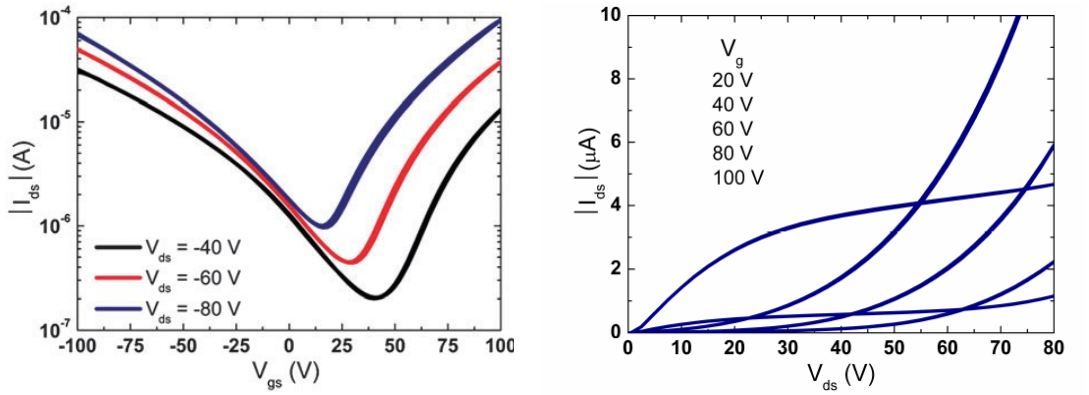


Figure 3.27: Organic field effect characteristics of **IGT-BT** a) Transfer characteristics at negative source drain bias for polymer annealed at 300 ºC. b) Output characteristics at positive source drain bias for polymer annealed at 300 ºC. Transistor dimensions: L = 20 μm and W = 1000 μm.

The transfer characteristics of an OFET device made from **IGT-BT** annealed at 300 ºC with a channel length of 20 μm and a channel width of 1000 μm are shown in **Figure 3.27 a**. The distinct V –shape of the curves indicates that the polymer is ambipolar. It is also evident from the both the transfer characteristics and the output characteristics (**Figure 3.27 b)** that they show minimal hysteresis thus indicating that the transistor devices show stable ambipolar behaviour.

The increase in the mobilities upon annealing is predominantly caused by a shift in the threshold voltages (V_T). As the annealing temperature is increased from 80 ºC to 300 ºC the threshold voltage decreases from ~130 V to ~60 V. Overall the average saturation mobility for holes and electrons determined from the transfer characteristics of transistor devices with channel lengths 5, 10 and 20 μm was 0.1 $cm^2V^{-1}s^{-1}$ for holes and 0.14 $cm^2V^{-1}s^{-1}$ for electrons. The maximum mobilities obtained were 0.16 $cm^2V^{-1}s^{-1}$ for holes and 0.14 $cm^2V^{-1}s^{-1}$ for electrons.

The effect of annealing the polymer above its melting point under nitrogen not only removes solvent impurities but may also help to remove electronegative impurities such as hydroxyl groups and oxygen thus improving electron transport.[191, 192] This partly explains why the electron transport improved with greater annealing temperature for the **IGT-BT** OFET devices. However, the effect of improved polymer microstructure can also play a role as by annealing the polymer the polymer has the energy required to reorganise into a more crystalline structure which can be more favourable for charge transport.[193]

3.3.7 AFM of IGT-BT copolymer

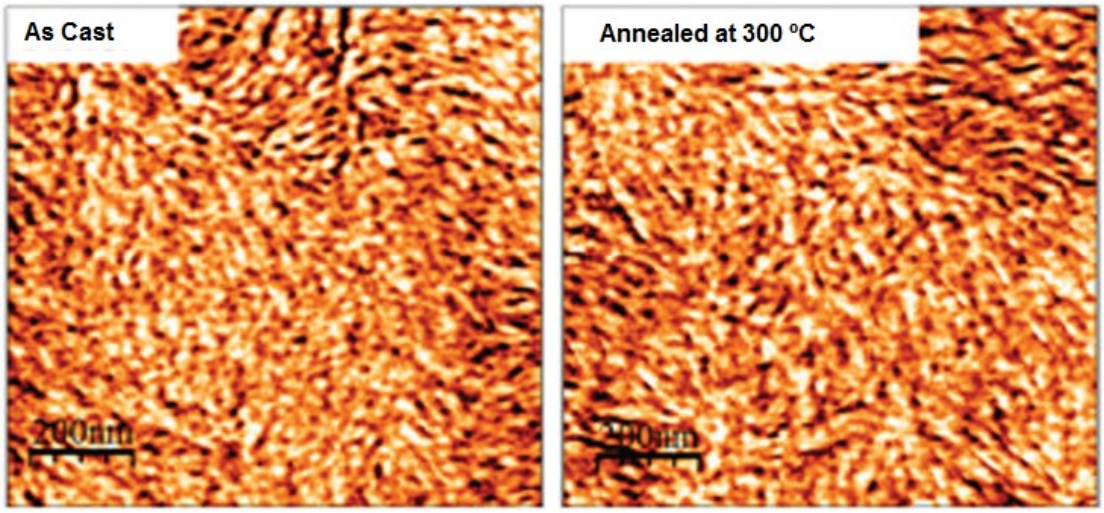


Figure 3.28: 2 μm × 2 μm AFM phase image of spin coated thin films of **IGT-BT**.

Atomic force microscopy (AFM) in tapping mode was used to see if any morphological changes take place upon annealing the polymer thin films. As it so happens no discernable changes were observed on going from the as cast to the annealed at 300 ºC film. The only measurable change was that the surface roughness increases slightly upon annealing going from 0.37 nm in the as cast film to 0.46 nm in the annealed film.

3.3.8 XRD of IGT-BT copolymer

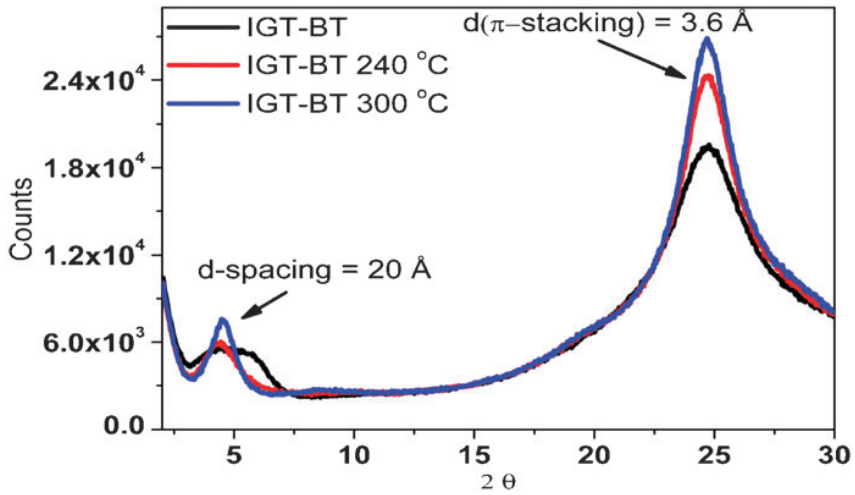


Figure 3.39: X-ray diffraction patterns of drop cast thin films of **IGT-BT** at various annealing temperatures.

Drop cast thin films for XDR analysis were prepared and the effect of changing the annealing temperature on the molecular packing of **IGT-BT** was studied. For the non-annealed drop cast film the XRD patterns shows a fairly broad reflection peak at the diffraction angle $2\theta = 4.4^{\circ}$ which corresponds to the 100 reflection of the crystal plane and is indicative of poorly ordered lamellar packing with a d spacing of roughly 20 Å. As the films are annealed the $2\theta = 4.4^{\circ}$ peak narrows and increases in intensity indicating improved lamellar packing. A similar trend is seen for the broad peak at $2\theta = 24.7^{\circ}$ which corresponds to a π-π stacking distance of roughly 3.6 Å. The narrowing of the $2\theta = 24.7^{\circ}$ peak and increase in intensity with increasing annealing temperature shows that annealing improves the π-π stacking, which is a phenomenon that is seen for other polymers.[194] The improvement in lamellar spacing and π-π stacking distance observed with increasing annealing temperature is another factor that can be attributed to improving the mobilities of the polymer at higher annealing temperatures. As from the AFM there was no observable change with annealing, it can be assumed that the crystalline domains detected in the XRD analysis are very small.

3.3.9 Density functional theory calculations for IGT-BT.

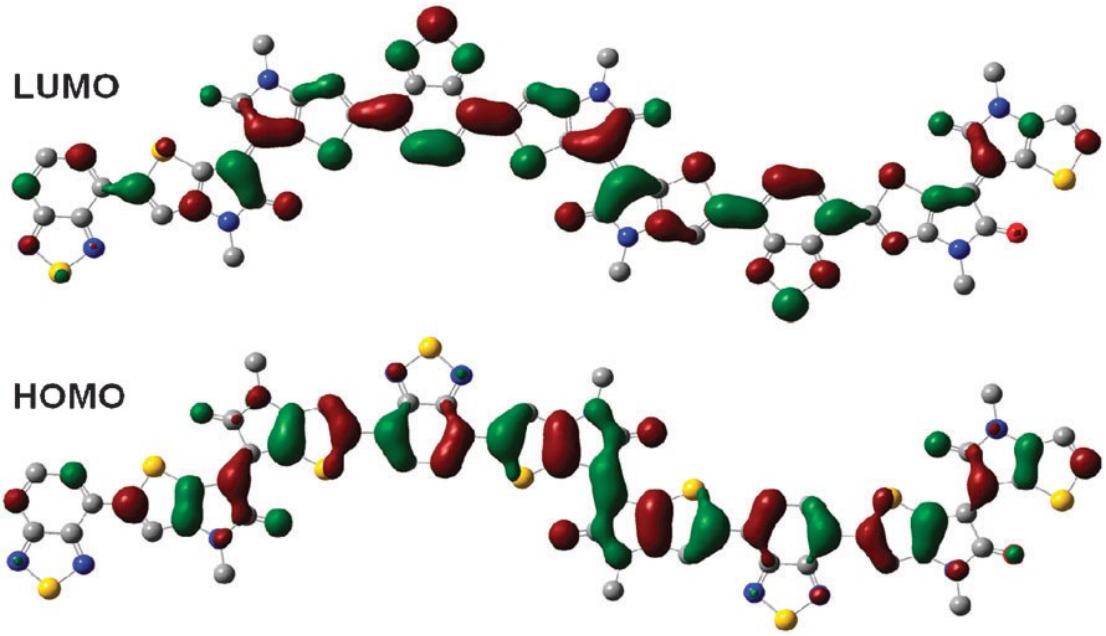


Figure 3.40: HOMO and LUMO distributions for the minimum energy conformations of methyl substituted **IGT-BT** trimers optimised with Gaussian 09 at the B3LYP/6-31G(d) level.

DFT calculations were carried out to ascertain the origins of the ambipolar nature of **IGT-BT**. Using Gaussian 09 the **IGT-BT** copolymer was simulated using methyl substituted trimers using a B3LYP/6-31G(d) functional and basis set. The HOMO and LUMO electron density distributions for the minimum energy conformations of the **IGT-BT** trimers are depicted in **Figure 3.40**, whereby the red and green colours represent the isosurfaces of wavefunctions with opposite phases. From looking at the HOMO electron density distribution, it is interesting to note that unlike the phenyl isoindigo shown in **Figure 3.12** the HOMO orbital is distributed on the nitrogen atom, with a bonding interaction that is distributed between both of the nitrogen atoms. In combination with the electron density provided by the electron rich thiophene units this makes the thiophene isoindigo considerably more electron rich than the analogous phenyl isoindigo. Additionally it can be seen that both the HOMO and LUMO energy levels are evenly delocalised over both the donor and the acceptor unit. This is contrary to conventional donor-acceptor copolymers in which the LUMO energy level is typically localised on just the acceptor unit within the copolymer backbone. For conventional polymers the localisation of the LUMO on the acceptor unit can hamper interchain electron transport, as interchain electron hopping requires a good alignment of the localised LUMO energy levels.[195] Thus the fact that the HOMO and LUMO energy levels are so delocalised for **IGT-BT** may to a certain extent explain the ambipolar nature observed.

3.3.10 Conclusion

In conclusion the **IGT-BT** copolymer synthesised from the novel branched thiophene isoindigo monomer (**3.25**) shows high ambipolar charge transport, with hole and electron mobilities exceeding 0.1 $cm^2V^{-1}s^{-1}$. This is considered to be as a result of the polymer's remarkably low band gap, crystallinity and extensively delocalised HOMO and LUMO energy levels.

3.4 Thiophene Isoindigo Part 2 – A Comparison with Phenyl Isoindigo

So far only one polymer of thiophene isoindigo **IGT-BT** has been thoroughly investigated. However this copolymer is in effect combining two acceptor units as the BT unit is an electron acceptor and to some extent the polar pyrrol functionality on the thiophene isoindigo acts as an electron accepting moiety. Thus to extend the range of polymers investigated to include more donor-acceptor characteristics into the polymer backbones, a range of electron rich and not so electron rich monomer units were copolymerised with the thiophene isoindigo monomer. To be able to make a valid comparison to phenyl isoindigo, the analogous copolymers of phenyl isoindigo were also synthesised.

3.4.1 Synthesis of thiophene isoindigo and phenyl isoindigo copolymers

Using the branched thiophene isoindigo monomer (**3.25**) and the phenyl isoindigo monomer (**3.6**) (for synthesis see sections **3.3.1** and **3.2.1** respectively) the monomers were copolymerised with electron rich thiophene and thieno[3,2-*b*]thiophene and the not so electron rich phenyl and napthalene monomers. The linear thiophene isoindigo monomer was also polymerised with thiophene but yielded a very low molecular weight oligomer M_n =2 kDa due to the poor solubility of the linear thiophene isoindigo monomer, and so will not be included in this thesis.

For the polymerisations involving thiophene and thieno[3,2-*b*]thiophene Stille coupling polymerisation was used. The reason for the choice of Stille coupling over Suzuki coupling in this case is due to the fact that electron rich boronate ester monomers are less stable than their tin based counterparts, and it has been found that when using thiophene boronates not only is deboronation a problem but also that the polymerisation can become terminated by aryl group transfer from the PPh_3 ligands employed.[196] So using catalytic $Pd_2(dba)_3$ with triphenylphosphine or tri(o-tolyl)phosphine ligands both the branched thiophene isoindigo monomer (**3.25**) and the phenyl isoindigo monomer (**3.6**) were copolymerised with both 2,5-bis(trimethylstannyl)thiophene (**3.11**) and 2,5-bis(trimethylstannyl)thieno[3,2-

b]thiophene (**3.12**) to give copolymers **IGT-T, IGT-TT, IGPh-T** and **IGPh-TT** respectively. These copolymers were all end capped with 2-trimethylstannyl thiophene (**3.13**) and 2-bromothiophene (**3.14**) to remove both tin and bromine moieties from the ends of the polymer chains to remove charge traps from the polymers[176, 180]. After precipitation into acidic methanol to quench any excess tin, the polymers were purified via Soxhlet extraction in acetone, hexane and chloroform. The chloroform fraction for each of the copolymers was each heated with sodium diethyldithiocarbamate trihydrate to remove residual palladium. The copolymers were finally re-precipitated into methanol and filtered and dried under high vacuum.

For the polymerisations involving phenyl and napthalene Suzuki polymerisation was used as the boronate esters of these monomers are stable and substantially less toxic to work with. So using $Pd(PPh_3)_4$ as catalyst, sodium carbonate as base and aliquat 336 as a phase transfer catalyst both the branched thiophene isoindigo monomer (**3.25**) and the phenyl isoindigo monomer (**3.6**) were copolymerised with both 1,4-phenyldiboronic acid bis pinacol ester (**3.27**) and 1,5-naphthalenediboronic acid bis pinacol ester (**3.28**) to give copolymers **IGT-Ph**, **IGT-Na**, **IGPh-Ph** and **IGPh-Na** respectively. Regrettably these polymers were not end capped due to a shortage of phenylboronic acid pinacol ester, but in this case as this is the case for both the thiophene isoindigo copolymers and the phenyl isoindigo copolymers a valid comparison can still be made. After precipitation into methanol, the polymers were purified via Soxhlet extraction in acetone, hexane and chloroform. The chloroform fraction for each of the copolymers was each heated with sodium diethyldithiocarbamate trihydrate to remove residual palladium. The copolymers were finally re-precipitated into methanol and filtered and dried under high vacuum.

The reaction schemes for the thiophene isoindigo copolymers are given in **Figure 3.41** and the reaction schemes for the phenyl isoindigo copolymers are given in **Figure 3.42**.

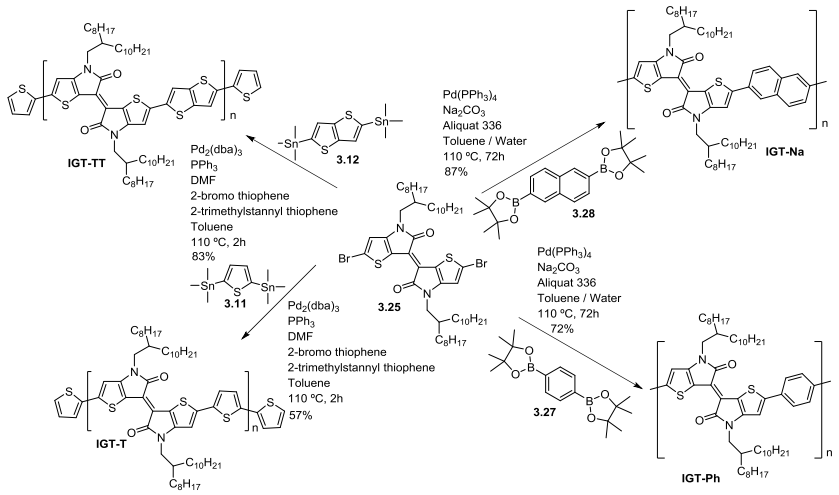


Figure 3.41: Synthesis of thiophene isoindigo based copolymers **IGT-T**, **IGT-TT**, **IGT-Ph** and **IGT-Na**.

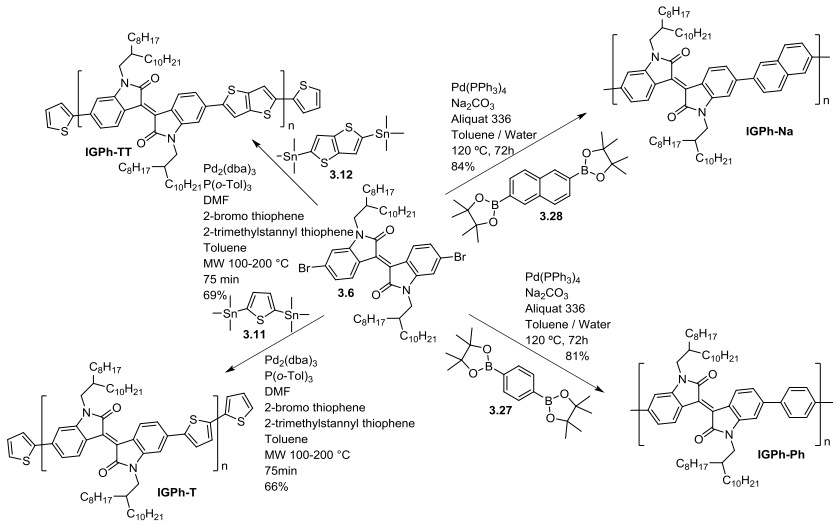


Figure 3.42: Synthesis of phenyl isoindigo based copolymers **IGPh-T**, **IGPh-TT**, **IGPh-Ph** and **IGPh-Na**.

Once the polymers were synthesised the polymers were further purified via preparative scale recycling size exclusion chromatography (recSEC). This technique has been shown to significantly enhance device performance for OPVs in other polymer systems.[197] The technique involves passing the polymers through an Agilent PLgel 10 μm MIXED-D column using chlorobenzene as eluent. It is important to keep the column temperature at 80 ºC to prevent the polymers from crashing out of solution and to minimise polymer chain aggregation. recSEC allows one to fractionate the polymers to separate out the high molecular weight fractions and obtain very narrow polydispersities. Additionally the technique helps to remove low molecular weight oligomers, defined as having a degree of polymerisation of less than 10 units, as well as polymer chains which are miscoupled or cross linked.

3.4.2 Physical properties of thiophene and phenyl isoindigo copolymers.

To determine the molecular weights of the collected polymer fractions, GPC calibrated against polystyrene standards was used. **Table 3.5** summarises the molecular weights obtained for each polymer that were used for subsequent characterisation.

Copolymer	M_n [kg/mol][a)]	M_w [kg/mol][b)]	PDI[c)]	DP_n[d)]
IGT-T	-	-	-	-
IGT-TT	-	-	-	-
IGT-Ph	40	69	1.73	44
IGT-Na	51	105	2.05	53
IGPh-T	10	12	1.86	11
IGPh-TT	26	71	2.74	27
IGPh-Ph	40	58	1.46	44
IGPh-Na	48	141	2.89	50

Table 3.5: Molecular weights of copolymers used for subsequent device characterisation a) M_n = number average molecular weight b) M_w = weight average molecular weight c) PDI = polydispersity index = $[M_w/M_n]$ d) DP_n = degree of polymerisation.

The molecular weights of **IGT-T** and **IGT-TT** could not be determined by GPC as it was found that the polymer strongly interacted with the column material. This was a problem also experienced by Van Pruissen et al[198] who was independently working on the 2-hexadecyl version of **IGT-T** and **IGT-Ph** at the same time as this work was being carried out. However, while Van Pruissen et al[198] were unable to obtain conclusive results for the molecular weight of the 2-hexadecyl version of **IGT-Ph**, the molecular weight of the **IGT-Ph** copolymer synthesised in this work was able to be determined. This may be due to the fact that in this work the alkyl chain was 2-octyldodecyl so being somewhat longer will enhance the solubility of the polymer, and may inhibit the interaction with the column. The initial molecular weight of the crude **IGT-Ph** copolymer was M_n = 29 kg/mol, M_w = 72 kg/mol, PDI = 2.48 but using recSEC was able to be fractionated into four fractions. The first fraction contained a small amount of extremely high molecular weight polymer with M_n = 168 kg/mol, M_w = 229 kg/mol, PDI = 1.36. The second fraction was M_n = 87 kg/mol, M_w = 129 kg/mol, PDI = 1.47. The third fraction was the one used for device

characterisation as it contained the largest yield of polymer and was comparable to the molecular weights of the other copolymers, M_n = 40 kg/mol, M_w = 69 kg/mol, PDI = 1.73. The fourth fraction contained the lowest molecular weight polymer with M_n = 18 kg/mol, M_w = 37 kg/mol, PDI = 1.97. From these values it can be seen that despite starting from a reasonably average M_n in the crude polymer with a large PDI, through using recSEC much higher molecular weights can be selected with narrower PDI distributions. Similar results were obtained for polymers **IGT-Na**, **IGPh-T**, **IGPh-TT** and **IGPh-Ph** although **IGPh-Na** was unable to be processed via recSEC due to insufficient solubility in room temperature chlorobenzene, a condition that is required to avoid fouling the column. Although this process effectively wastes polymer material, the resulting polymer obtained is purer and has a defined molecular weight and PDI. This means that the problems caused by polymer batch to batch variation which decreases device to device uniformity can be minimised resulting in more reliable electronic devices.

3.4.3 Optical properties of thiophene and phenyl isoindigo copolymers.

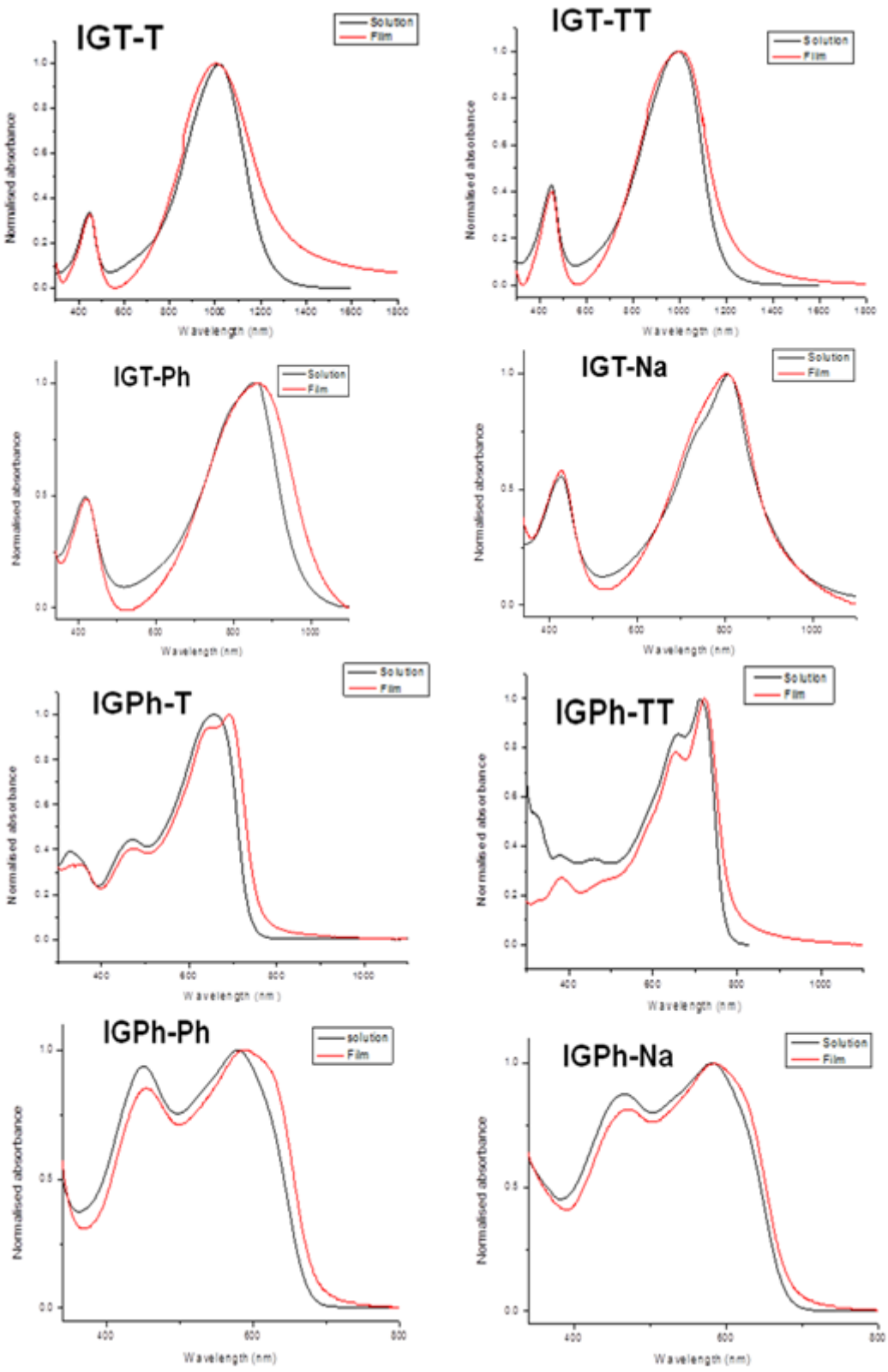


Figure 3.43: Solution (chlorobenzene at 25 ºC) and thin film UV-Vis absorption spectra of **IGT-T**, **IGT-TT**, **IGT-Ph**, **IGT-Na**, **IGPh-T**, **IGPh-TT**, **IGPh-Ph** and **IGPh-Na**.

Figure 3.43 shows the UV-Vis absorption spectra of **IGT-T**, **IGT-TT**, **IGT-Ph**, **IGT-Na**, **IGPh-T**, **IGPh-TT**, **IGPh-Ph** and **IGPh-Na** in dilute chlorobenzene solution at 25 ºC and in thin film spun from chlorobenzene solution (5 mg/mL, 1000 rpm, 1 min). Both the solution and thin film spectra for all of the polymers show π–π* transitions in the 400 nm wavelength region, although it is interesting to note that only the **IGPh-Ph** and **IGPh-Na** copolymers show a significantly high absorption in this region presumably as they contain the greatest number of π bonds out of all of the copolymers. With the exception of **IGT-T** and **IGT-Na** all of the polymers show a slight red shift in the maximum absorption wavelength in the charge transfer region with a slight broadening of the absorption upon going from solution to thin film, a condition that is expected due to increased molecular ordering. **IGT-T** however shows a slight blue shift of 13 nm on going from thin film to solution, a condition previously observed for **PFTFI** and **IGT-BT** and so may be due to the effect of side chain density affecting intermolecular packing. **IGT-Na** on the other hand shows no change in maximum absorption on going from solution to thin film indicating no change in molecular packing between neighbouring polymer chains. Unlike all of the other copolymers, **IGPh-T** and **IGPh-TT** show an additional peak in the charge transfer band which could be due to greater resolution of vibronic fine structure as these polymers are somewhat lower in molecular weight, or more likely a result of aggregation, as for **IGPh-T** this extra feature is only seen in the thin film and not in the solution. The data for these peaks are listed in **Table 3.6**.

Polymer	**Solution**		**Thin Film**		**Optical Band gap [eV]**[a)]
	π–π* transition (nm)	Charge transfer band (nm)	π–π* transition (nm)	Charge transfer band (nm)	
IGT-T	447	1019	448	1006	0.95
IGT-TT	451	988	452	1002	1.01
IGT-Ph	418	852	415	854	1.22
IGT-Na	426	809	424	809	1.35
IGPh-T	463	657	469	637, 692	1.64
IGPh-TT	462	657, 711	481	651, 723	1.57
IGPh-Ph	451	582	452	584	1.82
IGPh-Na	459	581	465	583	1.83

Table 3.6: Lambda max values and optical band gap for UV-Vis absorption of thiophene and phenyl isoindigo copolymers a) Optical band gap is derived from absorption onset.

The trend in going from thiophene to thieno[3,2-*b*]thiophene for the thiophene isoindigo copolymers is that the optical band gap increases due to the more aromatic nature of thieno[3,2-*b*]thiophene decreasing the amount of conjugation through the quinoidal effect. However this expected effect is not seen for the phenyl isoindigo copolymers presumably due to the fact that the **IGPh-T** copolymer is a very low molecular weight polymer and so may not have reached a high enough degree of polymerisation to have an effective persistence length. Thus for the **IGPh-Ph** copolymer presented in this work the lowest possible band gap may not have been attained, unlike that for **IGPh-TT**. So with a greater molecular weight the optical band gap for **IGPh-T** may be lower than **IGPh-TT**. Computational modelling in section **3.4.5** will be used to see if this hypothesis is correct though.

The trend in going from phenyl to naphthalene for both phenyl and thiophene isoindigo shows a blue shift, as naphthalene is more aromatic and so exhibits less electron delocalisation along the polymer backbone leading to the greater band gap.

On comparing thiophene against phenyl for **IGT-T** and **IGT-Ph** it can be seen that the thiophene copolymer is significantly more red shifted. This is due to the fact that the thiophene is more electron rich and thus there is greater donor acceptor character within this copolymer. This means that there is greater orbital hybridisation which helps to lower the band gap. Additionally the **IGT-T** is more planar as a result of there being less steric hindrance between the hydrogen atoms on the carbons alpha to the bonding carbon atoms between the monomer units. This planarisation of the polymer backbone also helps enhance electron delocalisation which lowers the band gap. These explanations are also valid for comparing **IGT-TT** against **IGT-Na**, or comparing **IGT-T** against **IGT-Na**, or comparing **IGT-TT** against **IGT-Ph**.

On comparing thiophene against phenyl for **IGPh-T** and **IGPh-Ph** it can be seen that the thiophene copolymer is significantly more red shifted. This is due to the fact that the thiophene is more electron rich and thus there is greater orbital hybridisation which helps to lower the band gap. Additionally the **IGPh-T** is more planar as a result of there being less steric hindrance between the neighbouring hydrogen atoms on the carbons alpha to the bonding carbon atoms between the monomer units. This planarisation of the polymer backbone also helps enhance electron delocalisation

which lowers the band gap. These explanations are also valid for comparing **IGPh-TT** against **IGPh-Na**, or comparing **IGPh-T** against **IGPh-Na**, or comparing **IGPh-TT** against **IGPh-Ph**.

When one compares the effect of the thiophene isoindigo monomer verses the phenyl isoindigo monomer all of the thiophene isoindigo copolymers exhibit much lower band gaps. This occurs despite the fact that the thiophene isoindigo monomer is more electron rich due to the electron rich thiophenes that make up the molecule, which would mean that it should show less of an acceptor character and thus give rise to less orbital hybridisation. Thus part of the explanation for the lower band gap lies in the fact that all of the thiophene isoindigo copolymers are more planar than the analogous phenyl isoindigo polymers due to the decrease in the effects of sterics between the neighbouring hydrogen atoms on the carbons alpha to the bonding carbon atoms between the monomer units. Thus one can see that for all of the polymers the band gap decreases as the inter monomer bond angles follow the order phenyl-phenyl, phenyl – thiophene, thiophene-thiophene due to the amount of steric hindrance decreasing. However if this was the only effect that lowers the band gap then **IGT-Ph** and **IGPh-T** would have similar maximum absorption values and optical gaps. As this is not the case it is evident that there is another factor at play here. From looking at the frontier molecular orbitals calculated with Gaussian 09 (see sections **3.2.5**, **3.3.9** and **3.4.5**) for phenyl and thiophene isoindigo it is evident that unlike the phenyl isoindigo the thiophene isoindigo has part of its HOMO energy level distributed on the nitrogen atom, with a bonding interaction that is distributed between both of the nitrogen atoms. This enhanced delocalisation, in addition to the effect of enhanced planarity, can also be attributed to causing the thiophene isoindigo copolymers to exhibit a much lower band gap.

3.4.4 PESA determination of energy levels of thiophene and phenyl isoindigo copolymers.

The HOMO energy levels of **IGT-T**, **IGT-TT**, **IGT-Ph**, **IGT-Na**, **IGPh-T**, **IGPh-TT**, **IGPh-Ph** and **IGPh-Na** were measured by PESA (photoelectron spectroscopy in air). For this measurement two thin films spin coated from chlorobenzene of each copolymer were measured and the average HOMO energy level was listed in **Table**

3.6 in relation to the vacuum energy level. Using the optical bandgaps, estimated from the absorption onset of the thin film UV-Vis spectrums the LUMO energy levels were calculated and also included in **Table 3.7**.

Copolymer	HOMO level [eV][a)]	LUMO level [eV][b)]	Optical Band gap [eV][c)]
IGT-T	-4.70	-3.75	0.95
IGT-TT	-4.63	-3.62	1.01
IGT-Ph	-4.84	-3.62	1.22
IGT-Na	-5.03	-3.68	1.35
IGPh-T	-5.30	-3.66	1.64
IGPh-TT	-5.26	-3.69	1.57
IGPh-Ph	-5.57	-3.75	1.82
IGPh-Na	-5.59	-3.76	1.83

Table 3.7: Energy levels of thiophene and phenyl isoindigo copolymers. a) Measured by PESA b) Estimated by addition of the absorption onset to the HOMO c) Determined from the absorption onset of the thin film UV-Vis spectrum.

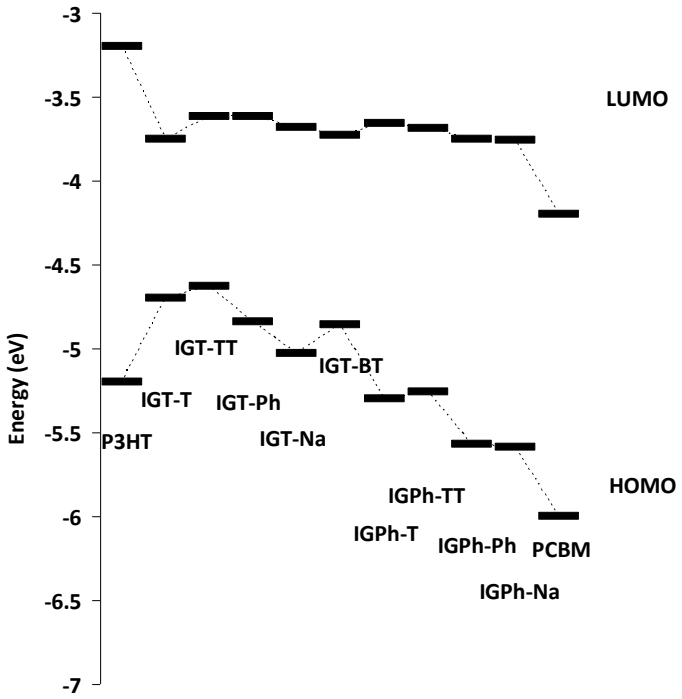


Figure 3.43: Visualisation of HOMO and LUMO energy levels for thiophene and phenyl isoindigo copolymers relative to P3HT and $PC_{60}BM$.

As can be seen from the data, **Figure 3.43**, there is a clear trend in the HOMO energy levels with the phenyl isoindigo copolymers being much lower than the thiophene

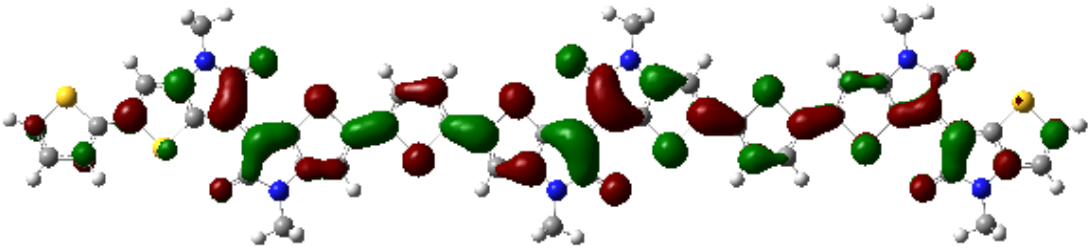
isoindigo copolymers. This is due to the fact that phenyl isoindigo monomer is much less electron rich than the thiophene isoindigo monomer. Another trend can be seen on going from a thiophene to a thieno[3,2-*b*]thiophene comonomer for both thiophene and phenyl isoindigo copolymers, with the thieno[3,2-*b*]thiophene HOMO level being higher due to it being more electron rich.

It is interesting to note that contrary to expectations on going from a phenyl to a naphthalene comonomer for both the thiophene and phenyl isoindigo copolymers the naphthalene based copolymers are lower in HOMO energy. One would expect that the naphthalene based copolymers would be higher in HOMO energy level as a result of increased conjugation within the naphthalene unit. However it may be the case that as the naphthalene unit is more aromatic than phenyl there is less electron delocalisation over the whole polymer backbone which leads to the overall HOMO energy level being lowered relative to phenyl. The alternative explanation could be that as only two samples for each polymer were measured and subsequently averaged, one of the samples from each set could be a statistical outlier which would thus skew the average. The results from DFT analysis (see section **3.4.5**) will help to determine if this is the case.

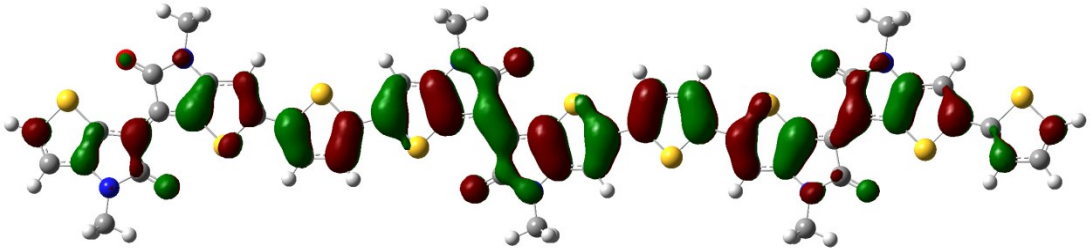
Despite the wide variation in HOMO energy levels the LUMO energy level going from thiophene isoindigo to phenyl isoindigo shows very little variation and seems to be also relatively unaffected by choice of comonomer.

3.4.5 DFT of thiophene and phenyl isoindigo copolymers.

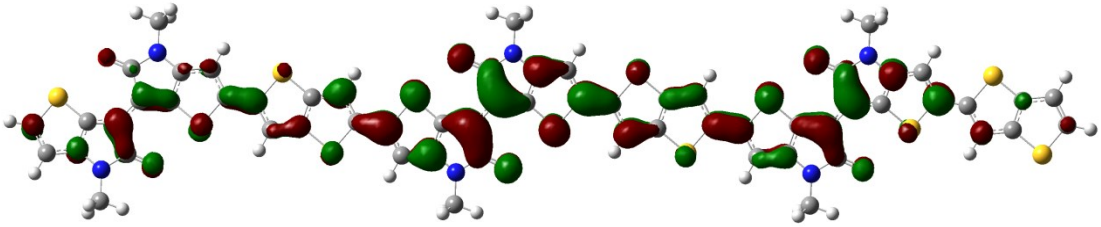
IGT-T
LUMO



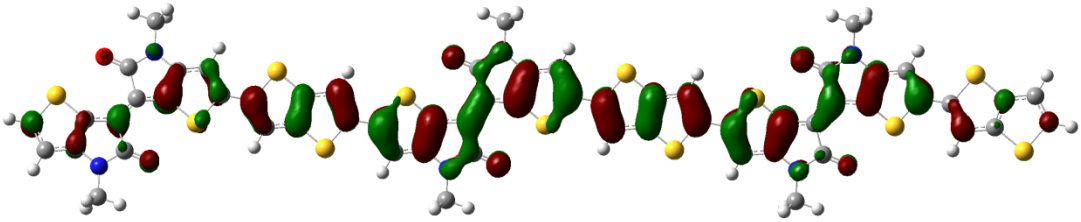
HOMO



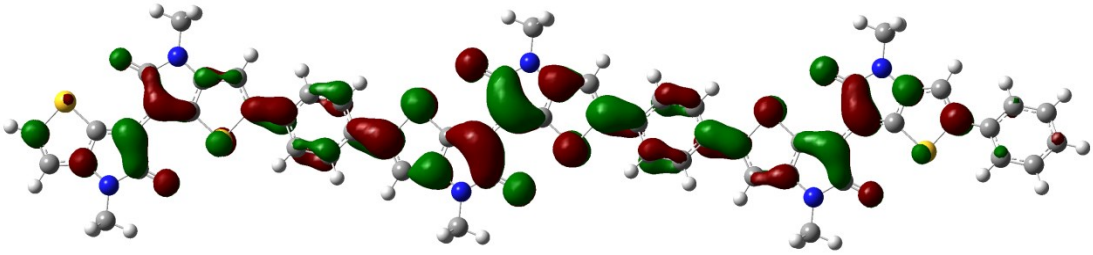
IGT-TT
LUMO



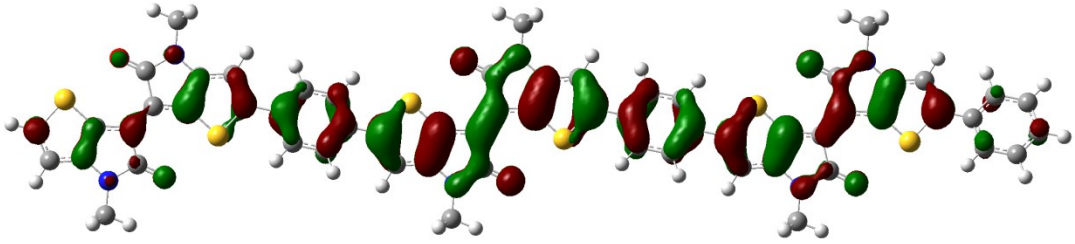
HOMO



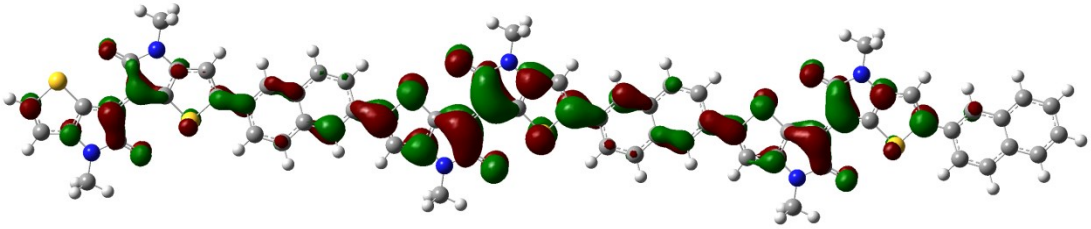
IGT-Ph
LUMO



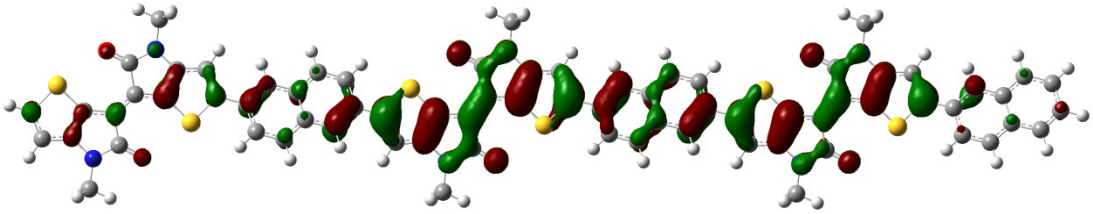
HOMO



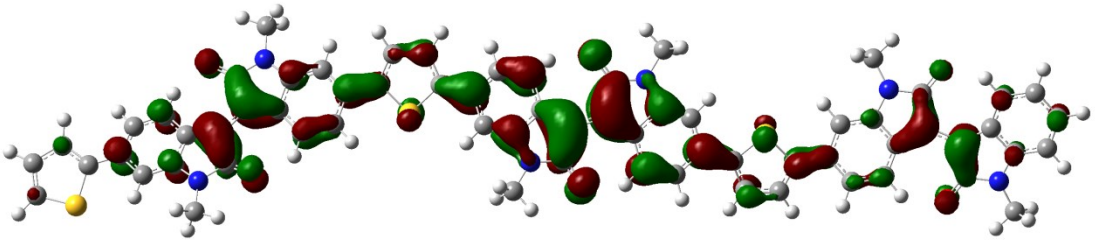
IGT-Na
LUMO



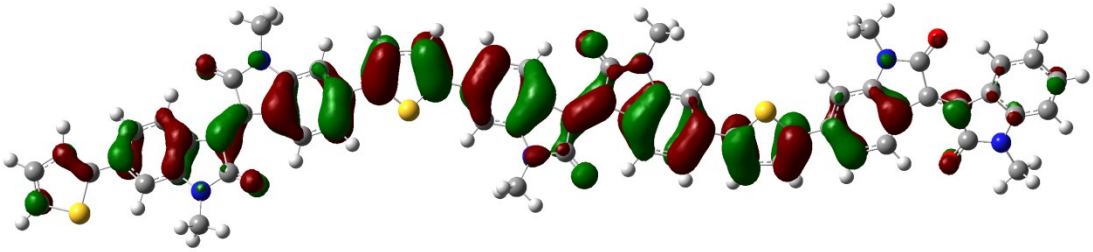
HOMO



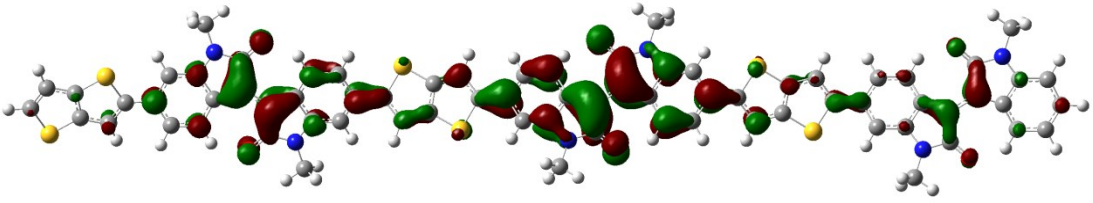
IGPh-T
LUMO



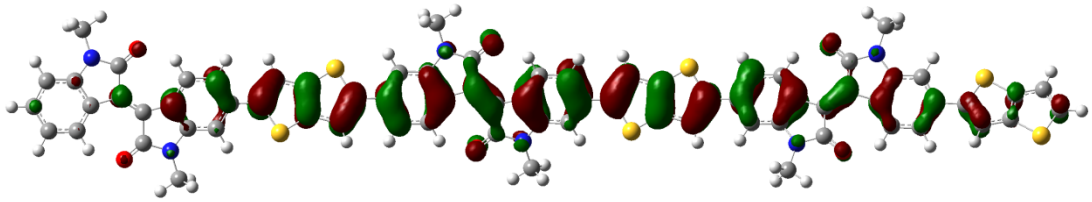
HOMO



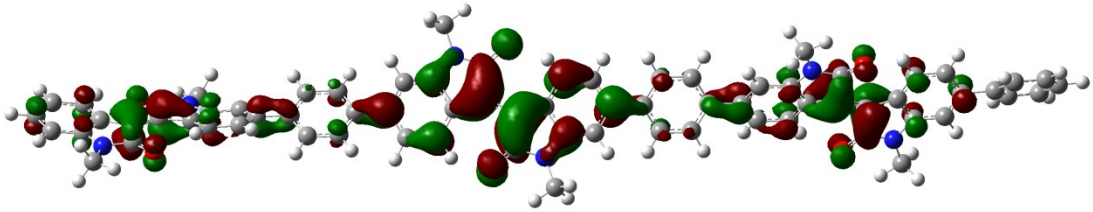
IGPh-TT
LUMO



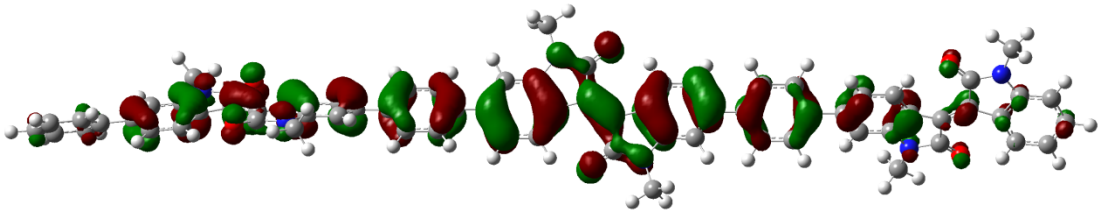
HOMO



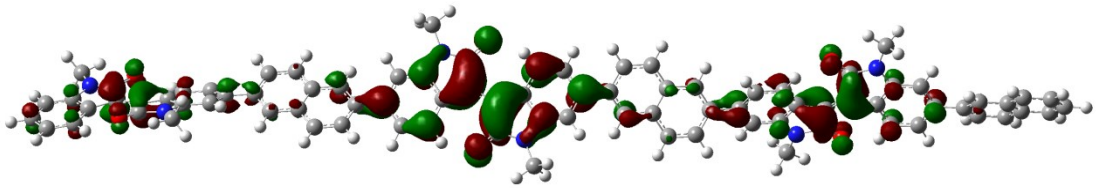
IGPh-Ph
LUMO



HOMO



IGPh-Na
LUMO



HOMO

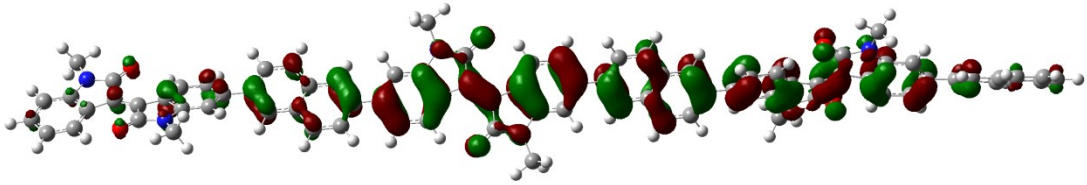


Figure 3.44: HOMO and LUMO distributions for the minimum energy conformations of methyl substituted **IGT-T**, **IGT-TT**, **IGT-Ph**, **IGT-Na**, **IGPh-T**, **IGPh-TT**, **IGPh-Ph** and **IGPh-Na** trimers optimised with Gaussian at the B3LYP/6-31G* level.

Quantum chemical calculations of the energy levels and band gaps of the thiophene and phenyl isoindigo copolymers were performed using DFT with Gaussian 09, in accordance to literature precedent.[185] The B3LYP/6-31G* functional and basis set was used to calculate optimised ground state geometries, from which the frontier

orbital energies were deduced. Methylated trimers were used as an approximation to the polymers. To calculate the optical band gaps, non adiabatic linear response calculations using time dependant density functional theory in Gaussian 09 were carried out. This involved using the same B3LYP/6-31G* functional and basis set as before. From these calculations the values shown in **Table 3.8** were obtained.

Copolymer	HOMO [eV]	LUMO [eV]	Optical band gap [eV]
IGT-T	-4.461	-3.182	1.2781
IGT-TT	-4.490	-3.211	1.2785
IGT-Ph	-4.629	-3.092	1.5367
IGT-Na	-4.662	-3.052	1.6093
IGPh-T	-5.108	-3.284	1.8235
IGPh-TT	-5.082	-3.293	1.7883
IGPh-Ph	-5.308	-3.194	2.1138
IGPh-Na	-5.281	-3.169	2.1112

Table 3.8: Calculated HOMO, LUMO and optical band gap for the minimum energy conformations of methyl substituted **IGT-T**, **IGT-TT**, **IGT-Ph**, **IGT-Na**, **IGPh-T**, **IGPh-TT**, **IGPh-Ph** and **IGPh-Na** trimers optimised with Gaussian at the B3LYP/6-31G* level.

The optical band gaps calculated for the series of copolymer trimers are all considerably larger than those obtained experimentally. This could be due to the optimal persistence length of the copolymers being longer than just three copolymer units long and thus the lowest band gap may not have been attained. Alternatively the minimum energy conformations obtained could have been local minima rather than global minima and so ideally a variety of alternative input conformations should be assessed to see whether a truly global low energy conformation can be attained. However, this process is computationally expensive and beyond the scope of this thesis.

Despite the fact that these calculations may not be fully optimised, some trends can still be observed. For example the HOMO level values for **IGT-T** and **IGT-TT** are very similar thus giving rise to optical band gaps which are very close, in which the band gap for **IGT-T** is smaller than **IGT-TT**, which was also observed experimentally. The discrepancy for the **IGT-T** and **IGT-TT** calculation however is

that the HOMO energy level is marginally higher for **IGT-T** which is not the case experimentally and also not expected as thieno[3,2-*b*]thiophene is more electron rich than thiophene and so would be expected to have a higher HOMO energy level. When comparing these values with the analogous **IGPh-T** and **IGPh-TT** copolymers the HOMO levels for **IGPh-T** and **IGPh-TT** show the correct trend in that the **IGPh-TT** HOMO is higher than the **IGPh-T**. Interestingly though unlike **IGT-T** and **IGT-TT** the calculated optical band gap of **IGPh-T** is calculated to be considerably larger than that of **IGPh-TT**. This was also seen experimentally, but was unexpected as thieno[3,2-*b*]thiophene is more aromatic and thus should give rise to less electron delocalisation leading to a lower band gap than with thiophene. Initially for the experimental result it was hypothesised that the discrepancy in the trend was due to the obtained **IGPh-T** having a lower molecular weight thus meaning that the optimal persistence length would not have been obtained which would give rise to the **IGPh-T** having a larger band gap than expected. However these DFT results show that this hypothesis is not completely correct. Thus the explanation may be found by looking at the visualisation of the copolymer backbones in **Figure 3.34.** It is evident that the backbones of **IGT-T** and **IGT-TT** are perfectly linear due to the antiperiplanar arrangement of the thiophene atoms that alternate in up and down positions along the polymer backbone. This enables the **IGT-T** and **IGT-TT** polymers to have fully delocalised energy levels which are thus only affected by the effects of the difference in aromaticity between the thiophene and the thieno[3,2-*b*]thiophene. For **IGPh-T** and **IGPh-TT** the situation is different. The **IGPh-T** copolymer exhibits a sine wave like backbone due to the 158.9º angle introduced by the incorporation of thiophene between two phenyl isoindigo units, whilst the **IGPh-TT** has a 179.2º angle between neighbouring phenyl isoindigo units meaning that the backbone of **IGPh-TT** is much straighter. As a result of backbone curvature the electrons in **IGPh-T** are less delocalised resulting in a greater band gap than that obtained for the more linear **IGPh-TT** copolymer.

The HOMO level for **IGT-Ph** is calculated to be higher than for **IGT-Na** whilst the calculation of the optical band gap shows that the optical band gap of **IGT-Ph** is significantly lower than that of **IGT-Na**. This accurately models the observed trends seen experimentally. As for **IGPh-Ph** and **IGPh-Na** the calculations show that **IGPh-Ph** has a higher HOMO energy level than **IGPh-Na** and that **IGPh-Ph** has a

marginally wider band gap than **IGPh-Na**. These results for **IGPh-Ph** and **IGPh-Na** are inconsistent with the trends observed for **IGT-Ph** and **IGT-Na** and are also inconsistent with the results obtained experimentally, although they do show that the optical band gaps are very close together which was observed experimentally.

The trend of the thiophene isoindigo based copolymers having a HOMO energy level that is considerably higher than the phenyl isoindigo based copolymers is evident from the calculations, and fits well with the results obtained experimentally. As can be seen from **Figure 3.44** the HOMO energy level is fully delocalised over the whole of the trimers for both thiophene and phenyl isoindigo. As seen for **IGT-BT** the HOMO for **IGT-T**, **IGT-TT**, **IGT-Ph** and **IGT-Na** is also fully delocalised over both of the nitrogen atoms of the thiophene isoindigo. The phenyl isoindigo copolymers **IGPh-T**, **IGPh-TT**, **IGPh-Ph**, **IGPh-Na** unlike **PFTFI** and **PFTTFI** show some electron density on the nitrogen atoms although this density is localised solely on the nitrogen atoms and is not distributed between them. This explains to some extent why the optical band gap of the thiophene isoindigo is much lower than that of phenyl isoindigo as the electrons are more delocalised in thiophene isoindigo. Looking at the electron distribution in the LUMO it is clear that for the phenyl isoindigo based copolymers the LUMO is predominantly localised on the phenyl isoindigo acceptor as is common for the majority of donor acceptor copolymers. The thiophene isoindigo polymers however show that the LUMO is more delocalised across the polymer chain which in conjunction with the raised HOMO as a result of the incorporation of the more electron rich thiophene may be another factor in lowering the optical band gap.

Copolymer	Interannular dihedral angle (º)	Optical band gap from experiment (eV)
IGT-T	1.63	0.95
IGT-TT	1.32	1.01
IGT-Ph	20.99	1.22
IGT-Na	22.47	1.35
IGPh-T	21.48	1.64
IGPh-TT	22.30	1.57
IGPh-Ph	35.15	1.82
IGPh-Na	35.05	1.83

Table 3.9: Comparison of interannular dihedral angles between thiophene or phenyl isoindigo unit and neighbouring thiophene, thieno[3,2-b]thiophene, phenyl or naphthalene unit derived from trimers modelled in **Figure 3.44** against experimental optical band gap.

The visualisations of the copolymer chains in **Figure 3.44** also show the degree of interannular dihedral twist between the isoindigo unit and the comonomer. It can be seen from **Table 3.9** that as you go from a thiophene-thiophene, thiophene-phenyl, phenyl – phenyl interannular linkage, the dihedral angle between the units increases. This is due to an increase in steric hindrance between the hydrogen atoms on the carbons adjacent to the bonding carbons linking the monomer units together. As such there is a rough trend that as dihedral angle increases the optical band gap decreases as a result of greater planarisation of the polymer backbone.

3.4.6 DSC of thiophene and phenyl isoindigo copolymers.

To see if there is a trend in crystallinity with increasing polymer backbone planarity, DSC measurements were taken.

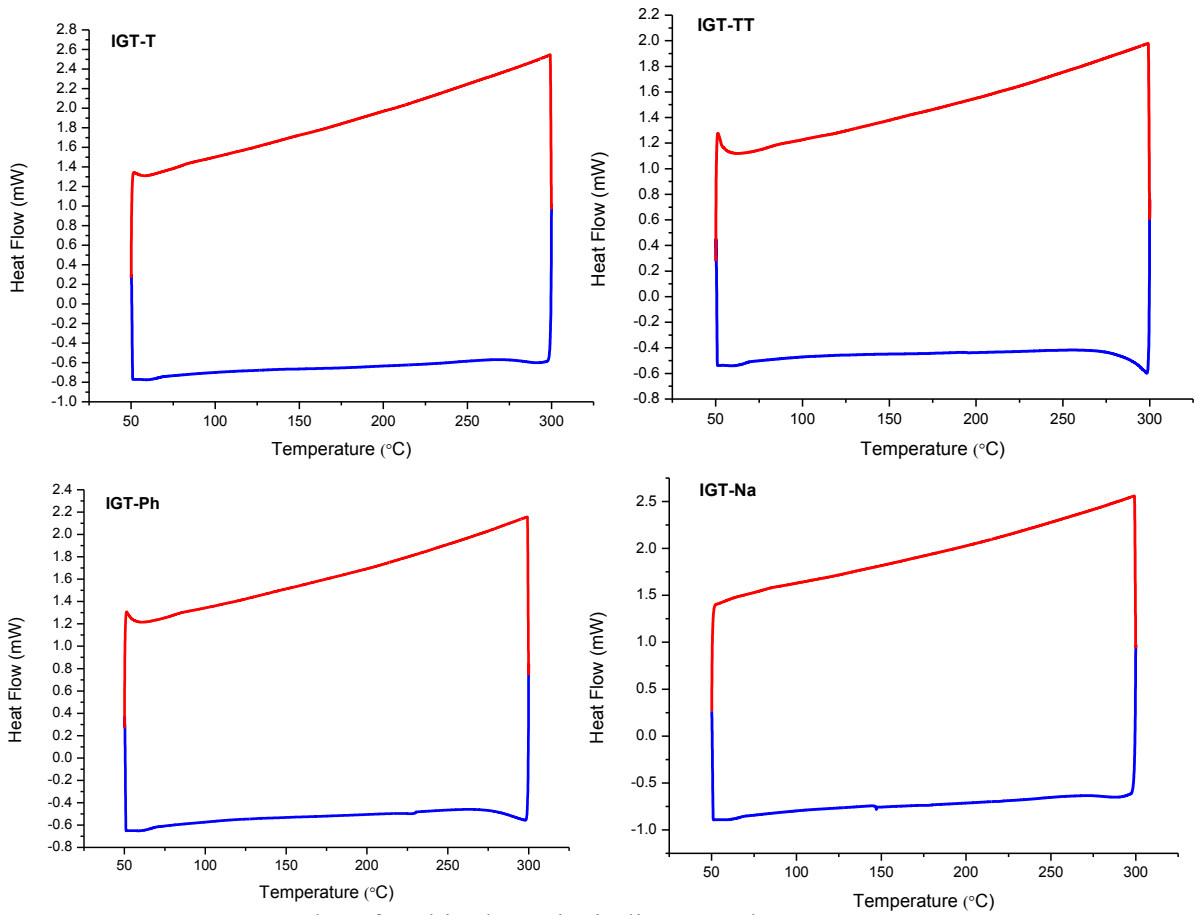


Figure 3.45: DSC data for thiophene isoindigo copolymers **IGT-T**, **IGT-TT**, **IGT-Ph** and **IGT-Na**. The red lines indicate heating while the blue lines indicate cooling. Positive peaks are endothermic events and negative peaks are exothermic events.

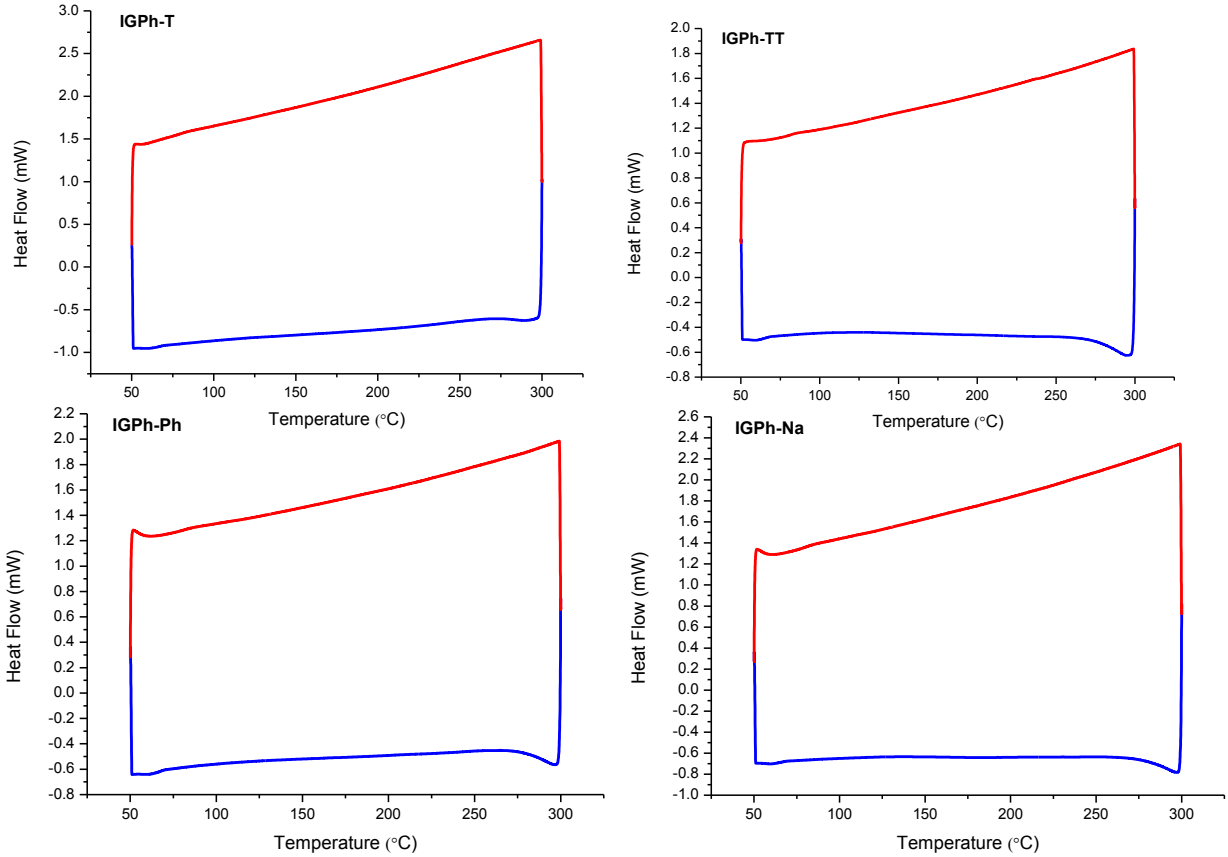


Figure 3.46: DSC data for phenyl isoindigo copolymers **IGPh-T**, **IGPh-TT**, **IGPh-Ph** and **IGPh-Na**. The red lines indicate heating while the blue lines indicate cooling. Positive peaks are endothermic events and negative peaks are exothermic events.

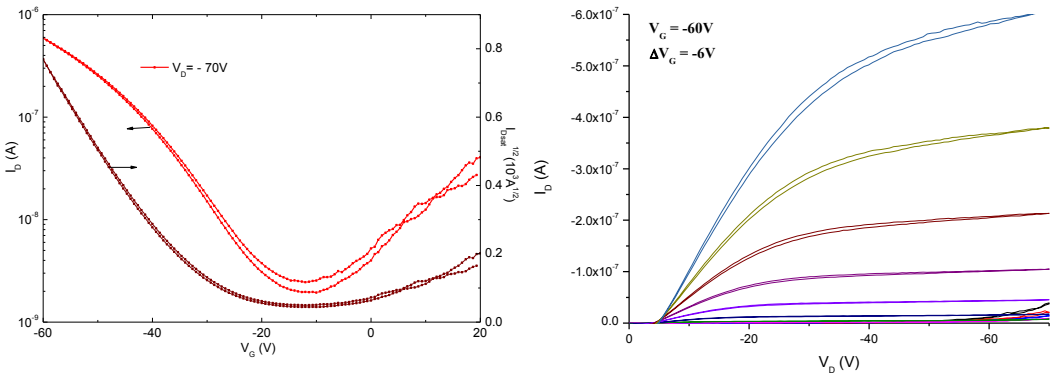
From the DSC data shown for the thiophene isoindigo based copolymers shown in **Figure 3.45** and the DSC data for the phenyl isoindigo based copolymers show in **Figure 3.46** it is clear that no transitions are observed for any of the polymers. Thus based purely on DSC data it is not possible to say if there is a trend in crystallinity for these polymers.

3.4.7 OFET device performance of thiophene and phenyl isoindigo copolymers

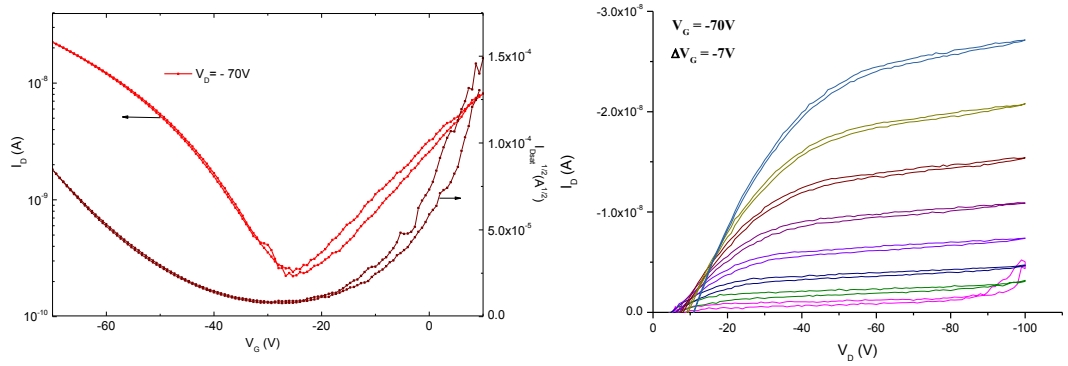
To study the charge carrier mobility of the polymers OFET devices were fabricated for **IGT-Ph**, **IGT-Na**, **IGPh-T**, **IGPh-TT**, **IGPh-Ph** and **IGPh-Na**. Unfortunately OFET devices were not produced for **IGT-T** and **IGT-TT** as as the molecular weight of these materials could not be properly determined it is likely that if these materials are a very low molecular weight then this would give false results. Top-gate, bottom-

contact OFETs were fabricated on glass with Au-PFBT electrodes, a CYTOP^{TM} dielectric and an Al gate. Polymer films were spin cast from dichlorobenzene solution and annealed at 200 °C for 10 min to ensure that any residual solvent was removed. The transfer and output characteristics for the devices are given in **Figure 3.47** below.

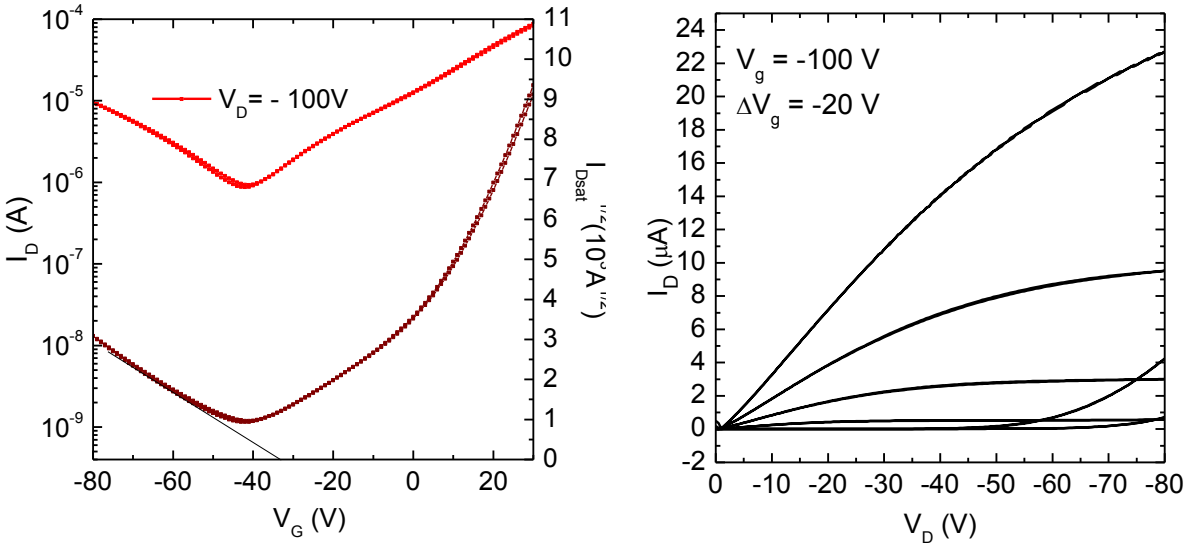
IGT-Ph



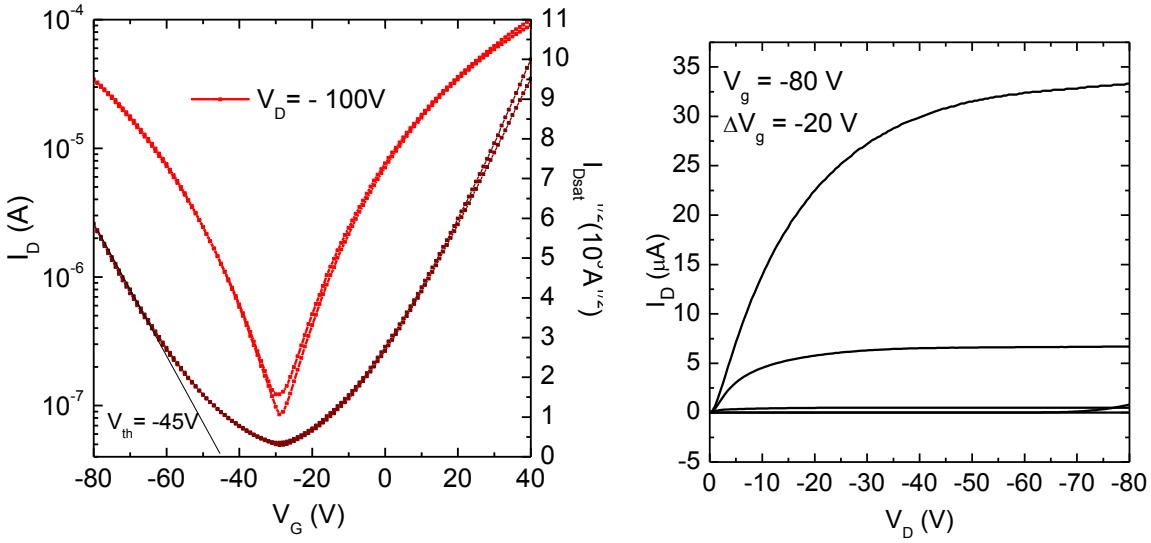
IGT-Na



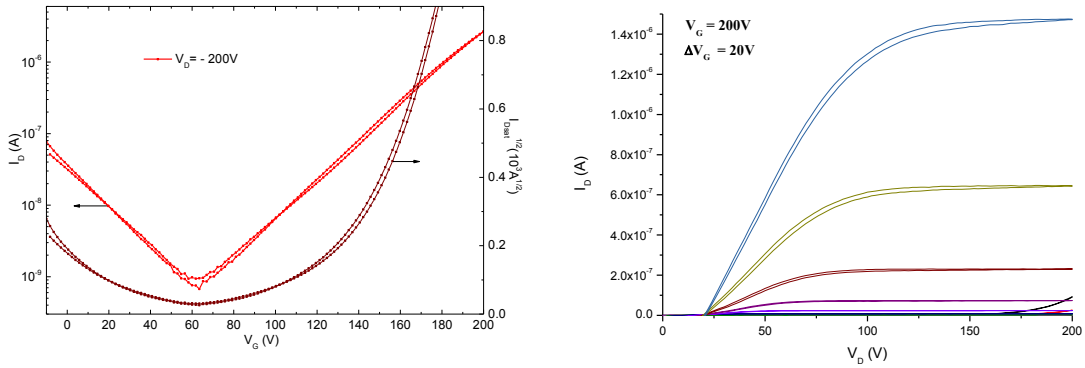
IGPh-T



IGPh-TT



IGPh-Ph



IGPh-Na

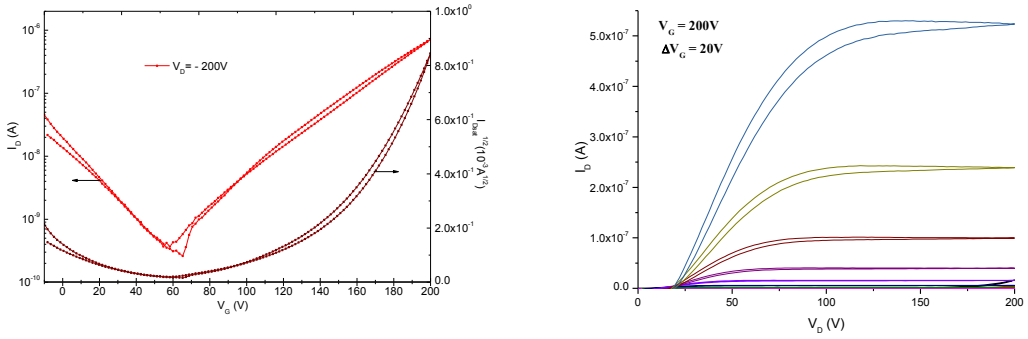


Figure 3.47: Transfer curves (left) and output characteristics (right) of **IGT-Ph**, **IGT-Na**, **IGPh-T**, **IGPh-TT**, **IGPh-Ph**, and **IGPh-Na** in descending order in top gate bottom contact devices, all annealed at 200 ºC.

The thiophene isoindigo copolymers **IGT-Ph** and **IGT-Na** were both found to be reasonably ambipolar with saturation hole mobilities of 1.93×10^{-2} and 1.65×10^{-3} $cm^2V^{-1}s^{-1}$ respectively and almost balanced saturation electron mobilities of 3.82×10^{-2}

and 3.94×10^{-2} $cm^2V^{-1}s^{-1}$ respectively. As the threshold voltages for these polymers were rather high, -27 and -40 V respectively with low on/off ratios this indicates that there is a high trap density within the polymers and that charge injection into the devices is not optimal. It should be noted that for the analogous **IGT-Ph** copolymer with 2-hexadecyl side chains synthesised by Van Pruissen et al[198] no electron transport was observed, although a much lower threshold voltage of 0 V was attained and also a lower saturation hole mobility of 5×10^{-3} $cm^2V^{-1}s^{-1}$.

The phenyl isoindigo copolymers, **IGPh-T** and **IGPh-TT** underwent more extensive device optimisation as the initial devices were annealed at 120 ºC and found to give saturation hole mobilities of 3.37×10^{-4} and 2×10^{-1} $cm^2V^{-1}s^{-1}$ respectively and saturation electron mobilities of 2.22×10^{-2} and 4.00×10^{-2} $cm^2V^{-1}s^{-1}$ respectively. However upon annealing both polymers at 200 ºC it was found that for **IGPh-T**, which at the lower annealing temperature showed poor device reproducibility and large differences in mobility for different channel lengths, the mobility increased by a factor of almost 100. Thus larger saturation hole mobilities of 3.86×10^{-2} and 3.30×10^{-1} $cm^2V^{-1}s^{-1}$ were obtained for **IGPh-T** and **IGPh-TT** respectively whilst the electron mobilities also increased substantially to 4.76×10^{-1} and 4.80×10^{-1} $cm^2V^{-1}s^{-1}$ presumably due to improved polymer morphology. It should be noted though that these polymers have been reported before and shown to give a hole mobility of 1.9×10^{-2} $cm^2V^{-1}s^{-1}$ for **IGPh-T**[199] with an on/off ratio of 10^6, and a hole mobility of 3.4×10^{-1} $cm^2V^{-1}s^{-1}$ for **IGPh-TT**[200] with an on/off ratio of $\sim10^5$-10^6, although no electron mobilities are reported for these polymers.

The phenyl isoindigo copolymers, **IGPh-Ph** and **IGPh-Na** which were not fully optimised show fairly low saturated hole mobilities of 5.32×10^{-3} and 7.87×10^{-3} $cm^2V^{-1}s^{-1}$ with electron mobilities that are an order of magnitude higher for both polymers, being 3.50×10^{-2} and 2.69×10^{-2} $cm^2V^{-1}s^{-1}$ respectively. The fact that these polymers exhibit greater n-type (electron transport) rather than p-type (hole transport) properties is one of interest. When isoindigo is homo polymerised its LUMO is so low that it becomes an n-type semiconductor.[201] However upon adding electron rich groups such as thiophene and thien[3,2-*b*]thiophene the HOMO level is raised allowing the polymers to exhibit more p-type character.[200] As the phenyl and naphthalene groups are not particularly electron rich the isoindigo unit retains its n-type nature as seen for

IGPh-Ph and **IGPh-Na**. It should be noted that some time after these polymers had been synthesised Prashant Sonar et al[202] independently reported the synthesis of **IGPh-Na** with a deeper HOMO at -5.66 eV with a hole mobility of 4×10^{-3} $cm^2V^{-1}s^{-1}$.

Copolymer	μ_h ($cm^2V^{-1}s^{-1}$)	μ_e ($cm^2V^{-1}s^{-1}$)	V_T (V)	I_{on}/I_{off}
IGT-Ph	1.93×10^{-2}	3.82×10^{-2}	-27	$\sim10^2$
IGT-Na	1.65×10^{-3}	3.94×10^{-2}	-40	$\sim10^2$
IGPh-T	3.86×10^{-2}	4.76×10^{-1}	-34	$\sim10^2$
IGPh-TT	3.30×10^{-1}	4.80×10^{-1}	-45	$\sim10^3$
IGPh-Ph	5.32×10^{-3}	3.50×10^{-2}	+46	$\sim10^2$
IGPh-Na	7.87×10^{-3}	2.69×10^{-2}	+45	$\sim10^2$

Table 3.10: Saturated hole and electron mobilities, threshold voltage and on/off ratio for top gate bottom contact devices of **IGT-Ph**, **IGT-Na**, **IGPh-T**, **IGPh-TT**, **IGPh-Ph** and **IGPh-Na**, all annealed at 200 ºC.

From looking at the values for hole and electron mobilities of the thiophene isoindigo and the phenyl isoindigo copolymers it is clear that they all exhibit ambipolar behaviour, but based on this data there is no clear trend that distinguishes the thiophene isoindigo from the phenyl isoindigo. The only trend that is clear is that with proper device optimisation, considerably higher mobilities could be obtained.

3.4.8 OPV device performance of thiophene and phenyl isoindigo copolymers

The copolymers **IGT-T**, **IGT-TT**, **IGT-Ph**, **IGT-Na**, **IGPh-T**, **IGPh-TT**, **IGPh-Ph** and **IGPh-Na** were tested in bulk heterojunction solar cells using the conventional device architecture ITO:PEDOT:PSS / polymer:$PC_{71}BM$ / Ca / Al. The photoactive layer was comprised of either a 1:2 or 1:4 (w/w) blend of polymer and $PC_{71}BM$ deposited from either *o*-dichlorobenzene (ODCB) or a chloroform : ODCB (9:1) mixture via spin coating. The *J-V* curves and EQE spectra of the highest performing devices are shown in **Figure 3.48** and the key photovoltaic parameters are given in **Table 3.11**. Unfortunately the *J-V* and EQE **IGPh-T**, **IGPh-Ph** and **IGPh-Na** were unable to be measured due to the polymers forming poor films. Additionally the EQE spectra of **IGT-T** and **IGT-TT** were not measured due to their poor device performance.

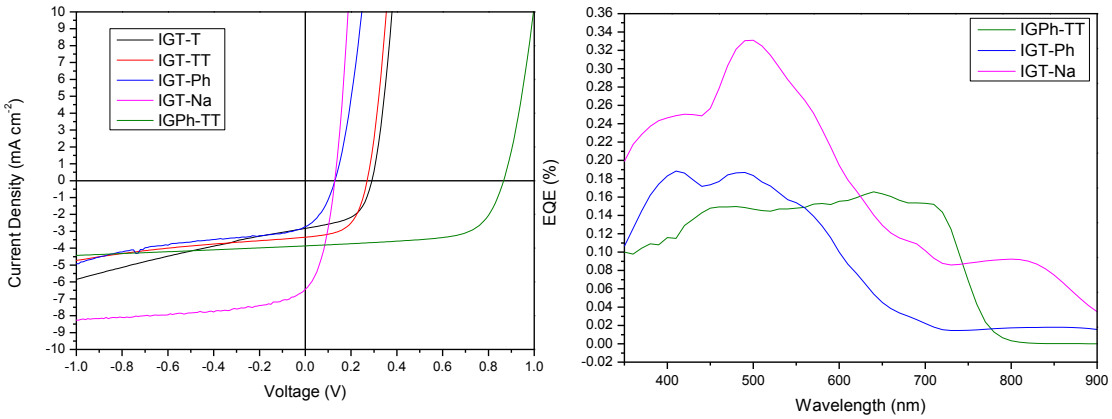


Figure 3.48: *J-V* characteristics (left) of **IGT-T**, **IGT-TT**, **IGT-Ph**, **IGT-Na**, and **IGPh-TT** and EQE spectra (right) of **IGT-Ph**, **IGT-Na** and **IGPh-TT** OPV devices under 100 mWcm^{-2} AM1.5G simulated solar illumination.

The lowest PCE obtained was for **IGT-T** with a PCE of 0.44%. This was due not only to the polymer exhibiting a low V_{oc} as a result of its high lying HOMO but also due to the low short circuit current density (2.83 mAcm^{-2}) that was obtained. Despite the fact that this polymer exhibits the lowest band gap of all the polymers and would thus be expected to have the highest photocurrent it actually shows the lowest J_{sc}. This could potentially be due to the polymer being a low molecular weight oligomer which would hinder charge transport within the device, or alternatively the device could be limited by poor charge separation as the band gap of the polymer may be too low, meaning that its LUMO energy level is too low to allow thermodynamically favourable charge transfer to the $PC_{70}BM$.

IGT-TT showed a marginally higher PCE of 0.52% than **IGT-T** despite the fact that its V_{oc} (0.27 V) was marginally lower due to its higher HOMO energy level. The improvement in PCE was down to the fact that **IGT-TT** exhibited a slightly larger Jsc (3.35 mAcm^{-2}) as well as a marginal improvement in fill factor (0.55). Further improvement in PCE is seen in **IGT-Ph** (0.68%) as the greater band gap as a result of incorporating phenyl lowers the HOMO and in turn improves the V_{oc} to 0.39 V. However the J_{sc} for **IGT-Ph** is still low (3.25 mAcm^{-2}) and it is not until the phenyl is replaced with naphthalene that the J_{sc} more than doubles to 7.39 mAcm^{-2} whilst still retaining the same V_{oc} of 0.39 V. This vastly increases the PCE to 1.64%. An explanation for this can be seen from looking at the EQE spectra in which the significantly larger EQE of **IGT-Na** enables the polymer to generate a greater

photocurrent. This is presumably due to the fact that naphthalene is a larger molecule than phenyl and so has a greater surface area over which to capture photons. Additionally as naphthalene is larger there is a greater possibility of intermolecular π-π stacking taking place as there is less alkyl chain density per unit length to hinder this stacking arrangement. This would enable **IGT-Na** to exhibit better charge transport than **IGT-Ph** which would result in the improvement in J_{sc}.

The highest PCE obtained for the solar cells was for **IGPh-TT** due to its high V_{oc} (0.87 V) as a result of its low lying HOMO energy level. However despite obtaining a moderate fill factor of 0.64, the PCE of 1.95% is still rather low as a result of poor current density (3.50 mA cm^{-2}) due to it having a fairly wide optical band gap. It should be noted that the synthesis of **IGPh-TT** and **IGPh-TT** with a shorter $CH_2CH(C_2H_5)C_4H_9$ side chain has been reported before by Guobing Zhang et al[203] but only the photovoltaic properties of the **IGPh-TT** with the shorter side chain were reported as V_{oc} = 0.84 V, J_{sc} = 3.90 $mAcm^{-2}$, FF = 53, and PCE = 1.74 %. It is evident that the **IGPh-TT** copolymer reported in this work shows a similar V_{oc} and J_{sc} but obtains a higher PCE as a result of its improved FF. This indicates that using longer alkyl chains may have improved the processability of the polymer thus allowing the morphology of the device to be improved leading to an enhancement in FF.

Copolymer	Polymer:$PC_{71}BM$ Ratio	Solvent	V_{oc} (V)	J_{sc} ($mAcm^{-2}$)	FF	PCE (%)
IGT-T	1:4	CF:ODCB (9:1)	0.29	2.83	0.53	0.44
IGT-TT	1:4	CF:ODCB (9:1)	0.27	3.35	0.55	0.52
IGT-Ph	1:2	ODCB	0.39	3.25	0.54	0.68
IGT-Na	1:2	ODCB	0.39	7.39	0.57	1.64
IGPh-TT	1:2	CF:ODCB (9:1)	0.87	3.50	0.64	1.95

Table 3.11: Photovoltaic properties of **IGT-T**, **IGT-TT**, **IGT-Ph**, **IGT-Na** and **IGPh-TT**.

3.4.9 Conclusion

A series of four thiophene isoindigo and four comparable phenyl isoindigo copolymers were synthesised via both Suzuki and Stille coupling polymerisation and

characterised with GPC, UV-Vis, PESA, DSC, OFET and OPV. The use of UV-Vis in combination with DFT calculations reveals that the thiophene isoindigo monomer is significantly more electron donating than the phenyl isoindigo monomer due to the greater delocalisation of electron density between the nitrogen atoms on the thiophene isoindigo core. The implication of the greater electron donation for **IGT-T** verses **IGT-TT** is that the electron donation of the thiophene isoindigo core into the neighbouring thiophene unit induces the quinoidal effect thus causing the band gap to be significantly lower than the thieno[3,2-*b*]thiophene copolymer. This effect is not observed for **IGPh-T** and **IGPh-TT** and so the band gap of **IGPh-TT** is lower than **IGPh-T** purely due to an increase in effective conjugation length. The OFET devices reveal that all the polymers are ambipolar with each polymer showing a slightly higher affinity for n-type charge transport behaviour due to all the polymers exhibiting a low lying LUMO energy level. The OPV devices show that whilst the thiophene isoindigo based polymers are capable of producing relatively higher current densities due to their low band gaps in the case of **IGT-Na**, the phenyl isoindigo based copolymers can achieve a higher PCE as a result of their lower HOMO energy level which produces a much greater V_{oc}.

3.5 Thiophene and Phenyl Isoindigo Based Terpolymers

So far it has been seen that the optical absorption of the thiophene isoindigo and phenyl isoindigo based copolymers can be modulated to absorb across the spectral range purely through changing the choice of comonomer. However the thiophene isoindigo based copolymers lack spectral absorption in the 400-500 nm wavelength region whilst the phenyl isoindigo based copolymers lack spectral absorption in the 800 nm and beyond region. By combining both the thiophene isoindigo monomer and the phenyl isoindigo monomer into the same polymer it is thought that the spectral properties of both monomers can be exploited. This should enable spectral absorption across the full range of the solar spectrum and allow one to traverse the parameter space between high J_{sc} obtained for thiophene isoindigo and high V_{oc} obtained for phenyl isoindigo to obtain high PCE solar cells. Thus to incorporate both monomers into one polymer there are a couple of ways that this can be achieved. Koen H. Hendriks et al[204] recently reported a method of incorporating DPP, thiophene and phenyl into a regular alternating DPP based terpolymer denoted **PDPP3TaltTPT**.

Whilst this polymer obtained an increased PCE of 8% over that of its parent polymers **PDPPTPT** and **PDPP3T** due to its improved optical absorption, which increased the J_{sc}, the synthesis of this polymer is somewhat cumbersome with separate monomers needing to be synthesised via mono brominating DPP, combining it with phenyl to make a DPP-phenyl-DPP monomer and then copolymerising this new unit with thiophene. An alternative method used by several groups involves combining either two acceptor units in varying proportions with a donor unit to give a terpolymer in which the individual acceptor units are randomly placed[205-210] or combining two donor units in varying proportions with an acceptor unit to give a terpolymer in which the donor units are randomly placed.[211-214] By systematically varying the ratios of either the two acceptor units or the two donor units it has been found that the spectral absorption of these polymers can be broadened thus enabling the PCE to be improved as a result of an enhanced J_{sc}. As this method of combining pre-existing monomers is synthetically appealing due to its simplicity and could be more industrially relevant in terms of lowering synthesis costs, it was decided that this method would be worth trying.

3.5.1 Synthesis of random thiophene isoindigo and phenyl isoindigo terpolymers

As Suzuki polymerisation conditions yielded the highest molecular weights for both the thiophene isoindigo and the phenyl isoindigo copolymers produced thus far, it was decided that this would be the method of choice. Thus the branched thiophene isoindigo monomer (**3.25**) was copolymerised with phenyl isoindigo monomer (**3.6**) and recrystallised commercially available 1,4-phenyldiboronic acid bis pinacol ester monomer (**3.27**) using $Pd(PPh_3)_4$ as catalyst, Na_2CO_3 as base, aliquat 336 as phase transfer catalyst and toluene and water as the solvents over the course of three days at 110 ºC. Three polymers were produced in this way with the ratio of thiophene isoindigo to phenyl to phenyl isoindigo being varied in the ratios 0.25:1:0.75 to give polymer **rIGPhPhIGT0.25**, 0.5:1:0.5 to give polymer **rIGPhPhIGT0.50** and 0.75:1:0.25 to give polymer **rIGPhPhIGT0.75**. After the three days the polymers were precipitated into methanol, filtered through a Soxhlet thimble and purified by Soxhlet extraction with acetone, hexane and chloroform. The chloroform fraction of each polymer was concentrated and heated with sodium diethyldithiocarbamate

trihydrate to remove residual palladium. The copolymers were finally re-precipitated into methanol and filtered using cellulose filter paper and dried under high vacuum.

The reaction schemes for the random thiophene isoindigo and phenyl isoindigo terpolymers are given in **Figure 3.49**.

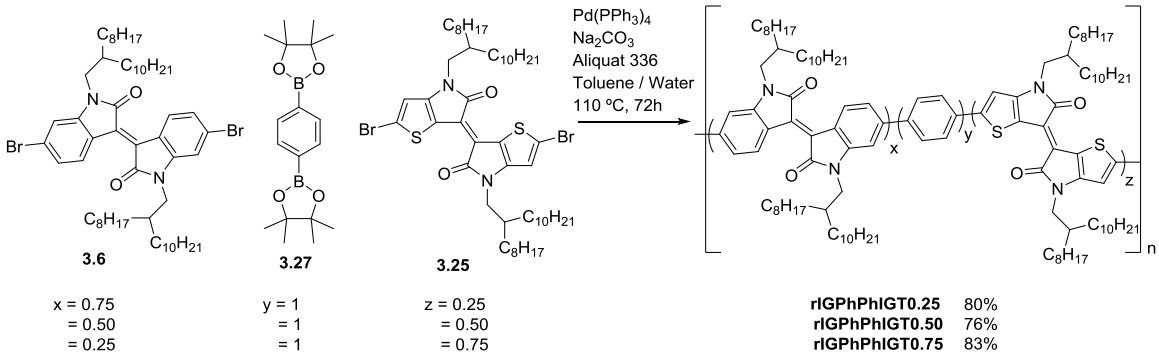


Figure 3.49: Synthesis of random thiophene and phenyl isoindigo based terpolymers **rIGPhPhIGT0.25**, **rIGPhPhIGT0.50** and **rIGPhPhIGT0.75**.

3.5.2 Properties of random thiophene isoindigo and phenyl isoindigo terpolymers

To determine the molecular weights of the collected polymer fractions, GPC calibrated against polystyrene standards was used. **Table 3.12** summarises the molecular weights obtained for each polymer.

Polymer	Phenyl isoindigo	Phenyl	Thiophene isoindigo	M_n [kg/mol][a)]	M_w [kg/mol][b)]	PDI[c)]
rIGPhPhIGT0.25	0.75	1	0.25	79	180	2.26
rIGPhPhIGT0.50	0.50	1	0.50	85	141	1.65
rIGPhPhIGT0.75	0.25	1	0.75	69	125	1.82

Table 3.12: Ratio of monomer units used in each terpolymer and molecular weights of terpolymers. a) M_n = number average molecular weight b) M_w = weight average molecular weight c) PDI = polydispersity index

As can be seen from **Table 3.12** the molecular weights for all of the polymers are exceedingly high considering that three monomer units had to be accurately weighed to achieve optimal monomer ratios. Despite the fact that these polymers have high

molecular weights they are all very soluble in chloroform and chlorobenzene, presumably due to the fact that as the monomers are randomly arranged in the polymer chains they are less likely to form π-π stacks and aggregate in solution.

3.5.3 Optical properties of random thiophene isoindigo and phenyl isoindigo terpolymers

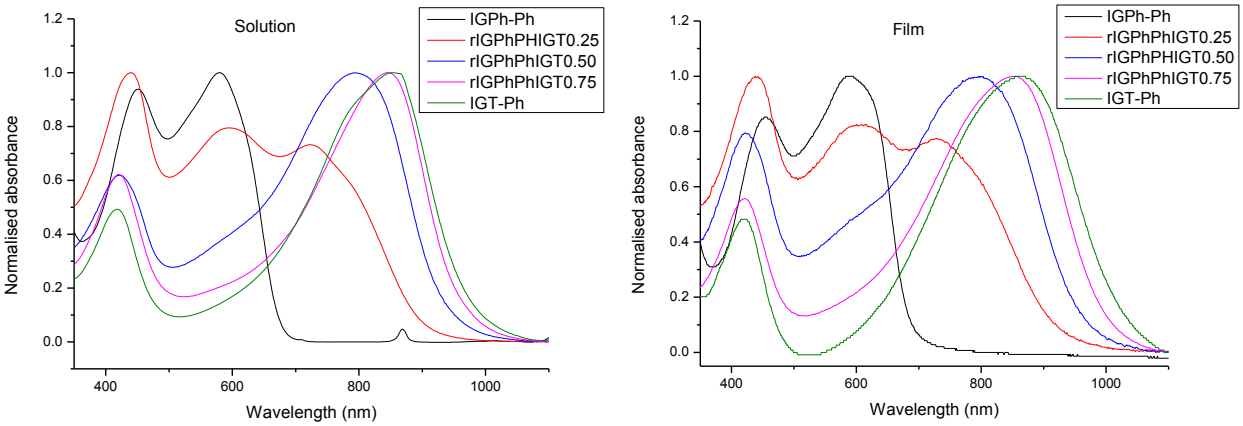


Figure 3.50: UV-Vis spectra of **IGPh-Ph**, **rIGPhPhIGT0.25**, **rIGPhPhIGT0.50**, **rIGPhPhIGT0.75** and **IGT-Ph** in chlorobenzene solution at 25 ºC (left) and in thin film spin coated from chlorobenzene solution, 5 mg/mL, 1000 rpm, 1 min (right).

From the solution UV-Vis spectra it can be seen that for **rIGPhPhIGT0.75** the UV-Vis absorption of the polymer is almost indistinguishable from the parent **IGT-Ph** polymer indicating that the phenyl isoindigo monomer plays a negligible part within the terpolymer. However as the thiophene isoindigo content of the terpolymer decreases the maximum absorption shifts from 847 nm for **rIGPhPhIGT0.75** to 792 nm for **rIGPhPhIGT0.50** although the broad shape of the **rIGPhPhIGT0.50** spectra still resembles the shape of the parent **IGT-Ph** polymer. It is only once the ratio of thiophene isoindigo has decreased to 0.25 equivalents that the influence of the phenyl isoindigo can be seen. For **rIGPhPhIGT0.25** it is evident that the two peaks at 439 nm and 594 nm resemble the respective π-π* transition and charge transfer band of the parent **IGPh-Ph** copolymer. However the peak at 724 nm is more reminiscent of a blue shifted charge transfer band of **IGT-Ph**, indicating that greater hybridisation of the thiophene isoindigo is taking place in this terpolymer.

On going from solution to thin film the charge transfer band for **rIGPhPhIGT0.75** red shifts to 736 nm, for **rIGPhPhIGT0.50** the charge transfer band red shifts to 798 nm and for **rIGPhPhIGT0.25** the charge transfer band assigned to thiophene isoindigo red shifts to 736 nm, indicating that all of the terpolymers exhibit a greater degree of molecular order and planarity in the solid state. It is interesting to note however that the thin film of **rIGPhPhIGT0.50** exhibits a more pronounced bump at 594 nm corresponding to the phenyl isoindigo charge transfer band and also exhibits a greater extinction coefficient for the π-π* absorption at 438 nm.

With regards to optical band gap it is evident that as the phenyl isoindigo content increased the optical band gap increased. This is due to the greater influence of steric effects between the hydrogen atoms between the phenyl isoindigo and the hydrogen atoms on the neighbouring phenyl unit as well as a decrease in the amount of electron density available for the quinoidal effect as the amount of electron rich thiophene isoindigo decreased. However compared to the parent polymer **IGPh-Ph**, the optical band gap of **rIGPhPhIGT0.25** is substantially reduced by 0.47 eV whereas the optical band gap of **rIGPhPhIGT0.75** is only increased by 0.01 eV compared to **IGT-Ph** indicating that the optical band gap of the terpolymers is most affected by the proportion of thiophene isoindigo present. The optical band gaps obtained are listed in **Table 3.13**.

Polymer	**Solution**			**Thin Film**			**Optical band gap (eV)**[c]
	π-π* (nm)	Charge transfer band (nm)[a]	Charge transfer band (nm)[b]	π-π* (nm)	Charge transfer band (nm)[a]	Charge transfer band (nm)[b]	
IGPh-Ph	451	582	-	452	584	-	1.82
rIGPhPhIGT0.25	439	594	724	438	607	736	1.35
rIGPhPhIGT0.50	420	-	792	422	593	798	1.28
rIGPhPhIGT0.75	420	-	847	421	-	851	1.23
IGT-Ph	418	-	852	420	-	854	1.22

Table 3.13: Optical properties of random thiophene and phenyl isoindigo terpolymers a) Charge transfer band corresponding to **IGPh-Ph** b) Charge transfer band corresponding to **IGT-Ph** c) Optical band gap calculated from absorption onset in thin film.

3.5.4 DSC of random thiophene and phenyl isoindigo terpolymers.

To see if there are any trends in crystallinity as the ratio of monomers within the terpolymers changes, DSC measurements were taken.

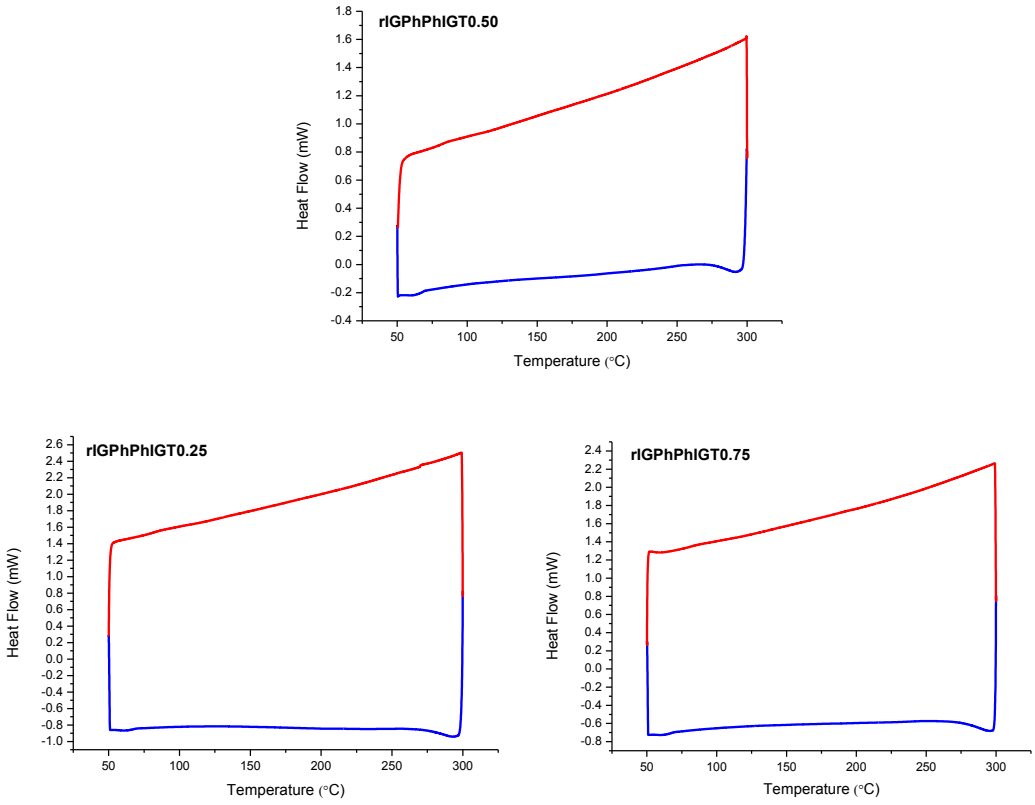


Figure 3.51: DSC data for random thiophene isoindigo and phenyl isoindigo terpolymers **rIGPhPhIGT0.25** (left), **rIGPhPhIGT0.50** (top), **rIGPhPhIGT0.75** (right). The red lines indicate heating while the blue lines indicate cooling. Positive peaks are endothermic events and negative peaks are exothermic events.

From the DSC data shown for the random thiophene isoindigo and phenyl isoindigo based terpolymers shown in **Figure 3.51** it is clear that no transitions are observed for any of the polymers. Thus based purely on DSC data it is not possible to say if there is a trend in crystallinity for these polymers.

3.5.5 PESA determination of energy levels of random thiophene and phenyl isoindigo terpolymers.

The HOMO energy levels of **rIGPhPhIGT0.25**, **rIGPhPhIGT0.50** and **rIGPhPhIGT0.75** were measured by PESA. For this measurement two thin films spin coated from chlorobenzene of each terpolymer were measured and the average

HOMO energy level was listed in **Table 3.14** in relation to the vacuum energy level. Using the optical band gaps, estimated from the absorption onset of the thin film UV-Vis spectrums the LUMO energy levels were calculated and also included in **Table 3.14**.

Polymer	HOMO (eV)[a)]	LUMO (eV)[b)]	Optical band gap (eV)[c)]
IGPh-Ph	-5.57	-3.75	1.82
rIGPhPhIGT0.25	-4.94	-3.59	1.35
rIGPhPhIGT0.50	-4.82	-3.54	1.28
rIGPhPhIGT0.75	-4.75	-3.52	1.23
IGT-Ph	-4.84	-3.62	1.22

Table 3.14: Energy levels of random thiophene and phenyl isoindigo terpolymers. a) Measured by PESA b) Estimated by addition of the absorption onset to the HOMO c) Determined from the absorption onset of the thin film UV-Vis spectrum.

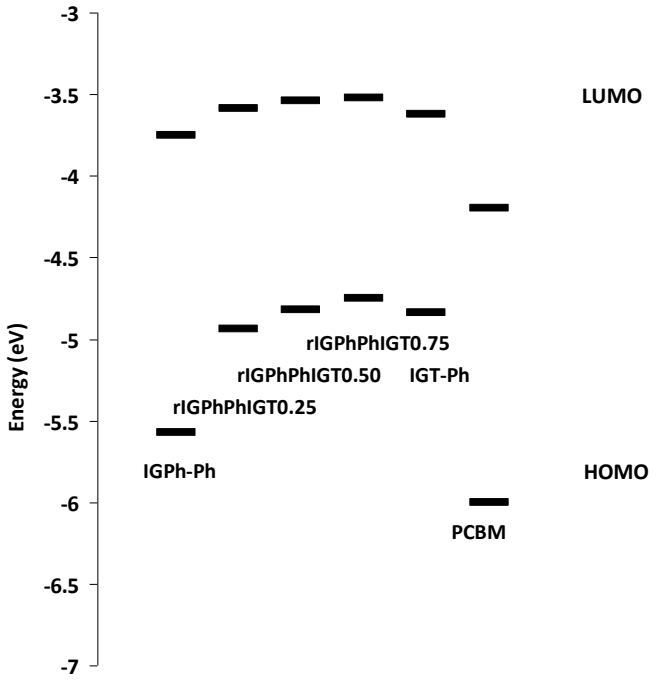


Figure 3.52: Visualisation of HOMO and LUMO energy levels for random thiophene isoindigo and phenyl isoindigo terpolymers relative to **IGPh-Ph**, **IGT-Ph** and $PC_{60}BM$.

From looking at the HOMO values it is clear to see that all of the terpolymers have a higher HOMO energy level than the parent **IGPh-Ph** copolymer due to the influence

of the electron rich thiophene isoindigo monomer. For **rIGPhPhIGT0.25** the HOMO value of -4.94 eV lies nicely in between that of **IGPh-Ph** and **IGT-Ph** as would be expected. **rIGPhPhIGT0.50** and **rIGPhPhIGT0.75** however have HOMO energy levels that are higher than that of the parent **IGT-Ph** copolymer despite the fact that they should contain less electron density due to containing a lower proportion of thiophene isoindigo. A possible explanation for this effect could be that as the molecular weights of **rIGPhPhIGT0.50** and **rIGPhPhIGT0.75** are much greater than that of **IGT-Ph**, each terpolymer chain contains more thiophene isoindigo than a **IGPh-Ph** copolymer chain and thus the films of **rIGPhPhIGT0.50** and **rIGPhPhIGT0.75** have a higher electron density which thus corresponds to a higher HOMO energy level.

The LUMO values for all of the terpolymers are also higher than both of the parent **IGPh-Ph** and **IGT-Ph** copolymers. The trend observed is that as the thiophene isoindigo content of the terpolymers increases the higher the LUMO energy level, despite the fact that the optical band gap decreases to reflect that of the parent **IGT-Ph** copolymer. The trend for the LUMO energy levels closely matches that of the HOMO energy levels in that as the HOMO energy levels increase the LUMO energy also increases. This would suggest that there is a minimum separation of HOMO and LUMO that is possible and in this case it is governed by the minimum band gap of the thiophene isoindigo monomer.

3.5.6 OPV device performance of random thiophene isoindigo and phenyl isoindigo terpolymers.

The terpolymers **rIGPhPhIGT0.25**, **rIGPhPhIGT0.50** and **rIGPhPhIGT0.75** were tested in bulk heterojunction solar cells using the conventional device architecture ITO:PEDOT:PSS / polymer:$PC_{71}BM$ / Ca / Al. The photoactive layer was comprised of a either a 1:2 or 1:4 (w/w) blend of polymer and $PC_{71}BM$ deposited from either *o*-dichlorobenzene (ODCB) or a chloroform : ODCB (9:1) mixture via spin coating. Despite repeated attempts to produce working devices from these polymers, by trying various solvents, blend ratios and deposition spin speeds, no current could be detected from the devices. This could be due to a variety of reasons such as poor morphology,

poor charge separation or poor charge transport. To see if charge transport was the issue OFET devices were prepared, the results of which are in section **3.5.7**.

3.5.7 OFET device performance of random thiophene isoindigo and phenyl isoindigo terpolymers.

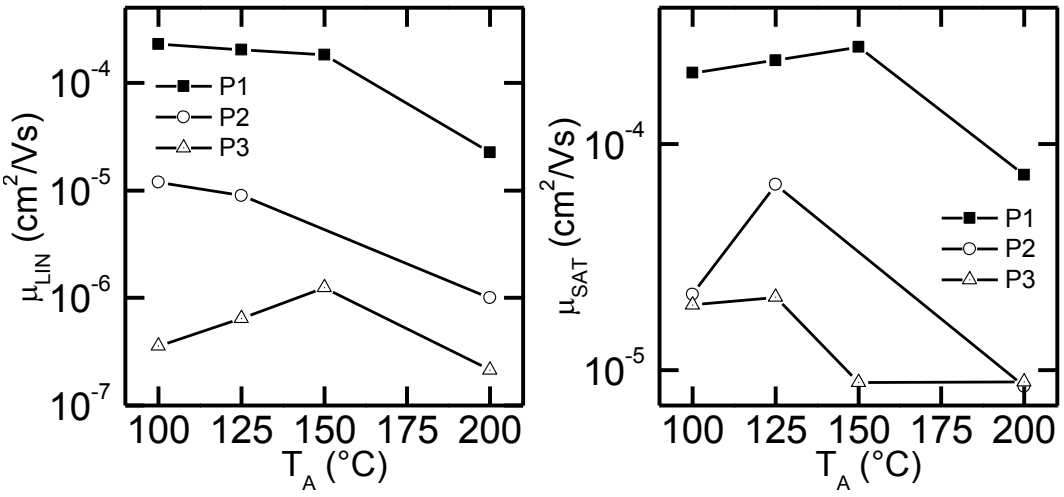


Figure 3.53: Linear (left) and saturated (right) hole mobilities of the random terpolymers at various annealing temperatures in bottom gate bottom contact OFETs. P1 corresponds to **rIGPhPhIGT0.75**, P2 corresponds to **rIGPhPhIGT0.50** and P3 corresponds to **rIGPhPhIGT0.25**.

To evaluate the charge transport properties of the terpolymers bottom-gate, bottom-contact transistor structures were fabricated using heavily doped p-type Si wafers acting as a common gate electrode and a 200 nm thermally grown SiO_2 layer as the dielectric. Using conventional photolithography, gold source-drain electrodes were defined with channel lengths and widths in the range of 1–40 μm and 1–20 mm, respectively. A 10 nm layer of titanium was used as an adhesion layer for the gold on the SiO_2 giving finished electrodes that were 100 nm thick. The SiO_2 surface was passivated with hexamethyldisilazane (HMDS) before the terpolymers **rIGPhPhIGT0.25**, **rIGPhPhIGT0.50** and **rIGPhPhIGT0.75** dissolved in chlorobenzene at a concentration of 5 mg/mL were spin coated on top of the electrodes at 2000 rpm for 30 seconds. The effect of annealing for 10 minutes at a variety of elevated temperatures, performed on a hotplate under a nitrogen atmosphere, was subsequently evaluated, with the results being seen in **Figure 3.53**. From **Figure**

3.53 it is evident that annealing up to 150 ºC has little impact on the linear mobility of **rIGPhPhIGT0.75** and **rIGPhPhIGT0.50** but increases the linear mobility of **rIGPhPhIGT0.25**. The saturation mobilities on the other hand seem to be at their maximum at 150 ºC for **rIGPhPhIGT0.75** and at 125 ºC for **rIGPhPhIGT0.50** and **rIGPhPhIGT0.25** (although the 150 ºC annealing temperature for the saturation mobility of **rIGPhPhIGT0.50**, was not tested). For all of the polymers it is apparent that annealing at a temperature of 200 ºC is detrimental for both the linear and hole mobility. Thus it is evident that annealing at the right temperature is important for maximising device performance. This is due to the fact that annealing not only removes residual chlorobenzene which has a boiling point of 131 ºC and can be detrimental for device performance, but also could potentially improve the crystallinity of the film thus enabling improved charge carrier mobilities.

The transfer and output characteristics of the devices are shown in **Figures 3.53**, **3.54** and **3.55**.

rIGPhPhIGT0.25

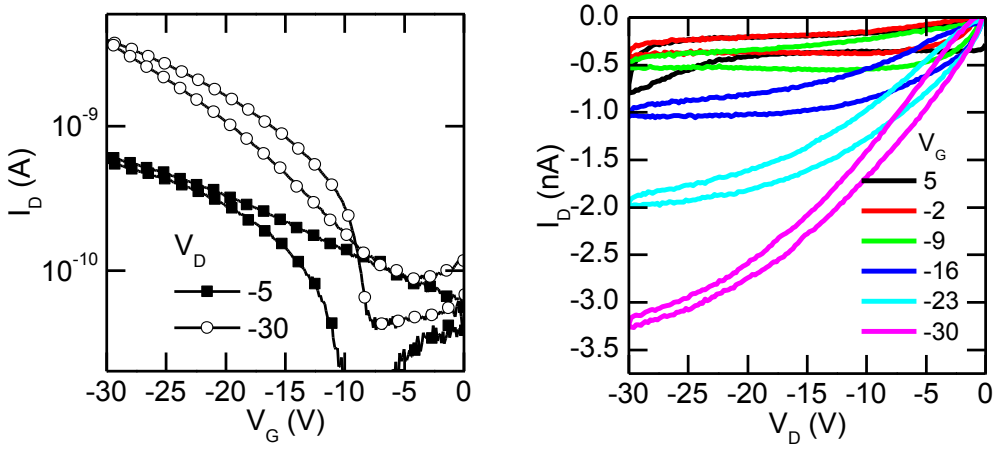


Figure 3.53: Transfer (left) and output (right) characteristics of bottom gate bottom contact OFETs using **rIGPhPhIGT0.25**. The channel width and length is 10mm and 5 µm respectively.

rIGPhPhIGT0.50

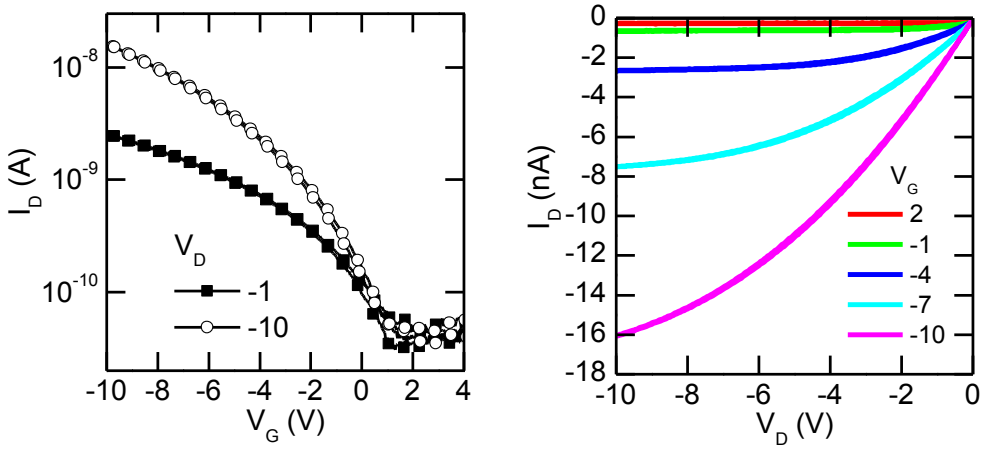


Figure 3.54: Transfer (left) and output (right) characteristics of bottom gate bottom contact OFETs using **rIGPhPhIGT0.50**. The channel width and length is 10mm and 5 µm respectively.

rIGPhPhIGT0.75

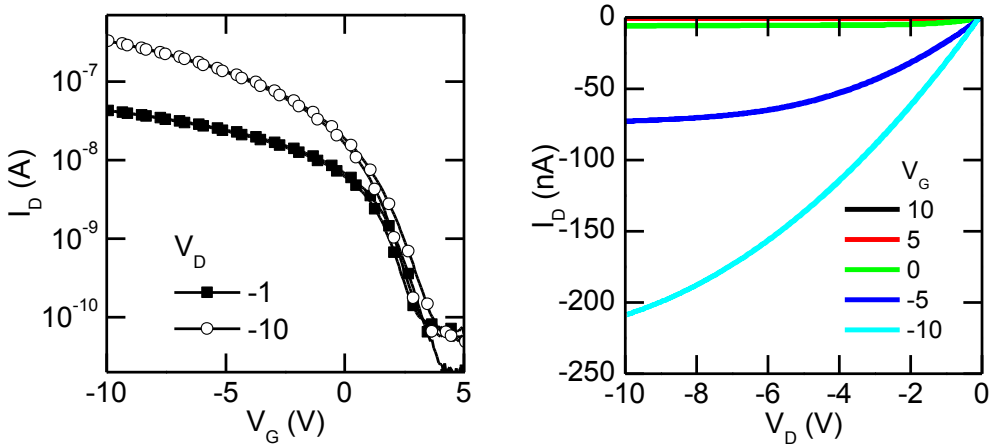


Figure 3.55: Transfer (left) and output (right) characteristics of bottom gate bottom contact OFETs using **rIGPhPhIGT0.75**. The channel width and length is 10mm and 10 µm respectively.

The mobilities for the terpolymers turn out to be substantially lower than that of the parent copolymers, possibly due to the random arrangement of monomers causing conformational disorder along the backbone, which thus disrupts the possibility for π-π stacking and the formation of lamella structures that are conducive to charge transport. The terpolymers all show p-type behaviour rather than the n-type behaviour exhibited by the parent copolymers presumably due to their raised HOMO energy level. The saturated hole mobilities of the polymers are given in **Table 3.15**.

Polymer	μ_h ($cm^2V^{-1}s^{-1}$)	V_T (V)	I_{on}/I_{off}
IGPh-Ph	5.32×10^{-3}	46	$\sim10^2$
rIGPhPhIGT0.25	2×10^{-5}	-2	7×10^1
rIGPhPhIGT0.50	2×10^{-4}	-1	3×10^2
rIGPhPhIGT0.75	6×10^{-4}	3	5×10^3
IGT-Ph	1.93×10^{-2}	-27	$\sim10^2$

Table 3.15: Saturated hole mobilities, threshold voltage and on/off ratio for bottom gate bottom contact devices of **rIGPhPhIGT0.25**, **rIGPhPhIGT0.50** and **rIGPhPhIGT0.75** compared to top gate bottom contact devices of **IGPh-Ph** and **IGT-Ph**.

Despite the fact that the random terpolymers showed fairly poor mobilities compared to the parent copolymers the mobilities obtained seem to be rather reproducible over a range of devices with different channel widths and lengths as depicted in **Figure 3.56**.

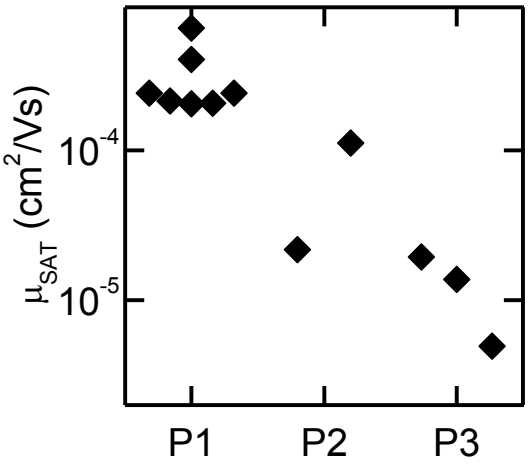


Figure 3.56: Saturation mobility for multiple devices with channel dimension ranging from 7.5-20 mm in width and 5-40 μm in length. P1 corresponds to **rIGPhPhIGT0.75**, P2 corresponds to **rIGPhPhIGT0.50** and P3 corresponds to **rIGPhPhIGT0.25**.

As can be seen from **Figure 3.56** as the content of thiophene isoindigo increases the saturation hole mobility increases in an almost linear fashion. This indicates that the introduction of thiophene isoindigo facilitates greater planarisation of the polymer backbone which could possibly enable the polymer to exhibit more crystalline attributes that are conducive to obtaining greater charge carrier mobilities.

3.5.8 Conclusion

A series of three new random thiophene isoindigo and phenyl isoindigo terpolymers **rIGPhPhIGT0.25**, **rIGPhPhIGT0.50** and **rIGPhPhIGT0.75** were synthesised via Suzuki coupling polymerisation and characterised with GPC, UV-Vis, PESA, DSC, OPV and OFET. All of the terpolymers showed remarkably high molecular weights and remained soluble in common solvents due to their random structure. The UV-Vis indicates that the attributes of both of the isoindigo monomers play a roll in both broadening the absorption and increasing the amount of absorption across the entire spectral range. PESA measurements show that the energy levels of all the terpolymers are dominated by the electron rich nature of the thiophene isoindigo. Unfortunately despite the improvement in optical absorption no current was observed in OPV devices possibly as a result of the reduced charge carrier mobilities observed in the OFETs.

3.6 Thiazole Isoindigo

From looking at both phenyl isoindigo and thiophene isoindigo it is apparent that the electron deficient nature of phenyl allows for the copolymers to have wide band gaps whilst the electron rich nature of thiophene isoindigo promotes very narrow band gaps. Additionally the structures of the two are very different with the phenyl ring of the phenyl isoindigo promoting steric hindrance with neighbouring monomer units by virtue of having a protruding hydrogen atom on the carbon atom beta to the carbon atom linking the monomers together. This steric hindrance is not present in the thiophene isoindigo and thus the polymer backbones of thiophene isoindigo based copolymers can exhibit greater planarity. So it would be evident that if one could combine the electron deficient nature of phenyl isoindigo with the planarising attributes of thiophene isoindigo it should produce copolymers that have intermediate band gaps that are better suited for absorbing photons in the 600-800 nm region of the solar spectrum. One such candidate for replacing phenyl and thiophene is thiazole. Thiazole is not only electron deficient by virtue of containing nitrogen in an electron withdrawing position in the form of an imine (C=N), but also has the same shape as thiophene. Thiazole has already been successfully exploited in a number of small molecules and polymers for both OPV and OFET devices in a variety of forms

including thiazole, bithiazole, 4-alkyl thiazole, thiazolothiazole, benzobisthiazole, pyrrolo[3,2-d:4,5-d']bisthiazole and carbonyl bridged bithiazole to name but a few.[215]

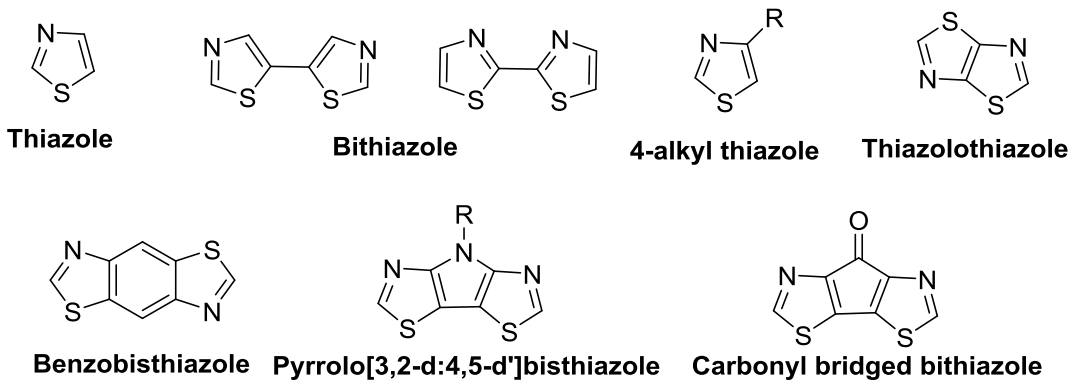


Figure 3.57: Chemical structures of thiazole, bithiazole, 3-alkyl thiazole, thiazolothiazole, benzobisthiazole, pyrrolo[3,2-d:4,5-d']bisthiazole and carbonyl bridged bithiazole.

Thus the next challenge was to attempt to incorporate thiazole into the isoindigo core. Unfortunately the end goal was not reached due to the task being synthetically challenging. Section **3.6.1** below outlines the steps taken to reach the target monomer.

3.6.1 Towards the synthesis of thiazole isoindigo.

A number of synthetic routes were attempted to produce thiazole isoindigo. The first route that was attempted followed that used to produce thiophene isoindigo as shown in **Figure 3.58**.

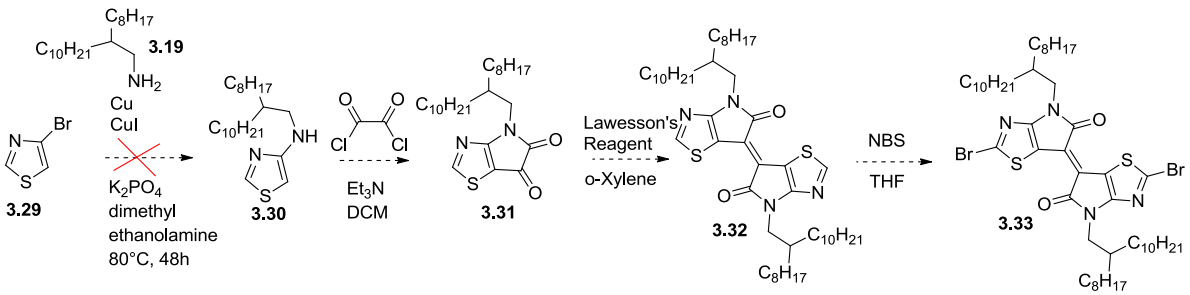


Figure 3.58: Initial route towards thiazole isoindigo monomer (**3.33**).

The initially planed route towards obtaining the thiazole isoindigo monomer (**3.33**) involved the amination of 4-bromothiazole (**3.29**) followed by the cyclization of the amine product (**3.30**) with oxalyl chloride and triethylamine to give the cyclised

thiazole (**3.31**) which would be subsequently dimerised with Lawesson's reagent to give dimer (**3.32**) and brominated with NBS to give the monomer (**3.33**). Unfortunately the initial Ullmann coupling reaction step failed to yield any product and only starting material was recovered, despite trying longer reaction times and higher reaction temperatures.

Thus an alternative method to aminate 4-bromothiazole (**3.29**) was attempted by using $Pd_2(dba)_3$ as a catalyst rather than copper, with BINAP ligands, amine (**3.19**) and sodium tert-butoxide as a strong base in refluxing toluene in accordance to a method used in the production of pyrrolo[3,2-d:4,5-d']bisthiazole.[216] However not only is this method more suitable for linking two aromatic units to the amine but as it turns out the thiazole also needs to be protected in the alpha positions, otherwise, as was observed in this reaction, the addition of the sodium tert- butoxide quickly decomposes the thiazole in under 10 minutes.[217]

As protecting the alpha positions of the thiazole for the amination was not a viable option an alternative route to obtaining the aminothiazole (**3.30**) was devised, **Figure 3.59**.

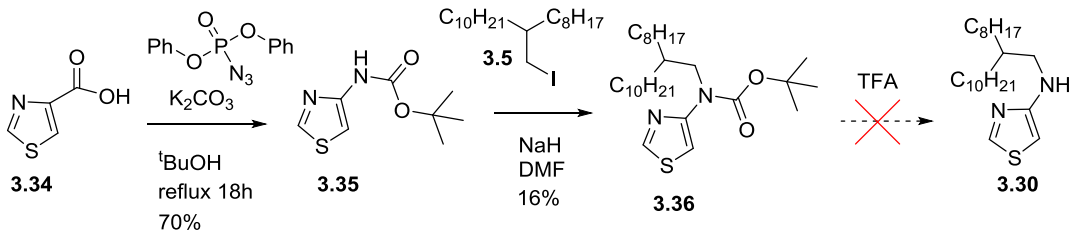


Figure 3.59: Synthesis route towards aminothiazole **(3.30)**.

Using 4-thiazole carboxylic acid (**3.34**) and diphenylphosphorylazide with potassium carbonate in refluxing tert-butanol the Boc protected amide could be formed via a Curtius rearrangement[218] in 70% yield. Subsequent deprotonation of the amide with mild base sodium hydride enabled the nitrogen to be alkylated with alkyl iodide (**3.5**)[219] to achieve the alkylated and Boc protected thiazole (**3.36**) in 16% yield after extensive purification. The next step was rather more problematic as initial attempts to remove the Boc protecting group with trifluoroacetic acid (TFA)[220, 221] over the course of 18 h in DCM at 25 ºC completely decomposed the thiazole. Subsequent attempts with TFA found that the thiazole decomposed after just 20 minutes. Thus

alternative Boc deprotection conditions were tried including using tertiary butyl amine fluoride (TBAF),[222] 4N HCl in dioxane/DCM at 25 ºC for 1 h[223] - which returned starting material, boiling water[224] - which returned starting material, heating in toluene at 200 ºC for 24 h[225] – which returned starting material and heating at 240 ºC under vacuum for 1.5 h at which point the thiazole decomposed. From all of these Boc deprotection attempts it is evident that the Boc group on the tertiary amine is surprisingly stable and that if the Boc group does become deprotected under very harsh acidic conditions or at very high temperatures then the resulting amine may not be stable enough to survive these conditions. Thus to see if the resulting amine could be stabilised, a ketone was introduced into the alkyl side chain. This means that that upon Boc deprotection instead of an amine being formed an amide would be formed, which is able to stabilise the lone pair of electrons on the nitrogen via delocalisation with the carbonyl group which thus forms a more stable molecule. For this purpose the Boc protected thiazole (**3.35**) was deprotonated with sodium hydride and reacted with palmitoyl chloride[219] to give the straight chain alkylated and Boc protected thiazole (**3.37**). The reason that palmitoyl chloride was used rather than a branched chain acid chloride was purely due to the fact that palmitoyl chloride is commercially available and thus faster progress in developing the synthetic methodology could be made. Additionally, thiazole isoindigo based polymers with linear alkyl side chains may also have a use in OFETs as linear alkyl side chains are more able to promote crystalline polymer behaviour than branched side chains.[110] Boc deprotection of thiazole (**3.37**) was subsequently attempted with TFA at rt over 2 h and also with 4N HCl in dioxane/DCM at 25 ºC for 2 h but both of these methods failed. However upon using a mild Boc deprotection method[226, 227] involving magnesium perchlorate at 50 ºC in acetonitrile the desired product (**3.38**) was obtained in 38% yield.

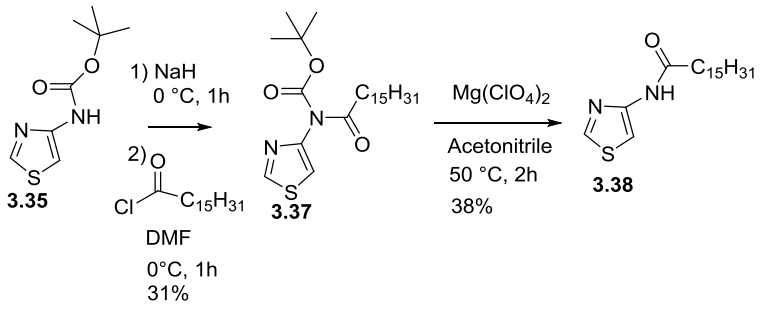


Figure 3.60: Synthesis of Boc deprotected thiazole (**3.38**)

It was at this stage that a collaboration with the company BASF revealed that a quicker and much easier synthesis to obtain a thiazole amide was possible.[228] Thus using 2-thiocyanatoacetonitrile (**3.39**) dissolved in acetic acid cooled to 10 ºC, the 2-thiocyanatoacetonitrile (**3.39**) could be instantaneously ring closed to form 2-bromothiazol-4-amine (**3.40**) upon the dropwise addition of a 33% solution of HBr in acetic acid. This product was produced in quantitative yield and could then be filtered off, washed and used without further purification. An interesting observation was made with this reaction when instead of using a 33% HBr solution in acetic acid, a 48% solution of HBr in acetic acid was used by mistake. It turns out that the reaction fails to work with a higher concentration of HBr indicating that the products and reactants exist in a finely balanced equilibrium as shown in **Figure 3.61**, which may explain why previous attempts to Boc deprotect compounds (**3.36**) and (**3.37**) with the strong acid TFA resulted in a loss of aromatic peaks in the NMR spectra.

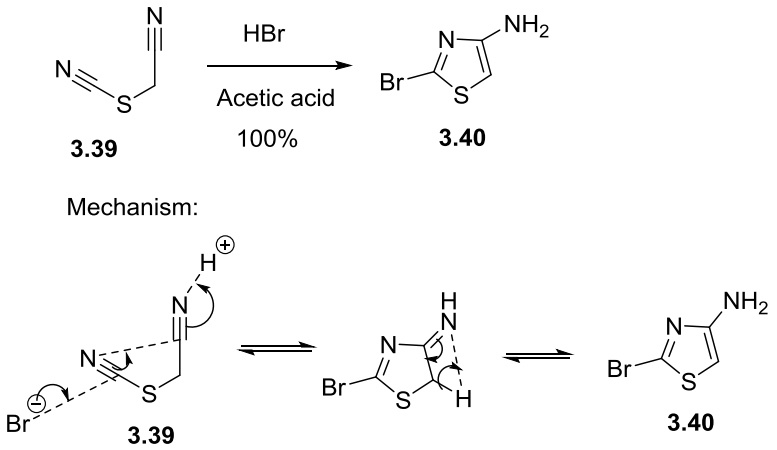


Figure 3.61: Reaction scheme and proposed mechanism for the formation of 2-bromothiazol-4-amine (**3.40**)

The next step, **Figure 3.62**, involved directly using the 2-bromothiazol-4-amine (**3.40**) by dissolving it in DCM, cooling it to 0 ºC and adding triethylamine and palmitoyl chloride. After 20 minutes the solvent and residual triethylamine was removed under reduced pressure and the amide product (**3.41**) obtained in quantitative yield was purified simply by washing with 1M HCl and water. Thus this method is not only quick, very high yielding and requires no purification but also installs a bromine atom in the required alpha position. The next step involved reducing the amide (**3.41**) to an amine (**3.42**) with lithium aluminium hydride ($LiAlH_4$), a step which unfortunately was found to also remove the bromine atom. Subsequently attempts were made to ring

close the amine (**3.42**) with oxalyl chloride. However despite repeated attempts the reaction failed as the 5 position of the thiazole was too electron deficient to undergo a nucleophilic Friedel Crafts attack on the acid chloride of the oxalyl chloride.

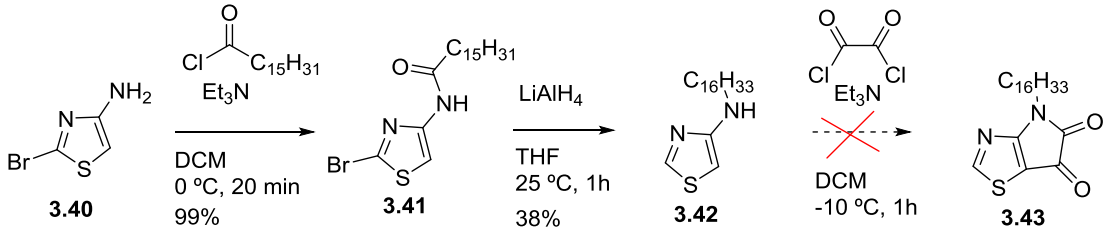


Figure 3.62: Attempted synthesis of ring closed thiazole (**3.43**).

As the 5 position of the thiazole was too electron deficient to be ring closed a variety of attempts were made to lithiate both the amine and the 5 position of thiazole (**3.42**) with two equivalents of LDA and subsequently ring close with oxalyl chloride. However all these attempts failed and so an alternative route based on the synthesis of phenyl isoindigo was tried.[229] Thus an initial attempt was made to produce a thiazole equivalent of an oximinoacetanilide via reacting amino thiazole (**3.40**) with chloral and sodium sulphate in 90 ºC water, **Figure 3.63**. However it was found that the amino thiazole (**3.40**) decomposed under these conditions.

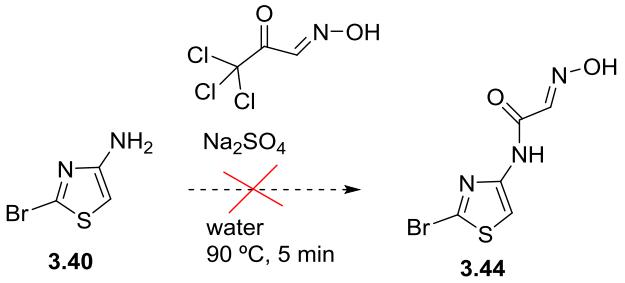


Figure 3.63: Attempted synthesis of (E)-N-(2-bromothiazol-4-yl)-2 hydroxyimino)acetamide (**3.44**).

To prevent the amino thiazole (**3.40**) from decomposing an alternative synthesis was devised. First the amino thiazole (**3.40**) was converted to N(2-bromothiazol-4-yl)-2,2,2 trichloroacetamide (**3.45**) to stabilise the lone pair of electrons on the nitrogen via conjugation with the neighbouring carbonyl group before heating thiazole (**3.45**) with hydroxylamine hydrochloride in water. This gave the desired (E)-N-(2-bromothiazol-4-yl)-2 hydroxyimino)acetamide (**3.44**) in quantitative yield, **Figure 3.64**. Subsequent attempted ring closure with sulphuric acid in water failed to produce

the desired ring close product (**3.45**). Despite varying the concentration of sulphuric acid and varying the reaction temperature only starting material was obtained.

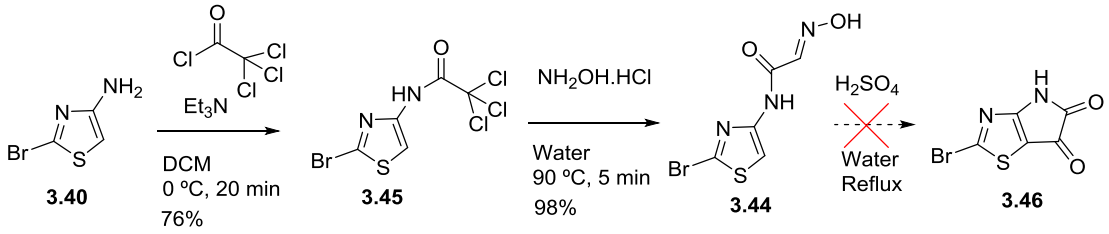


Figure 3.64: Attempted synthesis of ring closed thiazole (**3.46**).

The reason that the acid catalysed Friedel crafts reaction failed to work in this case was not only due to the fact that the thiazole is electron poor but the nitrogen contained within the thiazole ring can become protonated thus further decreasing the electron density of the thiazole ring.[230]

3.6.2 Conclusion

Although a lot of progress towards synthesising thiazole isoindigo was made with regards to developing a route to making alkyl thiazole amines, it became evident that due to the synthetic limitations of thiazole, the synthesis of thiazole isoindigo had to be abandoned to concentrate on more viable synthetic projects.

3.7 Furan Isoindigo

The use of furan as part of the isoindigo unit is anticipated to not only enhance the solid state order of the resulting polymers through having high backbone coplanarity and short inter-ring bond lengths,[174, 175] but also improve the solubility of the polymers.[176] As furan is more electron rich than thiophene, furan isoindigo would have a higher HOMO energy level than thiophene isoindigo and so is expected to produce polymers with an even lower band gap. Whilst this may be unsuitable for OPV applications as the LUMO-LUMO energy offset between the polymer and the PCBM may be less than the 0.3 eV offset required to allow thermodynamically favourable charge separation, the low band gap would be of benefit for allowing ambipolar charge transport in OFET devices.

Unfortunately the end goal was not reached due to the task being synthetically challenging. Section **3.7.1** below outlines the steps taken to reach the target monomer.

3.7.1 Towards the synthesis of furan isoindigo.

A number of synthetic routes were attempted to produce furan isoindigo. The first route that was attempted followed that used to produce thiophene isoindigo as shown in **Figure 3.65**.

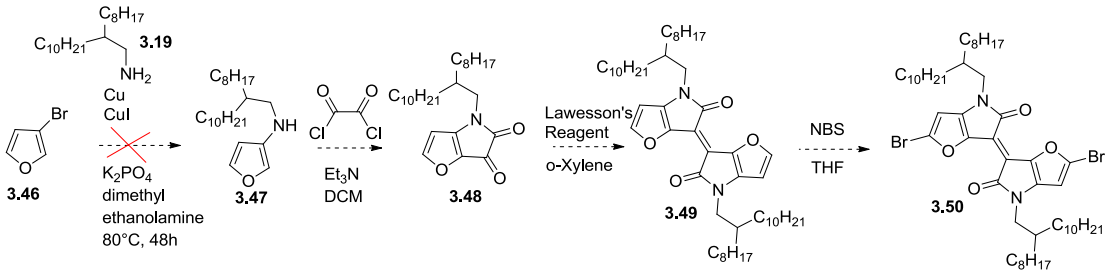


Figure 3.65: Initial route towards furan isoindigo monomer (**3.50**).

The initially planed route towards obtaining the furan isoindigo monomer (**3.50**) involved the amination of 3-bromofuran (**3.46**) followed by the cyclization of the amine product (**3.47**) with oxalyl chloride and triethylamine to give the cyclised furan (**3.48**) which would be subsequently dimerised with Lawesson's reagent to give dimer (**3.49**) and brominated with NBS to give the monomer (**3.45**). Unfortunately the initial Ullmann coupling reaction step failed to yield any product and only starting material was recovered, despite trying longer reaction times and higher reaction temperatures.

As copper catalysed reactions proved ineffective an alternative route to obtaining the amino furan (**3.47**) was devised, **Figure 3.66**.

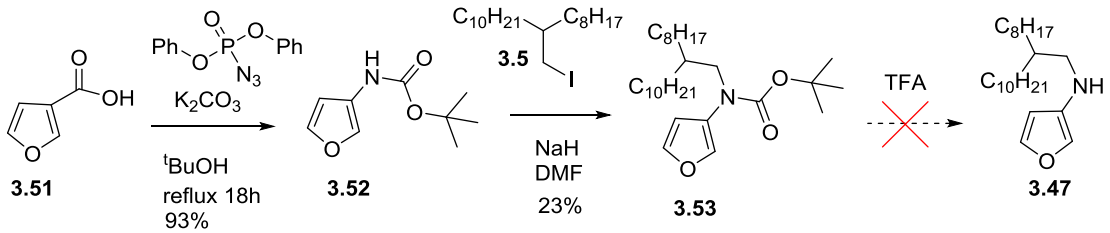


Figure 3.66: Synthesis route towards aminothiazole **(3.30)**.

Using furan-3-carboxylic acid (**3.51**) and diphenylphosphorylazide with potassium carbonate in refluxing tert-butanol the Boc protected amide was formed via a Curtius rearrangement[231] in 93% yield. Subsequent deprotonation of the amide with mild base sodium hydride enabled the nitrogen to be alkylated with alkyl iodide (**3.5**) to achieve the alkylated and Boc protected furan (**3.53**) in 23% yield after extensive purification.[219] The next step was rather more problematic as initial attempts to remove the Boc protecting group with TFA[221] over the course of 18 h in DCM at 25 ºC completely decomposed the furan. Subsequent attempts with TFA found that the furan decomposed after just 20 minutes. Thus alternative Boc deprotection conditions were tried including using TBAF,[222] phosphoric acid,[232] 4N HCl in dioxane/DCM at 25 ºC[223] for 1 h - which decomposed the furan, boiling water[224] for 12 minutes - which returned starting material, heating in toluene at 200 ºC for 24 h[225] – which returned starting material and heating at 240 ºC under vacuum for 1.5 h at which point the furan decomposed. From all of these Boc deprotection attempts it is evident that the Boc group on the tertiary amine is surprisingly stable and that if the Boc group does become deprotected under very harsh acidic conditions or at very high temperatures then the resulting amine may not be stable enough to survive these conditions. After trying to deprotect the Boc group of alkylated and Boc protected furan (**3.53**) with the mild method of using magnesium perchlorate in acetonitrile, returned only starting material it was realised that in order for the Boc deprotection mechanism of magnesium perchlorate to work a second ketone group on the alkyl side chain was required.[226] Thus for this purpose the Boc protected furan (**3.52**) was deprotonated with sodium hydride and reacted with palmitoyl chloride to give the straight chain Boc protected furan (**3.54**). The branched Boc protected furan (**3.58**) was also produced by reacting Boc protected furan (**3.52**) with sodium hydride and 2-octyldodecanoyl chloride (**3.57**). The 2-octyldodecanoyl chloride (**3.57**) was produced from reducing 2-octyldodecan-1-ol (**3.55**) with potassium permanganate in sulphuric acid[233] to produce 2-octyldodecanoic acid (**3.56**) which was subsequently converted into the acid chloride (**3.57**) with thionyl chloride and DMF.[234] Both the branched and linear Boc protected furans (**3.54**) and (**3.58**) were Boc deprotected with magnesium perchlorate in acetonitrile at 50 ºC for 2 h[226] to give the linear furan amide (**3.59**) and the branched furan amide (**3.60**) in 76% and 22% yields respectively. The next step proved to be tricky and involved reducing the furan amide (**3.59**) to produce furan amine (**3.61**). Initial attempts involved reducing the furan amide with 1 molar borane

in THF at 100 ºC for 3 h followed by an aqueous work up,[235] and reducing the furan amide with $LiAlH_4$ at 60 ºC over 1 h.[236] However these conditions proved to be too harsh and resulted in the complete decomposition of the furan. Additionally, 3 aminofurans are intrinsically unstable due to their remarkably low enthalpy of tautomerization (0.061 eV)[237] and have been shown to only be stable in solution at 0 ºC.[238] With this in mind the linear furan amide (**3.59)** was successfully reduced to the linear furan amine (**3.61**) by dissolving the linear furan amide (**3.59)** in anhydrous THF, adding a 1M solution of $LiAlH_4$ dropwise and allowing the reaction to stir at room temperature for 2.5 h. Next, using Schlenk line techniques to avoid contact with air and moisture, the anhydrous THF was removed under reduced pressure, before anhydrous hexane was added to precipitate out any excess $LiAlH_4$ and associated salts. The hexane was then decanted off via cannula to separate out the salts, and the hexane was removed under reduced pressure. After adding anhydrous DCM the isolated furan amine (**3.61**) was taken on directly to the next step and added dropwise to oxalyl chloride dissolved in anhydrous DCM at -10 ºC. After 30 minutes, triethylamine dissolved in anhydrous DCM was added dropwise to complete the ring closure and the reaction was allowed to warm to room temperature overnight. The resulting linear ring closed furan (**3.62**) was isolated by removing the DCM and triethylamine under reduced pressure and purifying via column chromatography in neat DCM to achieve a yield of 29% over the two steps.

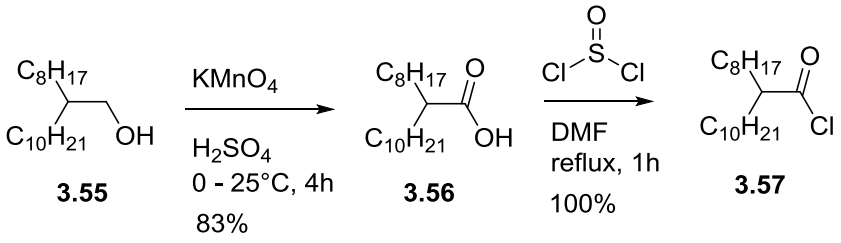


Figure 3.67: Synthesis of 2-octyldodecanoyl chloride (**3.57**).

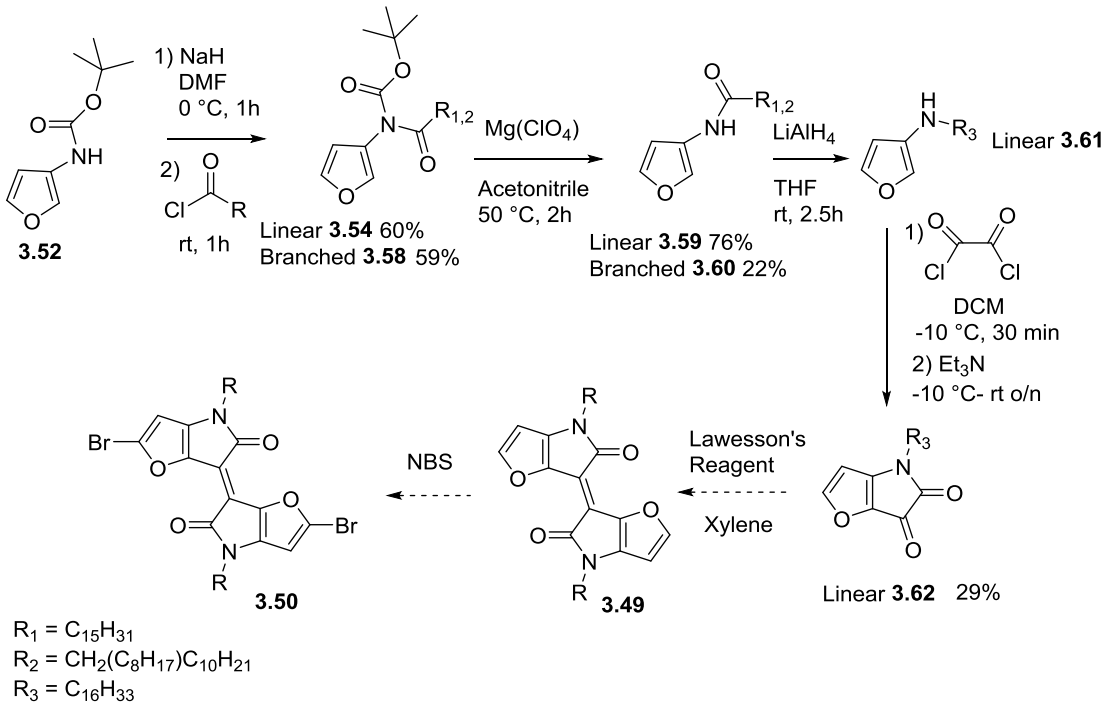


Figure 3.68: Synthetic route towards final monomer (**3.50**).

Unfortunately, out of 10 attempts to isolate the ring closed furan for both the linear and the branched versions, only the linear ring close furan (**3.62**) was isolated once on the first attempt. Despite trying to exactly replicate the ring closure procedure, and also trying various ways to modify it by introducing shorter reaction times, lower reaction temperatures and better filtration techniques to remove excess salts, the success of the very first attempt could not be repeated. Additionally, not enough of the linear ring closed furan (**3.62**) was obtained to carry on to the next step.

3.7.2 Conclusion

In spite of all the effort that has gone into making progress towards furan isoindigo, with the development of the ring closed furan (**3.62**) being realised, the project was sidelined to focus on more promising synthetic targets, due to the fact that it was very difficult to synthesise enough of the ring closed furan (**3.62**) to carry on.

Chapter 4 Pechmann Dyes

The most exciting phrase to hear in science, the one that heralds the most discoveries, is not "Eureka!" but "That's funny..."

Isaac Asimov (1920-1992). Professor of Biochemistry.

4.1 Introduction to Pechmann Dyes

The use of dyes can be traced back as far as 30000 years when it was used by prehistoric hunter gatherers to colour fabrics.[239] However the first synthetic dye didn't arrive until 1856 when William H. Perkin at the age of 18 years old accidentally discovered mauveine, whilst developing a synthesis for the antimalarial compound quinine.[240] With this dye Perkin started the modern dye industry and can be accredited with being the first person to successfully commercialise a scientific discovery.[241] Since the start of the dye industry thousands of new dyes have been developed which have been predominantly used for dying textiles.[242] More recently, dyes have become a source of inspiration for developing new building blocks for organic electronic materials. The reason for this is due to the fact that these dyes typically show semiconducting properties due to their conjugated structures and low band gaps.[243] Additionally dye molecules tend to be very chemically stable and typically show high extinction coefficients making them conducive to absorbing light in OPV devices.[244-246]

Thus by looking at the large selection of dyes that have been developed since the time of Perkin, Pechmann dyes look like a promising candidate for future applications in plastic electronics. Pechmann dyes were originally discovered by accident by Hans von Pechmann in 1882 as he tried to prepare 1,4-naphthoquinone from β-benzoyl acrylic acid.[247] The structure formed in this reaction was eventually shown to be a 3-butenolide dimer centred about an alkene bridge with a benzene ring at the 5 and 5' positions of the lactone rings (**Figure 4.1**) in 1924.[248] However unlike mauveine Pechmann dyes were never commercialised due to the fact that they are highly insoluble and rather difficult to purify.[241, 249]

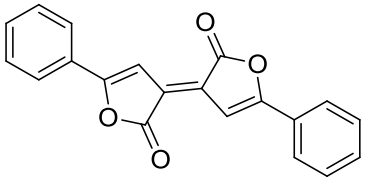


Figure 4.1: Pechmann Dye.

More recently interest in Pechmann dyes has resurfaced as the structure is rather similar to other chromophores such as DPP,[244] isoindigo[245] and N,N-

dialkylnaphthalene-1,8:4,5-tetracarboxydiimides (NDI)[246] all of which have been successfully incorporated into organic electronic devices. The similarities that these molecules possess are that they are all highly electron deficient as a result of their carbonyl / anhydride functional groups, they all contain conjugated ring systems which are highly planar and thus allow them to form efficient π-π stacking arrangements. Additionally they can all be alkylated or in the case of the Pechmann dyes amidated to introduce solubilising alkyl chains that are important for solubilising the resulting polymers. The side chains not only dictate polymer processing conditions but also have an influence over the aggregation and solid state packing arrangements of the polymer backbones which have important implications for OPV and OFET device performance.[110] In the case of Pechmann dyes it has been found that the optical band gap of the molecule can be modulated depending on whether or not the molecule is amidated, whether one or both of the lactone rings are amidated, whether the molecule has been thermally rearranged and is also dependant on the choice of aromatic ring that the molecule is made up of. **Figure 4.2** below shows some of the possible combinations that have appeared in the literature so far.

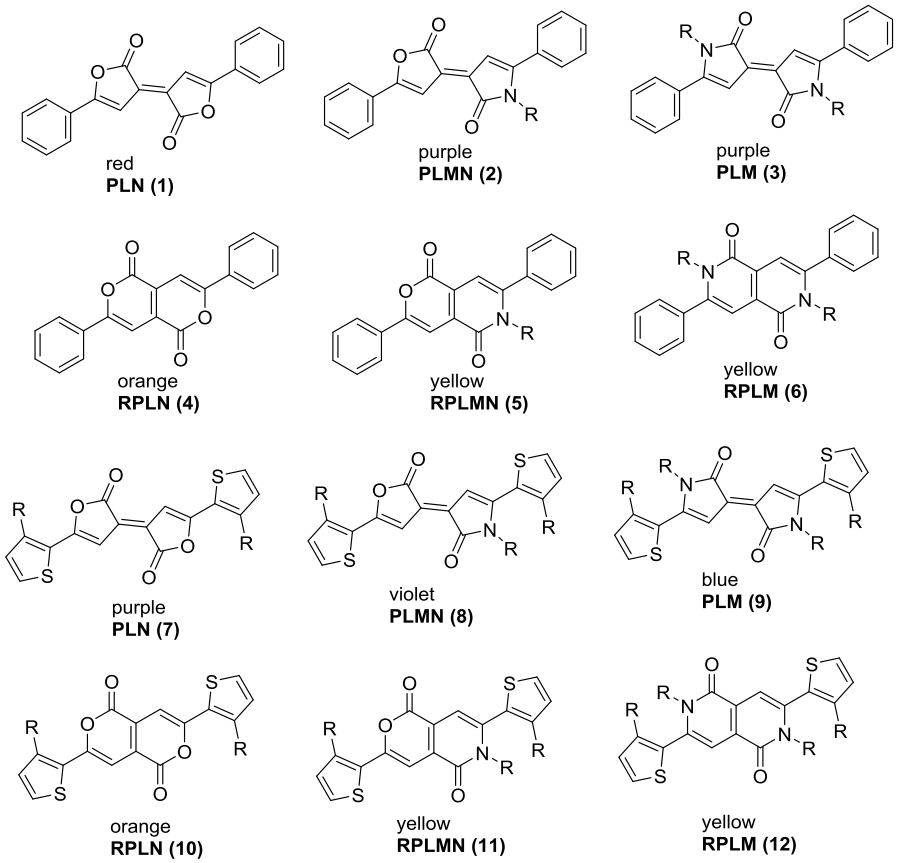


Figure 4.2: Variety of Pechmann dyes found in the literature. R = alkyl chain[241, 249-251]

As can be seen from **Figure 4.2** upon the stepwise, two fold amination of Pechmann lactone **PLN (1)** the absorption red shifts on going to the mono aminated Pechmann lactone **PLMN (2)** and a further red shift is observed on going to the di-aminated Pechmann lactone **PLM (3)**. The same observation can be made for the thiophene based Pechmann dyes on going from **PLN (7)** to **PLMN (8)** to **PLM (9)** although the thiophene based Pechmann dyes are considerably more red shifted. Both **PLN (1)** and **PLN (7)** can be thermally rearranged in aprotic solvents to give rearranged Pechmann lactones **RPLN (4)** and **RPLN (10)** respectively. However unlike **PLN (1)** and **PLN (7)** upon stepwise twofold amination of **RPLN (4)** and **RPLN (10)** to give the respective mono aminated rearranged Pechmann lactams **RPLMN (5)** and **RPLMN (11)** and respective di-aminated rearranged Pechmann lactams **RPLM (6)** and **RPLM (12)** a sequential blue shift is observed.

Despite the renewed interest in Pechmann dyes, no Pechmann dyes have been reported in the academic community to have been incorporated into polymers for organic electronics. Thus this presents an opportunity to further examine the properties of this class of materials.

4.2 Synthesis of Pechmann Dye Based Monomers

Based on the fact that the thiophene based Pechmann dyes show the lowest optical band gap and have a structure that is fairly similar to high performing DPP monomers it was decided that polymers incorporating this structure would be synthesised. As some synthetic difficulties were encountered, namely some very low yielding steps or reactions that simply failed to work, a number of synthetic routes towards obtaining a Pechmann dye based polymer were attempted.

The initial synthesis of a thiophene based Pechmann dye was carried out in accordance to the method patented by Jean-Charles Flores et al[252] and adapted to attempt to convert the Pechmann dye into a monomer.

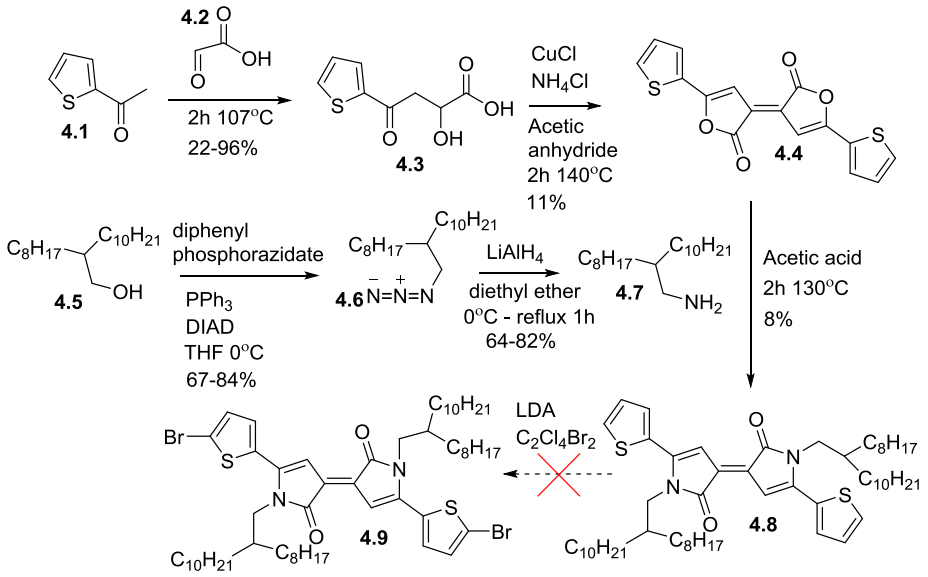


Figure 4.3: Attempted synthesis of Pechmann dye monomer (**4.9**)

The initial step involved the synthesis of carboxylic acid (**4.3**) from 2-acetyl thiophene (**4.1**) in neat glyoxylic acid (**4.2**) under vacuum at 107°C for 2 h. This gave varying yields (22-96%) of crude carboxylic acid (**4.3**) as a yellow oil, which could be used directly in the next step without purification. Cyclisation of carboxylic acid (**4.3**) with CuCl and ammonium chloride in acetic anhydride gave a dark purple solid which was purified by Soxhlet extraction to give a fairly insoluble Pechmann dye (**4.4**) in 11% yield. In tandem branched amine (**4.7**) was synthesised from alcohol (**4.5**) which was turned into azide (**4.6**) and reduced with $LiAlH_4$ to form the desired amine. Branched amine (**4.7**) was then reacted with Pechmann dye (**4.4**) to give branched amidated Pechmann dye (**4.8**) in 8% yield (as a side note the linear $C_{16}H_{33}$ amine was also synthesised but in 1% yield). Attempts to brominate the α thiophenes under mild conditions with LDA and 1,2 dibromotetrachloroethane to avoid the bromination of the central double bond failed as did attempts to borylate and also stannylate branched amidated Pechmann dye (**4.8**) both using LDA as a non nucleophilic base to lithiate the α positions on the thiophenes. Thus it was decided to introduce the bromines earlier on in the synthesis, as shown in **Figure 4.4**.

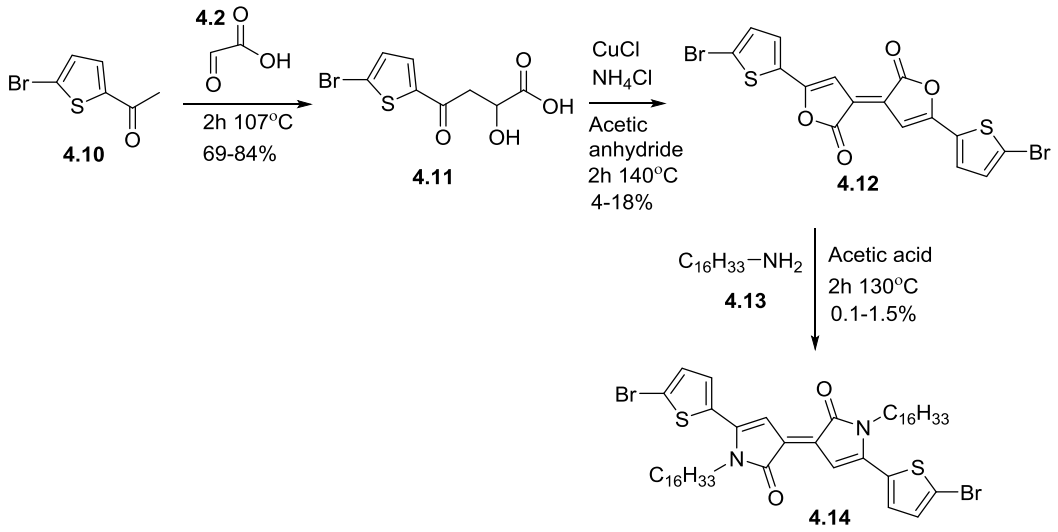


Figure 4.4: Synthesis of Pechmann dye monomer (**4.14**)

2-acetyl-5-bromothiophene (**4.10**) was heated in neat glyoxylic acid under vacuum for 2 h to form carboxylic acid (**4.11**) as a yellow solid in yields that varied from 69 to 84%. The yield varied due to the fact that as the reaction was being heated under vacuum the 2-acetyl-5-bromothiophene (**4.10**) had a tendency to sublime rather than react with the glyoxylic acid. Fortunately the conditions used for the work up enabled the product to be used in the next step without further purification. Reacting carboxylic acid (**4.11**) with CuCl and ammonium chloride in acetic anhydride at 140 ºC gave the brominated Pechmann dye (**4.12**) in initially very low yields of ~4%, due to the insoluble and hard to purify nature of the material. Eventually the highest yields of ~18% were obtained via Soxhlet extraction of the crude material in chloroform for 2 days. The next step involved aminating the brominated Pechmann dye (**4.12**) with commercially available linear hexadecylamine (**4.13**) to give the Pechmann dye monomer (**4.14**) in 0.1-1.5% yields. Unfortunately, as these reactions were so low yielding due to the insoluble nature of the initial Pechmann dye (**4.12**), there was not enough monomer to attempt a polymerisation and thus it was deemed not worth while to continue making this monomer, as ultimately a route which is so low yielding would never be commercialised. Thus an alternative strategy using alkylated thiophenes was envisaged based on the synthesis reported by Norsten et al,[251] **Figure 4.5**.

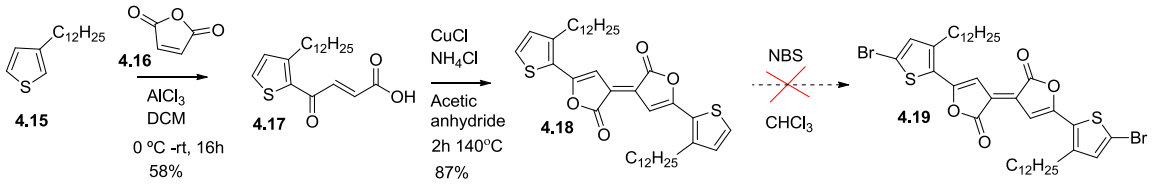


Figure 4.5: Attempted synthesis of Pechmann dye monomer (**4.19**)

Friedel Crafts acylation of 3-dodecylthiophene (**4.15**) with maleic anhydride (**4.16**) selectively acylated the 2 position of the thiophene to give the carboxylic acid (**4.17**) in 58% yield**.** Purification of carboxylic acid (**4.17**) was remarkably straightforward as it could be purified simply by triturating with hexane. Further reaction under the standard ring closure conditions of heating the carboxylic acid with CuCl and ammonium chloride in acetic anhydride at 140 ºC gave the alkylated Pechmann dye (**4.18**) in a much higher yield, 87%, due to the enhanced solubility of the compound. Additionally this compound was a lot easier to purify as due to the fact that it was so soluble it could be purified by column chromatography rather than a lengthy Soxhlet extraction process. Unfortunately, NBS bromination in chloroform at 0 °C failed to yield Pechmann dye monomer (**4.19**) as the bromine destroyed the central double bond. An alternative method to brominate the Pechmann dye (**4.18**) was also employed which involved using LDA at -78 °C with 1,2 dibromotetrachloroethane but unfortunately this also failed. By carrying out detailed NMR experiments with LDA and deuterium at a variety of reaction temperatures it was found that the LDA destroyed the Pechmann dye (**4.18)** at -40 °C after 10 minutes through attacking the lactone rings.

Thus it was decided to attempt to brominate the thiophene before the ring closure step. The attempted routes shown in **Figure 4.6**.

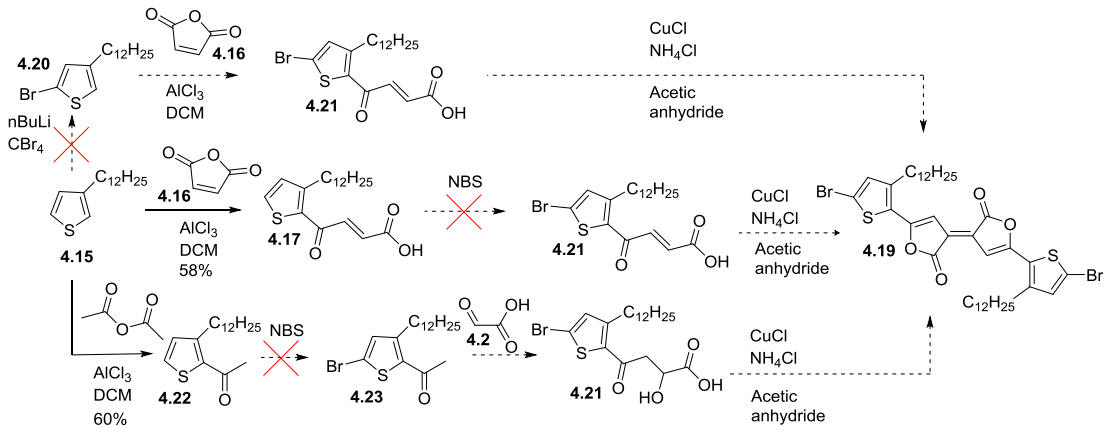


Figure 4.6: Attempted synthetic routes towards Pechmann dye monomer (**4.19**)

Initial attempts to brominate the 3-dodecylthiophene (**4.15**) to give 2 bromo 4 dodecylthiophene (**4.20**) in accordance to literature procedures[253] failed to give the required selectivity due to the fact that the literature only used thiophenes with side chains up to 8 carbon atoms long. This meant that the more solid 3-dodecylthiophene (**4.15**) froze at the -78 °C conditions required for the selective lithiation and bromination.

The next synthesis involved the attempted bromination of carboxylic acid (**4.17**) with NBS at 0 °C in various solvents including chloroform, THF, and a mixture of THF, DCM and acetic acid. However on each occasion the central double bound was brominated rather than the α position on the thiophene.

Thus it was decided to acylate 3-dodecylthiophene (**4.15**) in the 2 position via Friedel Crafts acylation with acetic anhydride. This gave a mixture of 40% 2-acetyl 4-dodecylthiophene and 60% of the required 2-acetyl-3 dodecylthiophene (**4.22**). The reason for this was so that there would be no double bond available for brominating in the next step. However it was found that upon NBS bromination of 2-acetyl-3 dodecylthiophene (**4.22**) the α position of the ketone was preferentially brominated rather than the α position on the thiophene.

The next synthetic strategy involved the synthesis of a higher yielding and more synthetically stable Pechmann dye that could be brominated in the final step. The synthetic route was based on that devised by Eric Assen B. Kantchev et al[3] with the

conditions for the final bromination step being elucidated by trial and error to convert Pechmann dye (**4.24**) into Pechmann dye monomer (**4.25**). The synthetic route is given in **Figure 4.7**.

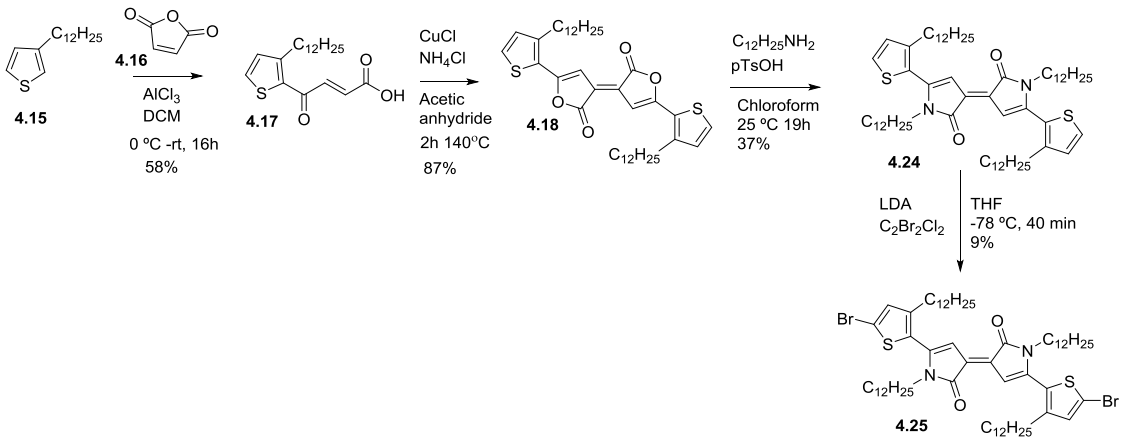


Figure 4.7: Synthesis of Pechmann dye (**4.25**).

Friedel Crafts acylation of 3-dodecylthiophene (**4.15**) with maleic anhydride (**4.16**) selectively acylated the 2 position of the thiophene to give the carboxylic acid (**4.17**) in 58% yield**.** Further reaction under the standard ring closure conditions of heating the carboxylic acid with CuCl and ammonium chloride in acetic anhydride at 140 ºC gave the alkylated Pechmann dye (**4.18**) in 87% yield. The next step involved the amidation of alkylated Pechmann dye (**4.18**) with dodecylamine to produce amidated Pechmann dye (**4.24**). For this step the literature[3] suggests to stir the alkylated Pechmann dye (**4.18**) with dodecylamine in chloroform with catalytic 4-dimethylaminopyridine (DMAP) for 16 h before adding p-toluene sulphonic acid (p-TsOH) and stirring for a further 3 h. However using this method only resulted in 3% yields but when the DMAP was omitted it was found that the yields increased to 37%. The bromination of amidated Pechmann dye (**4.24**) proved to be synthetically challenging. Initial attempts at lithiating the amidated Pechmann dye (**4.24**) with 2 equivalents of LDA at -78 °C for 30 minutes followed by quenching dibromotetrachloroethane and allowing the reaction mixture to return to room temperature returned starting material. Trying elevated temperatures of -40 °C and 0 °C also returned starting material. It was not until a vast excess of LDA (20 equivalents) was used at -78 °C for 10 minutes that a noticeable colour change in the reaction took place whereby the purple amidated Pechmann dye (**4.24**) turned blue-

green temporarily upon lithiation. At this point the lithiated species required immediate quenching with dibromotetrachloroethane. Additionally it was found that if the dibromotetrachloroethane was left in the reaction mixture for more than 10 minutes the Pechmann dye would completely decompose. Thus the reaction required quenching at a point whereby the greatest amount of product had been formed before the rate of decomposition destroyed all of the product and starting material. This meant that after each reaction which yielded between 1% and 9% brominated Pechmann dye monomer (**4.25**) the majority of the starting material could be recovered and re-reacted. Thus after 13 cycles of re-reacting the amidated Pechmann dye (**4.24**) enough Pechmann dye monomer (**4.25**) was obtained to try one polymerisation reaction.

4.3 Synthesis of Pechmann Dye Based Polymers

As the linear side chains on the Pechmann dye monomer (**4.25**) make it more suitable for transistor applications, thiophene was chosen as a suitable comonomer to enhance backbone planarity through the sulphur to sulphur antiperiplanar configuration in addition to the quinoidal effect. Thus the Pechmann dye monomer (**4.25**) was polymerised via $Pd_2(dba)_3$ catalysed Stille coupling with 2,5-bis(trimethylstannyl)thiophene (**4.26**) and end capped with 2-trimethylstannyl thiophene and 2-bromothiophene to remove both tin and bromine moieties from the ends of the polymer chain. After precipitation into acidic methanol to quench any excess tin the polymer was purified via Soxhlet extraction in acetone and hexane. Unfortunately the polymer all came out in the hexane fraction indicating that the polymer was a very low molecular weight. Subsequent GPC analysis showed that the polymer only achieved a molecular weight of Mn = ~1 kDa thus indicating that the reaction had failed.

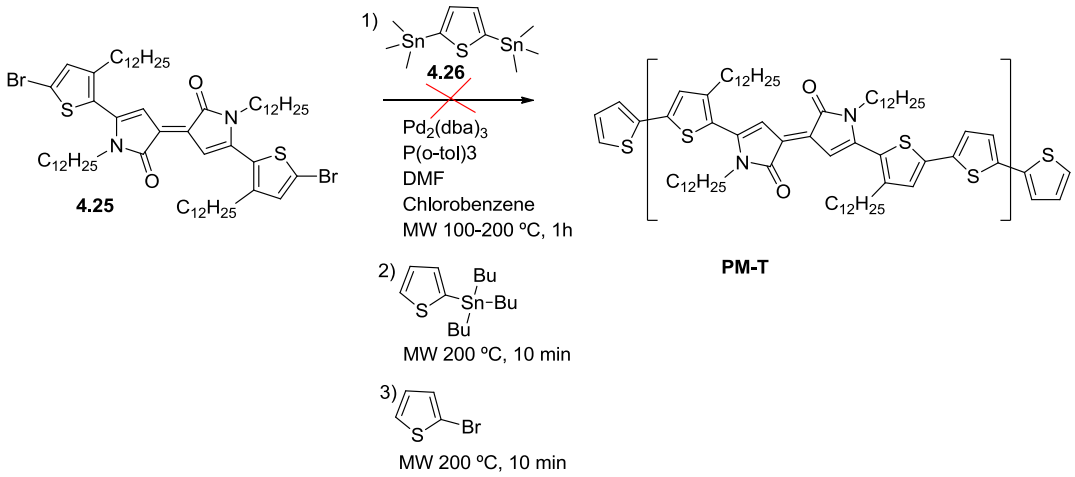


Figure 4.8: Attempted synthesis of Pechmann copolymer.

As sufficient quantities of the Pechmann dye monomer (**4.25**) was difficult to remake it was decided to form homo polymers from the non brominated Pechmann dye (**4.18**) and the amidated Pechmann dye (**4.24**) using $FeCl_3$ polymerisation in accordance to the procedure developed Hiroki Fukumoto et al.[254]

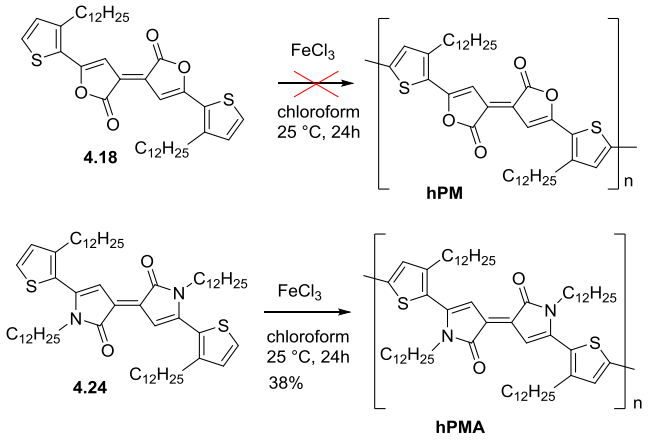


Figure 4.9: Formation of Pechmann homo polymer

Pechmann dye (**4.18**) and $FeCl_3$ were added to anhydrous chloroform at 0 °C and stirred for 24 h with a constant flow of Argon over the surface of the solution to ensure that the reaction was carried out in the absence of oxygen and water. However it soon became evident that the Pechmann dye (**4.18**) was not stable under these conditions as the purple Pechmann dye (**4.18**) turned yellow indicating that the lactone rings had ring opened.

Pechmann dye (**4.24**) and $FeCl_3$ were added to anhydrous chloroform at 0 °C and stirred for 24 h with a constant flow of Argon over the surface of the solution to ensure that the reaction was carried out in the absence of oxygen and water. After stirring for the required amount of time the reaction mixture was poured into methanol and the precipitate was collected by filtration. The crude product was subsequently dissolved in chloroform and de-doping of the aminated homo Pechmann polymer (**hPMA**) was attempted using aqueous hydrazine in accordance to literature procedures.[254] However it soon became evident that the Pechmann dye homo polymer (**hPMA**) was not stable under these conditions as the blue homo polymer (**hPMA**) turned yellow indicating that the lactone rings had ring opened. Thus the polymerisation reaction was carried out again using the same conditions but this time the de-doping purification step was omitted. The polymer (**hPMA**) was purified by Soxhlet extraction in acetone, hexane and chloroform and the chloroform fraction was reduced and poured dropwise into methanol to precipitate the purified polymer. The purified polymer was then collected by filtration and dried under high vacuum to afford the novel dark blue Pechmann dye homo polymer (**hPMA**).

4.4 Physical Properties of the Pechmann Dye Homo Polymer hPMA

The homo polymer (**hPMA**) was reasonably soluble in chloroform and chlorobenzene making it suitable for processing into a device.

The molecular weight of the polymer was measured by GPC calibrated against polystyrene standards. The analysis of **hPMA** gave a molecular weight that seemed rather low considering that it had been obtained from the chloroform fraction of the Soxhlet extraction with M_n = 2.5 kDa, M_w = 4.4 kDa and a PDI of 1.74. These results suggest that the degree of polymerisation for this polymer is between 2 and 3 indicating that only dimers and trimers had formed. However it is possible that like **IGT-T** and **IGT-TT** the polymer could interact with the column material and thus not give a true molecular weight. From looking at the optical properties it will become evident if the polymer is a dimer or trimer as vibronic coupling peaks would be observed if this is the case.

4.5 Optical Properties of Pechmann Dye Homo polymer hPMA

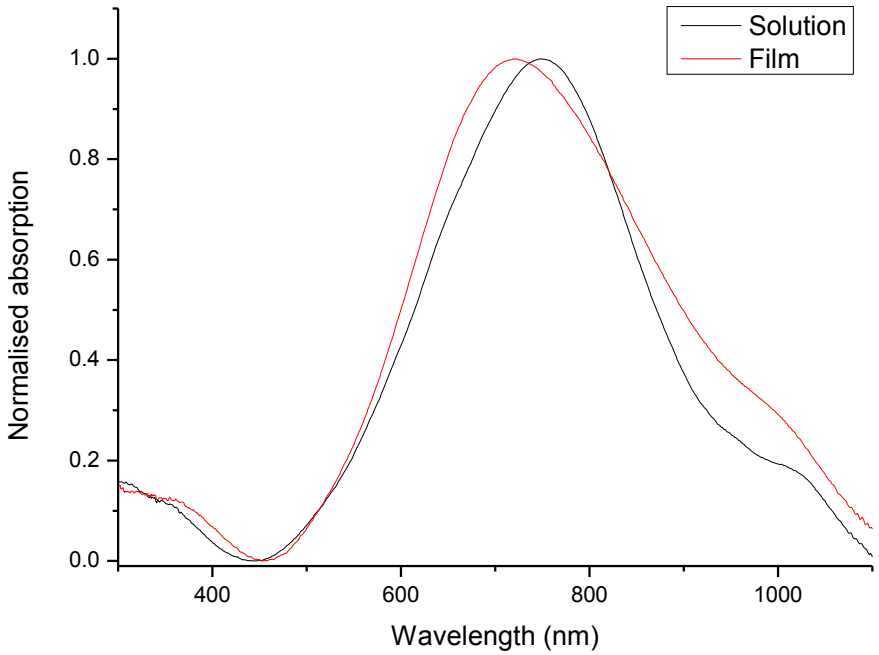


Figure 4.10: UV-Vis spectra of **hPMA** in solution (chlorobenzene at 25ºC) and in thin film (spun from chlorobenzene solution (5 mg/mL, 1000 rpm, 1 min).

Figure 4.10 shows the UV-Vis absorption spectra of **hPMA** in dilute chlorobenzene solution at 25 ºC and in thin film spun from chlorobenzene solution (5 mg/mL, 1000 rpm, 1 min). What is interesting about this polymer is that unlike both phenyl isoindigo copolymers **PFTFI**, **PFTTFI, IGPh-T, IGPh-TT, IGPh-Ph** and **IGPh-Na** and thiophene isoindigo copolymers **IGT-T, IGT-TT, IGT-Ph** and **IGT-Na** the Pechmann dye polymer **hPMA** does not exhibit a pronounced π-π* transition peak at around 400 nm for the solution and thin film spectra. Only a charge transfer peak at lambda max 749 nm for the solution and 722 nm for the thin film are observed with a slight aggregation peak at 1014 nm for the solution and 989 nm for the thin film. The fact that the lambda max of the thin film is blue shifted relative to the lambda max of the solution indicates that the film is less organised presumably due to the high density of alkyl side chains that disrupt the molecular packing. As there is no evidence of vibronic coupling in these UV-Vis spectra and the peaks appear broad, this suggests that lots of monomer units are coupled together. Thus it can be assumed

that **hPMA** is in fact a polymer and that like **IGT-T** and **IGT-TT** the homo polymer **hPMA** also interacts with the GPC column material to give false readings.

From the onset of the absorption of the thin film UV-Vis spectrum the bandgap of the homo polymer can be calculated to be 1.03 eV, indicating that the polymer should show ambipolar transistor behaviour and could potentially be useful as the low band gap layer in tandem solar cell devices.

4.6 DSC of Pechmann Dye Homo Polymer hPMA

To see if the side chain density of **hPMA** has an effect on polymer crystallinity DSC device measurements were taken.

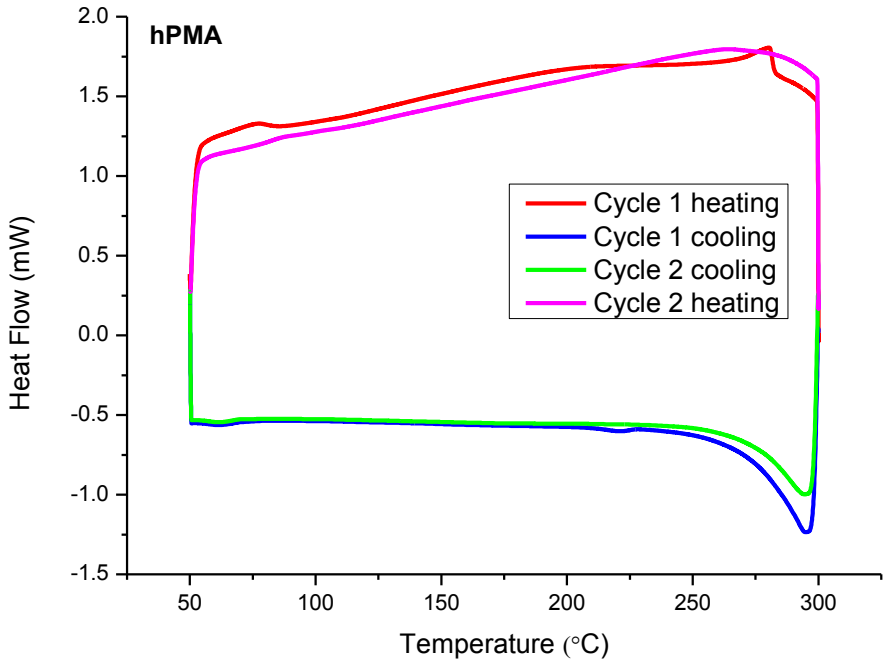


Figure 4.11: DSC of **hPMA** including first and second heating cycles. The red and pink lines indicate the first and second heating cycles respectively and the blue and green lines indicate the first and second cooling cycles respectively. Endothermic events are shown by positive peaks and exothermic events are shown by negative peaks.

From the DSC data shown in **Figure 4.11** it is evident that an endothermic event at 270 ºC occurs in the first heating cycle that is not subsequently seen in the second

cycle. As there is no corresponding exothermic event one can rule out the possibility of this being a melt transition. More likely this is due to either thermal decomposition of the polymer or is caused by the lactone structures within the Pechmann dye units thermally rearranging from the 5 membered exo structure as shown by **PLM (9)** to the 6 membered endo structure as shown by **RPLM (12)**.[251] If this is the case then the **hPMA** polymer could have potential uses in thermal curing nano imprinting lithography[255] in which the conductivity of the polymer could be altered via thermal patterning.

4.7 Optical Properties of Pechmann Dye Homo Polymer hPMA Revisited.

To see if the effect of heating the polymer at high temperatures whilst in thin film rearranged the structure of the lactone within the polymer, the thin film was thermally annealed at 270 ºC under argon for 10 minutes, before being analysed by UV-Vis spectroscopy, **Figure 4.12**.

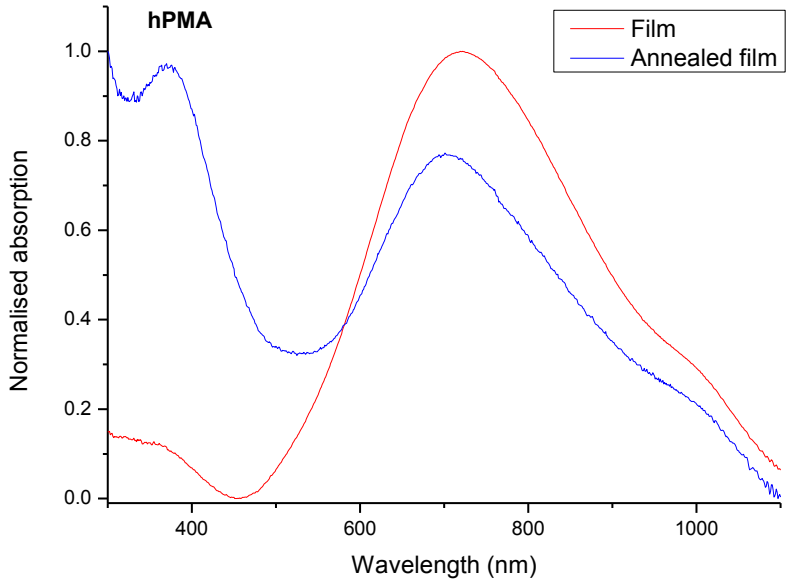


Figure 4.12: UV-Vis spectra of **hPMA** in thin film (spun from chlorobenzene solution (5 mg/mL, 1000 rpm, 1 min) and in a thin film thermally annealed at 270 ºC under argon for 10 minutes.

From **Figure 4.12** it is evident that the absorption of the π-π* transition at 376 nm of the polymer becomes much greater upon thermal annealing and that the maximum

absorption shows a blue shift from 722 nm in the thin film to 701 nm in the annealed film. Whilst the increase in the π-π* transition could be explained by thermal decomposition the blue shift in the maximum absorption would suggest that either the polymer is becoming more disordered or that the species being studied has changed. If the lactone ring is being thermally rearranged then one would expect to see a blue shift in absorption, although a somewhat greater blue shift would be expected. Thus it is difficult to make a definitive conclusion from these spectra as it is possible that either the polymer is decomposing or the thermal rearrangement may not have gone to full completion.

4.8 Energy Levels of Pechmann Dye Homo Polymer hPMA

The HOMO energy levels of **hPMA** and **hPMA** in a thermally annealed film at 270 ºC were measured by PESA and found to be -5.33 eV and -5.57 eV respectively in relation to the vacuum energy level. The fact that the HOMO energy level for the non annealed film is considerably higher than the annealed film could suggest that two different chemical species are being measured. Using the optical bandgap of **hPMA** (non annealed), estimated from the absorption onset of the thin film UV-Vis spectrum the LUMO energy level for **hPMA** was calculated to be -4.30 eV. As the optical band gap of the annealed film appears to be almost the same as the non annealed film it would suggest that the LUMO of the annealed polymer is a lot lower. However as it is not certain that the polymer species in the annealed film were either just degraded polymer or that not all of the lactone structures within the Pechmann dye units thermally having completely rearranged, it is not possible to conclusively make this determination.

4.9 OFET Device Performance of Pechmann Dye Homo Polymer hPMA.

To evaluate the charge transport properties of the Pechmann dye homo polymer **hPMA** bottom-gate, bottom-contact transistor structures were fabricated using heavily doped p-type Si wafers acting as a common gate electrode and a 200 nm thermally grown SiO_2 layer as the dielectric. Using conventional photolithography,

gold source-drain electrodes were defined with channel lengths and widths of 10 µm and 10 mm, respectively. A 10 nm layer of titanium was used as an adhesion layer for the gold on the SiO_2 giving finished electrodes that were 100 nm thick. The SiO_2 surface was passivated with hexamethyldisilazane (HMDS) before the homo polymer **hPMA** dissolved in chlorobenzene at a concentration of 10 mg/mL was spin coated on top of the electrodes at 2000 rpm for 30 seconds. The effect of annealing for 10 minutes at a variety of elevated temperatures, performed on a hotplate under a nitrogen atmosphere, was subsequently evaluated. **Figure 4.13** shows the transfer and output curves obtained.

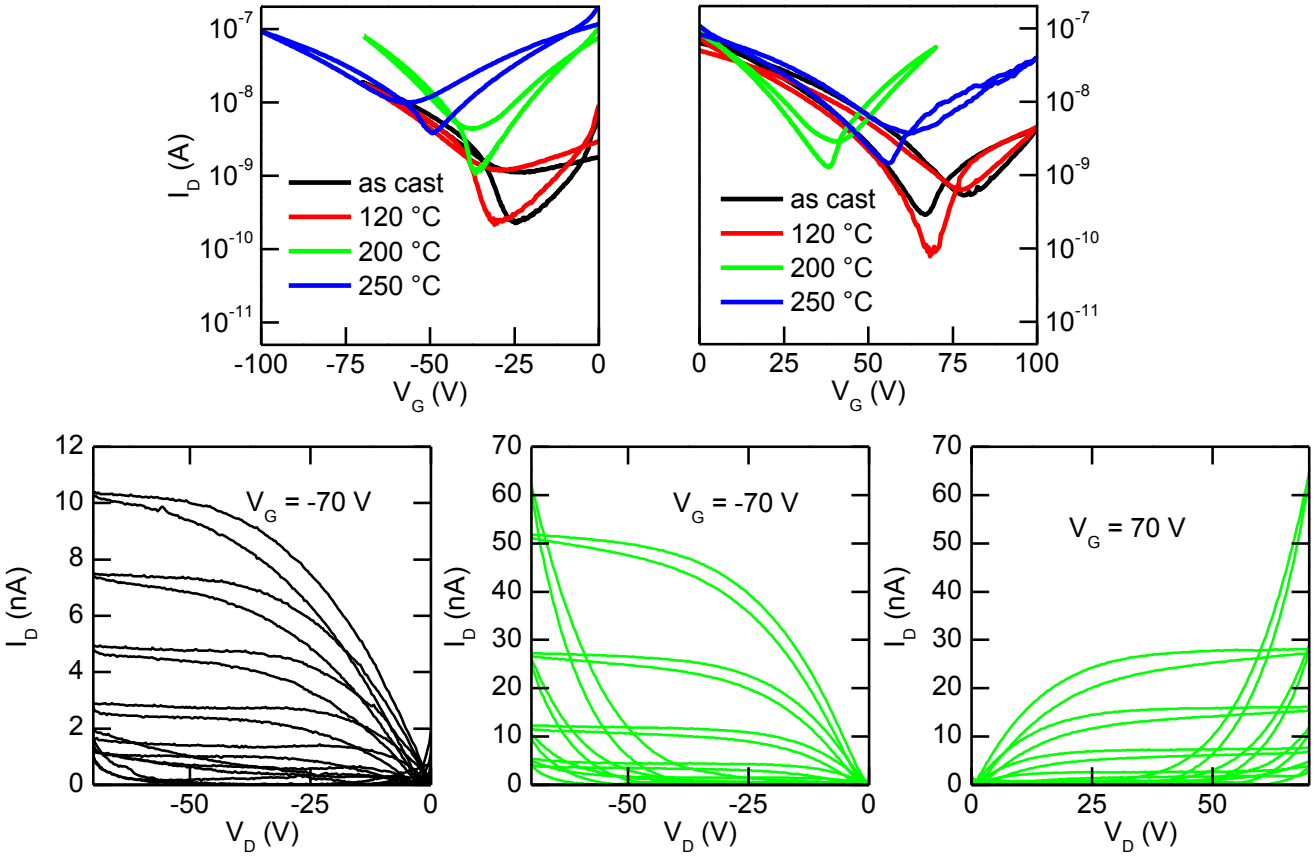


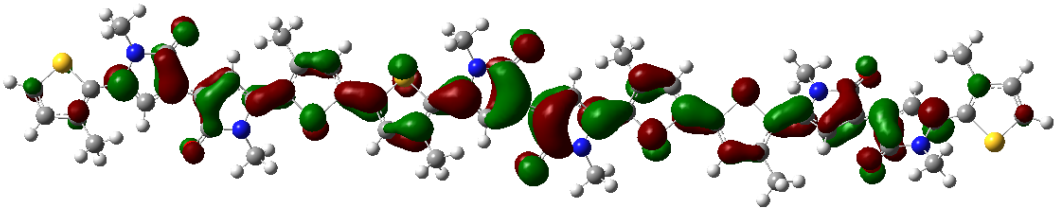
Figure 4.13: Transfer curves for p channel of the device (top left) and n channel of the device (top right) at various temperatures. Output characteristics for p channel of the device with as cast film (bottom left) and annealed film at 200 ºC (bottom middle). Output characteristics for n channel of device annealed at 200 ºC (bottom right). Transistors have channel dimensions 10 mm x 10 µm.

From the device characteristics in **Figure 4.13** it is clear that the homo Pechmann polymer **hPMA** shows ambipolar behaviour with saturated electron and hole mobilities that reach maximum values of around 10^{-6} $cm^2V^{-1}s^{-1}$ upon annealing at 200 ºC. Compared to other polymers such as the isoindigo based copolymers

produced in this thesis this mobility is rather low. This is presumably due to the fact that the alkyl chain density on the polymer backbone is so high that there is no room for alkyl chain interdigitation, which has been shown in other polymers such as **pBTTT** to enhance the lamellar structure of the polymer which in turn promotes the formation of crystalline domains and thus gives rise to high mobilities.[91]

4.10 Density Functional Theory Calculations for hPMA

LUMO



HOMO

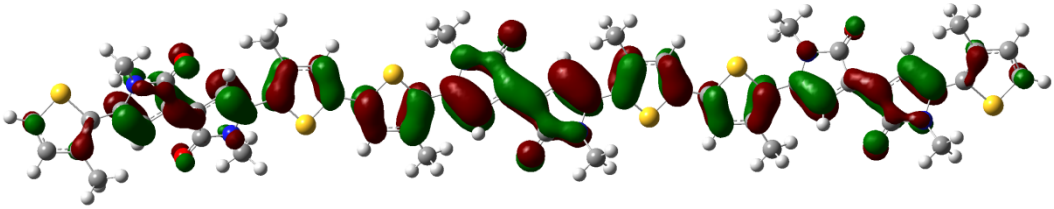
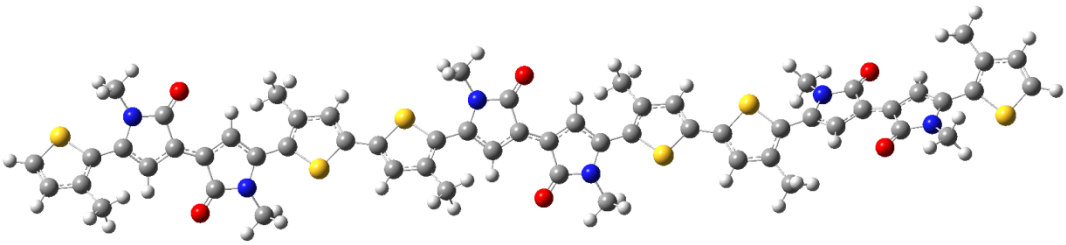


Figure 4.14: HOMO and LUMO distributions for the minimum energy conformations of a methyl substituted **hPMA** trimer optimised with Gaussian at the B3LYP/6-31G* level.

DFT calculations were carried out to ascertain the origins of the ambipolar nature of **hPMA**. Using Gaussian 09 the **hPMA** homopolymer was simulated using methyl substituted trimers using a B3LYP/6-31G(*) functional and basis set. The HOMO and LUMO electron density distributions for the minimum energy conformation of the **hPMA** trimer is depicted in **Figure 4.14**, whereby the red and green colours represent the isosurfaces of wavefunctions with opposite phases. The calculations gave the

value of the HOMO as -4.61 eV and a LUMO value of -3.22 eV giving a calculated band gap of 1.38 eV which is marginally higher than the experimentally determined optical band gap. From looking at the HOMO electron density distribution it is clear that both the HOMO and LUMO wavefunctions are evenly distributed over the whole of the trimer which gives rise to the ambipolar nature of the polymer. However from looking at just the face on view of the trimers it is not immediately evident why the mobility of this homo polymer is so low. When one looks at the side on view it is evident that the molecule is not planar as the steric hindrance of the alkyl chain on the thiophene and on the nitrogen atom sterically clash meaning that the alkyl chains are orientated in an antiperiplanar conformation to each other. This results in the sulphur of the thiophene ring and the nitrogen of the lactam ring adopting a synperiplanar conformation, but as the sulphur and nitrogen atoms are large they sterically clash with each other resulting in the molecule adopting an out of plane gauche conformation, **Figure 4.15**. This lack of planarity may result in the polymer being less crystalline and thus preventing adequate charge transport mobilities from being achieved.

Face on



Side on

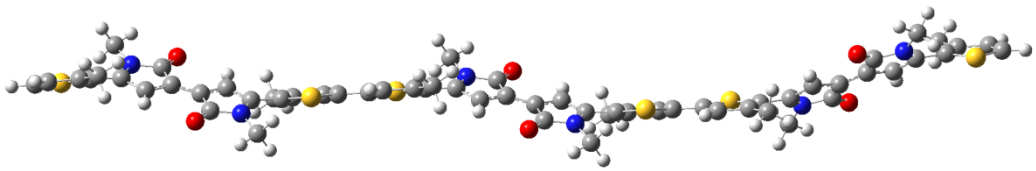


Figure 4.15: Face on (top) and side on (bottom) views of **hPMA**.

4.11 Conclusion and Broader Application

The development of a monomer to produce polymers from Pechmann dyes has been synthetically challenging with a variety of routes being tried in order to overcome the difficulties of obtaining low yields, producing intractable and difficult to purify intermediates, and intermediates that are unstable towards direct bromination. The synthesis of the homo polymer **hPMA** was finally achieved via the $FeCl_3$ catalysed polymerisation of the easily obtained Pechmann dye (**4.24**) in which the alkylated thiophenes were crucial to obtaining high yields while the inclusion of the nitrogen atom was crucial to the stability of the molecule. Although low mobilities were obtained in transistors due to the poor planarity of the molecule, the low band gap and broad absorption mean that further development of Pechmann dyes may be useful for future OPV applications.

Whilst this research was being carried out another research group developed a couple of small molecules based on Pechmann dyes which obtained remarkably high hole mobilities of 1.4 $cm^2V^{-1}s^{-1}$.[256] This shows that Pechmann dyes are a promising class of new material for future applications in plastic electronics, providing that the yields and difficulties with purification can be overcome if they are ever to be used in an industrial context.

Chapter 5 Experimental Procedures

‘Stick a thiophene in it’

Prof Iain McCulloch, Scottish Chemist and all round nice guy.

5.1 General Procedures

All reagents and solvents were purchased from commercial suppliers (Acros Organics, Alfa Aesar, Sigma Aldrich and VWR) unless otherwise stated. 3-dodecylthiophene and thieno[3,2-*b*]thiophene were purchased from Wawei Chemicals and all palladium catalysts were purchased from Strem Chemicals. Anhydrous solvents (diethyl ether, hexane and tetrahydrofuran) were obtained from Sigma Aldrich and used as received.

All glassware was oven dried before use and allowed to cool under an atmosphere of argon. All reactions, unless otherwise stated, were carried out under a protective argon atmosphere, using an argon filled dual manifold and standard Schlenk line techniques. Thin layer chromatography was performed on Merck TLC F254 silica gel 60 plates and developed under 254 or 336 nm ultraviolet light or developed with iodine. Column chromatography was performed using silica gel (Merck Kieselgel 60) or using Biotage ZIP columns. Microwave reactions were performed in a Biotage initiator V 2.3.

^{1}H NMR and ^{13}C NMR spectra were recorded on a BRUKER DRX400 spectrometer at 400MHz and 101 MHz respectively, with the peak due to the NMR solvent being used as the internal reference. HRMS was recorded on a micromass Autospec premier using EI or MALDI-TOF. Number-average (Mn) and weight-average (Mw) molecular weights were determined with an Agilent Technologies 1200 series GPC in chlorobenzene at 80 °C, using two PL mixed B columns in series, and calibrated against narrow polydispersity polystyrene standards. UV-Vis absorption spectra were recorded on a UV-1601 Shimadzu UV-Vis spectrometer. Cyclic voltammograms (CV) were carried out using a cylindrical platinum working electrode and a platinum mesh counter electrode in acetonitrile at a potential scan rate of 0.1 Vs^{-1}. Ag/Ag^{+} was used as a reference electrode and calibrated against ferrocene. All the measurements were carried out in an argon saturated solution of 0.1 M of tetrabutylammonium hexafluorophosphate (*n*-Bu_4NPF_6) in anhydrous acetonitrile. Photo Electron Spectroscopy in Air (PESA) measurements were recorded with a Riken Keiki AC-2 PESA spectrometer with a power setting of 5 nW and a power number of 0.5. AFM images were obtained with a Picoscan PicoSPM LE scanning probe in tapping and phase modes. X-ray diffraction (XRD) measurements were carried out with a

PANALYTICAL X'PERT-PRO MRD diffractometer equipped with a nickel-filtered Cu $K\alpha_1$ beam and a X' CELERATOR detector, using a current of 40 mA and an accelerating voltage of 40 kV.

5.2 Field Effect Transistor Fabrication and Characterisation.

Chapter 2

Field-effect transistors were fabricated by evaporating Au (23 nm) S/D contacts onto cleaned Corning glass substrates, followed by functionalization with a PFBT monolayer. Polymer solutions (10 mg/1.5mL in chlorobenzene) were spin coated in N_2 at 2000 rpm (acc=5s) for 60 s on top of the PFBT monolayer and then baked at 100 ºC for 10 min. CYTOP^{TM} was subsequently spin coated on top at 2000 rpm (acc = 9s) for 60 s and then baked at 95 ºC for 20 min. Al top gate electrodes were finally evaporated on top of the CYTOP^{TM} dielectric.

Chapter 3

Section 3.3.6

Polymer **IGT-BT** FETs were characterised by using the top-gate/bottom-contact (TGBC) configuration. Specifically, the gold source and drain bottom electrodes (with Cr as the adhesion layer) were patterned by photolithography on clean low sodium glass substrates. A layer of **IGT-BT** was then deposited on top by spin coating a polymer solution in anhydrous 1,2-dichlorobenzene (10 mg/mL) at a speed of 1500 rpm for 60 s. For as-spun FETs, solvent drying was performed at 80 °C for more than two hours. For annealed FETs, after solvent drying samples were further placed on a hotplate (preheated to the annealing temperature) for 30 minutes before cooling down to room temperature. Subsequently, a PMMA solution (45 mg/mL in *n*-butyl acetate) was then spin-coated onto the semiconducting polymer resulting in a dielectric layer of ~500 nm thick. Gate electrodes comprising a layer of gold (20-nm-thick) were then evaporated through a shadow mask onto the dielectric layer by thermal evaporation. Starting from the step of making the semiconductor polymer solution to the final step of FET measurements, all procedures/measurements were carried out inside a dry nitrogen glove box. Mobility values quoted in the text are averaged over typically 5-10 individual devices prepared under the same conditions.

Section 3.4.7

Top-gate, bottom-contact OFETs were fabricated by evaporating Au (23 nm) source drain contacts onto cleaned glass substrates. The electrodes were functionalised with a PFBT monolayer before the polymer films were spin cast on top under N_2 from dichlorobenzene solutions (10 mg/mL, 2000 rpm, acc = 5s, for 60 s) and subsequently annealed at 200 °C for 10 min to ensure that any residual solvent was removed. CYTOP™ was subsequently spin coated on top at 2000 rpm (acc = 9s) for 60 s and then baked at 95 ºC for 20 min. Al top gate electrodes were finally evaporated on top of the CYTOP™ dielectric.

Section 3.5.7

Bottom-gate, bottom-contact transistor structures were fabricated using heavily doped p-type Si wafers acting as a common gate electrode and a 200 nm thermally grown SiO_2 layer as the dielectric. Using conventional photolithography, gold source-drain electrodes were defined with channel lengths and widths in the range of 1–40 μm and 1–20 mm, respectively. A 10 nm layer of titanium was used as an adhesion layer for the gold on the SiO_2 giving finished electrodes that were 100 nm thick. The SiO_2 surface was passivated with hexamethyldisilazane (HMDS) before the terpolymers **rIGPhPhIGT0.25**, **rIGPhPhIGT0.50** and **rIGPhPhIGT0.75** dissolved in chlorobenzene at a concentration of 5 mg/mL were spin coated on top of the electrodes at 2000 rpm for 30 seconds. The devices were annealed at a variety of temperatures (100, 125, 150 and 200 ºC) for 10 minutes in a dynamic vacuum of 10^{-5} mbar. The electrical measurements were performed in vacuum using an HP 4155C semiconductor parameter analyzer.

Chapter 4

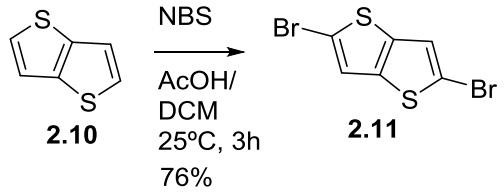
Field-effect transistors were fabricated using heavily doped silicon wafers as the common gate electrode with a 200 nm thermally oxidized SiO_2 layer as the gate dielectric. Using conventional photolithography, gold source and drain electrodes were defined in a bottom contact device configuration with a channel length of 10 μm and different widths. A 10 nm layer of titanium was used acting as an adhesion layer for the gold on SiO_2. The SiO_2 layer was exposed to the vapour of the primer hexamethyldisilazane for 60 min prior to semiconductor deposition in order to passivate the surface of the gate dielectric. Films were spun from a chloroform

solution at 1500 rpm for 30 s. Freshly prepared devices were annealed in a dynamic vacuum of 10^{-5} mbar at 200 °C for 72 h to remove traces of solvent. Electrical measurements were performed in vacuum using an HP 4155C semiconductor parameter analyzer.

5.3 Solar Cell Fabrication and Characterisation

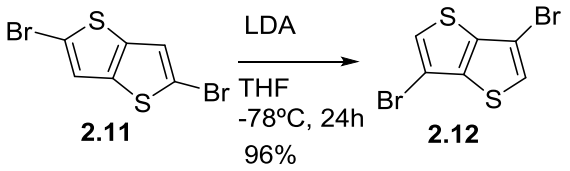
Photovoltaic devices were made by spin coating poly-(ethylenedioxythiophene):poly(styrene sulfonate) (PEDOT:PSS) (Clevios P, VP Al4083) onto pre-cleaned, patterned indium tin oxide (ITO) substrates (14 U per square) (Naranjo Substrates). The photoactive layer was deposited by spin coating a chlorobenzene or chloroform: chlorobenzene (described in the text) solution containing 6 mg mL^{-1} polymer and 12 mg mL^{-1} $PC_{70}BM$ for initial devices with the concentrations for the optimised devices described in the text. The counter electrode, consisting of LiF (1 nm) and Al (100 nm), was deposited by vacuum evaporation at ~3 × 10^{-7} mbar. The active area of the cells was as given in the text. J–V characteristics were measured under ~100 mW cm^{-2} white light from a tungsten–halogen lamp filtered by a Schott GG385 UV filter and a HoyaLB120 daylight filter, using a Keithley 2400 source meter. Short circuit currents under AM1.5G conditions were estimated from the spectral response and convolution with the solar spectrum. The spectral response was measured under simulated 1 sun operation conditions using bias light from a 532 nm solid state laser (Edmund Optics). Monochromatic light from a 50 W tungsten halogen lamp (Philips focusline) in combination with monochromator (Oriel, Cornerstone 130) was modulated with a mechanical chopper. The response was recorded as the voltage over a 50 Ω resistance, using a lock-in amplifier (Stanford Research Systems SR830). A calibrated Si cell was used as reference. The device was kept behind a quartz window in a nitrogen filled container. The thickness of the active layers in the photovoltaic devices was measured on a Veeco Dektak 150 profilometer.

5.4 Synthesis of 2,5-dibromothieno[3,2-*b*]thiophene (2.11)



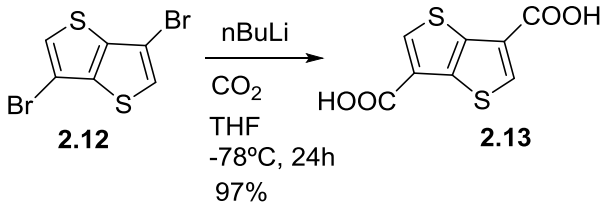
To a stirred solution of thieno[3,2-*b*]thiophene (**2.10**) (15 g, 107 mmol) in a mixture of DCM (248 mL) and acetic acid (AcOH) (119 mL) was slowly added NBS (38.1 g, 214 mmol) in small portions over a period of 40 min. After the addition, the mixture was stirred at room temperature for 3 h until TLC showed no starting material left. The mixture was washed twice with aqueous $NaHCO_3$ solution (5%) and three times with water, dried with anhydrous magnesium sulfate, and filtered. The product was obtained after evaporation of the solvent and dried in vacuo, resulting in 24.098 g (yield: 76%) of 2,5-dibromothieno[3,2-*b*]thiophene as white/greenish solid. ^{1}H NMR (400 MHz, $CDCl_3$): δ 7.17 (s, 2H). ^{13}C NMR (101 MHz, $CDCl_3$): δ 138.28, 121.77, 113.62 MS (EI): *m/z* 278 Calc. 279.79

5.5 Synthesis of 3,6-Dibromo-thieno[3,2-*b*]thiophene (2.12)



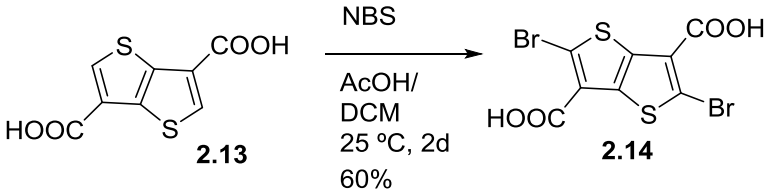
2,5-dibromo-thieno[3,2-*b*]thiophene (**2.11**) (24.098 g, 81 mmol) was dissolved in anhydrous THF (277 mL) and cooled to -78ºC. Lithium diisopropylamide (97 mL, 194 mmol, 2 M) was added dropwise and the solution was allowed to slowly warm to room temperature overnight. The solution was cooled to -78 ºC, diluted with hexanes (200 mL), and quenched with brine (200 mL). The organic layer was dried over anhydrous $MgSO_4$, flash columned directly onto silica under suction, washed through with toluene and the solvent removed under reduced pressure. The brownish solid obtained was flash columned again using toluene as eluent to give an off white solid which was washed with methanol and dried under high vacuum to give 23.148 g of white solid 3,6-dibromo-thieno[3,2-*b*]thiophene (**2.12**) in 96% yield. ^{1}H NMR (400 MHz, $CDCl_3$): δ 7.34 (2H, s). ^{13}C NMR (101 MHz, $CDCl_3$): δ 139.80, 125.15, 103.02 MS (EI): *m/z* 278 Calc. 279.79

5.6 Synthesis of thieno[3,2-*b*]thiophene-3,6-dicarboxylic acid (2.13)



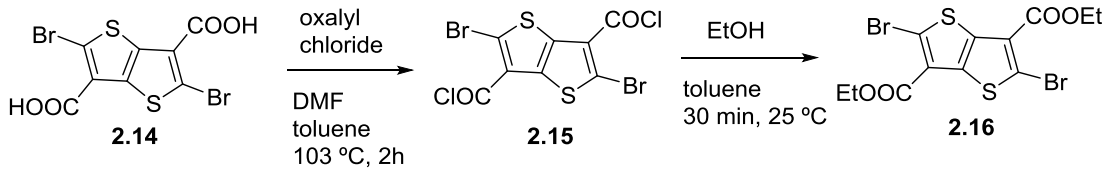
Dissolved 3,6 dibromothieno[3,2-*b*]thiophene (**2.12**) (5 g, 16.87 mmol) in anhydrous diethyl ether (300 mL) at room temperature under Ar. Cooled to -78 °C and added nBuLi in hexanes (14.76 mL, 36.9 mmol, 2.5 M). Stirred at -78 °C for 1.5 h before adding dry ice (5 g) and leaving to warm up over night. Added water (10 mL) to quench and then added diethyl ether (50 mL). Extracted the ether layer with sodium hydrogen carbonate (2*100 mL) and combined the aqueous layers. Acidified the aqueous layers with HCl (aq) (600 mL, 2 M) and filtered out the white precipitate under vacuum. The product obtained was dried under high vacuum to give 3.73 g of solid white thieno[3,2-*b*]thiophene-3,6-dicarboxylic acid in 97% yield. ^{1}H NMR (400MHz, DMSO-d_6): δ 13.35 (2H, s), 8.49 (2H, s). ^{13}C NMR (101 MHz, DMSO-d_6): δ 163.25, 138.40, 137.78, 126.75 MS (EI): *m/z* 228 Calc. 228.245

5.7 Synthesis of 2,5-dibromothieno[3,2-*b*]thiophene-3,6-dicarboxylic acid (2.14)



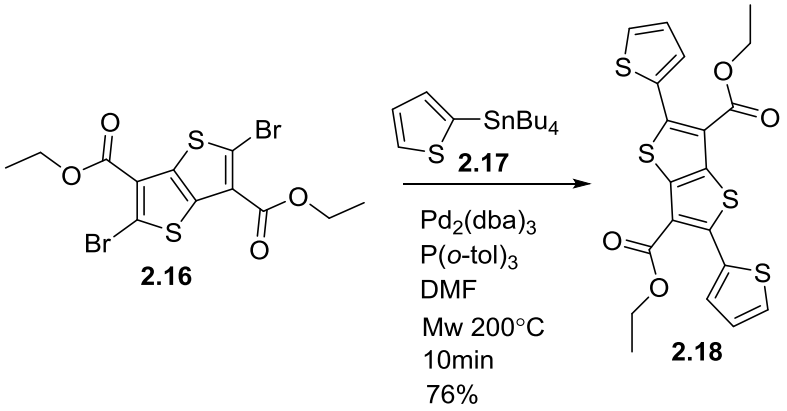
To a stirred solution of 3,6 thieno[3,2-*b*]thiophene dicarboxylic acid (1 g, 4.38 mmol) in a mixture of DCM (20.28 mL) and acetic acid (9.74 mL) in a 100 mL flask was slowly added NBS (3.12 g, 17.53 mmol) in small portions over a period of 10 min. After the addition, the mixture was stirred at room temperature for 2 days. The mixture was washed twice with aqueous $NaHCO_3$ solution (5%), filtered and washed with water. The beige solid obtained was dried in the vacuum oven overnight to give 1.02 g of 2,5-dibromothieno[3,2-*b*]thiophene-3,6-dicarboxylic acid in 60% yield. ^{1}H NMR (400 MHz, DMSO-d_6): δ14 (2H, s) ^{13}C NMR (101 MHz, DMSO-d_6): δ 161.77, 135.42, 124.51, 122.77 MS (EI): *m/z* 386 Calc. 386.037

5.8 Synthesis of diethyl 2,5-dibromothieno[3,2-*b*]thiophene-3,6-dicarboxylate (2.16)



Dissolved 2,5-dibromothieno[3,2-*b*]thiophene-3,6-dicarboxylic acid (0.1533 g, 0.39 mmol) in anhydrous toluene (50 mL) and added anhydrous DMF (0.2 mL) and oxalyl chloride (0.18 mL) under Ar at room temperature before heating the reaction mixture to 103 °C for 1 h. Stirred reaction mixture at room temperature for 1 h more, before quenching with ethanol (20 mL) and stirring at room temperature for 30 min. Evaporated off the solvent under reduced pressure to give the crude product as a reddish oil. The crude product was purified via column chromatography in DCM to give 0.108 g of diethyl 2,5-dibromothieno[3,2-*b*]thiophene-3,6-dicarboxylate as a white powdery solid in 62% yield. Rf = 0.82 in hexane. ^{1}H NMR (400 MHz, Acetone-d_6): δ4.46 (4H, q, J = 7.15Hz), 1.47 (6H, t, J = 7.04Hz) ^{13}C NMR (101 MHz, $CDCl_3$): δ 160.67, 135.80, 123.67, 123.52, 61.81, 14.27 MS (EI): *m/z* 440 (70%), 442 (100%), 444 (72%) Calc. 441.83668 (100%)

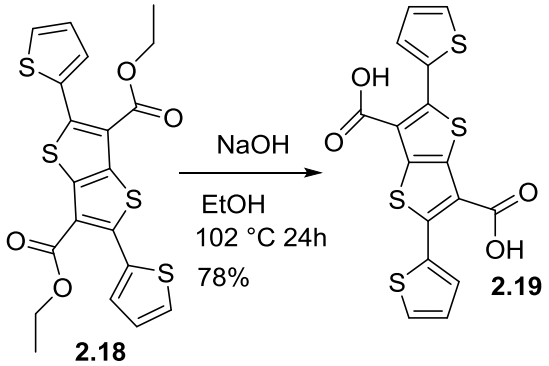
5.9 Synthesis of diethyl 2,5-di(thiophen-2-yl)thieno[3,2-*b*]thiophene-3,6-dicarboxylate (2.18)



A 10 mL glass vial was charged with a stirrer bar, tributyl(thiophen-2-yl)stannane (0.5 g, 1.131 mmol), $Pd_2(dba)_3$ (0.021 g, 0.023 mmol), P(*o*-tol)$_3$ (0.028 g, 0.09 mmol), dimethylformamide (0.087 mL, 1.131 mmol) and chlorobenzene (4 mL). The glass vial was purged under argon and securely sealed. The glass vial was placed into a microwave reactor (Biotage Initiator) and heated at 200 °C for 10 min with stirring. After cooling to room temperature, the reaction mixture was precipitated into a

mixture of methanol (20 mL) and HCl (2 mL, 2 M) and stirred for 5 min. The product was filtered off, dissolved up in hot ethyl acetate (90 °C) and filtered to remove the palladium. The product was flash columned on silica with DCM to give a yellow solid (0.423 g, 76%). ^{1}H NMR (400 MHz, $CDCl_3$): δ 7.59 (2H, dd, J = 0.97Hz, J = 3.76Hz), 7.51 (2H, dd, J = 1.13Hz, J = 5.22Hz), 7.148 (2H, dd, J = 3.02Hz, J = 3.76Hz), 4.42 (2H, q, J = 7.18Hz), 1.432 (2H, t, J = 7.09Hz) ^{13}C NMR (101 MHz, $CDCl_3$): δ 162.30, 146.42, 139.43, 137.15, 131.64, 129.70, 126.56, 119.39, 61.20, 14.41 MS (EI): *m/z* 448 Calc. 448.599

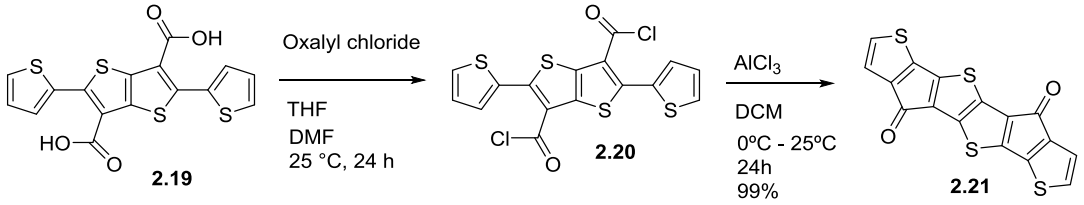
5.10 Synthesis of 2,5-di(thiophen-2-yl)thieno[3,2-*b*]thiophene-3,6-dicarboxylic acid (2.19)



2.18 **2.19**

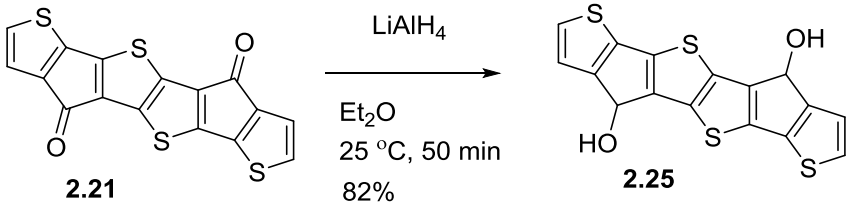
To a solution of sodium hydroxide (0.072 g, 1.808 mmol) in water (0.08 mL) and ethanol (0.7 mL) was added diethyl 2,5-di(thiophen-2-yl)thieno[3,2-*b*]thiophene-3,6-dicarboxylate (0.0245 g, 0.055 mmol). The mixture was refluxed under Ar for 3 h at a bath temperature of 102 °C and subsequently stirred at rt overnight. HCl (2 M, 5 mL) was added and the resultant yellow precipitate was filtered out and dried to give 0.0167 g, 78% of solid yellow 2,5-di(thiophen-2-yl)thieno[3,2-*b*]thiophene-3,6-dicarboxylic acid product. ^{1}H NMR (400 MHz, DMSO d_6): δ 13.72 (2H, s), 7.79 (2H, dd, J = 0.91Hz, J = 4.87Hz), 7.66 (2H, dd, J = 0.93Hz, J = 3.82Hz), 7.20 (2H, dd, J = 3.39Hz, J = 3.72Hz). ^{13}C NMR (101 MHz, DMSO d_6): δ 163.28, 145.26, 137.08, 133.76, 130.69, 130.16, 128.28, 120.66. MS (EI): *m/z* 391.9317 Calc. 391.93

5.11 Synthesis of thieno[3',2':4,5]cyclopenta[1,2-b]thieno[2'',3'':3',4']cyclopenta[1',2':4,5] thieno[2,3-d]thiophene-4,9-dione (2.21)



Dissolved 2,5-di(thiophen-2-yl)thieno[3,2-*b*]thiophene-3,6-dicarboxylic acid (2.77 g) in anhydrous THF (400 mL), degassed under Ar and added oxalyl chloride (0.11 mL). Added DMF (0.03 mL) dropwise and stirred at room temperature overnight. Removed THF and excess oxalyl chloride under reduced pressure. Added anhydrous DCM (3 mL) and stirred at 0 ºC for 10 min. In a separate round bottomed flask $AlCl_3$ (0.189 g) was suspended in anhydrous DCM (22 mL), degassed and stirred at 0 ºC. The acid chloride solution was added dropwise to the $AlCl_3$ suspension and left to stir and warm up overnight. The reaction mixture was added to ice cold HCl (2 M, 100ml) and stirred for 10 mins. Filtered off the solid precipitate and washed with HCl (20 mL, 2 M), water (20 mL) and acetone (20 mL) Obtained a black insoluble powder (2.5763 g, 99%). MS (EI) *m/z* 356 Calc. 356.462 Product was too insoluble to obtain ^{1}H and ^{13}C NMR.

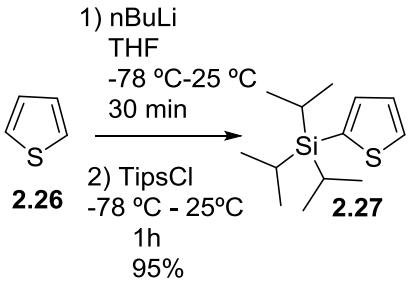
5.12 Synthesis of thieno[3',2':4,5]cyclopenta[1,2-b]thieno[2'',3'':3',4']cyclopenta[1',2':4,5] thieno[2,3-d]thiophene-4,9-diol (2.25)



Powdered lithium aluminium hydride (0.051 g, 1.35 mmol) was suspended in anhydrous diethyl ether (11 mL) and diketone compound (**2.21**) was slowly added. The reaction mixture was stirred for 50 min before ice cold water (3 mL) was added dropwise followed by HCl (5 mL, 2M). Filtered out the black solid product and washed with HCl (2 M) and water to give a crude product (0.1665 g, 82%) that was

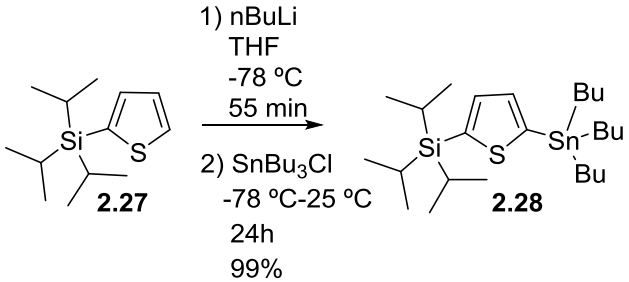
used in the next reaction without further purification due to its insoluble nature. MS (EI+): *m/z* 360 Calc. 359.941 Product was too insoluble for ^{1}H and ^{13}C NMR.

5.13 Synthesis of triisopropyl(thiophen-2-yl)silane (2.27)



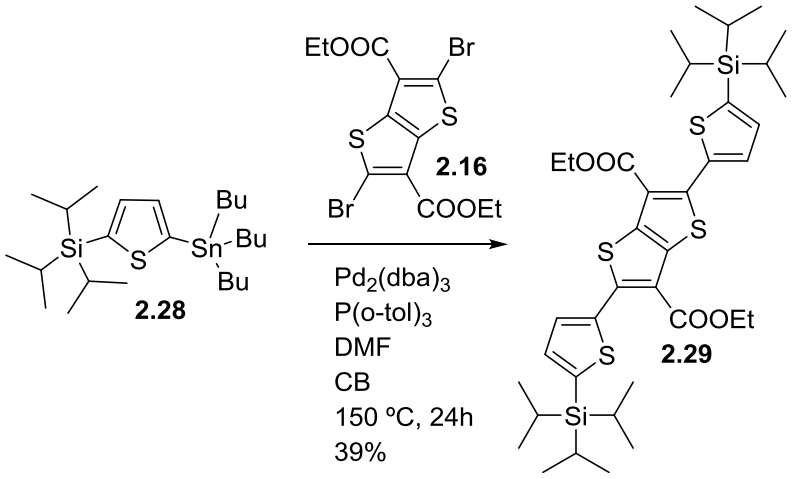
Thiophene (3.93 mL, 49.1 mmol) was dissolved in anhydrous THF (50 mL) and degassed under Ar for 20 min. After cooling to -78 °C in an acetone / dry ice bath, n-butyllithium (19.6 mL, 2.5 M in THF, 49.1 mmol) was added dropwise. The acetone / dry ice bath was removed and the reaction was allowed to warm to rt and stir over the course of 30 min. The reaction was cooled back down to -78 °C before chlorotriisopropylsilane (10.5 mL, 49.1 mmol) was added. The acetone / dry ice bath was once again removed and the reaction was allowed to warm to rt over the course of 1 h. The reaction was cooled to -78°C and water (3 mL) was added to quench the reaction. The reaction was allowed to warm to rt, extracted with diethyl ether, dried over $MgSO_4$, filtered and concentrated under reduced pressure to give the product as a yellow oil (11.15 g) in 95% yield. ^{1}H NMR (400 MHz, $CDCl_3$): δ 7.62 (1H, dd, J = 4.39, 0.98 Hz), 7.30 (1H, dd, J = 3.51, 0.97 Hz), 7.21 (1H, dd, J = 4.80, 3.50 Hz), 1.33 (3H, hept, J = 7.71 Hz), 1.11 (18H, d, J = 7.71 Hz). HRMS (EI): *m/z* 240.1368 Calc. 240.1368 Spectroscopic values agree with literature values.[257]

5.14 Synthesis of triisopropyl(5-(trimethylstannyl)thiophen-2-yl)silane (2.28)



Triisopropyl(thiophen-2-yl)silane (11.15 mL, 46.4 mmol) was dissolved in anhydrous THF (63 mL) and degassed under Ar for 20 min. After cooling to -78°C in an acetone / dry ice bath, n-butyllithium (18.5 mL, 2.5 M in THF, 46.4 mmol) was added dropwise over the course of 10 min. The acetone / dry ice bath was removed and the reaction was allowed to warm to rt and stir over the course of 45 min. The reaction was cooled back down to -78°C before chlorotrimethylstannane (50 mL, 1M in THF, 50 mmol) was added dropwise. The acetone / dry ice bath was once again removed and the reaction was allowed to stir under Ar overnight. Water (20 mL) was added to quench the reaction followed by petroleum ether (60-80°C) (30 mL). The organic layer was separated and washed with water (3 × 100 mL), dried over $MgSO_4$, filtered and concentrated under reduced pressure to give the product as a pale orange oil (18.51 g) in 99% yield. ^{1}H NMR (400 MHz, $CDCl_3$): δ 7.41 (d, J = 3.0 Hz, 1H), 7.30 (d, J = 3.2 Hz, 1H), 1.35 (hept, J = 7.4, 3H), 1.10 (d, J = 7.31 Hz, 18H), 0.37 (s, 9H). ^{13}C NMR (101 MHz, $CDCl_3$): δ 132.42, 135.70, 68.17, 25.76, 18.80, 12.10, 7.97 HRMS (EI): m/z 404.1035 Calc. 404.1016

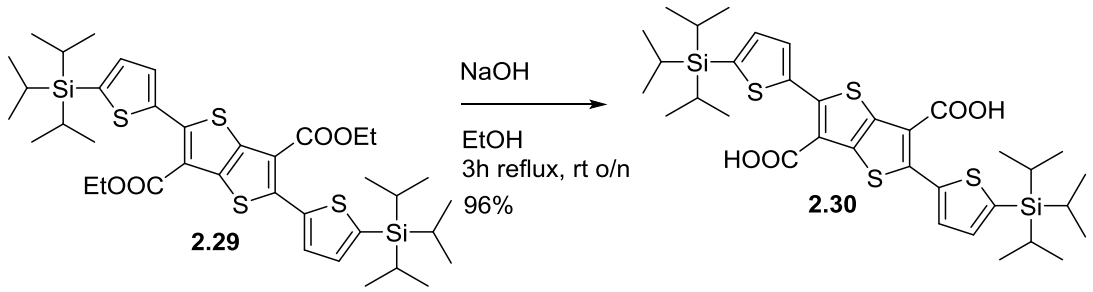
5.15 Synthesis of diethyl 2,5-bis(5-(triisopropylsilyl)thiophen-2-yl)thieno[3,2-*b*]thiophene-3,6-dicarboxylate (2.29)



Triisopropyl(5-(trimethylstannyl)thiophen-2-yl)silane (18.7 g, 46.4 mmol), diethyl 2,5-dibromothieno[3,2-*b*]thiophene-3,6-dicarboxylate (9.32 g, 21.08 mmol), $Pd_2(dba)_3$ (0.386 g, 0.422 mmol), $P(o\text{-}tol)_3$ (0.513 g, 1.686 mmol), dimethylformamide (1.63 mL, 21.08 mmol) and chlorobenzene (74.5 mL) were placed in a 3 necked 250 mL round bottomed flask and degassed under Ar for 45 min before being refluxed at a bath temperature of 150 ºC overnight. After cooling to room temperature, the reaction

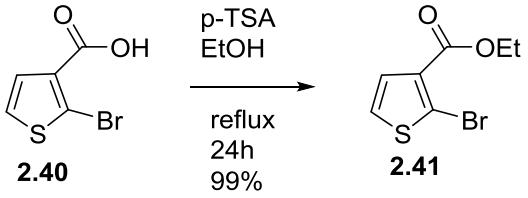
mixture was precipitated into a mixture of methanol (20 mL) and HCl (10 mL, 2 M) and stirred for 5 min. The precipitated product was filtered off, dissolved up in hot ethyl acetate (90 °C) and filtered to remove the palladium. Flash chromatography using silica and DCM as eluent gave the product as a yellow solid 6.2 g, 39%. ^{1}H NMR (400 MHz, $CDCl_3$): δ 7.69 (d, J = 3.6 Hz, 2H), 7.25 (d, J = 3.5 Hz, 2H), 4.40 (q, J = 7.1 Hz, 4H), 1.39 (t, J = 7.23 Hz, 6H), 1.38 (hept, J = 7.21, 6H), 1.14 (d, J = 7.3 Hz, 18H) ^{13}C NMR (101 MHz, $CDCl_3$): δ 162.20, 146.25, 139.24, 138.60, 137.52, 135.95, 130.86, 119.41, 61.42, 18.74, 14.41, 11.94. MS (MALDI): *m/z* 761.3 Calc. 760.26 (100%), 761.263

5.16 Synthesis of 2,5-bis(5-(triisopropylsilyl)thiophen-2-yl)thieno[3,2-*b*]thiophene-3,6-dicarboxylic acid (2.30)



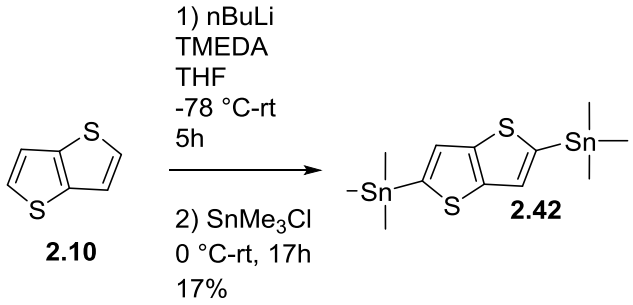
To a solution of sodium hydroxide (10.78 g, 270 mmol) in water (33ml) and ethanol (297 mL) was added diethyl 2,5-bis(5-(triisopropylsilyl)thiophen-2-yl)thieno[3,2-b]thiophene-3,6-dicarboxylate (6.20 g, 8.14 mmol). The mixture was initially sonicated for 10 min and then refluxed under Ar for 3 h at a bath temperature of 102 °C and subsequently stirred at rt overnight. HCl (2 M, 50 mL) was added and the resultant yellow precipitate was filtered out and dried to give 5.51 g, 96% of solid yellow product. ^{1}H NMR (400 MHz, DMSO-d_6): δ 8.32 (s, 2H), 7.79 (d, J = 3.6 Hz, 2H), 7.33 (d, J = 3.5 Hz, 2H), 1.34 (hept, J = 7.3 Hz, 6H), 1.08 (d, J = 7.4 Hz, 36H) ^{13}C NMR (101 MHz, DMSO-d_6): δ 162.93, 145.33, 138.21, 134.86, 131.63, 134.96, 129.77, 120.65, 18.77, 11.93. MS (EI): *m/z* 705 Calc. 704.197

5.17 Synthesis of 2 bromo thiophene 3 ethyl ester (2.41)



To a solution of 2 bromo -3 thiophenecarboxylic acid (9 g, 43.5 mmol) in ethanol (360 mL) was added p-toluenesulphonic acid (7.49 g, 43.5 mmol). The mixture was refluxed at 80°C overnight. The ethanol was removed under reduced pressure and DCM (40 mL) and saturated sodium hydrogen carbonate solution (40 mL) were added. The aqueous layer was extracted with DCM (3×100 mL) and the combined organics were dried over $MgSO_4$, filtered and concentrated under reduced pressure to give 10.09 g of 2 bromo thiophene 3 ethyl ester (**2a**) in 99% yield as an orange oil. R_f = 0.55 in hexane: ethyl acetate 4:1 ^{1}H NMR (400MHz, Acetone-d_6): δ 7.60 (1H, d, J = 5.81Hz), 7.40 (1H, d, J = 5.75Hz), 4.33 (2H, q, J = 7.19Hz), 1.37 (3H, t, J = 7.16Hz), ^{13}C NMR (400MHz, Acetone-d_6): δ 162.2, 132.5, 130.1, 128.0, 119.6, 61.5, 14.6 MS (EI): *m/z* 236 Calculated 235.10

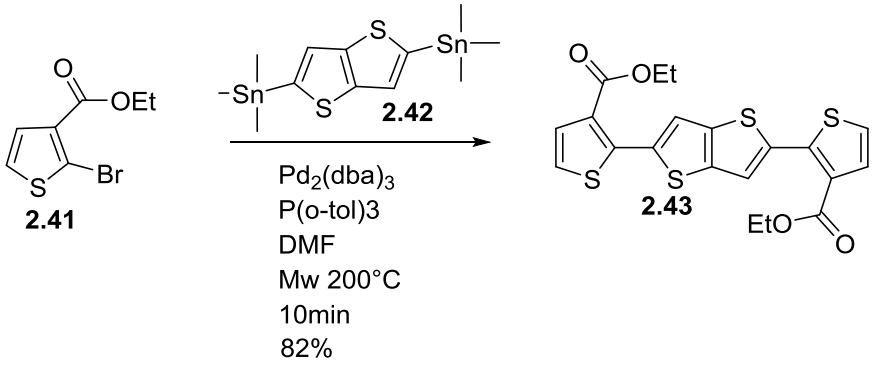
5.18 Synthesis of 2,5-bis(trimethylstannyl)thieno[3,2-b]thiophene (2.42)



A 500 mL 3 necked round bottomed flask was charged with thieno[3,2-b]thiophene (7 g), anhydrous tetrahydrofuran (THF) (140 mL) and tetramethylethylenediamine (TMEDA) (17 mL) and purged with Ar. The solution was cooled to -78 °C and a 2.5 M solution of nBuLi in hexanes was added over 10 mins. The reaction mixture was removed from the cooling bath and allowed to warm to room temperature, stirring for 5 h. The reaction mixture was cooled to 0 °C and trimethyltin chloride (25 g) was added as a solid in one portion. The reaction mixture was allowed to warm to room temperature stirring overnight for 17 h. The reaction mixture was quenched with water (100 mL) and extracted into ethyl acetate (100 mL). The organic extract was

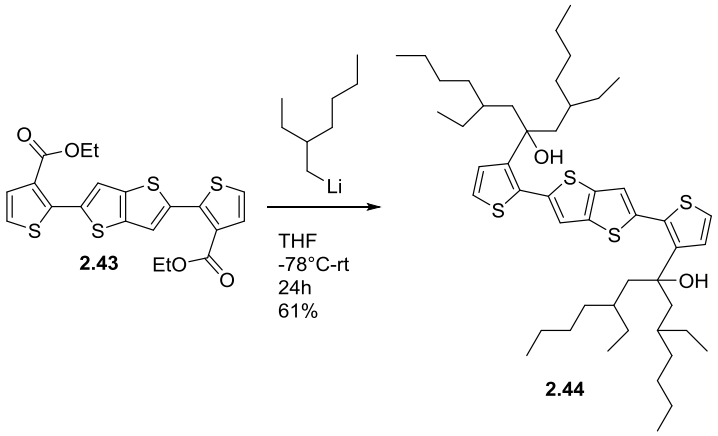
washed with water (2×100 mL) and brine (100 mL), dried over sodium sulfate (for 45 mins) and concentrated under vacuum to yield a brown solid. Recrystallisation (×3) from acetonitrile at 60 °C (with slow cooling in a water bath) gave 4 g of 2,5-bis(trimethylstannyl)thieno[3,2-*b*]thiophene in 17% yield as white crystals.[1]H NMR (400 MHz, Dimethylsulphoxide (DMSO) -d_6): δ 7.40 (2H, s), 0.37 (18H,s) MS (EI): *m/z* 466 Calc. 465.90. Spectroscopic values agree with literature values.[258]

5.19 Synthesis of diethyl 2,2'-thieno[3,2-b]thiene-2,5-diyldithiophene-3-carboxylate (2.43)



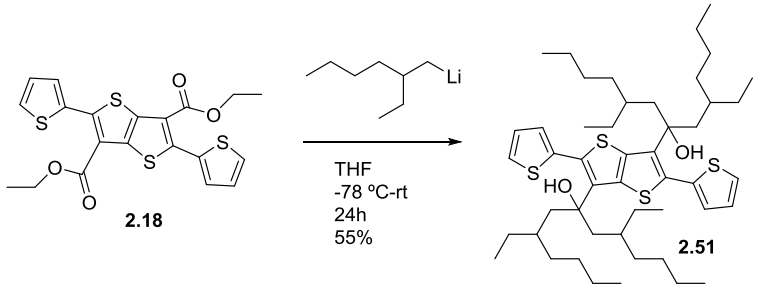
A 10 mL glass vial was charged with a stirrer bar, 2-bromothiophene-3-ethyl ester (1.8 g, 7.66 mmol), 2,5-bis(trimethylstannyl)thieno[3,2-*b*]thiophene (1.621 g, 3.48 mmol), $Pd_2(dba)_3$ (0.064 g, 0.07 mmol), P(*o*-tol)$_3$ (0.085 g, 0.278 mmol), dimethylformamide (0.269 mL, 3.48 mmol) and chlorobenzene (4 mL). The glass vial was purged under argon and securely sealed. The glass vial was placed into a microwave reactor (Biotage Initiator) and heated at 200 °C for 10 min with stirring. After cooling to room temperature, the reaction mixture was precipitated into a mixture of methanol (20 mL) and HCl (2 mL, 2 M) and stirred for 5 min. The product was filtered off, dissolved up in hot ethyl acetate (90 °C), precipitated out in room temperature ethanol and filtered off to give 1.28 g of diethyl 2,2'-thieno[3,2-*b*]thiene-2,5-diyldithiophene-3-carboxylate (**2.43**) as a bright orange solid in 82% yield. ^{1}H NMR (400 MHz, Acetone-d_6): δ 7.90 (2H, s), 7.59 (2H, d, J = 5.48Hz), 7.55 (2H, d, J = 5.52Hz), 4.32 (4H, q, J = 7.24Hz), 1.32 (6H, t, J = 7.17Hz) ^{13}C NMR (101 MHz, $CDCl_3$): δ 163.1, 142.9, 140.5, 136.2, 130.7, 128.4, 124.43, 121.3, 60.9, 29.7, 14.2 MS (EI): *m/z* 448 Calc. 448.60

5.20 Synthesis of 7,7'-(2,2'-(thieno[3,2-b]thiophene-2,5-diyl)bis(thiophene-3,2-diyl))bis(5,9-diethyltridecan-7-ol) (2.44)



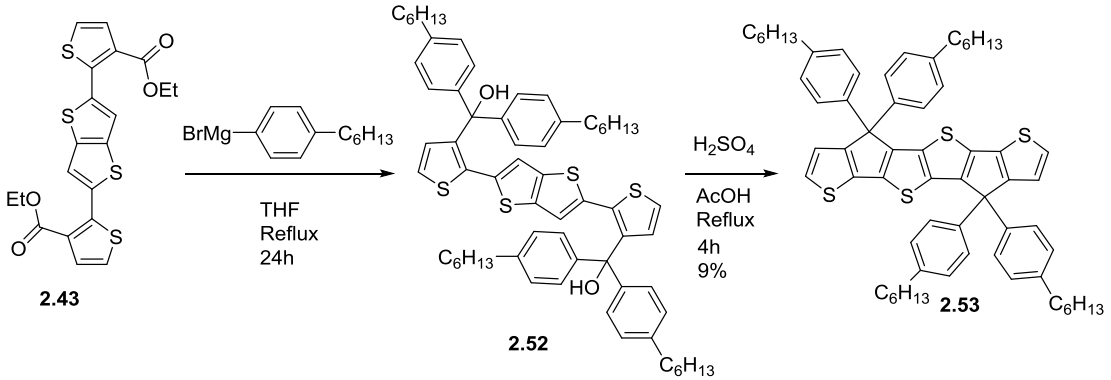
Diethyl 2,2'-thieno[3,2-*b*]thiene-2,5-diyldithiophene-3-carboxylate (0.74 g, 1.65 mmol) was dissolved in anhydrous THF (115 mL) and cooled to -78 °C. 2-ethylhexyllithium (5.43 mL, 9.90 mmol) was added dropwise over the course of 10 min and the reaction mixture was allowed to warm to room temperature overnight. The reaction mixture was quenched with methanol (10 mL) and then water (20 mL). The THF was rotary evaporated off and the remaining aqueous solution was extracted with ethyl acetate. The organic layer was dried over $MgSO_4$, filtered and reduced down to give a crude brown oil. The crude product was purified by column chromatography in hexane to give the product as a yellow oil (0.812 g) in 61% yield. ^{1}H NMR (400MHz, $CDCl_3$): δ 7.26 (2H, d, J = 5.26Hz), 7.25 (2H, s), 1.94 (2H, s), 1.84-1.76 (4H, m), 1.71-1.63 (4H, m), 1.48-1.00 (31H, m), 0.91-0.78 (6H, m), 0.72 (6H, t, J = 7.38Hz). ^{13}C NMR (101 MHz, $CDCl_3$): δ 145.95, 139.47, 137.47, 129.25, 128.58, 125.36, 121.43, 48.05, 34.64, 33.90, 31.60, 28.60, 26.47, 23.12, 14.14, 10.50. MS (EI): *m/z* 813.5 Calc. 813.376

5.21 Synthesis of 7,7'-(2,5-di(thiophen-2-yl)thieno[3,2-b]thiophene-3,6-diyl)bis(5,9-diethyltridecan-7-ol) (2.51)



Dissolved diethyl 2,5-di(thiophen-2-yl)thieno[3,2-b]thiophene-3,6-dicarboxylate (0.4 g, 0.829 mmol) in anhydrous THF (120 mL) at rt. Cooled to -78 °C and continued degassing under Ar. Added 2-ethyl hexyllithium (2.94 mL, 5.35 mmol) dropwise over 10 min and left to warm up overnight. The reaction mixture was quenched with methanol (10 mL) and then water (20 mL). The THF was rotary evaporated off and the remaining aqueous solution was extracted with ethyl acetate. The organic layer was dried over $MgSO_4$, filtered and reduced down to give a crude dark green oil. The crude product was purified by column chromatography in chloroform to give the product as a green oil (0.397 g, 55%). ^{1}H NMR (400 MHz, $CDCl_3$): δ 7.42 (2H, dd, J = 1.02Hz, J = 4.94Hz), 7.17 (2H, dd, J = 1.62Hz, J = 3.43Hz), 7.07 (2H, dd, J = 3.69Hz, J = 3.18Hz), 2.00 (2H, s), 1.72-1.62 (4H, m), 1.55-1.00 (38H, m), 0.95-0.75 (20H, m), 0.7-0.64 (6H, m). ^{13}C NMR (101 MHz, $CDCl_3$): δ 136.11, 129.92, 129.59, 127.51, 127.32, 126.77, 126.64, 39.24, 34.66, 28.60, 28.39, 26.58, 23.04, 14.22, 10.45 MS (EI): *m/z* 813 Calc. 813.376

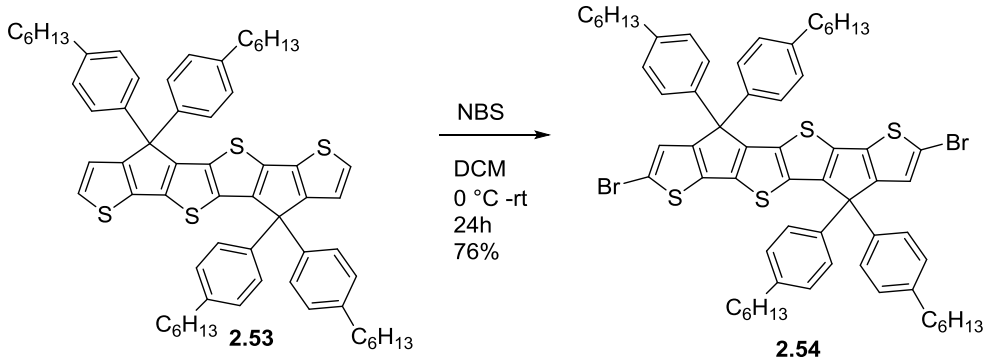
5.22 Synthesis of 4T (2.53)



To a solution of compound (**2.43**) (2.0 g, 4.46 mmol) in THF (20 mL) was added dropwise a solution of freshly prepared 4-*n*-hexylphenyl magnesium bromide (from 6.44 g, 26.72 mmol of 1-bromo-4-*n*-hexylbenzene in 10 mL THF). The solution was refluxed overnight and then allowed to cool to room temperature. Water (50 mL) and ethyl acetate (50 mL) were added and the layers separated. The organic fraction was washed with water (2 x 25 mL), dried ($MgSO_4$), filtered and concentrated *in vacuo* to afford viscous oil (**2.52**). The residue was subsequently dissolved in hot glacial acetic acid (100 mL) and conc. H_2SO_4 (5 mL) was added dropwise. The reaction mixture was then refluxed for 4 hours after which point water (200 mL) was added which afforded a dark solid which was isolated by filtration. Chloroform (100 mL) was

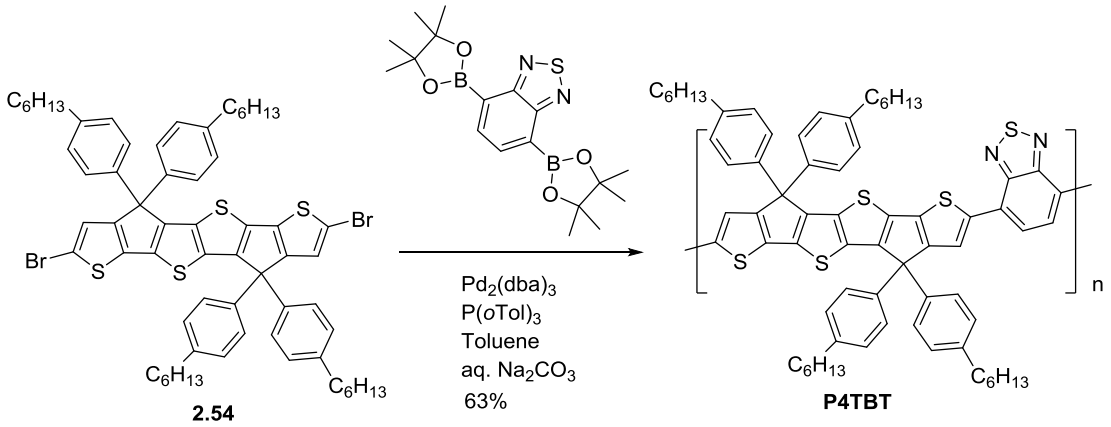
added and sonicated for 30 mins after which point the suspension was filtered and the filtrate concentrated *in vacuo*. The resulting black solid was purified by flash column chromatography (Hexanes) on silica gel to afford the product as a light yellow solid (389 mg, 9%). ^{1}H NMR (400 MHz, $CDCl_3$): δ 7.16 - 7.12 (m, 10H), 7.09 - 7.04 (m, 10H), 2.59 - 2.49 (m, 8H), 1.64 - 1.50 (m, 8H), 1.37 - 1.17 (m, 24H), 0.95 - 0.78 (m, 8H); ^{13}C NMR (101 MHz, $CDCl_3$): δ 141.7, 139.9, 137.1, 134.9, 128.6, 127.8, 125.2, 123.3, 61.9, 35.6, 31.7, 31.3, 29.1, 22.6, 14.1 MS (EI+): *m/z* 968 [M+H]+ Calc. 968.45

5.23 Synthesis of 4T-Br$_2$ (2.54)



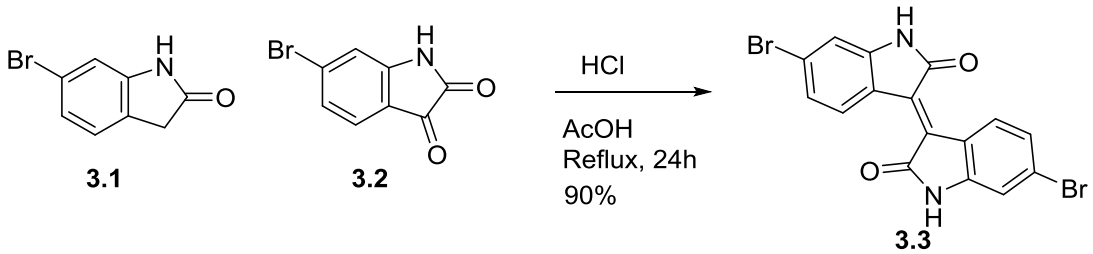
To a solution of **2.53** (0.2 g, 0.21 mmol) in dichloromethane (20 mL) at 0 °C was added N bromosuccinimide (81 mg, 0.45 mmol). The solution was allowed to warm to room temperature and stirred overnight. $Na_2S_2O_3$ (50 mL of a 2 M soln.) was added and the layers separated. The organic fraction was washed with water (3 x 25 mL), dried ($MgSO_4$), filtered and concentrated in vacuo. The resulting solid was recrystallized from acetone to afford compound (**2.54**) (180 mg, 76%) as a pale yellow solid. ^{1}H NMR (400 MHz, $CDCl_3$): δ 7.12 - 7.04 (m, 18H), 2.68 - 2.35 (m, 8H), 1.64 - 1.48 (m, 8H), 1.41 - 1.19 (m, 24H), 0.86 (t, *J* = 6.8 Hz, 8H); ^{13}C NMR (101 MHz, $CDCl_3$): δ 142.1, 139.1, 128.6, 127.7, 35.6, 31.7, 31.3, 29.1, 22.6, 14.1 MS (EI+): *m/z* 1127 [M+H]+ Calc. 1126.27

5.24 Synthesis of P4TBT



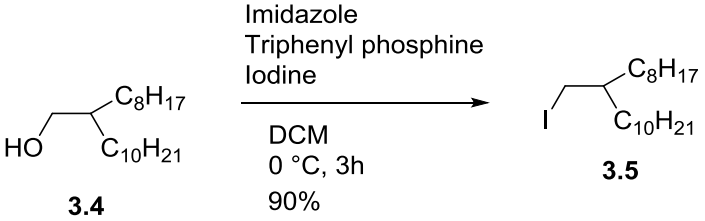
Compound (**2.54**) (0.160 g, 0.142 mmol), 4,7-bis(4,4,5,5- tetramethyl-1,3,2-dioxaborolan-2-yl)benzo[*c*][1,2,5]thiadiazole (0.055 g, 0.142 mmol), $Pd_2(dba)_3$ (3 mg, 0.003 mmol), P(*o*-tol)$_3$ (4 mg, 0.012 mmol) and Aliquat 336 (1 drop) were dissolved in toluene (6.5 mL). The mixture was thoroughly degassed with argon for 30 min, followed by the addition of degassed aqueous Na_2CO_3 (1.35 mL of a 1.0 M solution). The resulting mixture was degassed for a further 30 mins, sealed and heated at 120 ºC for 72 h. The polymer was precipitated by addition to methanol (150 mL) and collected by filtration. The polymer was further purified by Soxhlet extraction with acetone (24 h), hexanes (24 h) and finally chloroform (12 h). To the chloroform extract was added an aqueous solution of sodium diethyldithiocarbamate (~1 g/100mL) and the mixture was heated to 60 ºC with vigorous stirring for 2 h. After cooling to room temperature, the layers were separated and the organic fraction was washed with water (4 x 250 mL), and concentrated under vacuum. The resulting residue was dissolved in a minimum amount of chloroform and added dropwise to vigorously stirred methanol (250 mL). The resulting precipitate was isolated by filtration and dried *in vacuo* to afford the desired polymer as a dark solid (98 mg, 63%). ^{1}H NMR (400 MHz, $CDCl_3$): δ 8.13 (br s, 2H), 7.75 (br s, 2H), 7.40 - 6.95 (br m, 16H), 2.80 - 2.30 (br m, 8H), 1.70 - 1.45 (br m, 8H), 1.40 - 1.10 (br m, 24H), 0.90 0.70 (br m, 12H); ^{13}C NMR (101 MHz, $CDCl_3$): δ 128.7, 127.9, 35.6, 31.7, 31.3, 29.2, 22.6, 14.1. GPC (PS) M_n = 19 kDa, M_w = 50 kDa PDI = 2.6

5.25 Synthesis of (E)-6,6'-dibromo-[3,3'-biindolinylidene]-2,2'-dione (3.3).



To a suspension of 6-bromoindoline-2,3-dione (**3.1**) (1.275 g, 5.64 mmol) and 6-bromoindolin-2-one (**3.2**) (1.196 g, 5.64 mmol) in AcOH (35.7 mL) was added conc. HCl (37%) solution (0.113 mL). The mixture was refluxed for 24 h. The mixture was allowed to cool and filtered. The solid material was washed with water, ethanol, and ether. After drying under vacuum, brown (E)-6,6'-dibromo-[3,3'-biindolinylidene]-2,2'-dione (**3**) (2.138g, 90%) was obtained. ^{1}H NMR (400 MHz, DMSO-d_6): δ 11.10 (s, 2H), 8.99 (d, J = 8.7 Hz, 2H), 7.19 (dd, J = 8.6, 2.0Hz, 2H), 6.99 (d, J = 1.9 Hz, 2H) ^{13}C NMR (101 MHz, DMSO-d_6): δ 168.85, 145.51, 132.65, 130.91, 125.70, 123.98, 120.75, 112.37 MS (MALDI [M+]): *m/z* 419, 420, 421 Calc. 419.89

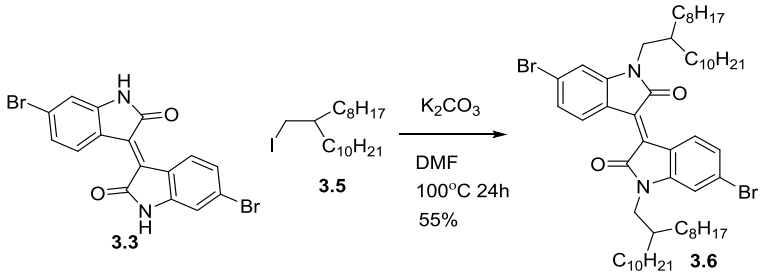
5.26 Synthesis of 9-(iodomethyl)nonadecane (3.5).



To a solution of 2-octyl-1-dodecanol (**3.4**) (100 mL, 281 mmol), triphenylphosphine (89 g, 338 mmol), imidazole (28.7 g, 422 mmol) in DCM (550 mL) at 0°C was added iodine (93 g, 366 mmol) portionwise. The reaction was allowed to stir in air and warm up overnight before being quenched with 25 mL of a saturated solution of Na_2SO_3 (aq). Two layers formed were separated and the aqueous layer was extracted with DCM. The DCM layers were combined, dried over $MgSO_4$, filtered and the DCM was evaporated off under reduced pressure. The crude oil obtained was passed through a plug of silica using hexane as eluent to obtain the product as a colourless oil (103.27 g, 90%). ^{1}H NMR (400 MHz, $CDCl_3$): δ 3.27 (d, J = 4.5 Hz, 2H), 1.35-1.17 (m, 32H), 1.15-1.08 (m, 1H), 0.88 (t, J = 6.7 Hz, 6H) ^{13}C NMR (101 MHz, $CDCl_3$): δ 39.02,

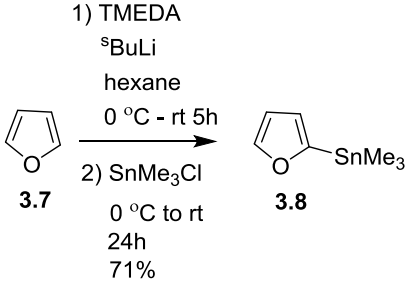
34.75, 32.26, 30.08, 29.98, 29.94, 29.91, 29.70, 29.65, 26.85, 23.03, 17.29, 14.47 HRMS (EI): *m/z* 407.2180 Calc. 407.2175

5.27 Synthesis of 6,6'-dibromo-N,N'-(2-octyldodecanyl)-isoindigo (3.6).



To a solution of (E)-6,6'-dibromo-[3,3'-biindolinylidene]-2,2'-dione (**3.3**) (1.571 g, 3.74 mmol), potassium carbonate (1.551 g, 11.22 mmol) in DMF (75 mL), 9-(iodomethyl)nonadecane (**3.5**) (3.820 g, 9.35 mmol) was added under argon. The mixture was stirred for 24 h at 100 °C and then the solvent was removed under reduced pressure. The residue was purified by silica gel chromatography with eluting (petroleum ether 60-80°C: chloroform = 3:1) to give 6,6'-dibromo-N,N'-(2-octyldodecanyl)-isoindigo (**3.6**) as a deep-red solid (2.007 g, 55%) ^{1}H NMR (400 MHz, $CDCl_3$): δ 9.07 (d, J = 8.7Hz, 2H), 7.16 (dd, J = 8.7, 1.9 Hz, 2H), 6.90 (d, J = 2 Hz, 2H), 3.62 (d, J = 7.4Hz, 4H), 1.93-1.85 (m, 2H), 1.43-1.20 (m, 48H), 0.92- 0.82 (m, 12H) ^{13}C NMR (101 MHz, $CDCl_3$): δ 168.51, 146.58, 132.97, 131.37, 127.03, 125.48, 120.76, 111.93, 45.05, 36.44, 32.26, 32.22, 31.84, 30.33, 29.98, 29.89, 29.69, 29.64, 26.70, 23.03, 14.47 HRMS (EI): *m/z* 979.5376 Calc. 978.5212

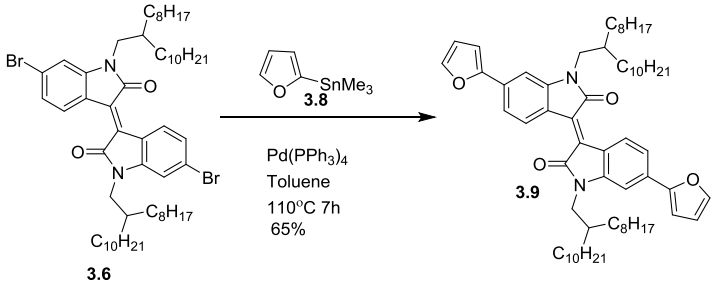
5.28 Synthesis of furan-2-yltrimethylstannane (3.8).



A solution of furan (**3.7**) (2 mL, 27.5 mmol) in anhydrous hexane (149 mL) was cooled to 0 °C. N,N,N′,N′-Tetramethylethylenediamine (TMEDA) (4.57 mL, 30.2 mmol) was added followed by the dropwise addition of sec BuLi (21.6 mL, 1.4 M in

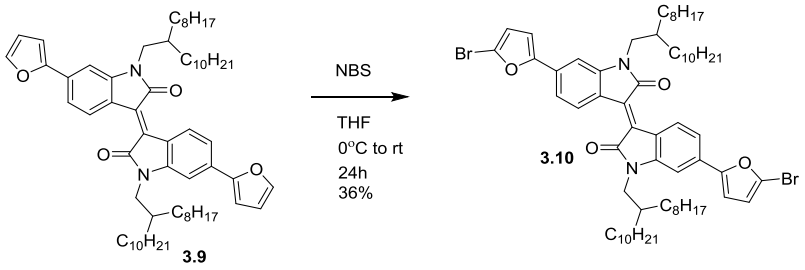
hexane, 30.2 mmol). The solution was stirred at 0 °C for 1h and then allowed to warm to rt over the course of 4 h. The solution was cooled back down to 0 °C before trimethyl tin chloride solution (38.5 mL, 1M in hexanes, 38.5 mmol) was added. The reaction mixture was allowed to stir and warm up to room temperature overnight before being quenched with saturated ammonium chloride (10 mL, aq), extracted with diethyl ether and dried over Na_2SO_4. The solvent was removed under reduced pressure leaving the product as an orange oil (4.512 g, 71%) which was used without further purification. ^{1}H NMR (400 MHz, $CDCl_3$): δ 7.77 (d, J = 1.8Hz, 1H), 6.65 (d, J = 3.2Hz, 1H), 6.47 (dd, J = 1.8, 3.2Hz, 1H), 0.39 (s, 9H). ^{13}C NMR (101 MHz, $CDCl_3$): δ 160.82, 147.30, 121.03, 109.49, -8.95. HRMS (EI): *m/z* 231.9900 calc 231.9910

5.29 Synthesis of (E)-6,6'-di(furan-2-yl)-1,1'-bis(2-octyldodecyl)-[3,3'-biindolinylidene]-2,2'-dione (3.9).



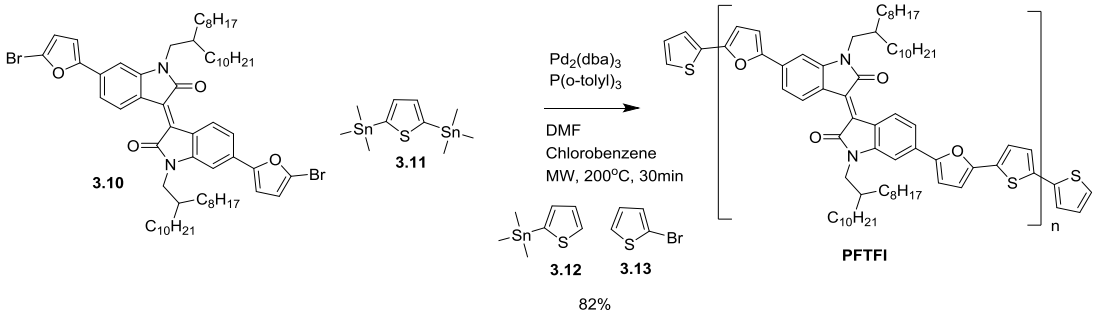
6,6'-dibromo-N,N'-(2-octyldodecanyl)-isoindigo (**3.6**) (1.5 g, 1.53 mmol) and furan-2-yltrimethylstannane (**3.8**) (0.847 g, 3.67 mmol) were dissolved in anhydrous toluene (75 mL) and degassed under Ar for 30 min. Tetrakis(triphenylphosphine)palladium (0) (0.141 g, 0.122 mmol) was added and the solution was degassed for a further 30 min before being heated at 110 °C overnight. The solvent was removed under reduced pressure and the residue was columned on silica gel using petroleum ether 60-80 °C and DCM (8:2). A dark red solid was obtained upon concentration of the main fractions (0.942 g, 65%). ^{1}H NMR (400 MHz, $CDCl_3$): δ 9.17 (d, J = 8.5 Hz, 2H), 7.52 (d, J = 2.2 Hz, 2H), 7.315 (dd, J = 8.3, 1.6 Hz, 2H), 7.07 (d, J = 1.7 Hz, 2H), 6.77 (d, J = 3.4 Hz, 2H), 6.52 (dd, J = 3.4, 1.9 Hz, 2H), 3.69 (d, J = 7.3 Hz, 4H), 1.95 (m, 2H), 1.45-1.31 (m, 16H), 1.29-1.19 (m, 48H), 0.88-0.83 (m, 12H). ^{13}C NMR (101 MHz, $CDCl_3$): δ 169.04, 154.13, 145.99, 143.32, 134.10, 132.36, 130.34, 121.26, 117.66, 112.51, 107.53, 103.41, 44.85, 32.24, 32.00, 30.35, 29.99, 29.94, 29.70, 29.65, 26.87, 23.02, 14.45 MS (MALDI (TOF)): *m/z* 956.0 Calc. 955.442

5.30 Synthesis of (E)-6,6'-bis(5-bromofuran-2-yl)-1,1'-bis(2-octyldodecyl)-[3,3'-biindolinylidene]-2,2'-dione (3.10).



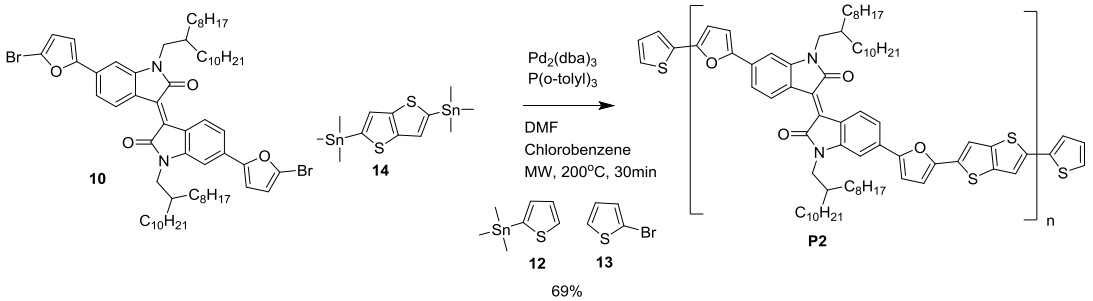
(E)-6,6'-di(furan-2-yl)-1,1'-bis(2-octyldodecyl)-[3,3'-biindolinylidene]-2,2'-dione (**3.9**) (0.8558 g, 0.896 mmol) was dissolved in anhydrous THF (20 mL) and cooled to 0°C in the dark. A solution of NBS (0.351 g, 1.97 mmol) in THF (5 mL) was added dropwise over the course of 20 min and the solution was allowed to stir and warm up to rt, in the dark, overnight. The solvent was removed under reduced pressure and the residue was dissolved in DCM and washed with water. The DCM fraction was dried over Na_2SO_4, filtered and the solvent was removed under reduced pressure. The crude product was purified by column chromatography using petroleum ether 60-80°C and DCM (9:1) to give the product as a dark blue solid (0.3585 g, 36%). ^{1}H NMR (400 MHz, TCE): δ 9.12 (d, J = 8.4Hz, 2H), 7.26 (d, J = 8.3Hz, 2H), 7.02 (s, 2H), 6.76 (d, J = 3.4Hz, 2H), 6.49 (d, J = 3.5 Hz, 2H), 3.69 (d, J = 7.2 Hz, 4H), 1.92 (m, 2H), 1.47-1.32 (m, 16H), 1.31-1.17 (m, 48H), 0.89-0.83 (m, 12H). ^{13}C NMR (101 MHz, $CDCl_3$): δ 168.74, 155.76, 145.86, 132.82, 132.23, 130.23, 123.04, 121.34, 117.05, 114.10, 109.57, 102.86, 44.63, 36.48, 32.07, 32.04, 31.82, 30.15, 29.81, 29.78, 29.74, 29.50, 29.46, 26.71, 22.83, 14.27 MS (MALDI (TOF)): *m/z* 1113.5 Calc. 1113.234

5.31 Synthesis of Poly((E)-6-(furan-2-yl)-1,1'-bis(2-octyldodecyl)-6'-(5-(thiophen-2-yl)furan-2-yl)-[3,3'-biindolinylidene]-2,2'-dione) (PFTFI).



(E)-6,6'-bis(5-bromofuran-2-yl)-1,1'-bis(2-octyldodecyl)-[3,3'-biindolinylidene]-2,2'-dione (**3.10**) (0.1 g, 0.09 mmol), 2,5-bis(trimethylstannyl)thiophene (**3.11**) (0.037 g, 0.09 mmol), $Pd_2(dba)_3$ (1.65 mg, 1.797 μmol), and tri(o-tolyl)phosphine (2.187 mg, 7.19 μmol) were placed in a microwave vial and degassed under Ar. Anhydrous chlorobenzene (3 mL) and anhydrous DMF (0.01 mL) were added and the reaction mixture was degassed for a further 10min. The reaction mixture was heated in a microwave for 5 min at 100 °C, 5 min at 120 °C, 5 min at 140 °C, 5 min at 160 °C, 10 min at 180 °C and 30 min at 200 °C. Tributyl(thiophen-2-yl)stannane (**3.12**) (2.9 μL, 0.09 mmol) was added and the reaction was heated to 200 °C for 10 min. 2-bromothiophene (**3.13**) (9.59 μL, 0.099 mmol) was added and the reaction was heated to 200 °C for a further 10 min. The reaction was allowed to cool to rt and the polymer was precipitated into methanol, filtered into a glass thimble and Soxhlet extracted in acetone, hexane and chloroform for 1 day in each solvent. The chloroform fraction was collected and sodium diethyldithiocarbamate trihydrate (0.3 g) dissolved in deionised water (100 mL) was added and the mixture was heated at 50 °C for 3 h. The aqueous layer was separated off and the chloroform layer was washed with water 5 times. The chloroform layer was concentrated and the polymer was precipitated into methanol, filtered off and dried under high vacuum to give **PFTFI** as a dark blue solid (0.0884 g, 82%, Mn 1.6×10^4 Da, Mw 4.1×10^4 Da, PDI 2.58) ^{1}H NMR (400 MHz, $CDCl_3$): δ 9.19 (s, 2H), 7.34 (s, 2H), 7.27 (s, 2H), 7.14 (s, 2H), 7.03 (s, 2H), 6.74 (s, 2H), 6.51 (s, 2H), 3.72 (s, 4H), 1.90 (s, 2H), 1.7-1.1 (m, 64H), 0.88 (m, 12H)

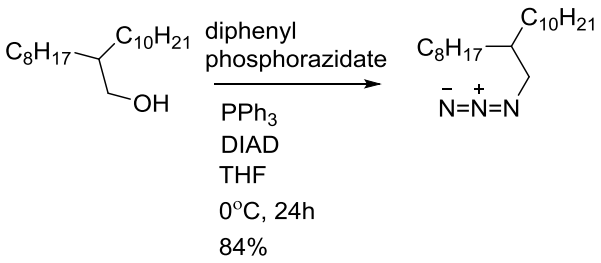
5.32 Synthesis of Poly((E)-6-(furan-2-yl)-1,1'-bis(2-octyldodecyl)-6'-(5-(thieno[3,2-b]thiophen-2-yl)furan-2-yl)-[3,3'-biindolinylidene]-2,2'-dione) (PFTTFI).



(E)-6,6'-bis(5-bromofuran-2-yl)-1,1'-bis(2-octyldodecyl)-[3,3'-biindolinylidene]-2,2'-dione (**3.10**) (0.1 g, 0.09 mmol), 2,5-bis(trimethylstannyl)thieno[3,2-b]thiophene (**3.14**) (0.042 g, 0.09 mmol), $Pd_2(dba)_3$ (1.65 mg, 1.797 μmol), and tri(o-tolyl)

phosphine (2.187 mg, 7.19 μmol) were placed in a microwave vial and degassed under Ar. Anhydrous chlorobenzene (3 mL) and anhydrous DMF (0.01 mL) were added and the reaction mixture was degassed for a further 10 min. The reaction mixture was heated in a microwave for 5 min at 100 °C, 5 min at 120 °C, 5 min at 140 °C, 5 min at 160 °C, 10 min at 180 °C and 30 min at 200 °C. Tributyl(thiophen-2-yl)stannane (**3.12**) (2.9 μL, 0.09 mmol) was added and the reaction was heated to 200 °C for 10 min. 2-bromothiophene (**3.13**) (9.59 μL, 0.099 mmol) was added and the reaction was heated to 200 °C for a further 10 min. The reaction was allowed to cool to rt and the polymer was precipitated into methanol, filtered into a glass thimble and Soxhlet extracted in acetone, hexane and chloroform, chlorobenzene and trichlorobenzene for 1 day in each solvent. The chloroform, chlorobenzene and trichlorobenzene fractions were collected and sodium diethyldithiocarbamate trihydrate (0.3 g) dissolved in deionised water (100 mL) was added to each fraction and the mixtures were heated at 50 °C for 3 h. The aqueous layer was separated off and the chlorinated solvent layers were washed with water 5 times. The chlorinated solvent layers were concentrated and the polymer was precipitated into methanol, filtered off and dried under high vacuum to give **PFTTFI** as a dark blue solid (Chloroform fraction: 0.0339 g, 30%, Mn 6.8×10^3 Da, Mw 1.4×10^4 Da, PDI 2.02. Chlorobenzene fraction: 0.0243 g, 22%, Mn 2.9×10^4 Da, Mw 7.6×10^4 Da, PDI 2.61. Trichlorobenzene fraction: 0.0192 g, 17%, Mn 4.9×10^4 Da, Mw 7.1×10^4 Da, PDI 1.46) ^{1}H NMR (400 MHz, $CDCl_3$, 323 K): δ 9.17 (s, 2H), 7.34 (s, 2H), 7.20 (s, 2H), 7.03 (s, 2H), 6.75 (m, 2H), 6.59 (s, 2H), 3.67 (s, 4H), 1.87 (s, 2H), 1.60-1.05 (m, 64H), 0.86 (m, 12H)

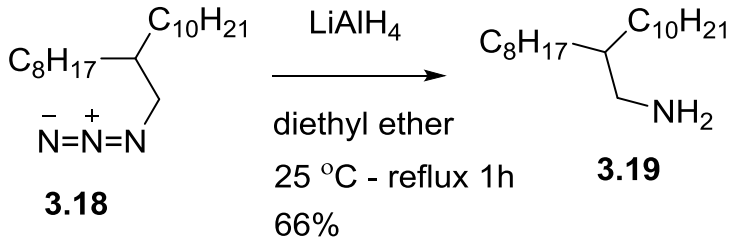
5.33 Synthesis of 9-(azidomethyl)nonadecane (3.18)



Triphenylphosphine (47.87 g, 183 mmol) and 2-octyldodecan-1-ol (**3.15**) (50 mL, 140 mmol) were dissolved in anhydrous THF (300 mL) and cooled to 0 °C. Diisopropyl

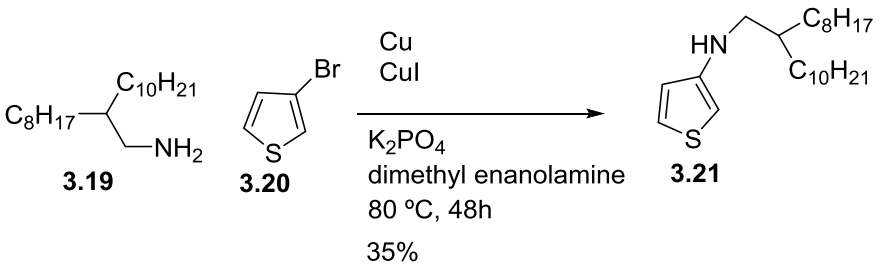
azodicarboxylate (DIAD) (35.87 mL, 182 mmol) was added dropwise followed by dropwise addition of diphenyl phosphorazidate (36.25 mL, 168 mmol) and the mixture was stirred under Ar overnight. After the evaporation of the solvent under vacuum, the viscous yellow residue was extracted with hexane. The combined hexane extracts were concentrated and subjected to silica gel chromatography (eluent heptane) to afford the pure azide as colourless oil (38.1 g, 84% yield). ^{1}H NMR (400MHz, $CDCl_3$): δ 3.23 (2H, d, J = 5.8Hz), 1.55 (1H, m), 1.35- 1.21 (32H, m), 0.88 (6H, t, J = 6.6Hz). ^{13}C NMR (101 MHz, $CDCl_3$): δ 55.27, 38.22, 31.93, 31.77, 31.62, 29.94, 29.66, 29.62, 29.58, 29.39, 29.33, 26.63, 22,71, 14.13 MS (EI): *m/z* 295 (-N_2) Calc. 323.33

5.34 Synthesis of 2-octyldodecan-1-amine (3.19)



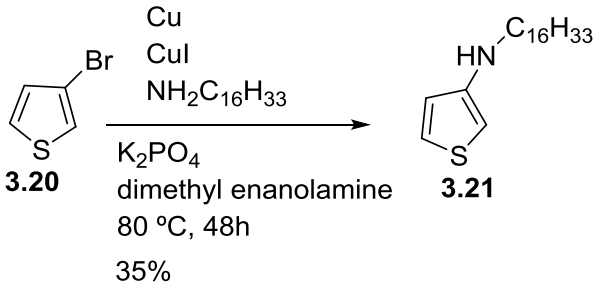
Dissolved 9-(azidomethyl)nonadecane (**3.18**) (11.807 g, 36.5 mmol) in anhydrous diethyl ether (50 mL) and degassed under vacuum and Argon. Added lithium aluminium hydride (50 mL, 1 M in hexane, 50mmol), dropwise over the course of 1 hour. After complete addition the reaction mixture was refluxed for 1 hour in a water bath at 40 °C. Cooled in an ice bath, added wet diethyl ether (50 mL) and then added 15% aqueous sodium hydroxide solution. The aqueous layer was removed; the ether layer was washed with water (4*125 mL) and dried over sodium sulphate. After removing the solvent under vacuum the amine was isolated as a clear off yellow oil (7.14 g, 66% yield). ^{1}H NMR (400 Hz, $CDCl_3$): δ 2.60 (2H, d, J = 5.0 Hz), 2.00 (1H, t, J = 5.0 Hz), 1.30-1.20 (32H, m), 0.89 (6H, t, J = 7.5 Hz). ^{13}C NMR (101 MHz, $CDCl_3$): δ 67.98, 45.23, 40.91, 31.93, 31.54, 30.13, 29.71, 29.66, 29.37, 26.80, 25.62, 22.70, 14.14 HRMS (EI): *m/z* 297.3398 Calc. 297.3396

5.35 Synthesis of n-(2-octyldodecyl)thiophen-3-amine (3.21 branched)



3-bromothiophene (2.87 mL, 30.7 mmol), 2-octyldodecan-1-amine (13.69 g, 46.0 mmol), copper (0.097 g, 1.533 mmol), copper(I) iodide (0.292 g, 1.533 mmol) and potassium phosphate tribasic (13.02 g, 61.3 mmol) were stirred in dimethyl aminoethanol (50 mL) at 80 °C for 48 h. The mixture was filtered and the solvent removed under vacuum. The crude product was then purified by chromatography over silica gel (2.5% EtOAc/hexanes) to obtain N-(2-octyldodecyl)thiophen-3-amine (**3.21 branched**) (4.08 g, 35%). ^{1}H NMR ($CDCl_3$, 400 MHz): δ 7.18 (dd, J = 2.92, 4.88Hz, 1H), 6.65 (d, J = 4.38 Hz, 1H), 5.95 (m, 1H), 3.61 (s, 1H), 3.01 (d, J = 6.05 Hz, 2H), 1.63 (m, 1H), 1.30-1.35 (bm, 32H), 0.92 (m, 6H). ^{13}C NMR (101 MHz, $CDCl_3$): δ 149.14, 124.99, 119.95, 94.79, 49.90, 37.84, 32.23, 31.94, 30.09, 29.67, 29.37, 26.82, 22.71, 14.14. MS (TOF MS ES+): *m/z* 380.33 (M+, 100%) Calc. 379.33

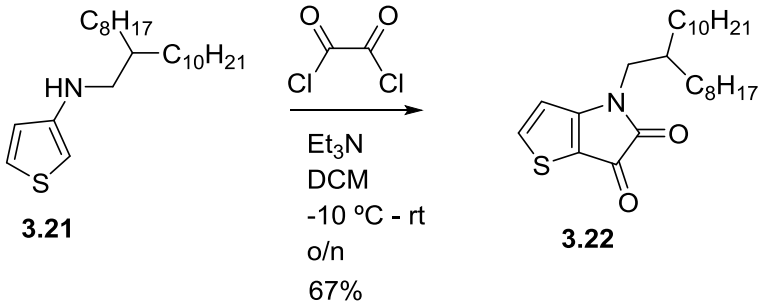
5.36 Synthesis of N-hexadecylthiophen-3-amine (3.21 linear)



3-bromothiophene (5 g, 2.87 mL, 30.7 mmol), hexadecan-1-amine (11.11 g, 46.0 mmol), copper (0.097 g, 1.533 mmol), copper(I) iodide (0.292 g, 1.533 mmol) and potassium phosphate tribasic (13.02 g, 61.3 mmol) were stirred in dimethyl aminoethanol (50 mL) at 80 °C for 48 h. The mixture was allowed to cool to rt, water (100 mL) was added and the solvent mixture was extracted with hexane. The hexane layer was dried over $MgSO_4$ and columned directly on silica gel using hexane as eluent. The solvent was removed under vacuum to give n-hexadecylthiophen-3-amine

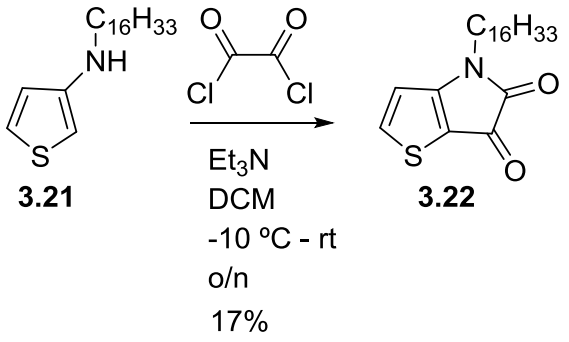
(**3.21 linear**) as a brown solid (3.5g, 35%). ^{1}H NMR (400 MHz, $CDCl_3$): δ 7.15 (dd, J = 2.94, 4.92 Hz, 1H), 6.62 (m, 1H), 5.95 (m, 1H), 3.06 (t, J = 7.31 Hz, 2H), 1.61 (m, 4H), 1.45-1.06 (m, 24H), 0.88 (t, J = 6.51, 3H). ^{13}C NMR (101 MHz, $CDCl_3$): δ 125.20, 119.82, 97.31, 95.37, 68.15, 58.42, 46.53, 45.98, 32.08, 30.33, 29.84, 29.77, 29.68, 29.61, 29.51, 27.36, 22.84, 14.28. MS (EI): *m/z* 323 Calc. 323.26

5.37 Synthesis of 4-(2-octyldodecyl)-4H-thieno[3,2-b]pyrrole-5,6-dione (3.22 branched)



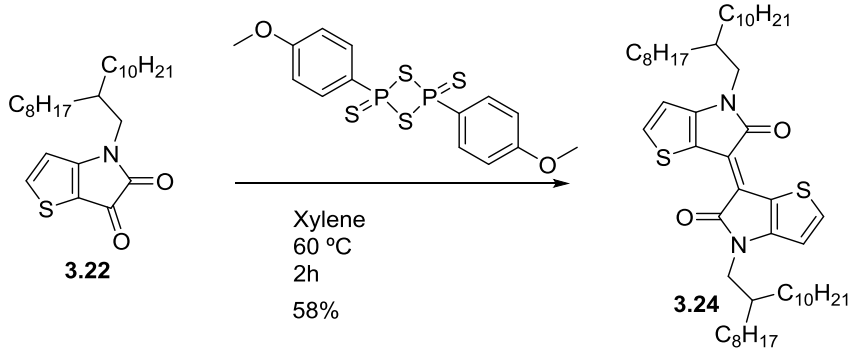
N-(2-octyldodecyl)thiophen-3-amine (3 g, 7.90 mmol) in anhydrous DCM (10 mL) was added dropwise to oxalyl chloride (0.9 mL, 10.64 mmol) in anhydrous DCM (20 mL) at 0°C. After 30 minutes, triethylamine (5 mL, 35.9 mmol) in DCM (5 mL) was added dropwise and stirred overnight at room temperature. The solvent was removed under vacuum and crude product was purified by chromatography on silica gel in DCM. 4-(2-octyldodecyl)-4*H*-thieno[3,2-*b*]pyrrole-5,6-dione (**3.22 branched**) was obtained as red oil (2.296 g, 67 %). ^{1}H NMR ($CDCl_3$, 400 MHz): δ 8.00 (d, 1H), 6.78 (d, 1H), 3.61 (d, 2H), 1.79 (m, 1H), 1.26-1.33 (bm, 32H), 0.89 (m, 6H) ^{13}C NMR (101 MHz, $CDCl_3$): δ 172.99, 165.54, 161.76, 143.75, 113.13, 111.07, 46.48, 37.00, 31.91, 31.86, 31.40, 29.91, 29.61, 29.56, 29.51, 29.33, 26.37, 22.68, 14.12. MS (TOF MS ES+): *m/z* 434.31 (M+,100%) Calc. 433.30

5.38 Synthesis of 4-(hexadecyl)-4H-thieno[3,2-b]pyrrole-5,6-dione (3.22 linear)



N-hexadecylthiophen-3-amine (3.54 g, 10.94 mmol) in anhydrous DCM (30 mL) was added dropwise to oxalyl chloride (1.29 mL, 10.64 mmol) in anhydrous DCM (20 mL) at 0°C. After 30 minutes, triethylamine (7.91 mL, 56.8 mmol) in anhydrous DCM (5 mL) was added dropwise and stirred overnight at room temperature. The solvent was removed under vacuum and crude product was purified by chromatography on silica gel in DCM. 4-(hexadecyl)-4*H*-thieno[3,2-*b*]pyrrole-5,6-dione (**3.22 linear**) was obtained as red solid in 17 % yield. ^{1}H NMR (400 MHz, $CDCl_3$): δ 8.00 (d, J = 4.9 Hz, 1H), 6.78 (d, J = 5.0 Hz, 1H), 3.65 (t, J = 7.2 Hz, 2H), 1.67 (p, J = 6.9 Hz, 2H), 1.38-1.22 (m, 26H), 0.87 (t, J = 6.6 Hz, 3H) ^{13}C NMR (101 MHz, $CDCl_3$): δ 173.20, 165.31, 161.61, 143.98, 114.03 113.07, 55.27, 42.29, 32.07, 29.84, 29.76, 29.68, 29.60, 29.51, 29.31, 28.33, 22.85, 14.28 HRMS (EI+): *m/z* 377.2395 Calc. 377.2389

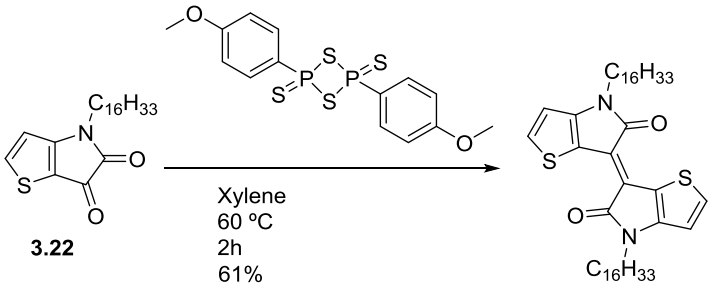
5.39 Synthesis of (E)-4,4'-bis(2-octyldodecyl)-[6,6'-bithieno[3,2-b]pyrrolylidene]-5,5'(4H,4'H)-dione (3.24 branched)



A solution of 4-(2-octyldodecyl)-4*H*-thieno[3,2-b]pyrrole-5,6-dione (0.561 g, 1.294 mmol) and Lawesson's Reagent (0.262 g, 0.647 mmol) in 15 mL *o*-xylene were stirred at 60 °C for 2 h. Progress of reaction was monitored by TLC and change in

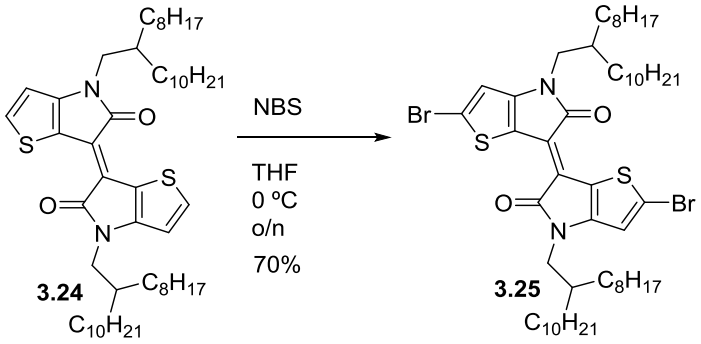
colour (from red to violet blue). The reaction mixture was then cooled down to room temperature. After removal of solvent, the crude product was purified by chromatography on silica gel in hexane : DCM mixture to give the product as an orange oil (0.3156 g, 58%). ^{1}H NMR (400 MHz, $CDCl_3$): δ 7.55 (d, 2H), 6.81 (d, 2H), 3.71 (d, 4H), 1.91 (m, 2H), 1.25-1.34 (bm, 64H), 0.89 (m, 12H) ^{13}C NMR (101 MHz, $CDCl_3$): δ 171.33, 151.57, 134.22, 121.08, 114.25, 111.36, 46.16, 31.88, 31.48, 29.95, 29.63, 29.57, 29.52, 29.35, 29.28, 26.42, 22.67, 14.12. MS (TOF MS ES+): *m/z* 834.61 (M+, 100%) Calc. 834.613

5.40 Synthesis of (E)-4,4'-dihexadecyl-[6,6'-bithieno[3,2-b]pyrrolylidene]-5,5'(4H,4'H)-dione (3.24 linear)



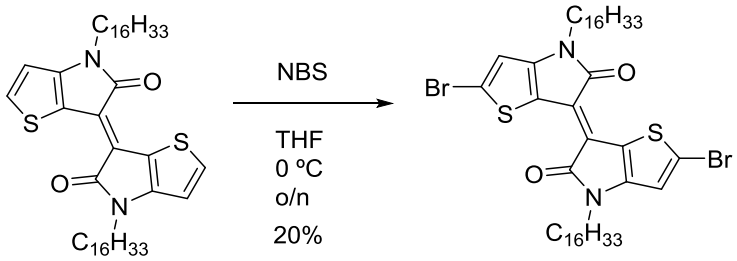
A solution of 4-(hexadecyl)-4*H*-thieno[3,2-*b*]pyrrole-5,6-dione (0.707 g, 1.87 mmol) and Lawesson's Reagent (0.379 g, 0.936 mmol) in *o*-xylene (15 mL) were stirred at 60 °C for 2 h. Progress of reaction was monitored by TLC and change in colour (from red to violet blue). The reaction mixture was then cooled down to rt. After removing the solvent under vacuum, the crude product was purified by flash chromatography on silica gel using hexane: DCM as eluent. The solvent was removed under vacuum to give the product as a purple solid (0.415 g, 61%). ^{1}H NMR (400 MHz, $CDCl_3$): δ 7.53 (d, J = 5.3 Hz, 2H), 6.81 (d, J = 5.1 Hz, 2H), 3.80 (t, J = 7.3 Hz, 4H), 1.73 (m, 4H), 1.40-1.16 (m, 52H), 0.87 (t, J = 6.61 Hz, 6H). ^{13}C NMR (101 MHz, $CDCl_3$): δ 134.51, 111.34, 41.94, 32.07, 29.81, 29.64, 29.51, 29.42, 28.74, 28.42, 27.06, 22.84, 14.27 MS (TOF LD+): *m/z* 723 Calc. 722.488

5.41 Synthesis of (E)-2,2'-dibromo-4,4'-bis(2-octyldodecyl)-[6,6'-bithieno[3,2-b]pyrrolylidene]-5,5'(4H,4'H)-dione (3.25 branched)



To an ice cold solution of (*E*)-4,4'-bis(2-octyldodecyl)-[6,6'-bithieno[3,2-b]pyrrolylidene]-5,5'(4*H*,4'*H*)-dione (0.410 g, 0.491 mmol) in THF (15 mL), NBS (0.188 g, 1.055 mmol) in THF (1 mL) was added dropwise over 30 minutes. The reaction progress was monitored by TLC. After completion, reaction was quenched by the addition of water (10 mL) and dichloromethane (50 mL) and the organic layer was separated off. The organic layer was washed with water (2 x 10 mL), brine (10 mL) and dried over $MgSO_4$. After removal of solvent, the crude product was purified by chromatography on silica gel using hexane and DCM as eluent. After filtering off the $MgSO_4$ and removing the solvent under vacuum, the crude product was purified by chromatography on silica gel using a hexane: DCM mixture as eluent. The solvent was removed under vacuum to give the product as a blue solid which was further purified by washing with methanol and dried under high vacuum to give the product **(3.25 branched)** (0.341 g, 70%). ^{1}H NMR (400 MHz, $CDCl_3$): δ 6.84 (s, 2H), 3.66 (d, 4H), 1.86 (m, 2H), 1.27-1.35 (bm, 64H), 0.89 (m, 12H) ^{13}C NMR (101 MHz, $CDCl_3$): δ 170.43, 150.21, 123.15, 119.73, 114.98, 114.72, 46.18, 37.19, 31.88, 31.39, 29.95, 29.64, 29.57, 29.52, 29.35, 29.30, 28.35, 22.68, 14.12. MS (TOF LD+): *m/z* 993 (M+, 100%) Calc. 993.432

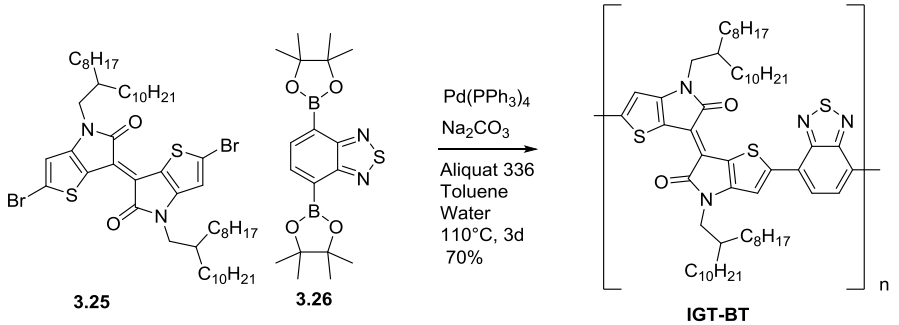
5.42 Synthesis of (E)-2,2'-dibromo-4,4'-dihexadecyl-[6,6'-bithieno[3,2-b]pyrrolylidene]-5,5'(4H,4'H)-dione (3.25 linear)



3.24 **3.25**

To an ice cold solution of (E)-4,4'-dihexadecyl-[6,6'-bithieno[3,2-b]pyrrolylidene]-5,5'(4H,4'H)-dione **(3.24 linear)** (0.4154 g, 0.574 mmol) in THF (25 mL), NBS (0.225 g, 1.264 mmol) in THF (1 mL) was added dropwise over 30 minutes. The reaction progress was monitored by TLC. After completion, reaction was quenched by the addition of water (10 mL) and dichloromethane (50 mL) and the organic layer was separated off. The organic layer was washed with water (2 x 10 mL), brine (10 mL) and dried over $MgSO_4$. After filtering off the $MgSO_4$ and removing the solvent under vacuum, the crude product was purified by chromatography on silica gel using hexane and DCM as eluent. After removal of solvent, the crude product was purified by chromatography on silica gel using a hexane: DCM mixture as eluent. The solvent was removed under vacuum to give the product as a blue solid which was further purified by washing with methanol and dried under high vacuum to give the product **(3.25 linear)** (0.10 g, 20%). ^{1}H NMR (400 MHz, $CDCl_3$): δ 6.86 (s, 2H), 3.74 (t, J = 7.3 Hz, 4H), 1.69 (m, 4H), 1.38-1.19 (m, 52H), 0.87 (t, J = 6.54 Hz, 6H). ^{13}C NMR (101 MHz, $CDCl_3$): δ 170.31, 150.05, 123.43, 119.99, 115.02, 114.82, 42.01, 29.84, 29.81, 29.76, 29.69, 29.62, 29.51, 29.36, 22.84, 14.28. MS (TOF LD+): *m/z* 881 Calc. 880.307

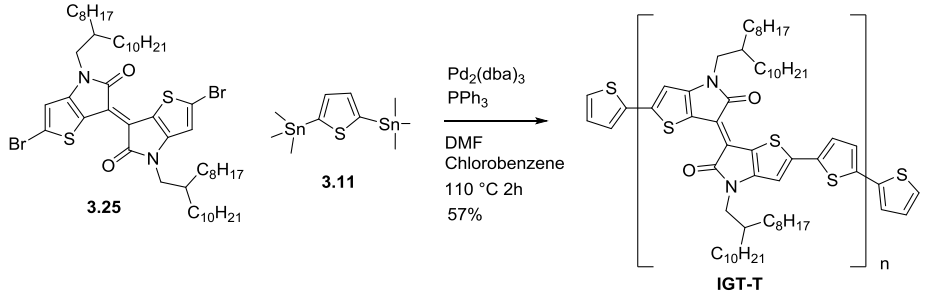
5.43 Synthesis of IGT-BT



3.25 **3.26** **IGT-BT**

Degassed toluene (1.5 mL), aqueous sodium carbonate (0.3 mL, 0.30 mmol, 1 M) and 2 drops of Aliquat 336 were added to (*E*)-2,2'-dibromo-4,4'-bis(2-octyldodecyl)-[6,6'-bithieno[3,2-b]pyrrolylidene]-5,5'(4*H*,4′*H*)-dione (**3.25 branched**) (0.050 g, 0.050 mmol), 4,7-bis(4,4,5,5-tetramethyl-1,3,2-dioxaborolan-2-yl)benzo[c][1,2,5]thiadiazole (0.020 g, 0.050 mmol) and $Pd(PPh_3)_4$ (1.164 mg, 1.007 μmol). The solution was thoroughly degassed under Argon, and then the Argon inlet was removed and the reaction heated for 72 h at 120 °C (oil bath temperature). After cooling to rt, the polymer was precipitated into methanol (100 mL), and filtered through a Soxhlet thimble. The polymer was Soxhlet extracted with methanol, acetone, hexane and, chloroform. The chloroform solution was concentrated and precipitated into methanol, and the precipitates were filtered and dried under vacuum to get **IGT-BT**, as a black solid. Obtained polymer was dried under high vacuum for 24 h. Yield (0.035 g, 70%). GPC (chlorobenzene, 80 ºC): M_n = 40000 g/mol, M_w = 90000 g/mol, PDI = 2.25 λ_{max} (film) = 1035 nm.

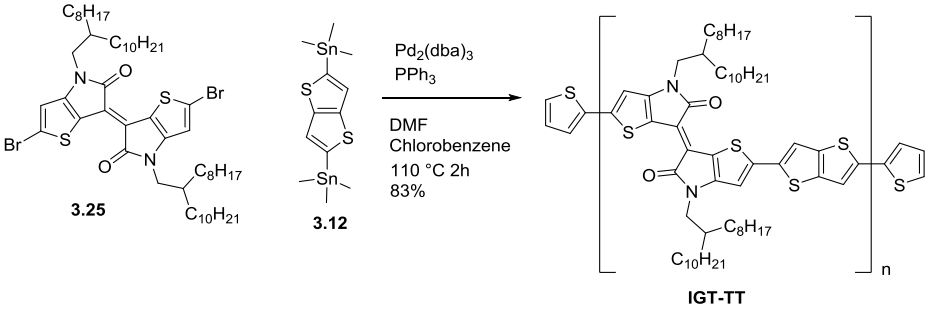
5.44 Synthesis of IGT-T



(*E*)-2,2'-dibromo-4,4'-bis(2-octyldodecyl)-[6,6'-bithieno[3,2-b]pyrrolylidene]-5,5'(4*H*,4′*H*)-dione (**3.25 branched**) (0.100 g, 0.101 mmol), 2,5-bis(trimethylstannyl)thiophene (**3.11**) (0.0413 g, 0.101 mmol), $Pd_2(dba)_3$ (3.69 mg, 4.03 μmol), and triphenylphosphine (2.139 mg, 8.16 μmol) were placed in a microwave vial and degassed under Ar. Anhydrous chlorobenzene (3 mL) and anhydrous DMF (0.01 mL) were added and the reaction mixture was degassed for a further 10 min. The reaction mixture was heated at 110 ºC for 2 h in an oil bath. Tributyl(thiophen-2-yl)stannane (**3.12**) (42 mg, 0.113 mmol) was added and the reaction was heated for a further 30 min at 110 °C. 2-bromothiophene (**3.13**) (37 mg, 0.227 mmol) was added and the reaction was heated for a further 30 min at 110 °C The reaction was allowed to cool to rt and the polymer was precipitated into methanol, filtered into a glass thimble and Soxhlet extracted in acetone, hexane and chloroform

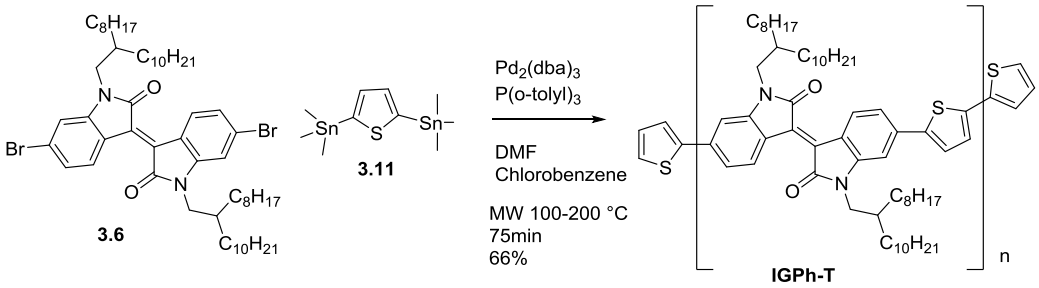
for 24 h in each solvent. The chloroform fraction was collected and sodium diethyldithiocarbamate trihydrate (0.3 g) dissolved in deionised water (100 mL) was added and the mixture was heated at 50 °C for 3 h. The aqueous layer was separated off and the chloroform layer was washed with water 5 times. The chloroform layer was concentrated and the polymer was precipitated into methanol, filtered off and dried under high vacuum to give **IGT-T** as a dark green solid (54.6 mg, 57%). Unable to GPC.

5.45 Synthesis of IGT-TT



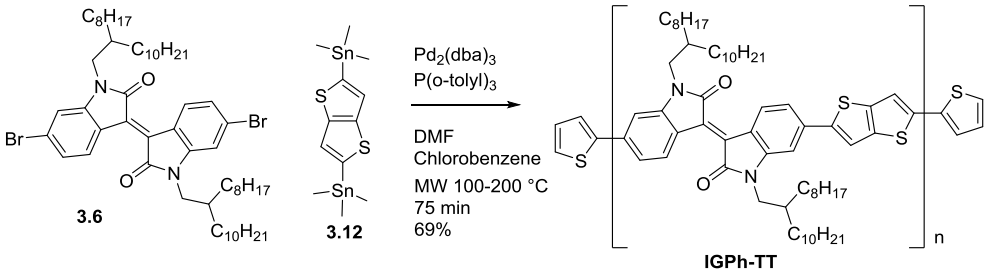
(*E*)-2,2'-dibromo-4,4'-bis(2-octyldodecyl)-[6,6'-bithieno[3,2-b]pyrrolylidene]-5,5'(4*H*,4'*H*)-dione (**3.25 branched**) (0.100 g, 0.101 mmol), 2,5-bis(trimethylstannyl)thieno[3,2-*b*]thiophene (**3.14**) (0.0469 g, 0.101 mmol), $Pd_2(dba)_3$ (3.69 mg, 4.03 μmol), and triphenylphosphine (2.139 mg, 8.16 μmol) were placed in a microwave vial and degassed under Ar. Anhydrous chlorobenzene (3 mL) and anhydrous DMF (0.01 mL) were added and the reaction mixture was degassed for a further 10 min. The reaction mixture was heated at 110 ºC for 2 h in an oil bath. Tributyl(thiophen-2-yl)stannane (**3.12**) (42 mg, 0.113 mmol) was added and the reaction was heated for a further 30 min at 110 °C. 2-bromothiophene (**3.13**) (37 mg, 0.227 mmol) was added and the reaction was heated for a further 30 min at 110 °C The reaction was allowed to cool to rt and the polymer was precipitated into methanol, filtered into a glass thimble and Soxhlet extracted in acetone, hexane and chloroform for 24 h in each solvent. The chloroform fraction was collected and sodium diethyldithiocarbamate trihydrate (0.3 g) dissolved in deionised water (100 mL) was added and the mixture was heated at 50 °C for 3 h. The aqueous layer was separated off and the chloroform layer was washed with water 5 times. The chloroform layer was concentrated and the polymer was precipitated into methanol, filtered off and dried under high vacuum to give **IGT-TT** as a dark green solid (95.3 mg, 83%). Unable to GPC.

5.46 Synthesis of IGPh-T



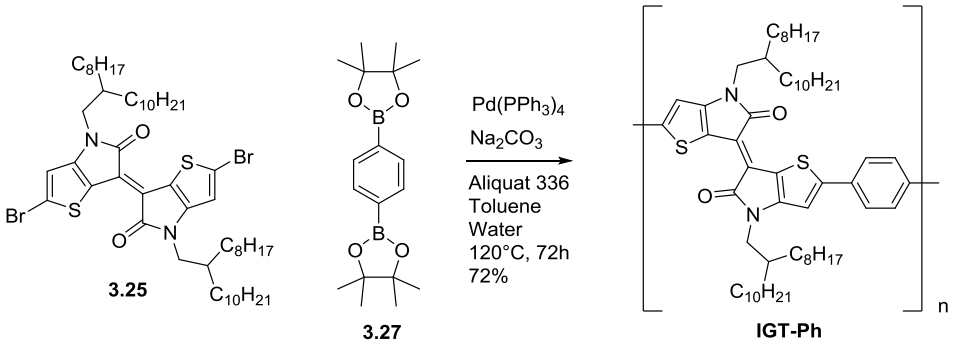
6,6'-dibromo-N,N'-(2-octyldodecanyl)-isoindigo (**3.6**) (0.100 g, 0.102 mmol), 2,5-bis(trimethylstannyl)thiophene (**3.11**) (0.042g, 0.102 mmol), $Pd_2(dba)_3$ (1.867 mg, 2.04 μmol), and tri(o-tolyl)phosphine (2.482 mg, 8.15μmol) were placed in a microwave vial and degassed under Ar. Anhydrous chlorobenzene (3 mL) and anhydrous DMF (0.01 mL) were added and the reaction mixture was degassed for a further 10 min. The reaction mixture was heated in a microwave for 5 min at 100 °C, 5 min at 120 °C, 5 min at 140 °C, 5 min at 160 °C, 10 min at 180 °C and 30 min at 200 °C. Tributyl(thiophen-2-yl)stannane (**3.12**) (0.032 mL, 0.102 mmol) was added and the reaction was heated to 200 °C for 10 min. 2-bromothiophene (**3.13**) (10.88 μL, 0.112 mmol) was added and the reaction was heated to 200 °C for a further 10 min. The reaction was allowed to cool to rt and the polymer was precipitated into methanol, filtered into a glass thimble and Soxhlet extracted in acetone, hexane and chloroform for 24 h in each solvent. The hexane fraction was collected and sodium diethyldithiocarbamate trihydrate (0.3 g) dissolved in deionised water (100 mL) was added and the mixture was heated at 50 °C for 3 h. The aqueous layer was separated off and the hexane layer was washed with water 5 times. The hexane layer was concentrated and the polymer was precipitated into acidic methanol, filtered off and dried under high vacuum to give **IGPh-T** as a dark solid (71.38 mg, 66%). The polymer was further purified by recycling gel permeation chromatography using chlorobenzene as eluent, the chlorobenzene was subsequently reduced under vacuum and the polymer was precipitated into methanol before being filtered and dried under high vacuum. The polymer was further purified by recycling gel permeation chromatography using chlorobenzene as eluent, the chlorobenzene was subsequently reduced under vacuum and the polymer was precipitated into methanol before being filtered and dried under high vacuum. GPC (chlorobenzene, 80 ºC): M_n = 10000 g/mol, M_w = 12000 g/mol, PDI = 1.86

5.47 Synthesis of IGPh-TT



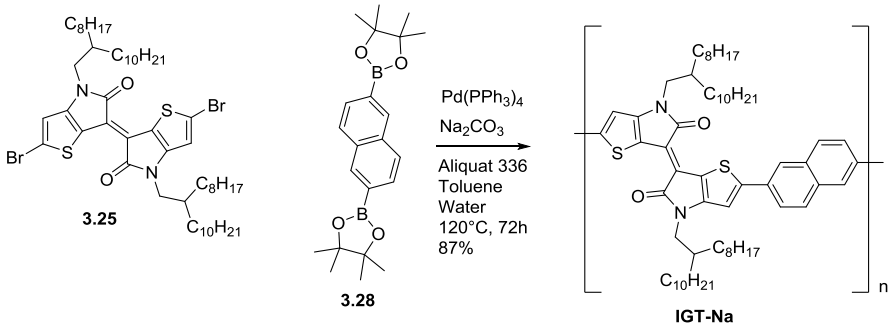
6,6'-dibromo-N,N'-(2-octyldodecanyl)-isoindigo (**3.6**) (0.100 g, 0.102 mmol), bis(trimethylstannyl)thieno[3,2-*b*]thiophene (**3.14**) (0.047 g, 0.102 mmol), $Pd_2(dba)_3$ (1.867 mg, 2.04 μmol), and tri(o-tolyl)phosphine (2.482 mg, 8.15 μmol) were placed in a microwave vial and degassed under Ar. Anhydrous chlorobenzene (3 mL) and anhydrous DMF (0.01 mL) were added and the reaction mixture was degassed for a further 10 min. The reaction mixture was heated in a microwave for 5 min at 100 °C, 5 min at 120 °C, 5 min at 140 °C, 5 min at 160 °C, 10 min at 180 °C and 30 min at 200 °C. Tributyl(thiophen-2-yl)stannane (**3.12**) (0.032 mL, 0.102 mmol) was added and the reaction was heated to 200 °C for 10 min. 2-bromothiophene (**3.13**) (10.88 μL, 0.112 mmol) was added and the reaction was heated to 200 °C for a further 10 min. The reaction was allowed to cool to rt and the polymer was precipitated into methanol, filtered into a glass thimble and Soxhlet extracted in acetone, hexane and chloroform for 24 h in each solvent. The chloroform fraction was collected and sodium diethyldithiocarbamate trihydrate (0.3 g) dissolved in deionised water (100 mL) was added and the mixture was heated at 50 °C for 3 h. The aqueous layer was separated off and the chloroform layer was washed with water 5 times. The chloroform layer was concentrated and the polymer was precipitated into acidic methanol, filtered off and dried under high vacuum to give **IGPh-TT** as a dark solid (79 mg, 69%). The polymer was further purified by recycling gel permeation chromatography using chlorobenzene as eluent, the chlorobenzene was subsequently reduced under vacuum and the polymer was precipitated into methanol before being filtered and dried under high vacuum. GPC (chlorobenzene, 80 ºC): M_n = 26000 g/mol, M_w = 71000 g/mol, PDI = 2.74

5.48 Synthesis of polymer IGT-Ph



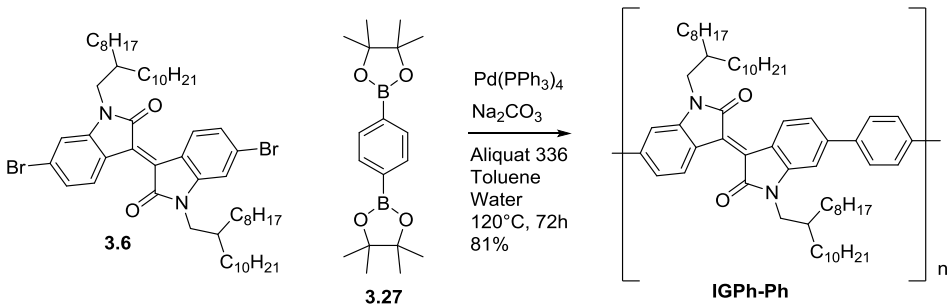
Degassed toluene (1.5 ml), aqueous sodium carbonate (0.3 mL, 0.30 mmol, 1 M) and 2 drops of Aliquat 336 were added to (*E*)-2,2'-dibromo-4,4'-bis(2-octyldodecyl)-[6,6'-bithieno[3,2-b]pyrrolylidene]-5,5'(4*H*,4′*H*)-dione (**3.25 branched**) (0.100 g, 0.101 mmol), 1,4-bis(4,4,5,5-tetramethyl-1,3,2-dioxaborolan-2-yl)benzene (0.033 g, 0.101 mmol) and $Pd(PPh_3)_4$ (2.00 mg, 1.73 μmol). The solution was thoroughly degassed under Argon, and then the Argon inlet was removed and the reaction heated for 72 h at 120 °C (oil bath temperature). After cooling to RT, the polymer was precipitated into methanol (100 mL), and filtered through a Soxhlet thimble. The polymer was Soxhlet extracted with acetone, hexane and chloroform. The chloroform fraction was collected and sodium diethyldithiocarbamate trihydrate (0.3 g) dissolved in deionised water (100ml) was added and the mixture was heated at 50 °C for 3 h. The aqueous layer was separated off and the chloroform layer was washed with water 5 times. The chloroform layer was concentrated and the polymer was precipitated into methanol, filtered off and dried under high vacuum for 24 h to give **IGT-Ph**, as a black solid. (67.8 mg, 72%) The polymer was further purified by recycling gel permeation chromatography using chlorobenzene as eluent, the chlorobenzene was subsequently reduced under vacuum and the polymer was precipitated into methanol before being filtered and dried under high vacuum. GPC (chlorobenzene, 80 °C): Mn = 40000 g/mol, Mw = 69000 g/mol PDI = 1.73

5.49 Synthesis of IGT-Na



Degassed toluene (1.5 mL), aqueous sodium carbonate (0.3 mL, 0.30 mmol, 1 M) and 2 drops of Aliquat 336 were added to (*E*)-2,2'-dibromo-4,4'-bis(2-octyldodecyl)-[6,6'-bithieno[3,2-b]pyrrolylidene]-5,5'(4*H*,4′*H*)-dione (**3.25 branched**) (0.100 g, 0.102 mmol), 2,6-bis(4,4,5,5-tetramethyl-1,3,2-dioxaborolan-2-yl)naphthalene (0.038 g, 0.102 mmol) and $Pd(PPh_3)_4$ (2.33 mg, 2.02 μmol). The solution was thoroughly degassed under Argon, and then the Argon inlet was removed and the reaction heated for 72 h at 120 °C (oil bath temperature). After cooling to rt, the polymer was precipitated into methanol (100 mL), and filtered through a Soxhlet thimble. The polymer was Soxhlet extracted with acetone, hexane and, chloroform. The chloroform solution was concentrated and precipitated into methanol, and the precipitates were filtered and dried under vacuum to get **IGT-Na**, as a black solid (87.1 mg, 87%). The polymer was further purified by recycling gel permeation chromatography using chlorobenzene as eluent, the chlorobenzene was subsequently reduced under vacuum and the polymer was precipitated into methanol before being filtered and dried under high vacuum. GPC (chlorobenzene, 80 °C): M_n = 51000 g/mol, M_w = 105000 g/mol, PDI = 2.05.

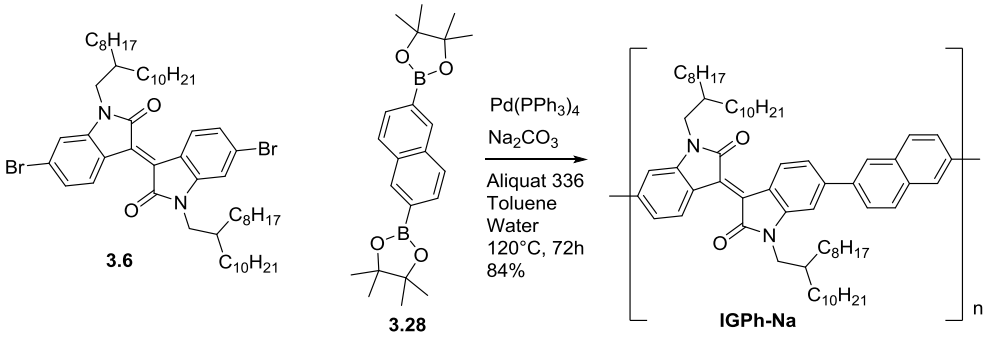
5.50 Synthesis of IGPh-Ph



Degassed toluene (1.5 mL), aqueous sodium carbonate (0.3 mL, 0.30 mmol, 1 M) and 2 drops of Aliquat 336 were added to 6,6'-dibromo-N,N'-(2-octyldodecanyl)-

isoindigo (**3.6**) (0.100 g, 0.102 mmol), 1,4-bis(4,4,5,5-tetramethyl-1,3,2-dioxaborolan-2-yl)benzene (0.034 g, 0.102 mmol) and $Pd(PPh_3)_4$ (2.36 mg, 2.04 μmol). The solution was thoroughly degassed under Argon, and then the Argon inlet was removed and the reaction was heated for 72 h at 120 °C (oil bath temperature). After cooling to rt, the polymer was precipitated into methanol (100 mL), and filtered through a Soxhlet thimble. The polymer was Soxhlet extracted with acetone, hexane and chloroform. The chloroform fraction was collected and sodium diethyldithiocarbamate trihydrate (0.3 g) dissolved in deionised water (100 mL) was added and the mixture was heated at 50 °C for 3 h. The aqueous layer was separated off and the chloroform layer was washed with water 5 times. The chloroform layer was concentrated and the polymer was precipitated into methanol, filtered off and dried under high vacuum to give **IGPh-Ph** as a dark blue solid (77 mg, 81%). The polymer was further purified by recycling gel permeation chromatography using chlorobenzene as eluent, the chlorobenzene was subsequently reduced under vacuum and the polymer was precipitated into methanol before being filtered and dried under high vacuum. GPC (chlorobenzene, 80 °C): M_n = 40000 g/mol, M_w = 58000 g/mol PDI = 1.46.

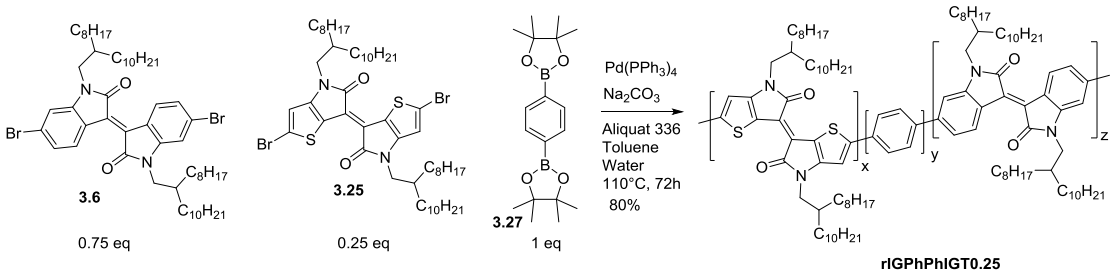
5.51 Synthesis of IGPh-Na



Degassed toluene (1.5 mL), aqueous sodium carbonate (0.3 mL, 0.30 mmol, 1 M) and 2 drops of Aliquat 336 were added to 6,6'-dibromo-N,N'-(2-octyldodecanyl)-isoindigo (**3.6**) (0.1 g, 0.102 mmol), 2,6-bis(4,4,5,5-tetramethyl-1,3,2-dioxaborolan-2-yl)naphthalene (0.039 g, 0.102 mmol) and $Pd(PPh_3)_4$ (2.36 mg, 2.04 μmol). The solution was thoroughly degassed under Argon, and then the Argon inlet was removed and the reaction was heated for 72 h at 120 °C (oil bath temperature). After cooling to rt, the polymer was precipitated into methanol (100 mL), and filtered through a Soxhlet thimble. The polymer was Soxhlet extracted with acetone, hexane

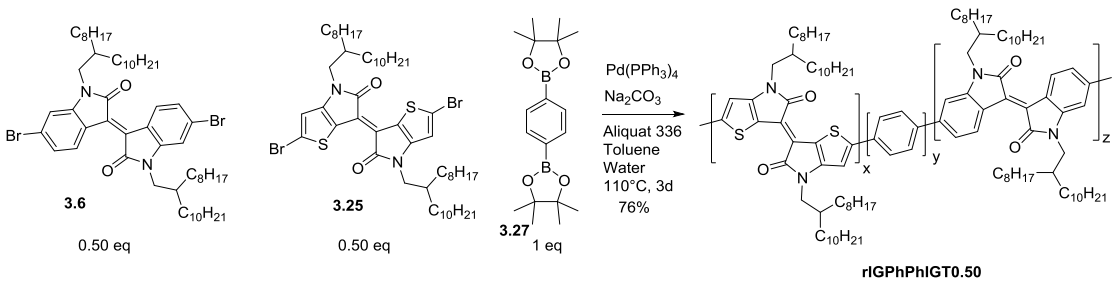
and chloroform. The chloroform fraction was collected and sodium diethyldithiocarbamate trihydrate (0.3 g) dissolved in deionised water (100 mL) was added and the mixture was heated at 50 °C for 3 h. The aqueous layer was separated off and the chloroform layer was washed with water 5 times. The chloroform layer was concentrated and the polymer was precipitated into methanol, filtered off and dried under high vacuum to give **IGPh-Na** as a dark blue solid (84 mg, 84%). GPC (chlorobenzene, 80 °C): M_n = 48000 g/mol, M_w = 141000 g/mol PDI = 2.89.

5.52 Synthesis of rIGPhPhIGT0.25



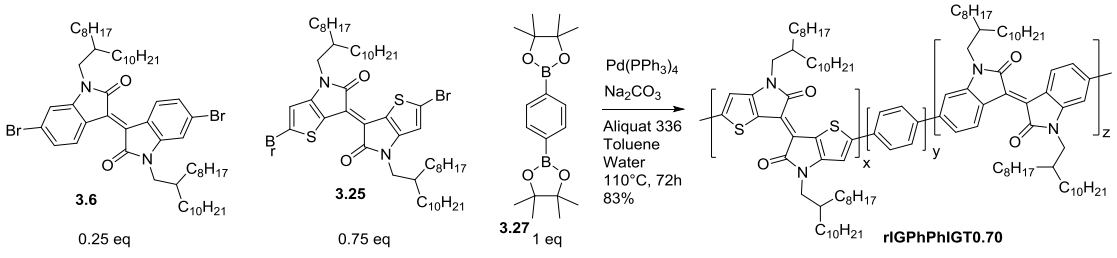
Degassed toluene (1.5 mL), aqueous sodium carbonate (0.3 mL, 0.30 mmol, 1M) and 2 drops of Aliquat 336 were added to 6,6'-dibromo-N,N'-(2-octyldodecanyl)-isoindigo (**3.6**) (0.074 g, 0.076 mmol), 1,4-bis(4,4,5,5-tetramethyl-1,3,2-dioxaborolan-2-yl)benzene (0.033 g, 0.101 mmol), (*E*)-2,2'-dibromo-4,4'-bis(2-octyldodecyl)-[6,6'-bithieno[3,2-b]pyrrolylidene]-5,5'(4*H*,4'*H*)-dione (**3.25 branched**) (0.025 g, 0.025 mmol) and $Pd(PPh_3)_4$ (2.327 mg, 2.014 μmol). The solution was thoroughly degassed under Argon, and then the Argon inlet was removed and the reaction was heated for 72 h at 110 °C. After cooling to rt, the polymer was precipitated into methanol (100 mL), and filtered through a Soxhlet thimble. The polymer was Soxhlet extracted with acetone, hexane and chloroform. The chloroform fraction was collected and sodium diethyldithiocarbamate trihydrate (0.3 g) dissolved in deionised water (100 mL) was added and the mixture was heated at 50 °C for 3 h. The aqueous layer was separated off and the chloroform layer was washed with water 5 times. The chloroform layer was concentrated and the polymer was precipitated into methanol, filtered off and dried under high vacuum to give **rIGPhPhIGT0.25** as a dark solid (142 mg, 80%). GPC (chlorobenzene, 80 °C): M_n = 79000 g/mol, M_w = 180000 g/mol PDI = 2.26.

5.53 Synthesis of rIGPhPhIGT0.50



Degassed toluene (1.5 mL), aqueous sodium carbonate (0.3 mL, 0.30 mmol, 1M) and 2 drops of Aliquat 336 were added to 6,6'-dibromo-N,N'-(2-octyldodecanyl)-isoindigo (**3.6**) (0.049 g, 0.05 mmol), 1,4-bis(4,4,5,5-tetramethyl-1,3,2-dioxaborolan-2-yl)benzene (0.033 g, 0.101 mmol), (*E*)-2,2'-dibromo-4,4'-bis(2-octyldodecyl)-[6,6'-bithieno[3,2-b]pyrrolylidene]-5,5'(4*H*,4′*H*)-dione (**3.25 branched**) (0.05 g, 0.05 mmol) and $Pd(PPh_3)_4$ (2.327 mg, 2.014 μmol). The solution was thoroughly degassed under Argon, and then the Argon inlet was removed and the reaction was heated for 72 h at 110 °C. After cooling to rt, the polymer was precipitated into methanol (100 mL), and filtered through a Soxhlet thimble. The polymer was Soxhlet extracted with acetone, hexane and chloroform. The chloroform fraction was collected and sodium diethyldithiocarbamate trihydrate (0.3 g) dissolved in deionised water (100 mL) was added and the mixture was heated at 50 °C for 3 h. The aqueous layer was separated off and the chloroform layer was washed with water 5 times. The chloroform layer was concentrated and the polymer was precipitated into methanol, filtered off and dried under high vacuum to give **rIGPhPhIGT0.50** as a dark solid (135 mg, 76%). GPC (chlorobenzene, 80 °C): M_n = 85000 g/mol, M_w = 141000 g/mol PDI = 1.65.

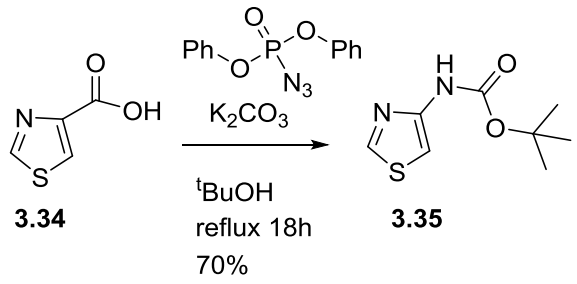
5.54 Synthesis of rIGPhPhIGT0.75



Degassed toluene (1.5 mL), aqueous sodium carbonate (0.3 mL, 0.30 mmol, 1M) and 2 drops of Aliquat 336 were added to 6,6'-dibromo-N,N'-(2-octyldodecanyl)-isoindigo (**3.6**) (0.025 g, 0.025 mmol), 1,4-bis(4,4,5,5-tetramethyl-1,3,2-

dioxaborolan-2-yl)benzene (0.033 g, 0.101 mmol), (*E*)-2,2'-dibromo-4,4'-bis(2-octyldodecyl)-[6,6'-bithieno[3,2-b]pyrrolylidene]-5,5'(4*H*,4′*H*)-dione (**3.25 branched**) (0.075 g, 0.076 mmol) and $Pd(PPh_3)_4$ (2.327 mg, 2.014 μmol). The solution was thoroughly degassed under Argon, and then the Argon inlet was removed and the reaction was heated for 72 h at 110 °C. After cooling to rt, the polymer was precipitated into methanol (100 mL), and filtered through a Soxhlet thimble. The polymer was Soxhlet extracted with acetone, hexane and chloroform. The chloroform fraction was collected and sodium diethyldithiocarbamate trihydrate (0.3 g) dissolved in deionised water (100 mL) was added and the mixture was heated at 50 °C for 3 h. The aqueous layer was separated off and the chloroform layer was washed with water 5 times. The chloroform layer was concentrated and the polymer was precipitated into methanol, filtered off and dried under high vacuum to give **rIGPhPhIGT0.75** as a dark solid (147 mg, 83%). GPC (chlorobenzene, 80 °C): M_n = 69000 g/mol, M_w = 125000 g/mol PDI = 1.82.

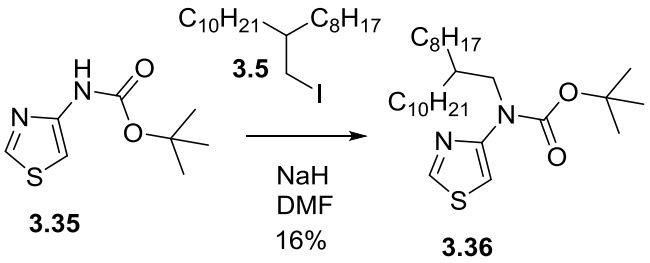
5.55 Synthesis of tert-butyl thiazol-4-ylcarbamate (3.35)



3.34 **3.35**

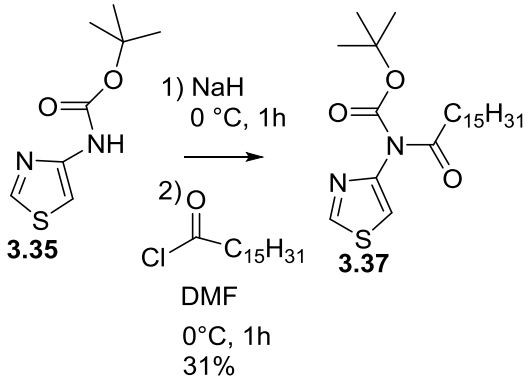
4 thiazole carboxylic acid (5 g, 38.7 mmol) was dissolved in tert-butanol (200 mL) and treated with triethylamine (7.56 mL, 54.2 mmol) and diphenylphosphorylazide (9.18 mL, 42.6 mmol). The mixture was heated at reflux for 18 h. The reaction mixture was cooled to room temperature, then concentrated to 50 mL and poured into saturated aqueous $NaHCO_3$. The mixture was stirred at 0 °C for 2 h. The solid was collected by filtration and dried under high vacuum. The crude reaction mixture was purified by flash chromatography using ethyl acetate as eluent to yield beige crystals (5.44 g, 70%). ^{1}H NMR (400 MHz, DMSO-d_6): δ 10.23 (s, 1H), 8.89 (d, J = 2.0 Hz, 1H), 7.73 (m, 1H), 1.46 (s, 9H) ^{13}C NMR (101 MHz, DMSO-d_6): δ 152.80, 151.81, 149.48, 98.29, 79.37, 28.07 HRMS (EI+): *m/z* 200.0631 Calc. 200.0619

5.56 Synthesis of tert-butyl (2-octyldodecyl)(thiazol-4-yl)carbamate (3.36)



To a solution of tert-butyl thiazol-4-ylcarbamate (1 g, 4.99 mmol) in DMF (10 mL) at 0 °C was added NaH (60% dispersion, 0.22 g, 5.49 mmol). The mixture was stirred at 0 °C for 1 h, and then 9-(iodomethyl)nonadecane (2.65 g, 6.49 mmol) was added. The reaction was heated at 50 °C overnight before the reaction mixture was partitioned between H_2O (50 mL) and ether (50 mL). The layers were separated, and the aqueous layer was extracted with ether. The combined organic layer was washed with H_2O, dried over $MgSO_4$, and concentrated under reduced pressure. The resultant oil was subjected to flash silica gel chromatography using EtOAc/hexane (2:8) as eluent with the product r.f. being 0.80. The product obtain was a colourless oil (0.389g, 16%). ^{1}H NMR (400 MHz, DMSO-d_6): δ 8.94 (d, J = 4.0 Hz, 1H), 7.42 (s, 1H), 3.78 (d, J = 7.6 Hz, 2H), 1.60 (m, 1H), 1.44 (s, 9H), 1.35-0.98 (m, 32H), 0.84 (m, 6H). ^{13}C NMR (101 MHz, DMSO-d_6): δ 152.81, 151.80, 149.47, 98.30, 79.37, 79.22, 78.95, 78.68, 51.40, 35.58, 31.22, 30.51, 29.30, 29.26, 28.75, 28.61, 28.60, 28.07, 25.55, 22.42, 22.04, 21.73, 13.92. HRMS (TOF MS ES+): *m/z* 481.3833 Calc. 481.3828

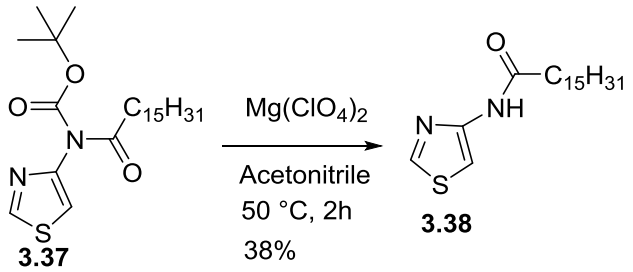
5.57 Synthesis of tert-butyl palmitoyl(thiazol-4-yl)carbamate (3.37)



To a solution of tert-butyl thiazol-4-ylcarbamate (3.1856 g, 15.91 mmol) in anhydrous DMF (29.1 mL) at 0 °C was added NaH (60% dispersion, 0.702 g, 17.56 mmol). The mixture was stirred at rt for 1 h, and then palmitoyl chloride (5.68 g, 20.68 mmol) was

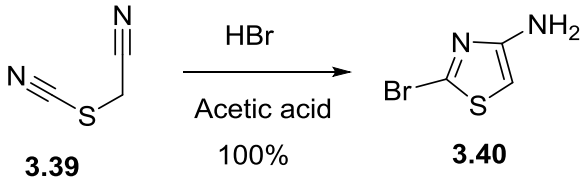
added. Stirring was continued for 1 h, and the reaction mixture was partitioned between H_2O (50 mL) and ether (50 mL). The layers were separated, and the aqueous layer was extracted with ether. The combined organic layer was washed with H_2O, dried over $MgSO_4$, and concentrated under reduced pressure. The resultant oil was subjected to flash silica gel chromatography using EtOAc/hexane (1:9) as eluent (rf 0.30). The product was obtained as a white solid (2.1484 g, 31%). ^{1}H NMR (400 MHz, $CDCl_3$): δ 8.75 (d, J = 2.4 Hz, 1H), 7.90 (d, J = 7.14 Hz, 1H), 2.92 (t, J = 7.5 Hz, 2H), 1.66 (h, J = 7.1 Hz, 2H), 1.40 (s, 9H), 1.36-1.20 (m, 24H), 0.88 (t, J = 6.48 Hz, 3H). ^{13}C NMR (101 MHz, $CDCl_3$): δ 179.01, 170.50, 150.47, 139.01, 118.15, 109.55, 82.28, 32.06, 29.82, 29.58, 29.51, 29.38, 29.20, 29.18, 28.73, 28.24, 22.83, 14.26 HRMS (TOF MS ES+): *m/z* 461.2811 Calc. 461.2814

5.58 Synthesis of N-(thiazol-4-yl)palmitamide (3.38)



Tert-butyl palmitoyl(thiazol-4-yl)carbamate (1.1668 g, 2.66 mmol) and magnesium perchlorate (0.594 g, 2.66 mmol) were placed under Ar and dissolved in acetonitrile (20 mL). The reaction mixture was heated at 50 °C for 2h before being cooled to 0 °C and quenched with water. The reaction mixture was extracted with diethyl ether and the organic layer was dried over anhydrous Na_2SO_4, filtered and concentrated under reduced pressure. The product was purified by column chromatography using petroleum ether (60-80 °C) and ethyl acetate in an 8:2 ratio to give a white oily solid (0.3427 g, 38%). ^{1}H NMR (400 MHz, $CDCl_3$): δ 8.63 (d, J = 2.2 Hz, 1H), 7.40 (d, J = 2.4 Hz, 1H), 2.35 (t, J = 7.6 Hz, 2H), 2.00 (q, J = 7.3 Hz, 2H), 1.58 (m, 4H), 1.37-1.14 (m, 22H), 0.87 (t, J = 7.4 Hz, 3H). ^{13}C NMR (101 MHz, $CDCl_3$): δ 170.94, 150.12, 138.09, 118.32, 34.44, 31.95, 30.99, 29.69, 29.59, 29.47, 29.39, 29.28, 29.05, 28.50, 28.15, 26.45, 24.81, 22.72, 14.16. HRMS (TOF MS ES+): *m/z* 339.2480 Calc 339.2470.

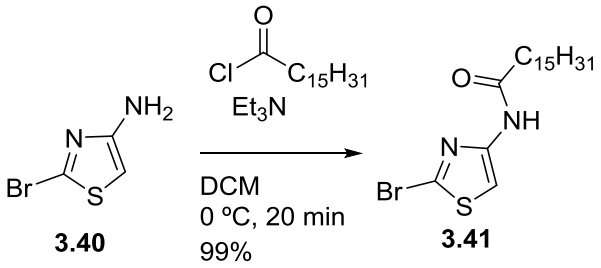
5.59 Synthesis of 2-bromothiazol-4-amine (3.40)



3.39 3.40

To a solution of 2-thiocyanatoacetonitrile (2g, 20.38 mmol) in acetic acid (6.6 mL) cooled to 10 °C was added HBr (10.71 mL, 61.1 mmol, 33% solution in acetic acid) dropwise. The reaction mixture was stirred for 10 min before diethyl ether (30 mL) was added and the precipitated product was filtered off as a light yellow powder. The product was further washed with diethyl ether and used without further purification (3.65 g, 100%). ^{1}H NMR (400 MHz, DMSO-d_6): δ 9.47 (s, 2H), 6.68 (s, 1H). HRMS (CI+): *m/z* 178.9271 Calc. 178.9279 Spectroscopic values are in accordance to literature.[228]

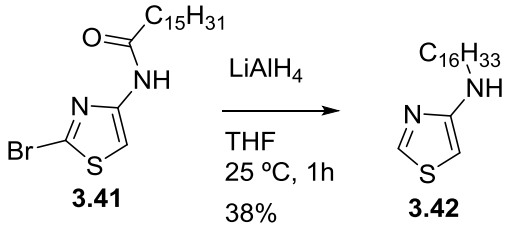
5.60 Synthesis of N-(2-bromothiazol-4-yl)palmitamide (3.41)



3.40 3.41

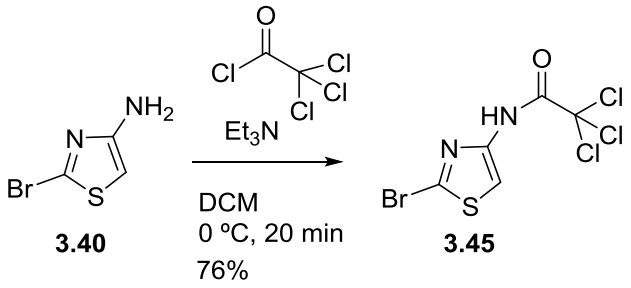
2-bromothiazol-4-amine (27.4g, 153 mmol) was dissolved in anhydrous DCM (200mL) and triethylamine (42 mL, 301 mmol) was added. The solution was cooled to 0 °C and palmitoyl chloride (42 g, 153 mmol) was added dropwise. The reaction mixture was stirred for 20 min before the DCM and triethylamine were removed under reduced pressure. Water (100 mL) was added and the product was filtered off. The product was subsequently washed with HCl (1 M) and water and dried under vacuum to give N-(2-bromothiazol-4-yl)palmitamide as a powdery white solid (63.33g, 99%). ^{1}H NMR (400 MHz, $CDCl_3$): δ 8.58 (s, 1H), 7.58 (s, 1H), 2.37 (t, J = 7.6Hz, 2H), 1.69 (m, 2H), 1.38-1.20 (m, 24H), 0.86 (t, J = 6.8 Hz, 3H). ^{13}C NMR (101 MHz, $CDCl_3$): δ 171.12, 146.89, 134.44, 105.27, 46.03, 37.00, 34.15, 32.05, 29.80, 29.72, 29.57, 29.49, 29.45, 29.29, 25.50, 22.81, 14.25, 8.75 HRMS (EI+): *m/z* 416.1509 Calc. 416.1497

5.61 Synthesis of N-hexadecylthiazol-4-amine (3.42)



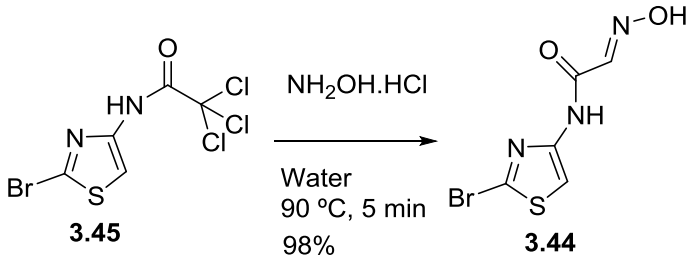
N-(2-bromothiazol-4-yl)palmitamide (**3.41**) was dissolved in anhydrous THF and lithium aluminium hydride (8.2 mL, 2M in THF, 16.40 mmol) was added dropwise and stirred at 25 ºC for 30 mins. The reaction mixture was quenched wet diethyl ether and washed with brine before being dried over $MgSO_4$ and purified via column chromatography using hexane and DCM to give the product as a brown oil (0.3 g, 38%). ^{1}H NMR (400 MHz, $CDCl_3$): δ 8.60 (d, J = 2.3 Hz, 1H), 7.72 (d, J = 2.3 Hz, 1H), 8.21 (s, 1H), 3.67 (t, J = 6.5 Hz, 2H), 1.67 (m, 2H), 1.44-1.20 (m, 26H), 0.91 (t, J = 6.8 Hz, 3H). ^{13}C NMR (101 MHz, $CDCl_3$): δ 170. 99, 150.14, 138.21, 69.34, 58.54, 42.14, 31.95, 30.98, 29.73, 29.58, 29.49, 29.37, 29.04, 28.49, 28.14, 26.45, 24.81, 22.73, 14.17 MS (EI): 325 Calc. 324.260

5.62 Synthesis of N-(2-bromothiazol-4-yl)-2,2,2-trichloroacetamide (3.45)



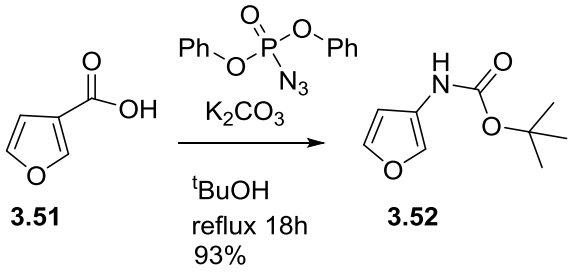
2-bromothiazol-4-amine (**3.40**) (4.56 g, 25.5 mmol) was suspended in anhydrous DCM (35 ml) and cooled to 0 ºC. Upon addition of triethylamine (6.99 mL, 50.2 mmol) the starting material fully dissolved. 2,2,2-trichloroacetyl chloride (2.86 mL, 25.5 mmol) was added dropwise and the reaction mixture was stirred for 2 h. The solvent was removed under vacuum and the crude product was purified via column chromatography using DCM as eluent to obtain the product as a white solid (6.3 g, 76%) ^{1}H NMR (400 MHz, $CDCl_3$): δ 9.20 (s, 1H), 7.66 (s, 1H). ^{13}C NMR (101 MHz, $CDCl_3$): δ 159.06, 144.83, 135.67, 107.63, 91.70 HRMS (EI+): *m/z* 321.8142 Calc 321.8137

5.63 Synthesis of (E)-N-(2-bromothiazol-4-yl)-2-(hydroxyimino)acetamide (3.44)



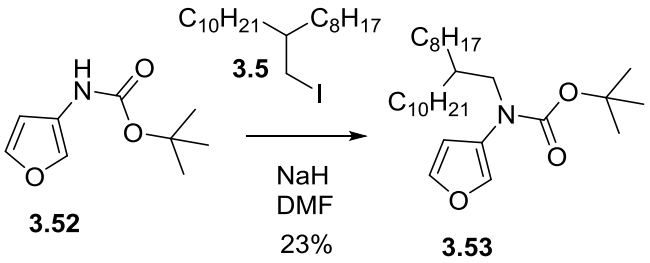
To n-(2-bromothiazol-4-yl)-2,2,2-trichloroacetamide (**3.45**) (0.925 g, 2.85 mmol) was added water (5.65 mL) and hydroxylamine hydrochloride (0.252 g, 3.62 mmol). The mixture was heated at 75 ºC for 30 min and allowed to cool to rt. The product was filtered off as a light brown solid, washed with water and dried (0.70 g, 98%). ^{1}H NMR (400 MHz, $CDCl_3$): δ 9.19 (s, 1H), 7.66 (s, 1H), 1.66 (s, 1H).). ^{13}C NMR (101 MHz, $CDCl_3$): δ 175.02, 173.97, 111.89, 79.11, 35.98 HRMS (CI+): *m/z* 249.9295 [M+H]+ Calc. 249.9286 [M+H]+

5.64 Synthesis of tert-butyl furan-3-ylcarbamate (3.52)



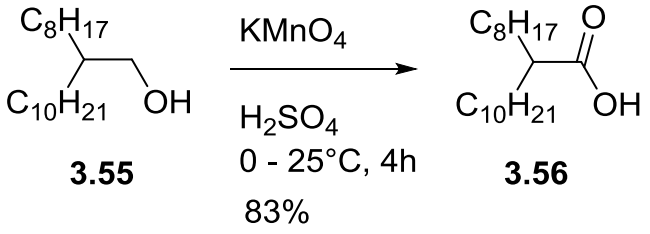
Furan-3-carboxylic acid (19.4 g, 173 mmol) was dissolved in *tert*-butanol (600 mL) and treated with triethylamine (33.8 mL, 242 mmol) and diphenylphosphorylazide (41 mL, 190 mmol). The mixture was heated at reflux for 18 h. The reaction mixture was cooled to room temperature, then concentrated to 50 mL and poured into saturated aqueous $NaHCO_3$. The mixture was stirred at 0 °C for 2 h. The solid was collected by filtration and dried under high vacuum. The crude reaction mixture was purified by flash chromatography using hexane and ethyl acetate (8:2) as eluent and recrystallised in ethyl acetate to give the product as white fluffy needles (29.45 g, 93%). ^{1}H NMR (400 MHz, DMSO-d_6): δ 9.25 (s, 1H), 7.64 (s, 1H), 7.46 (t, J = 1.8 Hz, 1H), 6.33 (s, 1H), 1.44 (s, 9H) ^{13}C NMR (101 MHz, DMSO-d_6): δ 152.65, 141.78, 129.27, 125.81, 104.93, 78.96, 28.09. HRMS (EI+): *m/z* 183.0889 Calc. 183.0895

5.65 Synthesis of tert-butyl furan-3-yl(2-octyldodecyl)carbamate (3.53)



To a solution of furan-2-yl carbamate (8.28 g, 45.2 mmol) in DMF (80 mL) at 0 °C was added NaH (60% dispersion, 1.996 g, 49.9 mmol). The mixture was stirred at 0 °C for 1 h, and then 9-(iodomethyl)nonadecane (24 g, 58.8 mmol) was added. Stirring was continued for 1 h, and the reaction mixture was partitioned between H_2O (50 mL) and ether (50 mL). The layers were separated, and the aqueous layer was extracted with ether. The combined organic layer was washed with H_2O, dried over $MgSO_4$, and concentrated under reduced pressure. The resultant oil was subjected to flash silica gel chromatography using EtOAc/hexane (1:9) as eluent with the product r.f. being 0.83. The product obtain was a yellow oil (4.8528 g, 23%). ^{1}H NMR (400 MHz, DMSO-d_6): δ 7.70 (m, 1H), 7.54 (t, J = 1.9 Hz, 1H), 6.56 (m, 1H), 3.46 (d, J = 7.4 Hz, 2H), 1.61 (m, 1H), 1.43 (s, 9H), 1.31-1.08 (m, 32H), 0.87-0.83 (m, 6H). ^{13}C NMR (101 MHz, DMSO-d_6): δ 152.92, 141.89, 129.10, 79.93, 79.23, 78.96, 78.69, 51.38, 35.59, 31.24, 30.50, 29.30, 29.25, 28.91, 28.76, 28.64, 28.60, 27.84, 25.54, 22.47, 22.05, 21.73, 13.91 HRMS (TOF MS ES+): *m/z* 464.4098 Calc. 464.4104

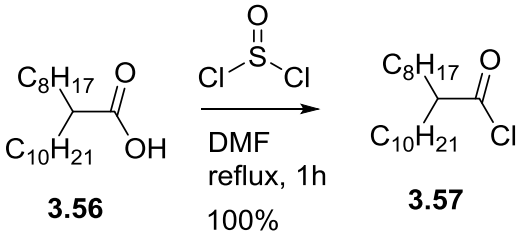
5.66 Synthesis of 2-octyldodecanoic acid (3.56)



To a cooled solution of 2-octyldodecan-1-ol in sulfuric acid (55.8 mL, 1.5 M, 84 mmol) potassium permanganate (21.17 g, 134 mmol) was added portionwise to ensure that the temperature did not exceed 15 °C. The reaction mixture was allowed to warmed up to room temperature and stirred for 4 h. The manganese dioxide formed was dissolved with aqueous sodium bisulphite solution and the mixture was extracted three times with diethyl ether (100 mL). The combined ether phases were extracted

with 10% sodium hydroxide solution, cooled to 10 °C and acidified with 10% HC1. The ether and HCl phases were further extracted three times with diethyl ether (100 mL) and the combined extracts were dried over $MgSO_4$, filtered, concentrated under reduced pressure and the residue was purified via column chromatography using petroleum ether / ethyl acetate (1:1) as eluent to give a pale yellow oil (21.775 g, 83%). ^{1}H NMR (400 MHz, $CDCl_3$): δ 2.83 (m, 1H), 1.63 (m, 2H), 1.46 (m, 2H), 1.39-1.22 (m, 28H), 0.90 (t, J = 6.7 Hz, 6H). ^{13}C NMR (101 MHz, $CDCl_3$): δ 45.43, 32.23, 31.94, 31.88, 29.63, 29.59, 29.50, 29.44, 29.36, 29.29, 27.40, 22.71, 14.16, 1.06 HRMS (EI+): *m/z* 312.3033 Calc. 312.3028

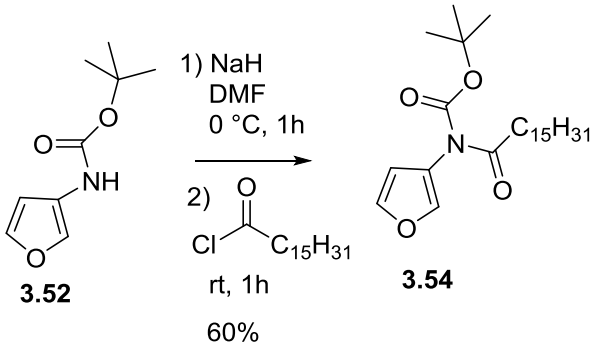
5.67 Synthesis of 2-octyldodecanoyl chloride (3.57)



3.56 **3.57**

To 2-octyldodecanoic acid (21.7 g, 69.4 mmol) in thionyl chloride (7.63 mL, 105 mmol) was added anhydrous dimethyl formyl amide (DMF) (2 drops) and the mixture was heated at reflux for 1 h. The thionyl chloride and DMF were removed under vacuum and the crude product was obtained as a brown oil (23 g, 100%) which was used without further purification. ^{1}H NMR (400 MHz, $CDCl_3$): δ 2.75 (m, 1H), 1.72 (m, 2H), 1.53 (m, 2H), 1.45-1.14 (m, 28H), 0.88 (t, J = 6.2 Hz, 6H). ^{13}C NMR (101 MHz, $CDCl_3$): δ 57.38, 49.10, 40.07, 32.14, 32.04, 31.96, 31.73, 29.78, 29.70, 29.65, 29.52, 29.45, 27.07, 26.72, 22.82, 14.25 HRMS (EI+): 330.2684 Calc. 330.2689

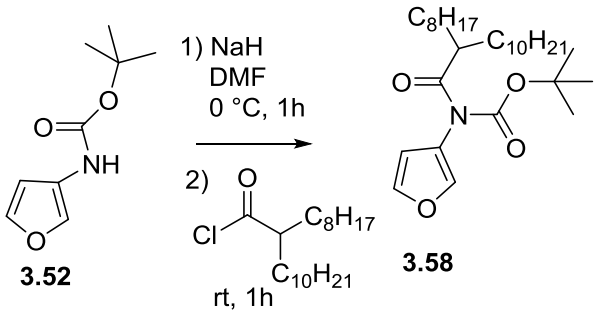
5.68 Synthesis of tert-butyl furan-3-yl(palmitoyl)carbamate (3.54)



3.52 **3.54**

To a solution of furan-2-yl carbamate (1 g, 5.46 mmol) in DMF (10 mL) at 0 °C was added NaH (60% dispersion, 0.241 g, 6.03 mmol). The mixture was stirred at rt for 1 h, and then palmitoyl chloride (1.5 g, 5.46 mmol) was added. Stirring was continued for 1 h, and the reaction mixture was partitioned between H_2O (50 mL) and ether (50 mL). The layers were separated, and the aqueous layer was extracted with ether. The combined organic layer was washed with H_2O, dried over $MgSO_4$, and concentrated under reduced pressure. The resultant oil was subjected to flash silica gel chromatography using EtOAc/hexane (1:9) as eluent (rf 0.33). The product which was initially a pale yellow oil spontaneously solidified at 20 °C to give a beige solid (1.38 g, 60%). ^{1}H NMR (400 MHz, $CDCl_3$): 7.39 (m, 1H), 7.38 (m, 1H), 6.29 (m, 1H), 2.85 (t, J = 7.5 Hz, 2H), 1.64 (m, 2H), 1.45 (s, 9H), 1.37-1.19 (m, 26H), 0.87 (t, J = 6.6 Hz, 3H). ^{13}C NMR (101 MHz, $CDCl_3$): δ 175.53, 152.52, 142.45, 138.97, 124.88, 110.60, 83.55, 38.03, 32.07, 29.83, 29.77, 29.66, 29.59, 29.51, 29.34, 28.44, 27.99, 25.16, 22.84 HRMS (EI +): *m/z* 421.3180 Calc. 421.3192

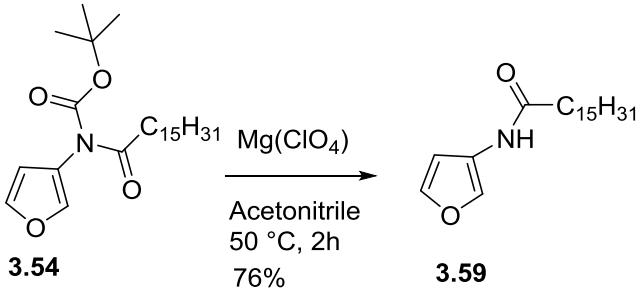
5.69 Synthesis of tert-butyl furan-3-yl(2-octyldodecanoyl)carbamate (3.58)



To a solution of tert-butyl thiazol-4-ylcarbamate (5 g, 27.3 mmol) in anhydrous DMF (50 mL) at 0 °C was added NaH (60% dispersion, 1.205 g, 30.1 mmol). The mixture was stirred at rt for 1 h, and then 2-octyldodecanoyl chloride (10.84 g, 32.8 mmol) was added. Stirring was continued for 1 h, and the reaction mixture was partitioned between H_2O (50 mL) and ether (50 mL). The layers were separated, and the aqueous layer was extracted with ether. The combined organic layer was washed with H_2O, dried over $MgSO_4$, and concentrated under reduced pressure. The resultant oil was subjected to flash silica gel chromatography using EtOAc/hexane (2:8) as eluent (rf 0.70). The product was obtained as a light brown oil (7.71 g, 59%). ^{1}H NMR (400 MHz, $CDCl_3$): δ 7.39 (m, 2H), 6.29 (d, J = 1.1 Hz, 1H), 3.35 (m, 1H), 2.34 (m, 2H),

1.62 (m, 2H), 1.48 (m, 2H), 1.46 (s, 9H), 1.37-1.16 (m, 28H), 0.87 (m, 6H). ^{13}C NMR (101 MHz, $CDCl_3$): δ 178.88, 142.38, 138.72, 110.46, 45.39, 31.94, 31.88, 29.64, 29.58, 29.49, 29.44, 29.36, 29.29, 29.08, 27.85, 27.40, 27.35, 27.28, 22.70, 14.15. HRMS (TOF MS ES+): *m/z* 500.3717 Calc. 500.3716.

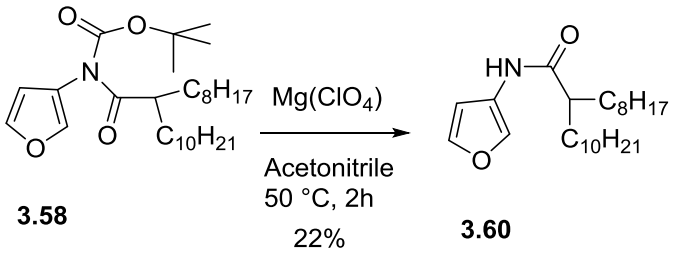
5.70 Synthesis of N-(furan-3-yl)palmitamide (3.59)



3.54 **3.59**

Tert-butyl furan-3-yl(palmitoyl)carbamate (1.3414 g, 3.18 mmol) and magnesium perchlorate (0.71 g, 3.18 mmol) were placed under Ar and dissolved in acetonitrile (20 mL). The reaction mixture was heated at 50 °C for 2 h before being cooled to 0 °C and quenched with water. The reaction mixture was extracted with diethyl ether and the organic layer was dried over anhydrous Na_2SO_4, filtered and concentrated under reduced pressure. The product was purified by column chromatography using petroleum ether (60-80 °C) and ethyl acetate in an 8:2 ratio to give a white solid (0.774 g, 76%). ^{1}H NMR (400 MHz, $CDCl_3$): δ 8.04 (d, J = 1.6 Hz, 1H), 7.29 (m, 1H), 7.01 (s, 1H), 6.29 (d, J = 1.9 Hz, 1H), 2.33 (t, J = 7.6 Hz, 2H), 1.70 (p, J = 7.3 Hz, 2H), 1.39-1.16 (m, 24H), 0.88 (t, J = 6.7 Hz, 3H). ^{13}C NMR (101 MHz, $CDCl_3$): δ 141.52, 132.67, 104.54, 36.87, 32.07, 29.81, 29.61, 29.51, 29.41, 25.72, 22.85, 14.29 HRMS (EI+): *m/z* 321.2672 Calc. 321.2668

5.71 Synthesis of N-(furan-3-yl)-2-octyldodecanamide (3.60)

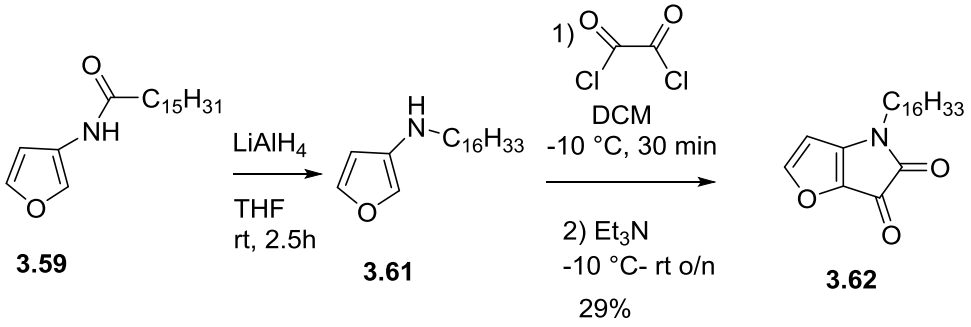


3.58 **3.60**

Tert-butyl furan-3-yl(palmitoyl)carbamate (7.70 g , 16.12 mmol) and magnesium perchlorate (3.60 g, 16.12 mmol) were placed under Ar and dissolved in acetonitrile

(69 mL). The reaction mixture was heated at 50 °C for 2 h before being cooled to 0 °C and quenched with water. The reaction mixture was extracted with diethyl ether and the organic layer was dried over anhydrous Na_2SO_4, filtered and concentrated under reduced pressure. The product was purified by column chromatography using DCM to give a light brown oil (1.33 g, 22%). ^{1}H NMR (400 MHz, $CDCl_3$): δ 8.07 (s, 1H), 7.30 (m, 1H), 6.97 (m, 1H), 6.31 (d, J = 1.9 Hz, 1H), 2.14 (m, 1H), 1.64 (m, 2H), 1.48 (m, 2H), 1.35-1.14 (m, 28H), 0.87 (m, 6H). ^{13}C NMR (101 MHz, $CDCl_3$): δ 173.71, 141.33, 132.65, 123.92, 104.51, 48.30, 33.20, 31.92, 31.86, 29.72, 29.61, 29.50, 29.47, 29.34, 29.28, 27.73, 27.41, 22.69, 14.12 HRMS (EI+): 377.3286 Calc. 377.3294

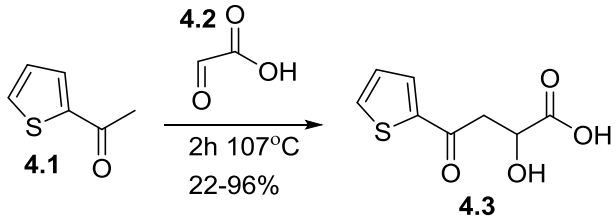
5.72 Synthesis of 4-hexadecyl-4H-furo[3,2-b]pyrrole-5,6-dione (3.62)



N-(furan-3-yl)palmitamide (0.5 g, 1.55 mmol) was dissolved in anhydrous THF and the solution was thoroughly degassed under Ar. Lithium aluminium hydride (2.131 mL, 1 M in THF, 2.131 mmol) was added dropwise at rt. The reaction mixture was stirred at rt for 2.5 h under Ar before the THF was removed under reduced pressure over the course of 30 min whilst still connected to the Schlenk line to avoid contact with oxygen. Upon full removal of the THF, anhydrous hexane was added and the residual lithium aluminium hydride and associated salts were precipitated out. The hexane was decanted off via cannula into a 2 necked round bottomed flask and removed under reduced pressure whilst still connected to the Schlenk line to avoid contact with oxygen. The resultant orange gel was dissolved up in anhydrous DCM (20 mL) and added dropwise over the course of 20 min to a solution of oxalyl chloride (0.184 mL, 2.089 mmol) dissolved in anhydrous DCM (7 mL) at -10 °C under Ar. After 30 min triethylamine (1.12 mL, 8.07 mmol) dissolved in anhydrous DCM (5 mL) was added dropwise and the reaction mixture was allowed to warm to rt overnight. The DCM and triethylamine was removed under reduced pressure and the crude

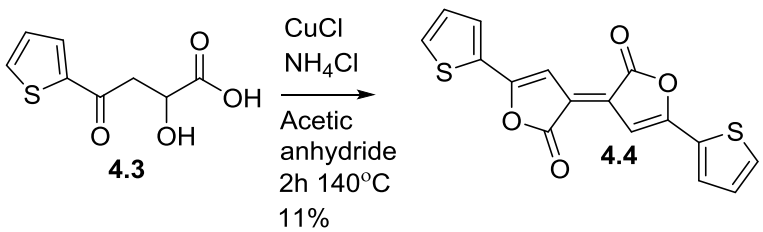
product was purified by column chromatography using DCM as eluent to give the product as a yellow solid (0.161 g, 29%). ^{1}H NMR (400 MHz, $CDCl_3$): δ 7.71 (d, J = 1.9 Hz, 1H), 6.38 (d, J = 1.9 Hz, 1H), 3.57 (t, J = 7.1 Hz, 2H), 1.63 (m, 4H), 1.41-1.08 (m, 24H), 0.87 (t, J = 6.4 Hz, 3H) ^{13}C NMR (101 MHz, $CDCl_3$): δ 155.09, 100.92, 53.47, 41.98, 31.96, 29.70, 29.55, 29.47, 29.40, 22.72, 14.17. (note: missing two quaternary carbons). HRMS (EI+): *m/z* 361.2628 calc 361.2617

5.73 Synthesis of 2-hydroxy-4-oxo-4-(thiophen-2-yl)butanoic acid (4.3)



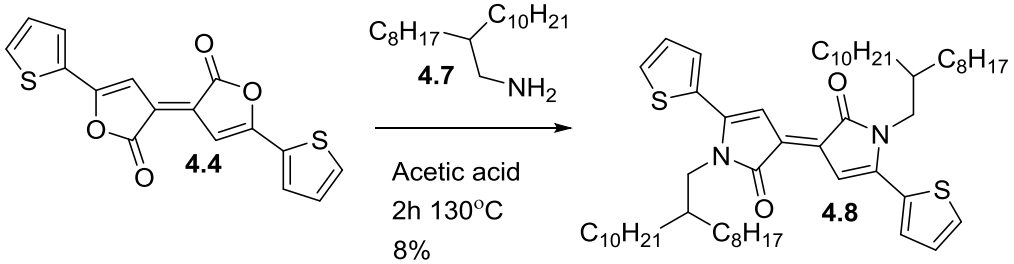
A 50% solution of glyoxylic acid in water (22.2 g, 0.15 mol) was heated under vacuum (50 mmHg) until 80% of the water was removed. 2- acetylthiophene (37.8 g, 0.3 mol) was added and the mixture was heated under vacuum for 2 h at 107 ºC. When cooled down to room temperature, 100 mK of water and Na_2CO_3 (8.7g) were added and the aqueous phase was washed several times with ether before being acidified to a pH value of around 1 and extracted several times with ethyl acetate. The organic phases were dried over Na_2SO_4 and evaporated to yield the product as a pale yellow oil (28.77 g, 96%). ^{1}H NMR (400MHz, $CDCl_3$): δ 9.73 (1H, s), 7.77 (1H, d, J = 3.9Hz), 7.71 (1H, d, J = 4.7Hz), 7.16 (1H, dd, J = 4.6Hz, J = 3.8Hz), 4.71 (1H, dd, J= 4.1Hz, J = 4.3Hz), 3.53 (1H, d, J = 4.0Hz), 3.51 (1H, d, J = 6.1Hz). ^{13}C NMR (101 MHz, $CDCl_3$): 190.85, 177.73, 135.13, 133.30, 128.47, 169.72, 42.42, 20.81 MS (EI): *m/z* 200 Calc. 200.212

5.74 Synthesis of (E)-5,5'-di(thiophen-2-yl)-2H,2'H-[3,3'-bifuranylidene]-2,2'-dione (4.4)



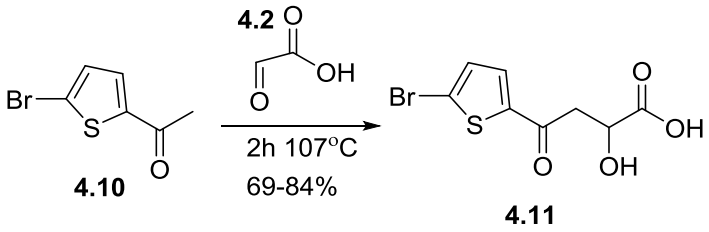
Dissolved ammonium chloride (5.76 g, 108 mmol), copper chloride (5.41 g, 54.6 mmol) and 2-hydroxy-4-oxo-4-(thiophen-2-yl)butanoic acid (28.77 g, 144 mmol) in acetic anhydride (150 mL). Heated at 140 °C for 2 h. Allowed to cool and stir overnight. When cooled down, the mixture was filtrated and the resulting black purple powder was washed several times with water, ethanol, ether acetic acid and methanol. Soxhlet extraction in chloroform over 2 days gave the black/purple product (5.04 g, 11% yield) as black crystals. ^{1}H NMR (400 MHz, $CDCl_3$): δ 7.64 (2H, d, J = 3.49Hz), 7.59 (2H, d, J =4.69Hz), 7.35 (2H, s), 7.18 (2H, dd, J = 3.8Hz, J = 3.9Hz) MS (EI): *m/z* 328 Calculated 327.99. Spectroscopic values are in accordance to literature.[241]

5.75 Synthesis of (E)-1,1'-bis(2-octyldodecyl)-5,5'-di(thiophen-2-yl)-[3,3'-bipyrrolylidene]-2,2'(1H,1'H)-dione (4.8)



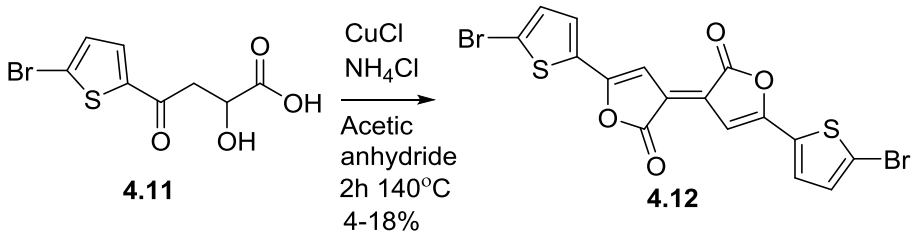
Dissolved 2-octyldodecan-1-amine (2.72 g, 9.14 mmol) and (E)-5,5'-di(thiophen-2-yl)-2H,2'H-[3,3'-bifuranylidene]-2,2'-dione (1 g, 3.05 mmol) in acetic acid (50 mL) and refluxed for 2.5 h. When cooled down, water and DCM were added and the DCM layer was washed several times with water, and evaporated. The resulting black oil was columned in hexane with 1% DCM to give the product as a blue oil (0.21 g, 8% yield). ^{1}H NMR (400 MHz, $CDCl_3$): δ 7.46 (2H, d, J = 5.0 Hz), 7.41 (2H, d, J = 3.8Hz), 7.12 (2H, dd, J = 3.91Hz, J = 3.9Hz), 3.78 (4H, d, J = 7.56Hz), 1.64 (2H, m), 1.30-1.12 (64H, m), 0.9-0.83 (12H, m). ^{13}C NMR (101 MHz, $CDCl_3$): δ 145.24, 136.84, 133.35, 128.29, 128.08, 127.90, 103.56, 89.39, 45.14, 37.44, 31.92, 29.93, 29.64, 29.52, 29.37, 29.30, 26.25, 22.70, 14.14 MS (EI): *m/z* 886 Calc. 886.64

5.76 Synthesis of 4-(5-bromothiophen-2-yl)-2-hydroxy-4-oxobutanoic acid (4.11)



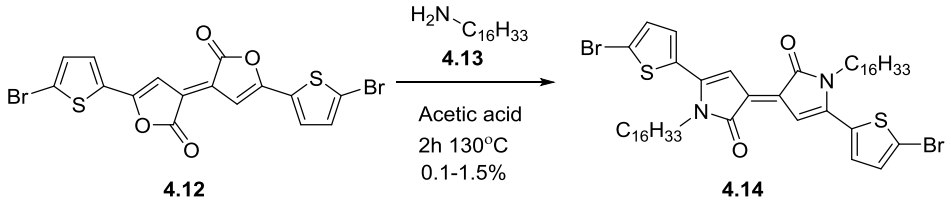
A 50% solution of glyoxylic acid in water (1.35 mL, 12 mmol) was heated under vacuum (50 mmHg) until 80% of the water was removed. Then, 2- acetyl 5-bromo-thiophene (5 g, 24.4mol) was added and the mixture was heated under vacuum for 2 h at 107 ºC. When cooled down to room temperature, water (100 mL) and Na_2CO_3 (0.7 g) were added and the aqueous phase was washed several times with ether and then acidified to a pH value of around 1 and extracted several times with ethyl acetate. The organic phases were dried over Na_2SO_4 and evaporated to give a yield of 2.86 g of crude product, 84% yield, as a beige solid which sparkles. ^{1}H NMR (400 MHz, DMSO-d_6): δ 12.76 (1H, s), 7.85 (1H, d, J = 4.0Hz), 7.41 (1H, d, J = 4.0Hz), 5.58 (1H, s), 4.45 (1H, dd, J = 7.6Hz, 4.7Hz), 3.32-3.15 (2H, m). ^{13}C NMR (101 MHz, DMSO-d_6): δ 190.20, 175.19, 146.14, 135.11, 132.90, 122.58, 67.13, 42.86. MS (EI): *m/z* 278 (-H) Calc. 279.10

5.77 Synthesis of (E)-5,5'-bis(5-bromothiophen-2-yl)-2H,2'H-[3,3'-bifuranylidene]-2,2'-dione (4.12)



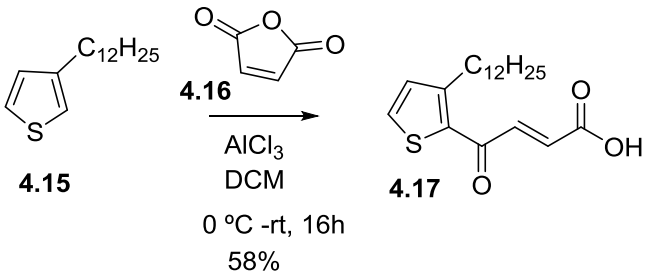
Dissolved ammonium chloride (1.343 g, 25.1 mmol), copper chloride (1.26 g, 12.7 mmol) and 4-(5-bromothiophen-2-yl)-2-hydroxy-4-oxobutanoic acid (9.345 g, 33.5 mmol) in acetic anhydride (25 mL). Heated at 140 °C for 2.5 h. Allowed to cool down to room temperature, filtered off the resulting black purple powder and washed the powder several times with acetic acid and ethanol. Soxhlet extraction in chloroform over 2 days gave the product as a dark purple shiny crystalline powder, (1.5 g, 18%). ^{1}H NMR (400 MHz, DMSO): δ 8.32 (s, 2H), 7.80 (d, J = 4.1 Hz, 2H), 7.41 (d, J = 4.1Hz, 2H) (note: not soluble enough for ^{13}C NMR) MS (E.I): *m/z* 486 Calc. 486.154

5.78 Synthesis of (E)-5,5'-bis(5-bromothiophen-2-yl)-1,1'-dihexadecyl-[3,3'-bipyrrolylidene]-2,2'(1H,1'H)-dione (4.14)



2-octyldodecan-1-amine (1.5 g, 6.21 mmol), (E)-5,5'-bis(5-bromothiophen-2-yl)-2H,2'H-[3,3'-bifuranylidene]-2,2'-dione (0.7 g, 1.4 mmol) was dissolved in acetic acid (70 mL) and refluxed at 130 °C for 2 h. When cooled down, water and DCM were added and the DCM layer was washed with water. The product was dried over $MgSO_4$ and directly columned in hexane and DCM. The obtained fractions were concentrated under vacuum and the product was precipitated into methanol. Obtained blue fibrous product (20.2 mg, 1.5%) ^{1}H NMR (400 MHz, $CDCl_3$): δ 7.12 (1H, d, J = 4.5Hz), 7.04 (1H, s), 6.98 (1H, d, J = 4.01), 1.35-1.23 (36H, m), 0.90 (6H, t, J = 6.55Hz) ^{13}C NMR (101 MHz, $CDCl_3$): δ 170.73, 144.31, 134.74, 131.12, 128.24, 127.93, 115.79, 103.68, 44.76, 30.11, 29.82, 29.75, 29.68, 29.64, 29.51, 29.37, 22.94, 14.30. MS (EI): *m/z* 933 Calc 933.035

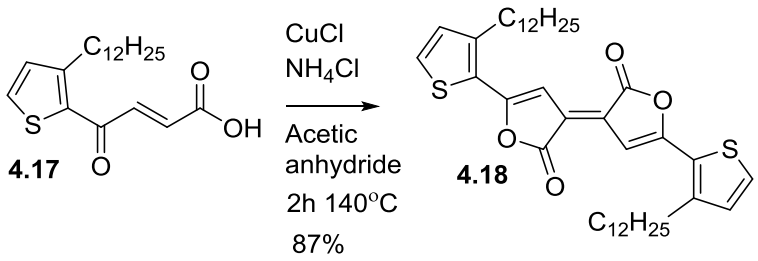
5.79 Synthesis of (E)-4-(3-dodecylthiophen-2-yl)-4-oxobut-2-enoic acid (4.17)



3-dodecylthiophene (5 g, 19.81 mmol) and maleic anhydride (1.996 g, 20.36 mmol) were dissolved with stirring in anhydrous DCM (100 mL) and the mixture cooled in an ice bath. $AlCl_3$ (5.81 g, 43.6 mmol) was added portion wise and the mixture stirred at rt for 16 h. The mixture was poured into a 10% HCl solution containing ice and stirred for 30 min. The organic layer was separated and the aqueous layer was extracted with 100 mL of DCM and the combined organic layers were washed with water and brine and dried over sodium sulfate. The solvent was removed and the solid

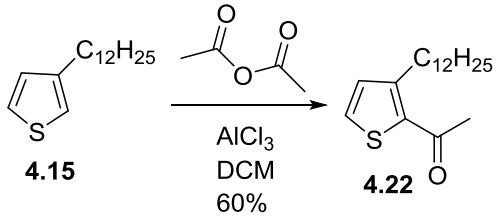
was triturated with hexanes and filtered yielding a light yellow powder which was used without further purification (3.99 g, 58%, literature value = 94%[251]) ^{1}H NMR ($CDCl_3$): 7.78 (d, 1H, *J* = 14.8 Hz), 7.56 (d, 1H, *J* = 5.2 Hz), 7.08 (d, 1H, *J* = 5.2 Hz), 6.88 (d, 1H, *J* = 4.8 Hz), 3.06 (t, 2H), 1.64 (m, 2H), 1.26 (M, 18H), 0.88 (t, 3H); ^{13}C NMR (DMSO-d_6): 170.79, 153.79, 141.15, 135.21, 132.62, 132.19, 130.83, 32.31, 31.03, 30.62, 29.98, 29.73, 23.07, 14.46; HRMS (EI): *m/z* 350.1914 (M+) Calc. 350.1916.

5.80 Synthesis of (E)-5,5'-(3-dodecylthiophen-2-yl)bifuranylidenedione (4.18)



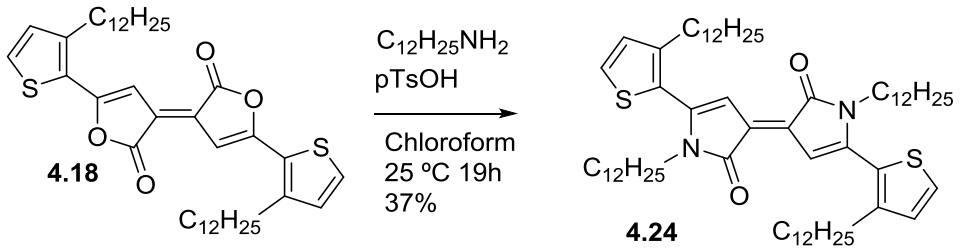
(E)-4-(3-dodecylthiophen-2-yl)-4-oxobut-2-enoic acid (3.99 g, 11.3 mmol), CuCl (0.34 g, 3.4 mmol) and ammonium chloride (0.359 g, 6.7 mmol) in acetic anhydride (25 mL) was placed in a 50 mL round bottomed flask. With stirring the mixture was brought to a boil at 140 °C at which time the mixture turned dark purple and was refluxed for 2 h. The mixture was cooled and the solid collected by vacuum filtration and washed with acetic acid and ethanol successively. The dark solid dissolved in chloroform and was filtered through a bed of celite to remove the insoluble copper salts yielding a purple solid after concentration (3.3 g, 87%, literature = 68%[251]). ^{1}H NMR (400 MHz, CD_2Cl_2): δ 7.53 (d, 2H, *J* = 5.2 Hz), 7.28 (s, 2H), 7.07 (d, 2H, *J* = 5.2 Hz), 2.93 (t, 4H), 1.73 (m, 4H), 1.29 (M, 36H), 0.88 (t, 6H); ^{13}C NMR (101 MHz, $CDCl_3$): δ 167.26, 155.29, 148.09, 131.98, 130.27, 125.77, 125.25, 104.29, 32.30, 30.83, 30.26, 29.85, 23.03, 14.51; HRMS (EI): *m/z* 664.3612 (M+) Calc. 664.3620.

5.81 Synthesis of 1-(3-dodecylthiophen-2-yl)ethanone (4.22)



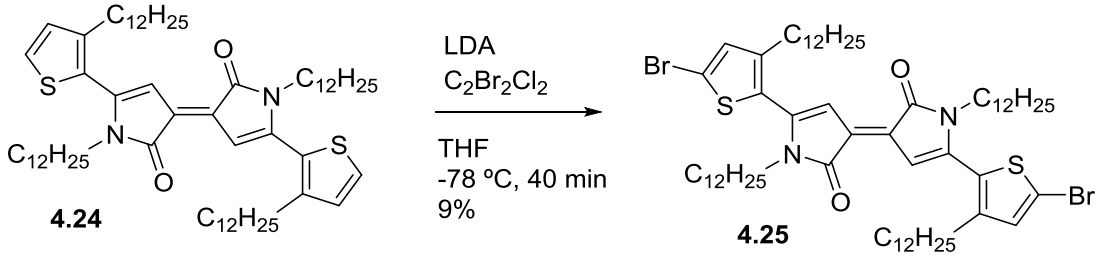
Dissolved 3-dodecylthiophene (2.568 g, 10.1 mmol) and acetic anhydride (1.0 mL, 10.7 mmol) in anhydrous DCM (60 mL) and then cooled to 0 °C under Ar. Added $AlCl_3$ (2.98 g, 22.4mmol) portionwise over the course of 10 min and stirred at 0 °C for 40 min. Removed ice bath and stirred at rt for 4 h. Added ice to quench and HCl (30 mL, 1 M) and stirred for 10 min. Extracted with DCM and dried over $MgSO_4$. Filtered and rotary evaporated off the DCM to give a crude yellow oil, which was columned in hexane and ethyl acetate to obtain the product as a yellow oil (2.98 g, 60%). ^{1}H NMR (400 MHz, $CDCl_3$): δ 7.42 (1H, d, J = 4.9Hz), 7.01 (1H, d, J = 5Hz), 3.01 (2H, m), 2.55 (3H, s), 1.41-1.22 (20H, m), 0.90 (3H, t, J = 6.7Hz) ^{13}C NMR (101 MHz, $CDCl_3$): δ 191.06, 150.57, 131.60, 129.64, 31.93, 30.31,30.25, 29.83,29.67, 29.64, 29.50, 29.36, 22.70, 14.14 MS (EI): *m/z* 294 Calc. 294.20

5.82 Synthesis of (E)-1,1'-didodecyl-5,5'-bis(3-dodecylthiophen-2-yl)-[3,3'-bipyrrolylidene]-2,2'(1H,1'H)-dione (4.24)



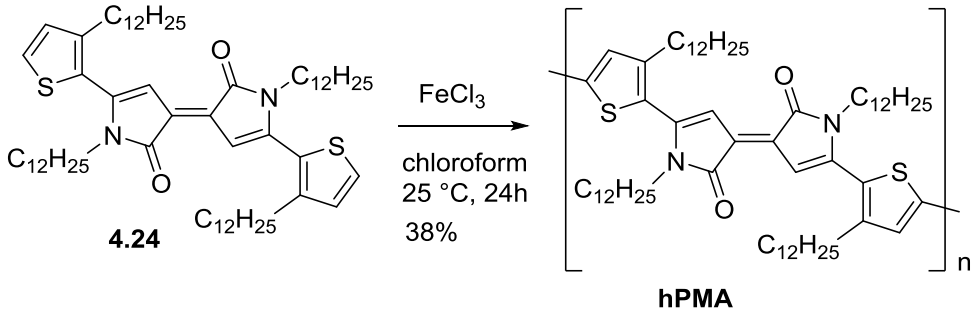
Pechmann dye (**4.18**) (4 g, 6.02 mmol) was dissolved in a chloroform solution (120 mL) containing n-dodecylamine (4.46 g, 24.06 mmol). After stirring over 16 h, additional chloroform (30 mL) and $TsOH \cdot H_2O$ (6.34 g, 33.3 mmol) were added. The dark blue solution reaction mixture was washed with 1 M HCl, saturated aqueous $NaHCO_3$ solution, dried over sodium sulfate, filtered and the solvent was removed under reduced pressure. The residue was subjected to flash chromatography on silica gel using hexane and ethyl acetate as eluent to afford the product (**4.24**) (2.2 g, 37%). ^{1}H NMR (400 MHz, $CDCl_3$): δ 7.40 (d, J = 5.0 Hz, 2H), 7.01 (d, J= 5.1 Hz, 2H), 6.86 (s, 2H), 3.60 (t, J = 7.5 Hz, 4H), 2.68 (t, J= 7.0 Hz, 4H) 1.63 (m, 4H), 1.45 (m, 4H), 1.39-1.09 (m, 72H), 0.90 (m, 12H). MS (MALDI (TOF LD+)) 998.7 Calc. 998.770 Spectroscopic values are in accordance to literature.[241]

5.83 Synthesis of (E)-5,5'-bis(5-bromo-3-dodecylthiophen-2-yl)-1,1'-didodecyl-[3,3'-bipyrrolylidene]-2,2'(1H,1'H)-dione (4.25)



(E)-1,1'-didodecyl-5,5'-bis(3-dodecylthiophen-2-yl)-[3,3'-bipyrrolylidene]-2,2'(1H,1'H)-dione (1 g, 1.0 mmol) was dissolved in anhydrous THF (60 mL) and cooled to -78 °C under Ar. Lithium diisopropylamide (LDA) (5 mL, 10 mmol, 2 M in THF) was added dropwise over the course of 30 min. Dibromotetrachloroethane (3.58 g, 11 mmol) was added in 1 portion and the reaction was stirred for 10 min. Water (20 mL) was added to quench the excess LDA and the reaction mixture was allowed to warm to rt. The reaction mixture was extracted with diethyl ether (3 × 50mL) and brine and the organics were dried over Na_2SO_4, filtered and the solvent was removed under reduced pressure. The residue was purified by column chromatography using hexane : chloroform (6:4) as eluent. The product was obtained as a blue solid (101 mg, 9%). ^{1}H NMR (400 MHz, $CDCl_3$): δ 6.98 (s, 2H), 6.83 (s, 2H), 3.58 (t, J = 6.3 Hz, 4H), 2.62 (t, J = 7.3 Hz, 4H), 1.43 (m, 8H), 1.36-1.07 (m, 72H), 0.87 (t, J = 6.2 Hz, 12H) ^{13}C NMR (101 MHz, $CDCl_3$): δ 170.37, 145.49, 132.32, 114.65, 105.78, 41.06, 32.07, 30.66, 29.80, 29.71, 29.51, 29.24, 26.78, 22.84, 14.27 MALDI (TOF LD+) 1156.5, 1157.0, 1157.5, 1158.0 Calc 1156.5886 (100%), 1157.5919

5.84 Synthesis of hPMA



Suspended $FeCl_3$ (0.065 g, 0.4 mmol) in anhydrous chloroform (25 mL) and degassed under Ar for 15 min. Pechmann dye **(4.24)** (0.1 g, 0.10 mmol) was added and the

reaction mixture was stirred for 24 h at room temperature with a constant stream of Ar blowing over the surface of the reaction mixture to remove any HCl gas generated. The reaction mixture was poured into methanol and filtered through a Soxhlet thimble. The polymer was Soxhlet extracted with methanol acetone, hexane and chloroform for 24 h in each solvent. The chloroform layer was concentrated and the polymer was precipitated into methanol, filtered off and dried under high vacuum to give **hPMA** as a blue solid (38.7 mg, 38%). GPC (chlorobenzene, 80 °C): M_n = 2500 g/mol, M_w = 4400 g/mol PDI = 1.74.

Chapter 6 References

"Copy from one, it's plagiarism; copy from two, it's research."
Wilson Mizner (1876-1933), American Playwright

1. R. L. Hills, *Power from Steam: A history of the stationary steam engine.*, Cambridge University Press, Cambridge, 1989.
2. I. p. o. C. C. (IPCC), *Climate Change 2007: Synthesis report*, 2007.
3. I. P. o. C. C. (IPCC), *Climate Change 2013 The Physical Science Basis*, 2013.
4. R. H. Socolow and S. W. Pacala, *Scientific American*, 2006, **September**, 50-57.
5. Intergovernmental-Panel-On-Climate-Change, 2014.
6. T. Ameri, N. Li and C. J. Brabec, *Energy & Environmental Science*, 2013, **6**, 2390-2413.
7. R. Po, A. Bernardi, A. Calabrese, C. Carbonera, G. Corso and A. Pellegrino, *Energy & Environmental Science*, 2014, **7**, 925-943.
8. N. S. Lewis and D. G. Nocera, *Proceedings of the National Academy of Sciences*, 2006, **103**, 15729-15735.
9. BP, 2013.
10. K. Yasuda and T.Okabe, *JOM*, 2010, **62**, 94-101.
11. M. C. Scharber, D. Mühlbacher, M. Koppe, P. Denk, C. Waldauf, A. J. Heeger and C. J. Brabec, *Advanced Materials*, 2006, **18**, 789-794.
12. S. R. Forrest, *Nature*, 2004, **428**, 911-918.
13. S. R. Forrest, *Chem. Rev.*, 1997, **97**, 1793-1896.
14. N. Espinosa, M. Hosel, D. Angmo and F. C. Krebs, *Energy Environ. Science*, 2012, **5**, 5117-5132.
15. N. Espinosa, R. Garcia-Valverde and F. C. Krebs, *Energy Environ. Science*, 2011, **4**, 1547-1557.
16. D. Yue, P. Khatav, F. You and S. B. Darling, *Energy Environ. Science*, 2012, **5**, 9163-9172.
17. S. B. Darling and F. You, *RSC Adv.*, 2013, **3**, 17633-17648.
18. *U.S department of energy*, 2005, ix, 9, 33.
19. H. E. Katz, Z. N. Bao and S. L. Gilat, *Acc. Chem. Res.*, 2001, **34**, 359-369.
20. M. L. Chabinyc, L. H. Jimison, J. Rivnay and A. Salleo, *MRS Bull.*, 2008, **33**, 683-689.
21. *Oxford Dictionary of English*.
22. P. W. Atkins., *Concepts in Physical Chemistry*, Oxford University Press, Oxford, UK, 1995.
23. L. Fumagalli, M. Binda, D. Natali, M. Sampietro, E. Salmoiraghi and P. Di Gianvincenzo, *J. Appl. Phys.*, 2008, **104**, 084513/084511-084513/084518.
24. R. J. Kline, M. D. McGehee, E. N. Kadnikova, J. Liu, J. M. J. Frechet and M. F. Toney, *Macromolecules*, 2005, **38**, 3312-3319.
25. J.-F. Chang, J. Clark, N. Zhao, H. Sirringhaus, D. W. Breiby, J. W. Andreasen, M. M. Nielsen, M. Giles, M. Heeney and I. McCulloch, *Physical Review B: Condensed Matter and Materials Physics*, 2006, **74**, 115318/115311-115318/115312.
26. J. F. Chang, H. Sirringhaus, M. Giles, M. Heeney and I. McCulloch, *Physical Review B*, 2007, **76**.
27. H. Klauk, *Organic electronics II: More materials and applications*, Wiley VCH, 2012.
28. J.-S. Kim, *Plastic Electronic Materials and Devices lecture notes*, 2009.
29. C. K. Chiang, C. R. Fincher, Y. W. Park, A. J. Heeger, H. Shirakawa, E. J. Louis, S. C. Gau and A. G. MacDiarmid, *Physical Review Letters*, 1977, **39**, 1098.
30. W. Pauli, *Z. Physik*, 1925, **31**, 765.

31. H. Hoppea and N. S. Sariciftci, *J. Mater. Res.*, 2004, **19**, 1924-1945.
32. J. L. Bredas, J. P. Calbert, D. A. d. S. Filho and J. Cornil, *PNAS*, 2002, **99**, 5804-5809.
33. H. Meier, U. Stalmach and H. Kolshorn, *Acta Polmerica*, 1997, **48**, 379-384.
34. T. M. Clarke and J. R. Durrant, *Chemical Reviews*, 2010, **110**, 6736.
35. I. McCulloch, *Synthesis and properties of organic semiconductors lecture notes*, 2009.
36. A. Pron, P. Gawrys, M. Zagorska, D. Djurado and R. Demadrille, *Chemical Society Reviews*, 2010, **39**, 2577-2632.
37. J.-L. Brédas, J. Cornil and A. J. Heeger, *Advanced Materials*, 1996, **8**, 447-452.
38. S. C. Graham, D. D. C. Bradley, R. H. Friend and C. Spangler, *Synthetic Metals*, 1991, **41**, 1277-1280.
39. D. E. Markov, E. Amsterdam, P. W. M. Blom, A. B. Sieval and J. C. Hummelen, *J. Phys. Chem*, 2005, **109**, 5266.
40. R. Koeppe and N. S. Sariciftci, *Photochem. Photobiol. Sci.*, 2006, **5**, 1122-1131.
41. S. Haque, *Molecular Electronic Materials lecture notes*, 2008.
42. I. McCulloch, M. Heeney, C. Bailey, K. Genevicius, I. MacDonald, M. Shkunov, D. Sparrowe, S. Tierney, R. Wagner, W. Zhang, M. L. Chabinyc, R. J. Kline, M. D. McGehee and M. F. Toney, *Nat Mater*, 2006, **5**, 328-333.
43. V. Coropceanu, J. Cornil, D. A. d. S. Filho, Y. Oliver, R. Silbey and J.-L. Bredas, *Chem Rev*, 2007, **107**, 926-952.
44. H. Bronstein, Z. Chen, R. S. Ashraf, W. Zhang, J. Du, J. R. Durrant, P. Shakya Tuladhar, K. Song, S. E. Watkins, Y. Geerts, M. M. Wienk, R. A. J. Janssen, T. Anthopoulos, H. Sirringhaus, M. Heeney and I. McCulloch, *Journal of the American Chemical Society*, 2011, **133**, 3272-3275.
45. J. Zaumseil and H. Sirringhaus, *Chem Rev*, 2007, **107**, 1296-1323.
46. B. C. Thompson and Jean M. J. Fréchet, *Angewandte Chemie International Edition*, 2008, **47**, 58-77.
47. H. Antoniadis, B. R. Hsieh, M. A. Abkowitz, S. A. Jenekhe and M. Stolka, *Synthetic Metals*, 1994, **62**, 265-271.
48. C. W. Tang, *Applied Physics Letters*, 1986, **48**, 183-185.
49. R. Kroon, M. Lenes, J. C. Hummelen, P. W. M. Blom and B. de Boer, *Polymer Reviews*, 2008, **48**, 531 - 582.
50. H. Spanggaard and F. C. Krebs, *Solar Energy Materials and Solar Cells*, 2004, **83**, 125-146.
51. G. Yu, J. Gao, J. C. Hummelen, F. Wudl and A. J. Heeger, *Science*, 1995, **270**, 1789-1791.
52. W. Ma, C. Yang, X. Gong, K. Lee and A. J. Heeger, *Advanced Functional Materials*, 2005, **15**, 1617-1622.
53. H.-Y. Chen, J. Hou, S. Zhang, Y. Liang, G. Yang, Y. Yang, L. Yu, Y. Wu and G. Li, *Nat Photon*, 2009, **3**, 649-653.
54. C. E. Small, S. Chen, J. Subbiah, C. M. Amb, S.-W. Tsang, T.-H. Lai, J. R. Reynolds and F. So, *Nat Photon*, 2009, **6**, 115-120.
55. Yongye Liang, Zheng Xu, Jiangbin Xia, Szu-Ting Tsai, Yue Wu, Gang Li, Claire Ray and L. Yu, *Advanced Materials*, 2010, **22**, 1-4.
56. Z. He, C. Zhong, S. Su, M. Xu, H. Wu and Y. Cao, *Nat Photonics*, 2012, **6**, 591.

57. N. S. Sariciftci, L. Smilowitz, A. J. Heeger and F. Wudl, *Science*, 1992, **258**, 1474.
58. C. J. Brabec, G. Zerza, G. Cerullo, S. D. Silvestri, S. Luzatti, J. C. Hummelen and S. Sariciftci, *Chem. Phys. Lett.*, 2001, **340**, 232.
59. Y.-J. Cheng, S.-H. Yang and C.-S. Hsu, *Chem. Rev.*, 2009, **109**, 5868-5923.
60. J. C. Hummelen, B. W. Knight, F. LePeg and F. Wudl, *J. Org. Chem.*, 1995, **60**, 532.
61. M. M. Wienk, J. M. Kroon, W. J. H. Verhees, J. Knol, J. C. Hummelen, P. A. van Hal and R. A. Janssen, *J. Angew. Chem. Int. Ed*, 2003, **42**, 3371.
62. W. Cao and J. Xue, *Energy & Environmental Science*, 2014.
63. R.Steim, F. R. Kogler and C. J. Brabec, *J. Mater. Chem.*, 2010, **20**, 2499-2512.
64. A. Elschner, F. Bruder, H. W. Heuer, F. Jonas, A. Karbach, S. Kirchmeyer, S. Thurm and R. Wehrmann, *Synthetic Metals*, **2000**, **111-112**, 139-143.
65. T. Wang, A. D. F. Dunbar, P. A. Staniec, A. J. Pearson, P. E. Hopkinson, J. E. MacDonald, S. Lilliu, C. Pizzey, N. J. Terrill, A. M. Donald, A. J. Ryan, R. A. L. Jones and D. G. Lidzey, *Soft Matter*, 2010, **6**, 4128-4134.
66. W. Y. Huang, S. Matsuoka, T. K. Kwei and Y. Okamoto, *Macromolecules*, 2001, **34**, 7166-7171.
67. E. Bundgaard and F. C. Krebs, *Solar Energy Materials and Solar Cells*, 2007, **91**, 954-985.
68. S. H. Park, A. Roy, S. Beaupre, S. Cho, N. Coates, J. S. Moon, D. Moses, M. Leclerc, K. Lee and A. J. Heeger, *Nat Photon*, 2009, **3**, 297-302.
69. T. Salim, L. H. Wong, B. Brauer, R. Kukreja, Y. L. Foo, Z. Bao and Y. M. Lam, *Journal of Materials Chemistry*, 2011, **21**, 242-250.
70. G. Griffini, J. D. Douglas, C. Piliego, T. W. Holcombe, S. Turri, J. M. J. Fréchet and J. L. Mynar, *Advanced Materials*, 2011, **23**, 1660-1664.
71. Z. Li, H. C. Wong, Z. Huang, H. Zhong, C. H. Tan, W. C. Tsoi, J. S. Kim, J. R. Durrant and J. T. Cabral, *Nat Commun*, 2013, **4**.
72. Y. S. Eo, H. W. Rhee, B. D. Chin and J.-W. Yu, *Synthetic Metals*, 2009, **159**, 1910-1913.
73. M. W. Rowell, M. A. Topinka, M. D. McGehee, H.-J. r. Prall, G. Dennler, N. S. Sariciftci, L. Hu and G. Gruner, 2006, pp. -.
74. J. Zhang, L. Gao, J. Sun, Y. Liu, Y. Wang and J. Wang, *Diamond and Related Materials*, 2012, **22**, 82-87.
75. J.-M. Yun, J.-S. Yeo, J. Kim, H.-G. Jeong, D.-Y. Kim, Y.-J. Noh, S.-S. Kim, B.-C. Ku and S.-I. Na, *Advanced Materials*, 2011, **23**, 4923-4928.
76. H. Pei, G. Cheng, C. Qingyu and G. Xiaojun, in *Communications and Photonics Conference and Exhibition, 2011. ACP. Asia*, 2011, pp. 1-4.
77. M. P. de Jong, L. J. van Ijzendoorn and M. J. A. de Voigt, *Applied Physics Letters*, 2000, **77**, 2255-2257.
78. T. Kristofer, A. Viktor, Z. Fengling and I. Olle, *Applied Physics Letters*, 2007, **91**, 123514.
79. X. Li, W. C. H. Choy, L. Huo, F. Xie, W. E. I. Sha, B. Ding, X. Guo, Y. Li, J. Hou, J. You and Y. Yang, *Advanced Materials*, 2012, **24**, 3046-3052.
80. G. Li, R. Zhu and Y. Yang, *Nat. Photonics*, 2012, **6**, 153-161.
81. J. You, L. Dou, K. Yoshimura, T. Kato, K. Ohya, T. Moriarty, K. Emery, C.-C. Chen, J. Gao, G. Li and Y. Yang, *Nat. Commun*, 2013, **4**, 1446.
82. P. W. M. Blom, V. D. Mihailetchi, L. J. A. Koster and D. E. Markov, *Advanced Materials*, 2007, **19**, 1551-1566.

83. P. Horowitz and W. Hill, *The Art of Electronics 2nd Ed.* , Cambridge University Press, 1990.
84. G. H. Gelinck, H. E. A. Huitema, E. van Veenendaal, E. Cantatore, L. Schrijnemakers, J. B. P. H. van der Putten, T. C. T. Geuns, M. Beenhakkers, J. B. Giesbers, B.-H. Huisman, E. J. Meijer, E. M. Benito, F. J. Touwslager, A. W. Marsman, B. J. E. van Rens and D. M. de Leeuw, *Nat Mater*, 2004, **3**, 106-110.
85. H. Sirringhaus, *Advanced Materials*, 2005, **17**, 2411-2425.
86. D. J. Gundlach, J. E. Royer, S. K. Park, S. Subramanian, O. D. Jurchescu, B. H. Hamadani, A. J. Moad, R. J. Kline, L. C. Teague, O. Kirillov, C. A. Richter, J. G. Kushmerick, L. J. Richter, S. R. Parkin, T. N. Jackson and J. E. Anthony, *Nat Mater*, 2008, **7**, 216-221.
87. A. Facchetti, M. H. Yoon and T. J. Marks, *Advanced Materials*, 2005, **17**, 1705-1725.
88. H. Peisert, M. Knupfer and J. Fink, *Applied Physics Letters*, 2002, **81**, 2400-2402.
89. J.-P. Hong, A.-Y. Park, S. Lee, J. Kang, N. Shin and D. Y. Yoon, *Applied Physics Letters*, 2008, **92**, 143311.
90. A. Dodabalapur, L. Torsi and H. E. Katz, *Science*, 1995, **268**, 270-271.
91. I. McCulloch, M. Heeney, C. Bailey, K. Genevicius, I. Macdonald, M. Shkunov, D. Sparrowe, S. Tierney, R. Wagner, W. Zhang, M. L. Chabinyc, R. J. Kline, M. D. Mcgehee and M. F. Toney, *Nat Mater*, 2005, **5**, 328-333.
92. R. J. Kline, M. D. McGehee, E. N. Kadnikova, J. Liu and J. M. J. Fréchet, *Advanced Materials*, 2003, **15**, 1519-1522.
93. A. Zen, J. Pflaum, S. Hirschmann, W. Zhuang, F. Jaiser, U. Asawapirom, J. P. Rabe, U. Scherf and D. Neher, *Advanced Functional Materials*, 2004, **14**, 757-764.
94. R. Pokrop, J.-M. Verilhac, A. Gasior, I. Wielgus, M. Zagorska, J.-P. Travers and A. Pron, *Journal of Materials Chemistry*, 2006, **16**, 3099-3106.
95. J.-M. Verilhac, R. Pokrop, G. LeBlevennec, I. Kulszewicz-Bajer, K. Buga, M. Zagorska, S. Sadki and A. Pron, *The Journal of Physical Chemistry B*, 2006, **110**, 13305-13309.
96. C. Jui-Fen, C. Jenny, Z. Ni, S. Henning, W. B. Dag, W. A. Jens, M. N. Martin, G. Mark, H. Martin and M. Iain, *Physical Review B (Condensed Matter and Materials Physics)*, 2006, **74**, 115318.
97. M. Brinkmann and P. Rannou, *Advanced Functional Materials*, 2007, **17**, 101-108.
98. B. D. Olsen, S.-Y. Jang, J. M. Luning and R. A. Segalman, *Macromolecules*, 2006, **39**, 4469-4479.
99. M. Urien, G. Wantz, E. Cloutet, L. Hirsch, P. Tardy, L. Vignau, H. Cramail and J.-P. Parneix, *Organic Electronics*, 2007, **8**, 727-734.
100. A. P. Kulkarni, X. Kong and S. A. Jenekhe, *The Journal of Physical Chemistry B*, 2004, **108**, 8689-8701.
101. C. Chunyan, I. Chan, E. Volker, Z. Andreas, L. Günter and W. Gerhard, *Chemistry - A European Journal*, 2005, **11**, 6833-6845.
102. E. J. W. List, R. Guentner, P. S. d. Freitas and U. Scherf, *Advanced Materials*, 2002, **14**, 374-378.
103. J. Fan, J. D. Yuen, M. Wang, J. Seifter, J.-H. Seo, A. R. Mohebbi, D. Zakhidov, A. Heeger and F. Wudl, *Advanced Materials*, 2012, **24**, 2186-2190.

104. N. Blouin, A. Michaud, D. Gendron, S. Wakim, E. Blair, R. Neagu-Plesu, M. Belletete, G. Durocher, Y. Tao and M. Leclerc, in *J. Am. Chem. Soc*, **2008**, pp. 732-742.
105. D. M. de Leeuw, M. M. J. Simenon, A. R. Brown and R. E. F. Einerhand, *Synthetic Metals*, 1997, **87**, 53-59.
106. M. S. Chen, J. R. Niskala, D. A. Unruh, C. K. Chu, O. P. Lee and J. M. J. Fréchet, *Chemistry of Materials*, 2013, **25**, 4088-4096.
107. I. McCulloch, R. S. Ashraf, L. Biniek, H. Bronstein, C. Combe, J. E. Donaghey, D. I. James, C. B. Nielsen, B. C. Schroeder and W. Zhang, *Accounts of Chemical Research*, 2012, **45**, 714-722.
108. J.-S. Kim, L. Lu, P. Sreearunothai, A. Seeley, K.-H. Yim, A. Petrozza, C. E. Murphy, D. Beljonne, J. r. m. Cornil and R. H. Friend, *Journal of the American Chemical Society*, 2008, **130**, 13120-13131.
109. M. Iain, H. Martin, L. C. Michael, D. Dean, R. J. Kline, C. Michael, D. Warren, F. Daniel, G. David, H. Behrang, H. Rick, R. Lee, S. Alberto, S. Maxim, S. David, T. Steven and Z. Weimin, *Advanced Materials*, 2009, **21**, 1091-1109.
110. H. Bronstein, D. S. Leem, R. Hamilton, P. Woebkenberg, S. King, W. M. Zhang, R. S. Ashraf, M. Heeney, T. D. Anthopoulos, J. d. Mello and I. McCulloch, *Macromolecules*, 2011, **44**, 6649-6652.
111. Z. Bao and A. J. Lovinger, *Chemistry of Materials*, 1999, **11**, 2607-2612.
112. A. Babel and S. A. Jenekhe, *Synthetic Metals*, 2005, **148**, 169-173.
113. A. Zen, M. Saphiannikova, D. Neher, U. Asawapirom and U. Scherf, *Chemistry of Materials*, 2005, **17**, 781-786.
114. I. Meager, R. S. Ashraf, S. Mollinger, B. C. Schroeder, H. Bronstein, D. Beatrup, M. S. Vezie, T. Kirchartz, A. Salleo, J. Nelson and I. McCulloch, *Journal of the American Chemical Society*, 2013, **135**, 11537-11540.
115. J. E. Anthony, M. Heeney and B. S. Ong, *MRS Bulletin*, 2008, **33**, 698.
116. H. Becker, H. Spreitzer, W. Kreuder, E. Kluge, H. Schenk, I. Parker and Y. Cao, *Advanced Materials*, 2000, **12**, 42-48.
117. G. Sabouraud, S. Sadki and N. Brodie, *Chemical Society Reviews*, 2000, **29**, 283-293.
118. N. Toshima and S. Hara, *Progress in Polymer Science*, 1995, **20**, 155-183.
119. R. S. Loewe, P. C. Ewbank, J. Liu, L. Zhai and R. D. McCullough, *Macromolecules*, 2001, **34**, 4324-4333.
120. Y.-J. Cheng and T.-Y. Luh, *Journal of Organometallic Chemistry*, 2004, **689**, 4137-4148.
121. J. Peet, J. Y. Kim, N. E. Coates, W. L. Ma, D. Moses, A. J. Heeger and G. C. Bazan, *Nat Mater*, 2007, **6**, 497-500.
122. Y. Zhang, J. Zou, H.-L. Yip, Y. Sun, J. A. Davies, K.-S. Chen, O. Acton and A. K.-Y. Jen, *J. Mater. Chem.*, 2011, **21**, 3895.
123. D. Mühlbacher, M. Scharber, M. Morana, Z. Zhu, D. Waller, R. Gaudiana and C. Brabec, *Advanced Materials*, 2006, **18**, 2884-2889.
124. S.-H. Chan, C.-P. Chen, T.-C. Chao, C. Ting, C.-S. Lin and B.-T. Ko, *Macromolecules*, 2008, **41**, 5519-5526.
125. G. Wang, J. Swensen, D. Moses and A. J. Heeger, *Journal of Applied Physics*, 2003, **93**, 6137-6141.
126. G. Zhao, Y. He and Y. Li, *Advanced Materials*, 2010, **22**, 4355-4358.

127. O. G. Reid, J. A. N. Malik, G. Latini, S. Dayal, N. Kopidakis, C. Silva, N. Stingelin and G. Rumbles, *Journal of Polymer Science Part B: Polymer Physics*, 2012, **50**, 27-37.
128. Y.-K. Lan and C.-I. Haung, *The Journal of Physical Chemistry B*, 2009, **113**, 14555-14564.
129. J. Peet, M. L. Senatore, A. J. Heeger, H. Geiger and G. C. Bazan, *Advanced Materials*, 2009, **21**, 1521-1527.
130. R. Zhang, B. Li, M. C. Iovu, M. Jeffries-EL, G. Sauvé, J. Cooper, S. Jia, S. Tristram-Nagle, D. M. Smilgies, D. N. Lambeth, R. D McCullough and T. Kowaelewski, *Journal of the American Chemical Society*, 2006, **128**, 3480-3481.
131. J. Roncali, *Macromol. Rapid Commun.*, 2007, **28**, 1761-1775.
132. M. Forster, K. O. Annan and U. Scherf, *Macromolecules*, 1999, **32**, 3159-3162.
133. J. L. Brédas, J. P. Calbert, D. A. d. S. Filho and J. Cornil, *Proc. Natl. Acad. Sci. USA*, 2002, **99**, 5804-5809.
134. Y. Liang, Y. Wu, D. Feng, S.-T. Tsai, H.-J. Son, G. Li and L. Yu, *Journal of the American Chemical Society*, 2009, **131**, 56-57.
135. S. Ando, J.-I. Nishida, H. Tada, Y. Inoue, S. Tokito and Y. Yamashita, *Journal of the American Chemical Society*, 2005, **127**, 5336-5337.
136. N.-S. Baek, S. K. Hau, H.-L. Yip, O. Acton, K.-S. Chen and A. K.-Y. Jen, *Chem. Mater*, 2008, **20**, 5734-5736.
137. W. M. Zhang, J. Smith, S. E. Watkins, R. Gysel, M. McGehee, A. Salleo, J. Kirkpatrick, S. Ashraf, T. Anthopoulous, M. Heeney and I. McCulloch, *Journal of the American Chemical Society*, 2010, **132**, 11437-11439.
138. X. Zhang, H. Bronstein, A. J. Kronemeijer, J. Smith, Y. Kim, R. J. Kline, L. J. Richter, T. D. Anthopoulos, H. Sirringhaus, K. Song, M. Heeney, W. Zhang, I. McCulloch and D. M. DeLongchamp, *Nat. Comm.*, 2013, **4**.
139. W. Zhang, J. Smith, S. E. Watkins, R. Gysel, M. McGehee, A. Salleo, J. Kirkpatrick, S. Ashraf, T. Anthopoulos, M. Heeney and I. McCulloch, *Journal of the American Chemical Society*, 2010, **132**, 11437-11439.
140. S.-H. Chan, Y.-S. Hsiao, L.-I. Hung, G.-W. Hwang, H.-L. Chen, C. Ting and C.-P. Chen, *Macromolecules*, 2010, **43**, 3399-3405.
141. Y.-C. Chen, C.-Y. Yu, Y.-L. Fan, L.-I. Hung, C.-P. Chen and C. Ting, *Chemical Communications*, 2010, **46**, 6503-6505.
142. L. Biniek, C. L. Chochos, N. Leclerc, G. Hadziioannou, J. K. Kallitsis, R. Bechara, P. Lévêque and T. Heiser, *J. Mater. Chem.*, 2009, **19**, 4946-4951.
143. L. Biniek, C. L. Chochos, G. Hadziioannou, N. Leclerc, P. Lévêque and T. Heiser, *Macromol. Rapid Commun*, 2010, **31**, 651-656.
144. L. Biniek, S. Fall, C. L. Chochos, D. V. Anokhin, D. A. Ivanov, N. Leclerc, P. Lévêque and T. Heiser, *Macromolecules*, 2010, **43**, 9779-9786.
145. X. Zhang, M. Köhler and A. J. Matzger, *Macromolecules*, 2004, **37**, 6306-6315.
146. L. S. Miguel and A. J. Matzger, *Macromolecules*, 2007, **40**, 9233-9237.
147. P. Liu, Y. Wu, H. Pan, Y. Li, S. Gardner, B. S. Ong and S. Zhu, *Chemistry of Materials*, 2009, **21**, 2727-2732.
148. Lidaris San Miguel, William W. Porter III and A. J. Matzger*, *Org. Lett.*, 2007, **9**, 1005-1008.
149. B. S. Furniss, A. J. Hannaford, P. W. G. Smith and A. R. Tatchell, *Vogel's Textbook of Practical Organic Chemistry*, John Wiley & Sons, Inc, 1994.

150. A. Yoshio, I. Yutaka, U. Masashi and U. Masato, in *WO2012JP52018 20120130* ed. W. J. 20120130, WO2012JP52018 20120130
151. S. Van Mierloo, P. J. Adriaensens, W. Maes, L. Lutsen, T. J. Cleij, E. Botek, B. Champagne and D. J. Vanderzande, *The Journal of Organic Chemistry*, 2010, **75**, 7202-7209.
152. R. K. Haynes, S. C. Vonwiller and M. R. Luderer, in *Encyclopedia of Reagents for Organic Synthesis*, John Wiley & Sons, Ltd, 2001.
153. H. Bronstein, R. S. Ashraf, Y. Kim, A. J. P. White, T. Anthopoulos, K. Song, D. James, W. Zhang and I. McCulloch, *Macromolecular Rapid Communications*, 2011, **32**, 1664-1668.
154. S.-H. Chan, C.-P. Chen, T.-C. Chao, C. Ting, C.-S. Lin and B.-T. Ko, *Macromolecules*, 2008, **41**, 5519-5526.
155. Y.-C. Chen, C.-Y. Yu, Y.-L. Fan, L.-I. Hung, C.-P. Chen and C. Ting, *Chemical Communications*, 2010, **46**, 6503-6505.
156. W. L. Leong, G. C. Welch, L. G. Kaake, C. J. Takacs, Y. Sun, G. C. Bazan and A. J. Heeger, *Chemical Science*, 2012, **3**, 2103-2109.
157. W. R. Mateker, J. D. Douglas, C. Cabanetos, I. T. Sachs-Quintana, J. A. Bartelt, E. T. Hoke, A. El Labban, P. M. Beaujuge, J. M. J. Frechet and M. D. McGehee, *Energy & Environmental Science*, 2013, **6**, 2529-2537.
158. K. T. Nielsen, K. Bechgaard and F. C. Krebs, *Macromolecules*, 2005, **38**, 658-659.
159. M. M. Erwin, J. McBride, A. V. Kadavanich and S. J. Rosenthal, *Thin Solid Films*, 2002, **409**, 198-205.
160. K.-S. Chen, Y. Zhang, H.-L. Yip, Y. Sun, J. A. Davies, C. Ting, C.-P. Chen and A. K. Y. Jen, *Organic Electronics*, 2011, **12**, 794-801.
161. Y.-J. Cheng, C.-H. Chen, T.-Y. Lin and C.-S. Hsu, *Chem. Asian J.*, 2012, **7**, 818-825.
162. X. Shi, J. Chang and C. Chi, *Chem. Comm.*, 2013, **49**, 7135.
163. M.Seefelder, *Indigo in Culture, Science and Technology*, Ecomed, Landsberg, Germany, 1994.
164. E. D. Glowacki, L. Leonat, G. Voss, M.-A. Bodea, Z. Bozkurt, A. M. Ramil, M. Irimia-Vladu, S. Bauer and N. S. Sariciftci, *AIP Advances*, 2011, **1**, 042132-042131 - 042132-042136.
165. A. Wahl, *Bulletin de la Société Chimique de France*, 1910, **5**, 1039.
166. T. Maugard, E. Enaud, P. Choisy and M. D. Legoy, *Phytochemistry*, 2001, **58**, 897-904.
167. H. v. Eller-Pandraud, *Acta Crystallogr*, 1960, **13**, 936-938.
168. Y. Mao-Sen, F. Qi, J. Lei and Y. Wen-Tao, *Acta Crystallogr., Sect.E: Struct. Rep. Online*, 2007, **63**, o4342.
169. Yu. K. Voronina, D. B. Krivolapov, A. V. Bogdanov, V. F. Mironov and I. A. Litvinov, *Journal of Structural Chemistry*, 2012, **53**, 413-416.
170. J. Mei, K. R. Graham, R. Stalder and J. R. Reynolds, *Organic Letters*, 2010, **12**, 660-663.
171. R. Stalder, J. Mei and J. R. Reynolds, *Macromolecules*, 2010, **43**, 8348-8352.
172. E. Wang, Z. Ma, Z. Zhang, P. Henriksson, O. Inganäs, F. Zhang and M. R. Andersson, *Chemical Communications*, 2011, **47**, 4908-4910.
173. E. Wang, Z. Ma, Z. Zhang, K. Vandewal, P. Henriksson, O. Inganäs, F. Zhang and M. R. Andersson, *Journal of the American Chemical Society*, 2011, **133**, 14244-14247.

174. O. Gidron, Y. Diskin-Posner and M. Bendikov, *Journal of the American Chemical Society*, 2010, **132**, 2148-2150.
175. U. H. F. Bunz, *Angewandte Chemie International Edition*, 2010, **49**, 5037-5040.
176. A. T. Yiu, P. M. Beaujuge, O. P. Lee, C. H. Woo, M. F. Toney and J. M. J. Fréchet, *Journal of the American Chemical Society*, 2012, **134**, 2180-2185.
177. M. S. Chen, O. P. Lee, J. R. Niskala, A. T. Yiu, C. J. Tassone, K. Schmidt, P. M. Beaujuge, S. S. Onishi, M. F. Toney, A. Zettl and J. M. J. Fréchet, *Journal of the American Chemical Society*, 2013.
178. B. Classon, Z. Liu and B. Samuelsson, *J. Org. Chem.*, 1988, **53**, 6126-6130.
179. Z. Ma, E. Wang, M. E. Jarvid, P. Henriksson, O. Inganäs, F. Zhanga and M. R. Andersson, *J. Mater. Chem.*, 2012, **22**, 2306.
180. J. K. Park, J. Jo, J. H. Seo, J. S. Moon, Y. D. Park, K. Lee, A. J. Heeger and G. C. Bazan, *Advanced Materials*, 2011, **23**, 2430-2435.
181. M. P. Nikiforov, B. Lai, W. Chen, S. Chen, R. D. Schaller, J. Strzalka, J. Maser and S. B. Darling, *Energy & Environmental Science*, 2013, **6**, 1513-1520.
182. B. C. Schroeder, C. B. Nielsen, Y. J. Kim, J. Smith, Z. Huang, J. Durrant, S. E. Watkins, K. Song, T. D. Anthopoulos and I. McCulloch, *Chemistry of Materials*, 2011, **23**, 4025-4031.
183. C.-C. Ho, S.-Y. Chang, T.-C. Huang, C.-A. Chen, H.-C. Liao, Y.-F. Chen and W.-F. Su, *Polymer Chemistry*, 2013, **DOI 10.1039/C3PY00119A**.
184. J. S. Kim, J. H. Lee, J. H. Park, C. Shim, M. Sim and K. Cho, *Advanced Functional Materials*, 2010, **21**, 480-486.
185. J. Kirkpatrick, C. B. Nielsen, W. Zhang, H. Bronstein, R. S. Ashraf, M. Heeney and I. McCulloch, *Adv. Energy Mater.*, 2012, **2**, 260-265.
186. H. Bronstein, M. Hurhangee, E. C. Fregoso, D. Beatrup, Y. W. Soon, Z. Huang, A. Hadipour, P. S. Tuladhar, S. Rossbauer, E.-H. Sohn, S. Shoaee, S. D. Dimitrov, J. M. Frost, R. S. Ashraf, T. Kirchartz, S. E. Watkins, K. Song, T. Anthopoulos, J. Nelson, B. P. Rand, J. R. Durrant and I. McCulloch, *Chemistry of Materials*, 2013, **25**, 4239-4249.
187. P. P. Boix, M. M. Wienk, R. A. J. Janssen and G. Garcia-Belmonte, *The Journal of Physical Chemistry C*, 2011, **115**, 15075-15080.
188. R. S. Ashraf, A. J. Kronemeijer, D. I. James, H. Sirringhaus and I. McCulloch, *Chemical Communications*, 2012, **48**, 3939-3941.
189. G. Kim, A. R. Han, H. R. Lee, J. Lee, J. H. Oh and C. Yang, *Chemical Communications*, 2013, **50**, 2180-2183.
190. W. Hong, B. Sun, H. Aziz, W.-T. Park, Y.-Y. Noh and Y. Li, *Chemical Communications*, 2012, **48**, 8413-8415.
191. H. Sirringhaus, *Advanced Materials*, 2009, **21**, 3859-3873.
192. L.-L. Chua, J. Zaumseil, J.-F. Chang, E. C. W. Ou, P. K. H. Ho, H. Sirringhaus and R. H. Friend, *Nature*, 2005, **434**, 194-199.
193. Z. Chen, M. J. Lee, R. Shahid Ashraf, Y. Gu, S. Albert-Seifried, M. Meedom Nielsen, B. Schroeder, T. D. Anthopoulos, M. Heeney, I. McCulloch and H. Sirringhaus, *Advanced Materials*, 2011, **24**, 647-652.
194. T. L. Nelson, T. M. Young, J. Liu, S. P. Mishra, J. A. Belot, C. L. Balliet, A. E. Javier, T. Kowalewski and R. D. McCullough, *Advanced Materials*, 2010, **22**, 4617-4621.

195. C. L. Donley, J. Zaumseil, J. W. Andreasen, M. M. Nielsen, H. Sirringhaus, R. H. Friend and J.-S. Kim, *Journal of the American Chemical Society*, 2005, **127**, 12890-12899.
196. I. A. Liversedge, S. J. Higgins, M. Giles, M. Heeney and I. McCulloch, *Tetrahedron Letters*, 2006, **47**, 5143-5146.
197. R. S. Ashraf, B. C. Schroeder, H. A. Bronstein, Z. Huang, S. Thomas, R. J. Kline, C. J. Brabec, P. Rannou, T. D. Anthopoulos, J. R. Durrant and I. McCulloch, *Advanced Materials*, 2013, **25**, 2029-2034.
198. G. W. P. V. Pruissen, F. Gholamrezaie, M. M. Wienk and R. e. A. J. Janssen, *J. Mater. Chem.*, 2012, **22**, 20387.
199. T. Lei, Y. Cao, Y. Fan, C.-J. Liu, S.-C. Yuan and J. Pei, *J. Am. Chem. Soc*, 2011, **133**, 6099-6101.
200. T. Lei, Y. Cao, X. Zhou, Y. Peng, J. Bian and J. Pei, *Chem. Mater.*, 2012, **24**, 1762-1770.
201. R. Stalder, J. Mei, J. Subbiah, C. Grand, L. A. Estrada, F. So and J. R. Reynolds, *Macromolecules*, 2011, **44**, 6303-6310.
202. P. Sonar, H.-S. Tan, S. Sun, Y. M. Lam and A. Dodabalapur, *Polymer Chemistry*, 2013, **4**, 1983-1994.
203. G. Zhang, Y. Fu, Z. Xie and Q. Zhang, *Macromolecules*, 2011, **44**, 1414-1420.
204. K. H. Hendriks, G. H. L. Heintges, V. S. Gevaerts, M. M. Wienk and R. A. J. Janssen, *Angewandte Chemie*, 2013, **125**, 8499-8502.
205. J.-M. Jiang, H.-C. Chen, H.-K. Lin, C.-M. Yu, S.-C. Lan, C.-M. Liu and K.-H. Wei, *Polymer Chemistry*, 2013, **4**, 5321-5328.
206. J. Zhou, S. Xie, E. F. Amond and M. L. Becker, *Macromolecules*, 2013, **46**, 3391-3394.
207. B. Burkhart, P. P. Khlyabich and B. C. Thompson, *Macromolecular Chemistry and Physics*, 2012, **214**, 681-690.
208. G. Zhang, Y. Fu, L. Qiu and Z. Xie, *Polymer*, 2012, **53**, 4407-4412.
209. B. Burkhart, P. P. Khlyabich and B. C. Thompson, *ACS Macro Letters*, 2012, **1**, 660-666.
210. T. E. Kang, H.-H. Cho, H. j. Kim, W. Lee, H. Kang and B. J. Kim, *Macromolecules*, 2013, **46**, 6806-6813.
211. Z. Zhu, D. Waller, R. Gaudiana, M. Morana, D. Muhlbacher, M. Scharber and C. Brabec, *Macromolecules*, 2007, **40**, 1981-1986.
212. M.-C. Yuan, M.-Y. Chiu, C.-M. Chiang and K.-H. Wei, *Macromolecules*, 2010, **43**, 6270-6277.
213. J. Li, K.-H. Ong, P. Sonar, S.-L. Lim, G.-M. Ng, H.-K. Wong, H.-S. Tan and Z.-K. Chen, *Polymer Chemistry*, 2013, **4**, 804-811.
214. C. B. Nielsen, R. S. Ashraf, B. C. Schroeder, P. D'Angelo, S. E. Watkins, K. Song, T. D. Anthopoulos and I. McCulloch, *Chemical Communications*, 2012, **48**, 5832-5834.
215. Y. Lin, H. Fan, Y. Li and X. Zhan, *Advanced Materials*, 2012, **24**, 3087-3106.
216. M. Al-Hashimi, J. G. Labram, S. Watkins, M. Motevalli, T. D. Anthopoulos and M. Heeney, *Organic Letters*, 2010, **12**, 5478-5481.
217. M. W. Hooper, M. Utsunomiya and J. F. Hartwig, *The Journal of Organic Chemistry*, 2003, **68**, 2861-2873.
218. T. Heinrich, H. Koolman and M. Reggelin, *Synthesis*, 2010, **18**, 3152-3162.
219. A. Padwa, S. K. Bur and H. Zhang, *The Journal of Organic Chemistry*, 2005, **70**, 6833-6841.

220. Q. Zeng, J. G. Allen, M. P. Bourbeau, X. Wang, G. Yao, S. Tadesse, J. T. Rider, C. C. Yuan, F.-T. Hong, M. R. Lee, S. Zhang, J. A. Lofgren, D. J. Freeman, S. Yang, C. Li, E. Tominey, X. Huang, D. Hoffman, H. K. Yamane, C. Fotsch, C. Dominguez, R. Hungate and X. Zhang, *Bioorganic & Medicinal Chemistry Letters*, 2010, **20**, 1559-1564.
221. D. M. Shendage, R. FrÃ¶hlich and G. n. Haufe, *Organic Letters*, 2004, **6**, 3675-3678.
222. S. Routier, L. Saugé, N. Ayerbe, G. Coudert and J.-Y. Mérour, *Tetrahedron Letters*, 2002, **43**, 589-591.
223. T. Kimura, D. Shuto, Y. Hamada, N. Igawa, S. Kasai, P. Liu, K. Hidaka, T. Hamada, Y. Hayashi and Y. Kiso, *Bioorganic & Medicinal Chemistry Letters*, 2005, **15**, 211-215.
224. J. Wang, Y.-L. Liang and J. Qu, *Chemical Communications*, 2009, 5144-5146.
225. A. Padwa, M. A. Brodney, S. M. Lynch, P. Rashatasakhon, Q. Wang and H. Zhang, *The Journal of Organic Chemistry*, 2004, **69**, 3735-3745.
226. J. A. Stafford, M. F. Brackeen, D. S. Karanewsky and N. L. Valvano, *Tetrahedron Letters*, 1993, **34**, 7873-7876.
227. S. Kiren, X. Hong, C. A. Leverett and A. Padwa, *Tetrahedron*, 2009, **65**, 6720-6729.
228. F. Johnson and W. A. Nasutavicus, *The Journal of Organic Chemistry*, 1963, **28**, 1877-1883.
229. H.-Q. Liu, W. Wang, W. De-Cai, O. Fei and Ping-Kai, *Chinese Chemical Letters*, 2013, **24**, 929-933.
230. J. V. Metzger, *The Chemistry of Heterocyclic Compounds, Thiazole and Its Derivatives*, Wiley, 2009.
231. T. P. Heffron, B. Wei, A. Olivero, S. T. Staben, V. Tsui, S. Do, J. Dotson, A. J. Folkes, P. Goldsmith, R. Goldsmith, J. Gunzner, J. Lesnick, C. Lewis, S. Mathieu, J. Nonomiya, S. Shuttleworth, D. P. Sutherlin, N. C. Wan, S. Wang, C. Wiesmann and B.-Y. Zhu, *Journal of Medicinal Chemistry*, 2011, **54**, 7815-7833.
232. B. Li, M. Berliner, R. Buzon, C. K. F. Chiu, S. T. Colgan, T. Kaneko, N. Keene, W. Kissel, T. Le, K. R. Leeman, B. Marquez, R. Morris, L. Newell, S. Wunderwald, M. Witt, J. Weaver, Z. Zhang and Z. Zhang, *The Journal of Organic Chemistry*, 2006, **71**, 9045-9050.
233. S. Barth and F. Effenberger, *Tetrahedron: Asymmetry*, 1993, **4**, 823-833.
234. A. R. Murphy, J. M. J. Fréchet, P. Chang, J. Lee and V. Subramanian, *Journal of the American Chemical Society*, 2004, **126**, 1596-1597.
235. S. R. G, *US4382143 (A)*, 1983, 1-14.
236. C. Mikhail, C. Sultan, F. Robert, F. Jianmin, K. Rajender, L. Shifeng, R. Vandna, S. B. Mehran, S. Jianyu and S. Serguei, *WO2008046082 (A2)*, 2008.
237. N. Bodor, M. J. S. Dewar and A. J. Harget, *J. Am. Chem. Soc*, 1970, **92**, 2929-2936.
238. A. R. Lingham, T. J. Rook and H. M. Hugel, *Aust. J. Chem.*, 2002, **55**, 795-798.
239. E. Kvavadze, O. Bar-Yosef, A. Belfer-Cohen, E. Boaretto, N. Jakeli, Z. Matskevich and T. Meshveliani, *Science*, 2009, **325**, 1359.
240. W. H. Perkin, *Journal of the Chemical Society, Transactions*, 1879, **35**, 717-732.
241. E. A. B. Kantchev, T. B. Norsten, M. L. Y. Tan, J. J. Y. Ng and M. B. Sullivan, *Chem. Eur. J*, 2012, **18**, 695-708.

242. H. Zollinger, *Colour Chemistry: Syntheses, Properties, and Applications of Organic Dyes and Pigments*, Wiley-VCH, 2003.
243. W. Wu, Y. Liu and D. Zhu, *Chemical Society Reviews*, 2010, **39**, 1489-1502.
244. Y. Li, P. Sonar, L. Murphy and W. Hong, *Energy & Environmental Science*, 2013, **6**, 1684-1710.
245. E. Wang, W. Mammo and M. R. Andersson, *Advanced Materials*, 2014, **26**, 1801-1826.
246. Y. Kim and E. Lim, *Polymers*, 2014, **6**, 382-407.
247. H. v. Pechmann, *Ber. Dtsch. Chem. Ges.*, 1882, **15**, 881-892.
248. M. T. Bogert and J. J. Ritter, *Journal of the American Chemical Society*, 1924, **46**, 2871-2878.
249. H. Irikawa and N. Adachi, *Heterocycles*, 2000, **53**, 135-142.
250. H. Hashimoto, K. Shiratori, K. Kawakita, T. Tanaka, R. Sekine and H. Irikawa, *Heterocycles*, 2005, **65**, 1385-1392.
251. T. B. Norsten, E. A. B. Kantchev and M. B. Sullivan, *Organic Letters*, 2010, **12**, 4816-4819.
252. J.-C. Flores, U. Berens, F. Bienewald, H. J. Kirner and M. Turbiez, WO 2009 / 053291 PCT / EP2008 / 063919.
253. A. A. El-Shehawy, N. I. Abdo, A. A. El-Barbary and J.-S. Lee, *Tetrahedron Letters*, **51**, 4526-4529.
254. H. Fukumoto, Y. Omori and T. Yamamoto, *Polymer Journal*, 2013, **45**, 462-465.
255. H. Lee and G.-Y. Jung, *Microelectronic Engineering*, 2004, **77**, 168-174.
256. Z. Cai, Y. Guo, S. Yang, Q. Peng, H. Luo, Z. Liu, G. Zhang, Y. Liu and D. Zhang, *Chemistry of Materials*, 2013, **25**, 471-478.
257. A. Yassar, F. Garnier, F. Deloffre, G. Horowitz and L. Ricard, *Advanced Materials*, 1994, **6**, 660.
258. M. Sato, A. Asami, G. Maruyama, M. Kosuge, J. Nakayama, S. Kumakura, T. Fujihara and K. Unoura, *Journal of Organometallic Chemistry*, 2002, **654**, 56-65.

Chapter 7 Appendix

"Don't let it end like this. Tell them I said something."

- last words of Pancho Villa (1877-1923) Mexican Revolutionary general.

7.1 The X-ray crystal structure of 4T-Br_2 (2.54)

Crystal data for 4T-Br_2: $C_{64}H_{70}Br_2S_4$, M = 1127.26, monoclinic, C2/c (no. 15), a = 24.9447(14), b = 16.6835(10), c = 14.2293(13) Å, β = 104.097(7)°, V = 5743.4(7) $Å_3$, Z = 4 [C_i symmetry], D_c = 1.304 g cm_{-3}, μ(Cu-Kα) = 3.432 mm_{-1}, T = 173 K, yellow thin needles, Oxford Diffraction Xcalibur PX Ultra diffractometer; 5510 independent measured reflections (R_{int} = 0.0683), F_2 refinement, R_1(obs) = 0.0695, wR_2(all) = 0.2203, 2661 independent observed absorption-corrected reflections [$|F_o| > 4\sigma(|F_o|)$, $2\theta_{max}$ = 145°], 341 parameters. CCDC 833875.

Despite a ca. 83 hour data collection time for an experiment using Cu-Kα radiation and that was designed to collect just the unique monoclinic data to a resolution of only 0.83 Å, the overall intensity of the data set was still very low, the mean I/σ being ca. 3.9. This was primarily a result of the crystals being thin needles so that only a comparatively small volume of material could be bathed in the X-ray beam (the crystal studied had dimensions of ca. 0.25 mm × 0.03 mm × 0.01 mm), and thus the scattering was very weak. As a consequence, the ratio of observed to unique reflections is low (ca. 0.48) and the final R-factors are relatively high (this is most easily seen in the wR_2(all) value of 0.2203). Despite this weak data however, there is little doubt as to the identity of the species present.

The molecule was found to have a centre of symmetry in the middle of the C(9)–C(9A) bond, and the C(11) to C(22) 4-n-hexylphenyl group was found to be disordered. Two orientations were identified of ca. 58 and 42% occupancy, their geometries optimised (including the phenyl rings being treated as idealised hexagonal rigid bodies), the thermal parameters of adjacent atoms restrained to be similar, and only the non-hydrogen atoms of the - 7 - major occupancy orientation were refined anisotropically (the remainder were refined isotropically).